TARGETED DELIVERY OF CPG-OLIGODEOXYNUCLEOTIDE TO BREAST CANCER CELLS BY POLY-AMIDOAMINE DENDRIMER-MODIFIED MAGNETIC NANOPARTICLES

A THESIS SUBMITTED TO
THE GRADUATE SCHOOL OF NATURAL AND APPLIED SCIENCES
OF
MIDDLE EAST TECHNICAL UNIVERSITY

BY

NEGAR TAGHAVI POURIANAZAR

IN PARTIAL FULFILLMENT OF THE REQUIREMENTS
FOR
THE DEGREE OF DOCTOR OF PHILOSOPHY
IN
BIOTECHNOLOGY

FEBRUARY 2016

Approval of the thesis

TARGETED DELIVERY OF CPG-OLIGODEOXYNUCLEOTIDE TO BREAST CANCER CELLS BY POLY-AMIDOAMINE DENDRIMER-MODIFIED MAGNETIC NANOPARTICLES

submitted by **NEGAR TAGHAVI POURIANAZAR** in partial fulfillment of the requirements for the degree of **Doctor of Philosophy in Biotechnology Department, Middle East Technical University** by,

Prof. Dr. Gülbin Dural Ünver _____
Dean, Graduate School of **Natural and Applied Sciences**

Assoc. Prof. Dr. Çağdaş Devrim Son _____
Head of Department, **Biotechnology**

Prof. Dr. Ufuk Gündüz _____
Supervisor, **Biology Dept., METU**

Prof. Dr. Güngör Gündüz _____
Co-supervisor, **Chemical Engineering Dept., METU**

Examining Committee Members:

Assoc. Prof. Dr. Dilek Keskin _____
Engineering Sciences Dept., METU

Prof. Dr. Ufuk Gündüz _____
Biology Dept., METU

Assoc. Prof. Dr. Çağdaş Devrim Son _____
Biology Dept., METU

Assoc. Prof. Dr.Özlem Darcansoy İşeri _____
Institute of Transplantation and Gene Sciences, Başkent Uni.

Assoc. Prof. Dr. Serap Yalçın Azarkan _____
Food Engineering Dept., Ahi Evran Uni.

Date: 04.02.2016

I hereby declare that all information in this document has been obtained and presented in accordance with academic rules and ethical conduct. I also declare that, as required by these rules and conduct, I have fully cited and referenced all material and results that are not original to this work.

Name, Last name: Negar Taghavi Pourianazar

Signature:

ABSTRACT

TARGETED DELIVERY OF CPG-OLIGODEOXYNUCLEOTIDE TO BREAST CANCER CELLS BY POLY-AMIDOAMINE DENDRIMER-MODIFIED MAGNETIC NANOPARTICLES

Taghavi Pourianazar, Negar

Ph.D., Department of Biotechnology

Supervisor: Prof. Dr. Ufuk Gündüz

Co-supervisor: Prof. Dr. Güngör Gündüz

February 2016, 175 pages

One major application of nanotechnology in cancer treatment involves designing nanoparticles to deliver drugs, oligonucleotides, and genes to cancer cells. Nanoparticles should be engineered so that they could target and destroy tumor cells with minimal damage to healthy tissues.

This research aims to develop an appropriate and efficient nanocarrier, having the ability of interacting with and delivering CpG-oligodeoxynucleotides (CpG-ODNs) to tumor cells. CpG-ODNs activate Toll-like receptor 9 (TLR9), which can generate a signal cascade for cell death. In our study, we utilized three-layer magnetic nanoparticles composed of a Fe3O4 magnetic core, an aminosilane (APTS) interlayer and a cationic poly(amidoamine) (PAMAM) dendrimer. The detailed characterization of synthesized nanoparticles was performed by X-ray photoelectron spectroscopy (XPS), Fourier transform infrared spectroscopy (FTIR), transmission electron microscopy (TEM),

scanning electron microscope (SEM), dynamic light scattering (DLS), zeta-potential, and vibrating sample magnetometer (VSM) analyses. TEM and SEM images indicated that synthesized dendrimer-coated magnetic nanoparticles (DcMNPs) have mono-disperse size distribution with an average particle diameter of 40±10 nm. DcMNPs were found to be superparamagnetic through VSM analysis. The synthesis, aminosilane modification, and dendrimer coating of iron oxide nanoparticles were validated by FTIR and XPS analyses. Cellular internalization of nanoparticles was studied by using fluorescence microscopy for FITC-bound nanoparticles. Results demonstrated that the synthesized DcMNPs, with their functional groups, symmetry perfection, size distribution, magnetic properties, and nontoxic characteristics could be suitable nanocarriers for targeted cancer therapy upon loading with various anticancer agents.

Successful transfer of the CpG-ODN to the tumor site is dependent on the development of an efficient delivery vector to overcome various hurdles, such as rapid degradation by serum nucleases and poor diffusion across the cell membrane. In the second part of this study, CpG-ODN was efficiently bound onto the surface of newly synthesized DcMNPs which can be targeted to the tumor site under magnetic field. The validation of CpG-ODN binding to DcMNPs was performed using agarose gel electrophoresis, UV-spectrophotometer, zeta-potential, and XPS analyses. Then, internalization of CpG-bound nanoparticles was evaluated in MDA-MB231, SKBR3, MCF7, and Doxorubicin-resistant MCF7 (MCF7/Dox) cell lines with Prussian blue staining method. Cytotoxicity of conjugates was assessed in fore-mentioned cell lines based on cell viability by XTT and flow cytometric analyses. Our results indicated that the synthesized DcMNPs having high positive charges on their surface could attach efficiently to CpG-ODN molecules via electrostatic means and induce cell death in breast tumor cells and could be considered a suitable targeted delivery system for CpG-ODN in biomedical applications. The magnetic core of these nanoparticles represents a promising option for selective drug targeting as they can be concentrated and held in position by means of an external magnetic field.

In the next part, we investigated the expression profiles of apoptosis-related genes, such as *Bax*, *Noxa*, *Puma*, *Bcl-2*, *Survivin*, and *C-Flip* before and after treatment with CpG-

loaded nanoparticles in breast cancer cells. The results indicated that after treatment of the cells, the expression profile of apoptosis-related genes showed a change compared to untreated cells which indicates triggering of the apoptotic pathways in the cells.

Studies show that the TLR9 activation with CpG-ODN may induce a Th1-like cytokine response in various cells, therefore, the release of IL-6, IL-10, and TNF-α was examined after treating the cells with different concentrations of free CpG, unloaded nanoparticles, and CpG-loaded nanoparticles and compared with the amount of release by the untreated cells. The results showed an increase in the released amount of IL-6 after treatment with CpG-loaded nanoparticles in breast cancer cells.

Keywords: Cancer, PAMAM-coated magnetic nanoparticles, CpG-ODN, TLR9, targeted therapy.

ÖZ

CPG-OLİGODEOKSİNÜKLEOTİTLERİN MEME KANSERİ HÜCRELERİNE POLİ-AMİDOAMİN DENDRİMER KAPLI MANYETİK NANOPARÇACIKLAR İLE HEDEFLENMESİ

Taghavi Pourianazar, Negar

Doktora, Biyoteknoloji Bölümü

Tez Yöneticisi: Prof. Dr. Ufuk Gündüz

Ortak Tez Yöneticisi: Prof. Dr. Güngör Gündüz

Şubat 2016, 175 sayfa

Kanser tedavisindeki nanoteknolojik uygulamalardan en önemlisi kanser hücrelerine ilaç, oligonükleotit ve gen taşımak için üretilen nanoparçacıklardır. Nanoparçacıklar tümör hücrelerini hedefleyip öldürürken, sağlıklı dokulara en az düzeyde zarar verecek şekilde tasarlanmalıdır.

Bu çalışmada CpG oligodeoksinükleotiti uygun ve etkili bir şekilde tümör hücrelerine taşıması için CpG-ODN ile etkileşime giren nanoparçacıkların geliştirilmesi amaçlanmıştır. CpG-ODN ler hücre ölümü için sinyal kaskadını oluşturan Toll benzeri reseptör 9' u (TLR9) uyarmaktadır. Bu çalışmada Fe_3O_4 manyetik çekirdek, aminoasilan (APTS) ara katmanı ve katyonik poli-amidoamin (PAMAM) dendrimerden oluşan üç katmanlı manyetik nanoparçacıklar sentezlenmiştir. Nanoparçacıkların karakterizasyonu X-Ray Fotoelektron Spektroskopisi (XPS), Fourier Dönüşümlü Kızılötesi Spektroskopisi (FTIR), Geçirimli Elektron Mikroskobu (TEM), Taramalı Elektron Mikroskobu (SEM), Dinamik ışık saçılımı (DLS),

Titreşimli Örnek Manyetometresi (VSM), ve zeta potansiyel analizleri ile yapılmıştır. TEM ve SEM görüntülerinden sentezlenen dendrimer kaplı manyetik nanoparçacıkların (DcMNPs) boyut bakımından uniform karakterde ve ortalama 40±10 nm çapa sahip oldukları görülmüştür. VSM analizi yapılarak DcMNP'lerin süperparamanyetik özellikte oldukları bulunmuştur. Demir oksit nanoparçacıkların sentezi, aminoasilan ile modifiye edilmesi ve dendrimer ile kaplanması FTIR ve XPS analizleri ile valide edilmiştir. Nanoparçacıkların hücre içine alımı FITC bağlı nanoparçacık kullanılarak floresan mikroskobu ile gözlemlenmiştir. Sonuçlar DcMNP'lerin fonksiyonel grupları, simetri mükemmelliği, boyut dağılımı, manyetik özelliği ve toksik olmaması açısından hedeflenmiş kanser tedavisinde ilaç taşıyıcı olarak kullanılabileceğini göstermiştir.

CpG-ODN'lerin, çeşitli engelleri aşarak tümör bölgesine başarılı bir şekilde taşınması etkili bir taşıyıcı vektörün kullanılmasına bağlıdır. Çünkü CpG-ODN'ler serumdaki nükleazlar tarafından hızlı bir şekilde yıkıma uğrayabilir ve hücre zarından difüzyonla geçemeyebilirler. Bu çalışmanın ikinci kısmında, CpG-ODN'ler yeni nesil bir polimer olan ve başarılı bir şekilde sentezlenen DcMNP'lerin yüzeyine etkili bir şekilde bağlanmış ve manyetik alan varlığında tümör bölgesine hedeflenmiştir. CpG-ODN'nin, DcMNP'nin yüzeyine bağlandığı agaroz jel elektroforezi, UV spektrofotometre, zeta potansiyel ve XPS analizleri ile belirlenmiştir. Daha sonra, CpG-ODN bağlı DcMNP'lerin hücre içine alındığı MDA-MB231, SKBR3, MCF7, and Doksorubisin dirençli MCF7 hücre hatlarında Prussian Blue boyama yöntemiyle gösterilmiştir. Aynı hücre hatlarında, hücre çoğalma analizi ve akış sitometrisi analizleri yapılarak konjüge nanoparçacıklar için sitotoksisite belirlenmiştir. Sonuçlar sentezlenen DcMNPlerin yüzeyinde çok miktarda pozitif yük bulundurması sebebiyle meme kanseri dokusunda hücre ölümüne sebep olan CpG-ODN molekülleri ile etkili şekilde elektrostatik etkileşime girdiğini; bu nedenle de hedeflenmiş kanser tedavisinde CpG-ODN taşımak için uygun bir taşıyıcı olabileceğini göstermiştir. Bu nanoparçacıklardaki manyetik çekirdek sayesinde harici manyetik alan kullanılarak ilaçların istenilen bölgeye hedeflenmesi sağlanabilmektedir.

Çalışmanın bir sonraki kısmında, CpG yüklü nanoparçacıklarının meme kanseri hücrelerine uygulamadan önce ve uygulamadan sonra apoptozla ilgili *Bax*, *Noxa*, *Puma*,

Bcl-2, *Survivin*, ve *C-Flip* genlerinin ifade düzeylerinde meydana gelen değişiklikler araştırılmıştır. Elde edilen sonuçlara göre CpG yüklü nanoparçacıklarının meme kanseri hücrelerine uygulanmasından sonra apoptozla ilgili genlerin ifade düzeylerinde apoptozu tetikleyecek şekilde değişiklik olduğu gösterilmiştir.

Yapılan diğer çalışmalar, farklı hücre hatlarında CpG-ODN ile TLR9'un aktivasyonu, Th1 benzeri sitokin cevabını uyardığını göstermektedir. Bu nedenle farklı konsantrasyonlarda serbest CpG, CpG yüklenmemiş nanoparçacıklar ve CpG yüklenmiş nanoparçacıklar hücrelere uygulanmadan önce ve uygulandıktan sonra IL-6, IL-10, ve TNF-α salımı açısından karşılaştırılmıştır. Sonuçlar CpG yüklenmiş nanoparçacıklar uyguladıktan sonra meme kanseri hücrelerinde IL-6 salımında bir artış olduğunu göstermiştir.

Anahtar Kelimeler: Kanser, PAMAM kaplı manyetik nanoparçacık, CpG-ODN, TLR9, hedeflenmiş tedavi

To my precious family and to my love Kaveh…

ACKNOWLEDGEMENTS

I would like to convey my thanks to those people who made this thesis possible. First I would like to express my gratitude to my advisor Prof. Dr. Ufuk Gündüz for her generous support, wholehearted help and thoughtful guidance throughout the Ph.D. candidature.

I would like to acknowledge my co-adviser Prof. Dr. Güngör Gündüz with my all sincerity for his supports.

I thank to the members of examining committee, Assoc. Prof Dr. Çağdaş Devrim Son, Assoc. Prof. Dr. Dilek Keskin, Assoc. Dr. Serap Yalçın Azarkan, and Assoc. Dr. Özlem Darcansoy İşeri.

I am indebted to Prof. Dr. İnci Eroğlu and Assoc. Prof. Dr. Bora Maviş for providing me an opportunity to use their laboratory during some parts of the research.

I would like to express my special appreciation and thanks to Assoc. Prof. Dr. Pelin Mutlu for her insightful comments and advice.

I am grateful to Çağrı Urfalı who as a good friend, was always willing to help and give her best suggestions. I would like to thank my other labmates, Maryam Parsian, Ayca Nabioğlu, Esra Metin, Hasan Hüseyin Kazan, Murat Erdem, Aktan Alpsoy, for the stimulating discussions and for all the fun we have had in the last three years.

Lastly and most notably, I would like to thank my family. I am deeply indebted to my mother and my sisters for their endless love, trust, and support in every step of my life especially throughout my years of study and through the process of researching and writing this thesis. I also thank my kind, extraordinary husband, Kaveh, with unfailing support and continuous encouragement. I specially dedicate this thesis to my father.

This study is supported by the Scientific and Technical Research Council of Turkey (TÜBİTAK-grants 2215 and 1002) and Middle East Technical University (BAP-07-02-2012-71).

TABLE OF CONTENTS

ABSTRACT v

ÖZ viii

ACKNOWLEDGEMENTS xii

TABLE OF CONTENTS xiii

LIST OF TABLES xix

LIST OF FIGURES xx

LIST OF ABBREVIATIONS xxv

CHAPTERS

1 INTRODUCTION 1

1.1 Cancer 1

1.2 Breast Cancer 2

1.3 The Most Common Therapy Options for Breast Cancer 3

1.3.1 Surgery 3

1.3.1.1 Lumpectomy 3

1.3.1.2 Mastectomy 3

1.3.2 Radiotherapy 3

1.3.3 Hormone Therapy 3

1.3.4 Chemotherapy 4

1.3.5 Targeted Cancer Therapies 4

1.3.5.1 Passive Targeting 6

1.3.5.2 Active Targeting 7

1.4 Targeted Delivery Using Magnetic Nanoparticles 8

1.4.1 Superparamagnetism 10
1.4.2 Synthesis of Magnetic Nanoparticles 11
1.5 Dendrimers for Surface Coating of Magnetic Nanoparticles 12
1.5.1 Poly(amidoamine) Dendrimers 13
1.5.2 Strategies for Synthesizing PAMAM Dendrimers 15
1.5.2.1 Divergent Synthesis……15
1.5.2.2 Convergent Synthesis…….16
1.5.2.3 Combined Convergent-Divergent Synthesis……..17
1.5.2.4 Click Synthesis……...18
1.6 Toll-Like Receptors 19
1.6.1 Toll-Like Receptor 9 20
1.6.2 The Expression of TLR9 21
1.6.3 CpG-ODN as TLR9 Agonist 22
1.6.3.1 Classes of Synthetic CpG-Oligodeoxynucleotides ……22
1.6.4 Signaling Pathway 25
1.6.5 Therapeutic Applications of CpG-ODN 27
1.6.5.1 Immunomodulation by CpG-ODN ……..……..……28
1.6.5.2 Anti-tumor Therapy Using CpG-ODN……...……29
1.6.5.3 Cytokine Production……...……30
1.6.5.3.1 Interleukin 6 (IL-6)…….....……31
1.6.5.3.2 Interleukin 10 (IL-10)……. ……...….....……32
1.6.5.3.3 Tumor necrosis factor-α (TNF-α)…..…….....…….……32
1.7 Aim of the Study 33
2 MATERIALS AND METHODS 35

2.1 Synthesis of Magnetic Nanoparticles 35
2.2 Surface Modification of Magnetic Core with Aminosilane 36
2.3 Growth of PAMAM Dendrimer on the Surface of APTS-Modified MNPs 36
2.4 Characterization of Synthesized Bare and PAMAM-Coated Magnetic Nanoparticles 37
2.5 Preparation of CpG-ODN Stock Solution 37
2.6 CpG Binding 37
2.7 Characterization of CpG-Bound DcMNPs 38
2.7.1 NanoDrop Spectrophotometer Analysis 38
2.7.2 Gel Electrophoresis 38
2.7.3 X-Ray Photoelectron Spectroscopy 39
2.7.4 Scanning Electron Microscopes 39
2.7.5 Transmission Electron Microscopy 40
2.7.6 Fourier Transform Infrared Spectroscopy 40
2.7.7 Zeta-Potential 40
2.8 *In Vitro* Stability of CpG-ODN/DcMNP Conjugate 40
2.9 Cell Culture and Culture Conditions 40
2.10 Subculturing of Cells 41
2.11 Freezing the Cells 42
2.12 Thawing the Frozen Cells 42
2.13 Cell Counting 42
2.14 Cellular Internalization 43
2.14.1 Detection of Internalized Nanoparticles by Fluorescence Microscopy 43
2.14.2 Detection of Internalized Nanoparticles by Prussian Blue Staining 44
2.15 Targeting Properties of MNP Core 44

2.16 RNA Isolation 45
2.17 Quality Control of the Isolated RNA 46
2.17.1 Checking RNA Quantity and Purity 46
2.17.2 Checking RNA Integrity 46
2.18 DNase I Treatment 46
2.19 cDNA Synthesis 47
2.20 Quantitative Real-Time Polymerase Chain Reaction (qRT-PCR) 47
2.21 Analyzing qRT- PCR Data by the Comparative C_T Method 49
2.22 XTT Cell Proliferation Assay 49
2.23 Apoptotic Gene Expression Analysis 50
2.24 Evaluation of Apoptosis by Flow Cytometry 52
2.25 Determination of IL-6, IL-10, and TNF-α Release by ELISA Assay 54
2.26 Statistical Analysis 55
3 RESULTS AND DISCUSSION 57
3.1 Synthesis of DcMNPs 57
3.2 Characterization of Bare and PAMAM-Coated Magnetic Nanoparticles 58
3.2.1 Fourier Transform-Infrared Spectroscopy (FTIR) 58
3.2.2 Transmission Electron Microscopy Analysis (TEM) 59
3.2.3 Scanning Electron Microscopy (SEM) 60
3.2.4 Vibrating Sample Magnetometer Analysis (VSM) 61
3.2.5 Zeta (ζ) Potential Analysis 62
3.3 Cellular Internalization of Dendrimer-Coated Magnetic Nanoparticles 65
3.3.1 Fluorescence Microscopy 65
3.4 Validation of CpG Loading on DcMNPs 66
3.4.1 NanoDrop Spectroscopy Analysis 67

3.4.2 Agarose Gel Electrophoresis Shift Assay 69

3.4.3 CpG-ODN Loading Validation by Zeta-Potential Analysis 70

3.4.4 Validation of CpG-ODN Loading by X-Ray Photoelectron Spectroscopy (XPS).....72

3.4.5 The Hydrodynamic Size Measurement of G_7DcMNP by Dynamic Light Scattering (DLS) 74

3.4.6 Evaluation of CpG-DcMNP Internalization by Cells Using Prussian Blue Staining Assay.....74

3.5 Targeting Properties of Free and CpG-Loaded DcMNP.....77

3.6 CpG-Loaded DcMNPs Stability Studies.....78

3.7 *TLR9* Expression Analysis 79

3.7.1 Isolation of Total RNA.....79

3.7.2 Quantitative Real-Time Polymerase Chain Reaction (qRT-PCR).....80

3.8 Cytotoxicity of CpG-Bound DcMNPs 82

3.9 Annexin V/PI Staining (Flow Cytometry) 86

3.10 Apoptotic Gene Expression Analysis After Treatment with CpG-Loaded DcMNPs 92

3.10.1 Isolation of Total RNA.....92

3.10.2 Quantitative Real-Time Polymerase Chain Reactin (qPCR): Expression Analysis of *Bax, Noxa, Bcl-2, Survivin, Puma, C-Flip,* and *β-actin* Genes.....94

3.11 Enzyme-Linked Immunosorbent Assay (ELISA): Changes in Secreted IL-6, TNF-α, and IL-10 Levels.....100

4 CONCLUSIONS.....113

REFERENCES.....117

APPENDICES

A. BUFFERS AND SOLUTIONS.....137

B. THRESHOLD CYCLE VALUES.....139

C. AMPLIFICATION CURVES, MELT CURVES, STANDARD CURVES, AND AGAROSE GEL IMAGES.....141

D. CELL CULTURE MEDIUM.....153

E. CELL PROLIFERATION GRAPHS.....155

F. NANODROP SPECTROPHOTOMETER.....163

G. FLOW CYTOMETRY GRAPHS.....163

CURRICULUM VITAE.....169

LIST OF TABLES

TABLES

Table 1.1 Comparison of D, K, C and P-type oligodeoxynucleotide. 24

Table 2.1 PCR mix for expression analysis of TLR9 gene.....48

Table 2.2 Reaction conditions for TLR9 gene expression.....48

Table 2.3 Primers used in gene expression analyses.....51

Table 2.4 qRT-PCR conditions of *Bax, Noxa, Bcl-2, Survivin, Puma, C-Flip,* and *β-actin* genes.....52

Table 2.5 Various treatments for MDA-MB231, SKBR3, MCF7/S, and MCF7/1000Dox cell lines. 53

Table 3.1 Determination of RNA concentration (ng/µl) and the purity of sample using NanoDrop spectrophotometer. 80

Table 3.2 IC_{50} amounts of unloaded DcMNP, free CpG, and DcMNPs bearing CpG-ODN treatments after on MDA-MB-231, SKBR3, MCF7, and MCF7/Dox cell lines. ..84

Table 3.3 Determination of RNA concentration (µg/ml) and the purity of sample using NanoDrop spectrophotometer. 93

Table 3.4 Expression levels of apoptotic-related genes in untreated and treated MDA-MB231, SKBR3, MCF7, and MCF7/Dox cell lines. 100

Table B.1 Threshold cycle (C_t) values of qRT-PCR analysis……..….139

Table B.2 Threshold cycle (C_t) values of qRT-PCR analysis……139

Table D.1 Formulation of RPMI 1640 Medium……..……..……153

Table F.1 Determination of ssDNA concentration (free CpG-ODN) using NanoDrop spectrophotometer……...163

Table F.2 Determination of ssDNA concentration (free CpG-ODN) in the stability test using NanoDrop spectrophotometer……...164

LIST OF FIGURES

FIGURES

Figure 1.1 Acquired capabilities of cancer.....1
Figure 1.2 The anatomy of breast.....2
Figure 1.3 Representation of EPR effect in malignant tissue. 6
Figure 1.4 A) Passive targeting of nanocarriers. B) Active targeting strategies in which ligands grafted at the surface of nanocarriers bind to receptors (over)expressed by cancer cells or angiogenic endothelial cells.....8
Figure 1.5 A summary of nanoparticles that have been explored as carriers for drug delivery in cancer therapy, together with illustrations of biophysicochemical properties. 9
Figure 1.6 Schematic representation of magnetic nanoparticle-based drug delivery system.....10
Figure 1.7 Dendrimer structure. 14
Figure 1.8 Structure of dendritic macromolecules: A) structural elements, B) dendron, and C) dendrimer.....16
Figure 1.9 Convergent method for synthesis of dendrimers. 17
Figure 1.10 Convergent-divergent method for dendrimer synthesis.....18
Figure 1.11 Copper-catalyzed azide-alkyne cycloaddition (CuAAC). 19
Figure 1.12 Schematic representation of A) the molecular structure of TLR9 and B) its position in lysosomes after CpG-ODN entry. 21
Figure 1.13 Intracellular TLR9 traffic.....25
Figure 1.14 The signaling pathway for TLR9.....27
Figure 1.15 Survey on intracellular TLR-9-mediated signaling MyD88-dependent pathways and the role of nanoparticles as a potent TLR-agonist delivery device for cytokine release. 31
Figure 2.1 Arrangement for experimental setup for MNP synthesis. 36
Figure 3.1 Stepwise modification of magnetic nanoparticle modified with APTS and PAMAM dendrimer. 58

Figure 3.2 FTIR spectra of bare MNP, MNP-APTS, G5, and G7DcMNPs. 59
Figure 3.3 TEM results showing A) bare MNP (magnetite core) and B) G_7DcMNP. 60
Figure 3.4 SEM results showing G_7DcMNP with an average grain size of 40±10 nm...61
Figure 3.5 Variation of magnetization of the MNPs, APTS-modified MNPs and DcMNPs with applied field at 37°C showing superparamagnetic nature of MNPs with zero coercivity. 62
Figure 3.6 ζ Potential measurements of free MNP. 63
Figure 3.7 ζ Potential measurements of A) APTS-modified MNP and B) G7DcMNP…64
Figure 3.8 Fluorescence microscope images 66
Figure 3.9 CpG binding percent on different generations of DcMNP (G_3-G_8) (CpG-ODN:DcMNP ratio (w/w) was 1:70). 68
Figure 3.10 CpG binding percent on different ratios of CPG-ODN:G_7DcMNP (w/w)...69
Figure 3.11 Agarose gel electrophoresis of loading optimization of CpG-ODN on DcMNPs at pH 7.. 70
Figure 3.12 Zeta Potential Analysis of CpG-ODN/G7DcMNP Complex 71
Figure 3.13 Zeta potentials of bare MNP, APTS-modified MNP, unloaded DcMNP, CpG-loaded DcMNP in H2O. 72
Figure 3.14 X-ray photoelectron spectroscopy (XPS) spectra of A) unloaded G_7DcMNP and B) CpG/G7DcMNP conjugates 73
Figure 3.15 The hydrodynamic size distribution of G_7DcMNPs measured by DLS analysis. 74
Figure 3.16 Prussian blue stained images of untreated (A) MDA-MB231, (B) SKBR3, (C) MCF7/S, and (D) MCF7/Dox. 75
Figure 3.17 Prussian blue stained images of (A) and (B) MDA-MB231, (C) and (D) SKBR3, (E) and (F) MCF7/S, and (G) and (H) MCF7/Dox. Cells were incubated with CpG-DcMNP complexes with a concentration of 100 µg DcMNP for 5 h. 76
Figure 3.18 Evaluation of the role of MNP core as targeting agent in MDA-MB231 cells. 77
Figure 3.19 CpG-ODN release percent determined by release assay followed up to 8 weeks in PBS (pH 7.2) at 37˚C…….78

Figure 3.20 Total RNAs isolated from MDA-MB231 (Lane 1), SKBR3 (Lane 2) and MCF7/S (Lane 3), MCF7/Dox cells (Lane 4) on 1% agarose gel.....79
Figure 3.21 Amplification curves for a) TLR9 and b) *β-actin* genes in MDA-MB231, SKBR3, MCF7/S, and MCF7/Dox cell lines. 80
Figure 3.22 TLR9 mRNA-expression in MDA-MB231, SKBR3, MCF7/S, and MCF7/Dox cell lines 81
Figure 3.23 Cytotoxicity of unloaded G_7DcMNPs on MDA-MB-231, SKBR3, MCF7, and MCF7/Dox cell lines. 82
Figure 3.24 IC50 amounts (µg ml^{-1}) of free CpG-ODN for MDA-MB-231, SKBR3, MCF7, and MCF7/Dox cell lines. 83
Figure 3.25 Cytotoxicity of CpG ODN-loaded G_7DcMNPs on MDA-MB-231, SKBR3, MCF7, and MCF7/Dox cell lines. 84
Figure 3.26 Flow cytometric analysis of MDA-MB231 cells by double labeling with Annexin V-FITC and PI.. 88
Figure 3.27 Flow cytometric analysis of SKBR3 cells by double labeling with Annexin V-FITC and PI.....89
Figure 3.28 Flow cytometric analysis of MCF7 cells by double labeling with Annexin V-FITC and PI.....90
Figure 3.29 Flow cytometric analysis of MCF7/Dox cells by double labeling with Annexin V-FITC and PI. 91
Figure 3.30 Total RNAs isolated from untreated MDA-MB231 cells (Lane 1), MDA-MB231 cells treated with 0.5 µg/ml CpG-DcMNP complex (Lane 2), untreated SKBR3 cells (Lane 3), SKBR3 cells treated with 0.5 µg/ml CpG-DcMNP complex (Lane 4), untreated MCF7 cells (Lane 5), MCF7 cells treated with 0.5 µg/ml CpG-DcMNP complex (Lane 6), untreated MCF7/Dox cells (Lane 7), and MCF7/Dox cells treated with 0.5 µg/ml CpG-DcMNP complex (Lane 8) on 1% agarose gel. 93
Figure 3.31 Expression levels of apoptotic-related genes in untreated and treated MDA-MB23 cell line with 0.29 mg/ml CpG-loaded DcMNPs for 48 h, when $p<0.05$. 96
Figure 3.32 Expression levels of apoptotic-related genes in untreated and treated SKBR3 cell line with 0.29 mg/ml CpG-loaded DcMNPs for 48 h, when $p<0.05$.....97

Figure 3.33 Expression levels of apoptotic-related genes in untreated and treated MCF7/Dox cell line with 0.29 mg/ml CpG-loaded DcMNPs for 48 h, when p<0.05.....98
Figure 3.34 Expression levels of apoptotic-related genes in untreated and treated MCF7 cell line with 0.29 mg/ml CpG-loaded DcMNPs for 48 h, when p<0.05. 99
Figure 3.35 Quantification of released IL-6 in a) MDA-MB231, b) SKBR3, c) MCF7, and d) MCF7/Dox cell lines.....102
Figure 3.36 Model for the role of the EGF receptor in IL-6-induced STAT3 signaling. 105
Figure 3.37 Quantification of released TNF-α in a) MDA-MB231, b) SKBR3, c) MCF7, and d) MCF7/Dox cell lines. 106
Figure 3.38 Quantification of released IL-10 in a) MDA-MB231, b) SKBR3, c) MCF7, and d) MCF7/Dox cell lines.....109
Figure C.1 Cycling profile (upper), melt curve (middle) and standard curve (lower) for *Bax* amplicon……. 141
Figure C.2 Cycling profile (upper), melt curve (middle) and standard curve (lower) for *Noxa* amplicon……..……..142
Figure C.3 Cycling profile (upper), melt curve (middle) and standard curve (lower) for *Bcl-2* amplicon……..……..143
Figure C.4 Cycling profile (upper), melt curve (middle) and standard curve (lower) for *Survivin* amplicon…….……..144
Figure C.5 Cycling profile (upper), melt curve (middle) and standard curve (lower) for *Puma* amplicon……..……...……..145
Figure C.6 Cycling profile (upper), melt curve (middle) and standard curve (lower) for *C-Flip* amplicon……..146
Figure C.7 Cycling profile (upper), melt curve (middle) and standard curve (lower) for *B-actin* amplicon……..……..147
Figure C.8 Expression levels of *β-actin (ACTB)*……...……148
Figure C.9 Expression levels of *Bax* ……149
Figure C.10 Expression levels of *Noxa*…….……149
Figure C.11 Expression levels of *Bcl-2*……...….…….……150

Figure C.12 Expression levels of *Survivin*……..……150
Figure C.13 Expression levels of *Puma*……..……151
Figure C.14 Expression levels of *C-Flip* (long)…….……....151
Figure E.1 Profile of cell proliferation of a) MDA-MB231, b) SKBR3, c) MCF7/S, and d) MCF7/Dox cell lines at increasing concentrations of unloaded DcMNP at three different incubation times……...…155
Figure E.2 Profile of cell proliferation of a) MDA-MB231, b) SKBR3, c) MCF7/S, and d) MCF7/Dox cell lines at increasing concentrations of free CpG-ODN at three different incubation times……..……158
Figure E.3 Profile of cell proliferation of a) MDA-MB231, b) SKBR3, c) MCF7/S, and d) MCF7/Dox cell lines at increasing concentrations of CpG-loaded DcMNP at three different incubation times……..…….....160
Figure G.1 Profile of programmed cell death of MDA-MB231 cells after five different treatments determined by flow cytometric analysis……...165
Figure G.2 Profile of programmed cell death of SKBR3 cells after five different treatments determined by flow cytometric analysis……...166
Figure G.3 Profile of programmed cell death of CF7 cells after five different treatments determined by flow cytometric analysis…….……....167
Figure G.4 Profile of programmed cell death of MCF7/Dox cells after five different treatments determined by flow cytometric analysis……...168

LIST OF ABBREVIATIONS

APTS	(3-Aminopropyl)trimethoxysilane
bp	Base Pair
cDNA	Complementary Deoxyribonucleic Acid
c-FLIP	Cellular FLICE-Like Inhibitory Protein
CpG-ODN	CpG-Oligodeoxynucleotide
C_T	Threshold Cycle Value
DcMNP	Dendrimer-Coated Magnetic Nanoparticles
DEPC	Diethylpyrocarbonate
dH_2O	Distilled Water
DMSO	Dimethyl Sulfoxide
DNA	Deoxyribonucleic Acid
Dox	Doxorubicin
dNTP	Deoxy Nucleotide Triphosphate
EDTA	Ethylenediaminetetraacetic Acid
ELISA	Enzyme-Linked Immunosorbent Assay
Emu g^{-1}	Electromagnetic Unit per Gram
EtBr	Ethidium Bromide

FBS	Fetal Bovine Serum
$FeCl_2.4H_2O$	Iron (II) Chloride Tetrahydrate
$FeCl_3.6H_2O$	Iron (III) Chloride Hexahydrate
FTIR	Fourier Transform Infrared Spectroscopy
G_7DcMNP	Generation 7 Dendrimeric-Coated Mangetic Nanoparticles
IC_{50}	Inhibitory Concentration 50
IL	Interleukin
kDa	kilo Dalton
MCF-7/S	Sensitive MCF-7 (Michigan Cancer Foundation-7)
MCF-7/1000Dox	1000 nM Doxorubicin-Resistant MCF7 Cell Line
MNP	Magnetic Nanoparticle
MRI	Magnetic Resonance Imaging
NF-κB	Nuclear Factor-Kappa B
PBS	Phosphate Buffered Saline
PCR	Polymerase Chain Reaction
PUMA	p53 Upregulated Modulator of Apoptosis
qRT-PCR	Quantitative Real-Time Polymerase Chain Reaction
RNA	Ribonucleic Acid
rpm	Revolution per Minute

SEM	Scanning Electron Microscope
SEM	Standart Error of the Means
ssDNA	Single-Stranded DNA
TAE	Tris-Acetate-EDTA
TEM	Transmission Electron Microscopy
TGA	Thermal Gravimetric Analysis
TLR	Toll-Like Receptor
V	Volt
VSM	Vibrating Sample Magnetometer
v/v	Volume per Volume
w/v	Weight per Volume
XTT	2,3-Bis-(2-Methoxy-4-Nitro-5-Sulfophenyl)-2H-Tetrazolium-5-Carboxanilide

CHAPTER 1

INTRODUCTION

1.1 Cancer

Cancer, also known as a malignant tumor, is a complex group of diseases comprising abnormal growth of cells. The biological capabilities dictating malignant growth are acquired during the multistep development of human tumors which include (Figure 1.1): self-sufficiency in growth signals, limitless replicative potential, evading growth suppressing signals, resistance to programmed cell death (apoptosis), sustained angiogenesis, tissue invasion and metastasis. Underlying these hallmarks is genome instability, which generates the genetic diversity that accelerates their acquisition and inflammation, which fosters multiple hallmark functions. Conceptual progress in the last decade has added two emerging hallmarks to this list—reprogramming of energy metabolism and evading immune destruction (Hanahan and Weinberg 2000).

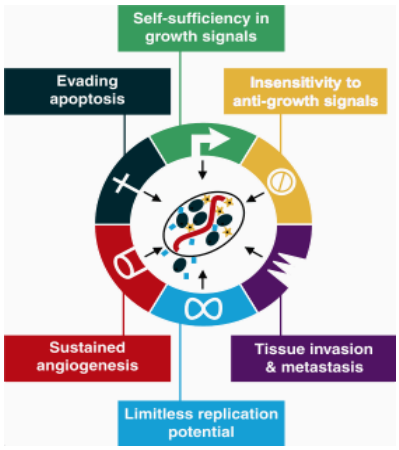

Figure 1.1 Acquired capabilities of cancer. Retrieved from (Hanahan and Weinberg 2000).

1.2 Breast Cancer

Breast cancer is the most common kind of cancer affecting females and the second cause of mortality in women in the United States in 2010 (Lee and Nan 2012). In these patients, it is not the primary tumor, but its metastases at distant sites that are the main cause of death (Weigelt et al. 2005).

Breast cancer usually starts off in the inner lining of milk ducts or the lobules that supply them with milk (Figure 1.2). A breast cancer that started off in the lactiferous duct (milk duct), known as ductal carcinoma, is the most common type, while one that developed from the lobules, known as lobular carcinoma, is much less common. A malignant tumor can spread to other parts of the body. The most common sites of breast cancer metastases are to lymph nodes, lung, liver, bone and brain (Grobmyer et al. 2012).

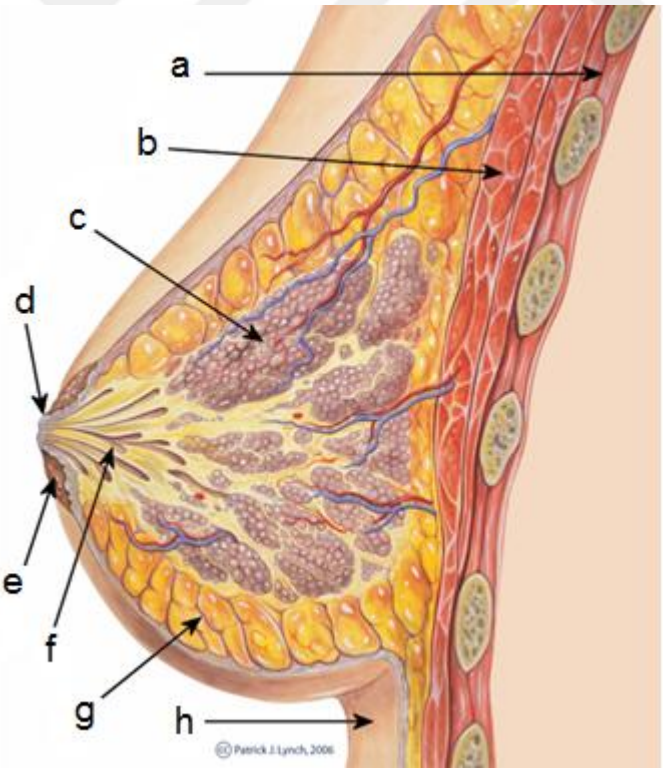

Figure 1.2 The anatomy of breast. a) chest wall, b) pectoralis muscles. C) lobules glands that make milk, d) nipple surface, e) areola, f) lactiferous duct tube that carries milk to the nipple, g) fatty tissue, and h) skin. Retrieved from (http://www.medicalnewstoday.com/articles/37136.php).

1.3 The Most Common Therapy Options for Breast Cancer

1.3.1 Surgery

Surgery is usually considered as the primary treatment for breast cancer with the aim of removing the entire tumor from the breast. Some of the lymph nodes from the underarm area (axillary nodes) may also be removed to see if cancer cells are present. Two main types of surgery to remove breast cancer include *Lumpectomy* and *Mastectomy*.

1.3.1.1 Lumpectomy

In this treatment, also called breast-conserving surgery or wide excision, the tumor and a little bit of healthy tissue around it are removed.

1.3.1.2 Mastectomy

During this surgery, removal of the entire breast, sometimes along with other nearby tissues is occurred.

1.3.2 Radiotherapy

Radiotherapy is a treatment for cancer that uses carefully measured and controlled high energy x-rays. This high-energy rays or particles are produced by a machine called a linear accelerator, which focuses on the exact area to be treated. Radiation to the breast is often given after breast-conserving surgery to help lower the chance that the cancer will come back in the breast or nearby lymph nodes.

1.3.3 Hormone Therapy

Most types of hormone therapy for breast cancer either lower estrogen levels or stop estrogen from acting on breast cancer cells. This kind of treatment is helpful for hormone receptor-positive breast cancers, but it does not help patients whose tumors are hormone receptor negative (both estrogen- and progesterone-negative). This type of

therapy is given to people with primary invasive breast cancer to reduce the risk of the breast cancer coming back.

1.3.4 Chemotherapy

Chemotherapy is a treatment with using anti-cancer (also called cytotoxic) drugs that may be given intravenously (injected into a vein) or by mouth. The drugs travel through the bloodstream to reach cancer cells in most parts of the body.

The main drawback in cancer chemotherapy is systemic toxicity, as the activity of the cancer drug circulating throughout the body, is not limited to the tumor cells and leads to various undesirable effects on normal tissues and organs. To lower the toxicity of these agents, two objectives required to be accomplished; decreasing the level of drug presented systematically while maintaining its amount in the tumor microenvironment. The most possible way to this, is targeting the drug to the tumor mass. Various delivery systems have been able to provide enhanced therapeutic activity and reduced toxicity due to anticancer agents, mainly by altering their pharmacokinetics and biodistribution (Gang et al. 2007).

1.3.5 Targeted Cancer Therapies

Targeted cancer therapies are treatments that target specific characteristics of cancer cells, such as a protein that allows the cancer cells to grow in a rapid or abnormal way. Targeted therapies are generally less likely than chemotherapy to harm normal, healthy cells. A targeted therapy is a drug designed to attack a certain molecular agent or pathway involved in the development of cancer. For example, the drug trastuzumab (Herceptin) targets a certain gene's protein called HER2/neu that is found on the surface of some cancer cells.

Almost a century ago, developing of a hypothetical drug called the “magic bullet” was proposed by Paul Ehrlich, which had the potential to selectively demolish disease cells while it did not possess any harm effect on normal cells. After that, some drugs were designed that could specifically target the site of action. The targeted drug delivery

system contains three different constituents: a therapeutic agent, a carrier system, and a targeting component. The therapeutic agents can be incorporated into the carrier system by either encapsulation or complexation. That is to say, in order to deliver the drug molecules, they can be either encapsulated within the delivery agent or attached to its terminal functional groups via electrostatic or covalent bonds. The selection of the carrier molecule is very important since it considerably influences the pharmacokinetics and pharmacodynamics of the drugs (Park et al. 2010).

An alternative to overcome the limitations of specificity of conventional chemotherapeutic agents was to use targeted drug delivery with nanoparticles. High amounts of drugs can be loaded and targeted to the tumor mass via nanoparticles. Delivery of drugs by utilizing nanoparticles enhances the half-life and decreases toxic side effects of drugs, by improving their pharmacokinetic profile and therapeutic efficacy (Shubayev et al. 2009).

In order to better understand how the targeted systems work, a brief description about the tumor microenvironment is provided.

The tumor microenvironment (TME) is the cellular environment in which the tumor exists, including surrounding blood vessels, immune cells, fibroblasts, bone marrow-derived inflammatory cells, lymphocytes, signaling molecules and the extracellular matrix (ECM). The tumor and the surrounding microenvironment are closely related and interact constantly. Tumors can influence the microenvironment by releasing extracellular signals, promoting tumor angiogenesis and inducing peripheral immune tolerance, while the immune cells in the microenvironment can affect the growth and evolution of cancerous cells, such as in immuno-editing (Balkwill et al. 2012; Mbeunkui and Johann 2009).

The metabolic microenvironment of solid tumors is characterized by insufficient blood perfusion, an oxygen deficiency (hypoxia), and increased anaerobic glycolysis leading to extracellular acidosis and ATP depletion. Correspondingly, tumor cells switch to anaerobic glycolysis, resulting in an excessive amount of lactate and low glucose

concentrations, pronounced extracellular acidosis with pH values in some instances even below 6.5, and lack of ATP (Justus et al. 2013; Lotz et al. 2007).

1.3.5.1 Passive Targeting

Enhanced permeability and retention (EPR) effect is a passive phenomenon as a result of the unique abnormalities of tumor vasculature. Most solid tumors possess a higher vascular density (hypervasculature) compared to normal tissues and organs, i.e., angiogenesis that is one of the most important features of tumors to preserve their rapid growth. Tumor vascular angiogenesis (vascular bed) is even indicated in tumor nodules smaller than 0.2 mm in size. Furthermore, irregular or contradictory blood flow is detected in tumors. In addition, most solid tumors acquire blood vessels with poorly aligned defective endothelial cells, such as wide fenestrations (up to 4 μm), lacking smooth muscle layer or innervations, with relatively wide lumen and impaired receptor function for vasoactive mediators especially angiotensin II, so that macromolecules could escape from tumor blood vessels and accumulate selectively in tumor tissues, whereas they could not cross normal blood vessels which will result in less side effects (Figure 1.3) (Iyer et al. 2006; Maeda et al. 2013).

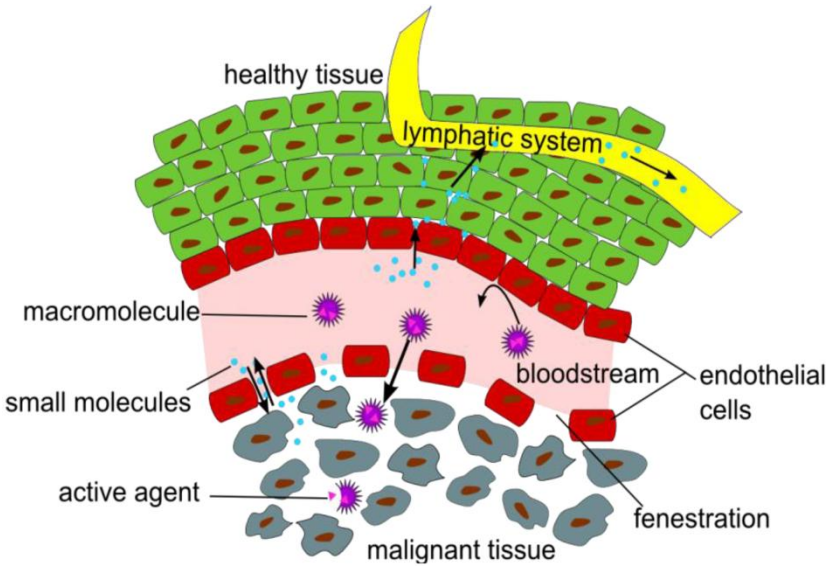

Figure 1.3 Representation of EPR effect in malignant tissue. Retrieved from (Stockhofe et al. 2014).

Moreover, the enhanced permeability of tumor blood vessels is partly referred to the hyperproduction of vascular mediators, such as bradykinin, nitric oxide (NO), vascular endothelial growth factor (VEGF) and carbon monoxide (CO) and therefore, it is considered as a landmark principle in the development of the EPR based tumor targeting (Fang et al. 2011; Greish 2010). It is the mostly used mechanism for the uptake of nanoparticles or polymers at oncological target sites in pre-clinical and clinical studies (Stockhofe et al. 2014). Nanocarriers can transport into the tumor interstitium and cells through leaky tumor capillary fenestrations by passive targeting (Figure 1.4A) (Danhier et al.2010).

1.3.5.2 Active Targeting

Specific nanocarrier systems are designed with the targeting ligands present on their surface which could bind specifically to the receptors expressed on the target cells. This is called active targeting (Figure 1.4B). The ligand is chosen to bind to a receptor overexpressed by tumor cells or tumor vasculature and not expressed by normal cells. Moreover, targeted receptors should be expressed homogeneously on all targeted cells. The binding affinity of the ligands influences the tumor penetration because of the "binding-site barrier." For targets in which cells are readily accessible, typically the tumor vasculature, because of the dynamic flow environment of the bloodstream, high affinity binding appears to be preferable (Danhier et al. 2010).

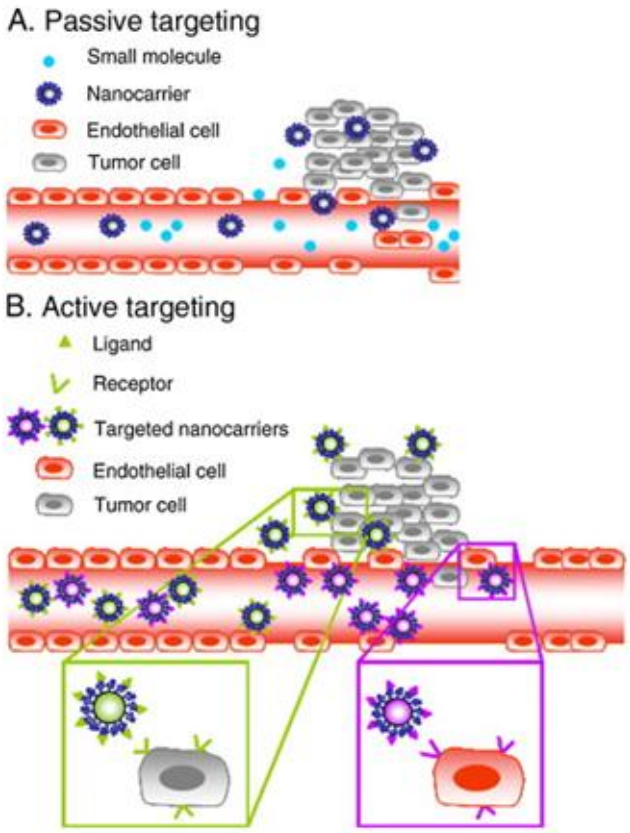

Figure 1.4 A) Passive targeting of nanocarriers. B) Active targeting strategies in which ligands grafted at the surface of nanocarriers bind to receptors (over)expressed by cancer cells or angiogenic endothelial cells. Retrieved from (Danhier et al. 2010).

1.4 Targeted Delivery Using Magnetic Nanoparticles

Delivery of antitumor agents by nanocarrier systems such as nanoparticles possesses various advantages compared with traditional therapy methods. These carriers could deliver higher amounts of drug molecules into tumor cells or enhance the delivery of therapeutic agents with relatively low solubility in water. Furthermore, the drug is protected from harsh environments in the way to the target (such as high stomach acid or the low pH in the lysosomes of the cells or the enzymes present in the blood circulation) which could, in turn, enhance the plasma half-life of the therapeutic agent. Targeting the drug to the specific cells or tissues by the nanocarriers could maximize the efficiency of the treatment while reducing the systemic side effects. Moreover, these delivery systems

have controlled release of drugs and also they can deliver more than one type of therapeutic agents (combination therapy) in order to overcome multidrug resistance (Figure 1.5) (Sun et al. 2014).

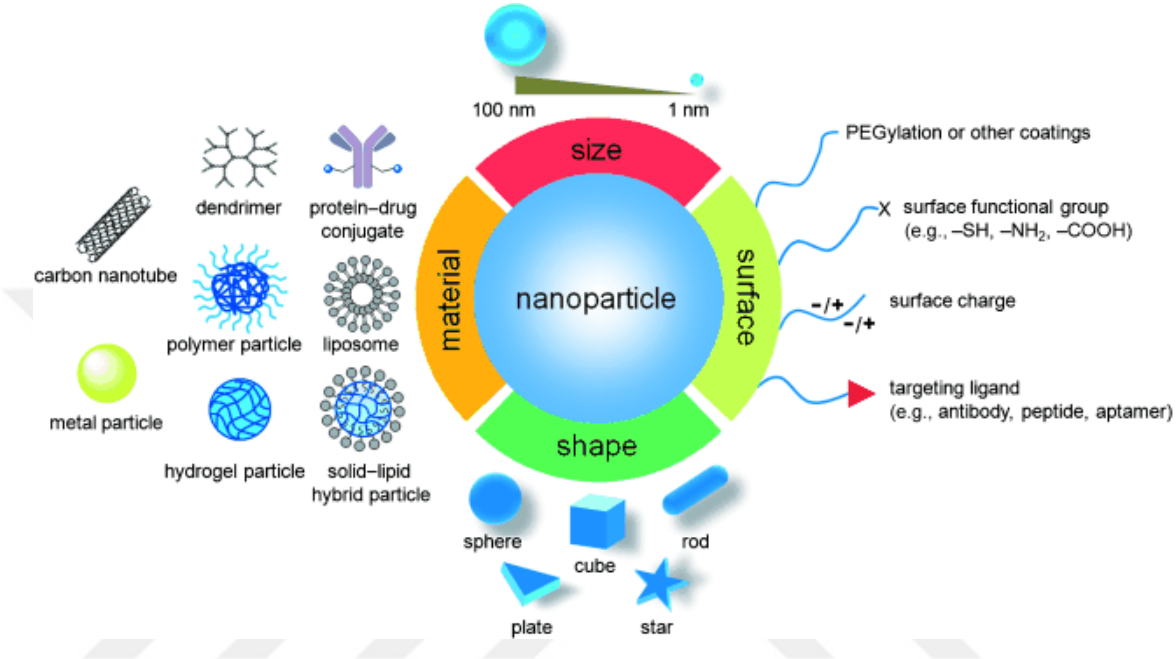

Figure 1.5 Various types of nanoparticles utilized as drug delivery system in cancer therapy and their biophysicochemical characteristics. Retrieved from (Sun et al. 2014).

Magnetism-based targeted delivery was first described in 1978. Magnetic nanoparticle technology offers the potential to achieve selective and efficient delivery of therapeutic drugs and genes by using external magnetic fields, and also allows simultaneous imaging to monitor the delivery *in vivo* (Figure 1.6) (Li et al. 2012).

The most important characteristic of these nanoparticles as efficient delivery systems is that they behave magnetic only under the influence of external magnetic field and render inactive when the external magnetic field is removed. Such magnetic properties are usually acquired by very small nanoparticles within the size range of less than 20 nm, due to the presence of single domain state (Mody et al. 2014).

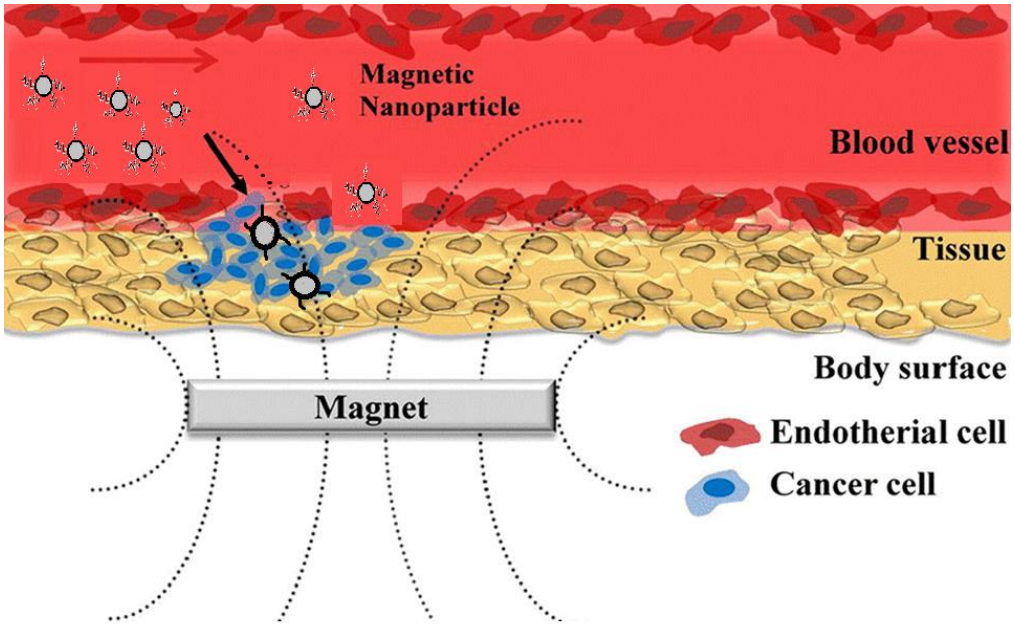

Figure 1.6 Schematic representation of magnetic nanoparticle-based drug delivery system. Retrieved from (Park et al. 2010).

1.4.1 Superparamagnetism

For the first time, Frenkel and Dorfman stated that a ferromagnetic particle with the size below 15 nm would consist of a single magnetic domain. In other words, this particle called superparamagnetic particle, would be considered as a particle which possess a uniform magnetization at any field (Tartaj et al. 2003). At present, it is preferred to use the superparamagnetic particles for biomedical applications. However, in order to utilize them in medical diagnosis and therapy, properties such as stability in water at neutral pH is absolutely important, which is dependent to the size, charge and surface characteristics of the particles. Superparamagnetic iron oxide nanoparticles (SPIONs) coated with an appropriate polymer could be loaded or encapsulated with a therapeutic agent and then directed to the target cells or tissue by using an external magnet. The main characteristic of these nanoparticles is considered as “superparamagnetism”. In other words, when an external magnetic field is applied, they are magnetized up to their saturation magnetization and once the applied magnetic field is removed, no residual magnetism of these particles is remained. This characteristic is size-dependent and the supermagnetic property is present in the nanoparticles with the size range of 10–20 nm.

As it is mentioned before, superparamagnetism is the most important property for nanoparticles which are designed to utilize as drug delivery systems, since they can precisely direct the therapeutic agents to their target site by applying a magnetic field. Furthermore, when the magnetic field is removed, they no longer exhibit any residual magnetic interaction at room temperature and then, they do not agglomerate (i.e., they are easily dispersed) and so, they do not lead to thrombosis or blockage of blood capillaries. Their high dispersion causes their evasion from uptake by phagocytes and also, their plasma half-life is increased (Bucak et al. 2012; Wahajuddin and Arora 2012). In other words, when the size of the particles are small enough, they do not precipitate because of the gravitation forces, and also, their charge and surface chemistry give rise to both, steric and coulombic repulsions. Moreover, the small size of the particles facilitates their passing through the capillary systems of the organs after injection and prevents vessel embolism. They should possess a suitable magnetization so that their movement in the blood can be controlled with a magnetic field and so that they can be immobilized close to the targeted pathological tissue (Tartaj et al. 2003).

1.4.2 Synthesis of Magnetic Nanoparticles

They have been reported various methods for synthesizing Fe_3O_4 nanoparticles, such as co-precipitation of hydroxides, hydrothermal synthesis, sol-gel transformation and ball milling, etc (Kandpal et al. 2015). Co-precipitation method is a suitable one for obtaining monodispersed and uniform Fe_3O_4 nanoparticles both in size and shape. In this method, ferrous and ferric ions are at the molar ratio of 1 to 2 in alkaline medium. Chemical co-precipitation can produced fine, stoichiometry particles of single and multi-component metal oxides (Hariani et al. 2013). Most of Fe_3O_4 nanoparticles obtained by the co-precipitation method are spherical shaped (Shen et al. 2014; Yigit et al. 2012). Magnetic particles should be coated with a biocompatible polymer to meet some of the essential properties required for *in vivo* applications, such as avoiding the formation of large aggregates, changes from the original structure and biodegradation when exposed to the biological system. The binding of various drugs and therapeutic agents is allowed via the polymer by covalent attachment, adsorption or entrapment on the particles.

1.5 Dendrimers for Surface Coating of Magnetic Nanoparticles

The synthesis of SPION cores is followed by their coating with an appropriate polymer which endows some essential characteristics to these nanoparticles that are important for their utilizing as drug delivery systems. An increase in the dispersibility and colloidal stability of the uncoated nanoparticles and a considerable decrease in their aggregation tendency, protecting their surface from oxidation, presenting a surface for conjugation of drug molecules and targeting agents, enhancing the blood circulation time by preventing clearance by the reticuloendothelial system, increasing the biocompatibility of the particles and minimizing nonspecific interactions, thus reducing toxicity, and improving their internalization efficiency by target cells are the advantages which is obtained after their coating with a suitable polymer (Wahajuddin and Arora 2012).

Dendrimers are very symmetric and monodispersed three-dimensional polymers (Cheng et al. 2008; Shcharbin et al. 2009; Tomalia 2005; Yoo et al. 1999). The term of "dendrimer" derived from two Greek words, dendron (tree) and meros (part). Their hyper-branched property causes them to have a globular shape containing a core attached to peripheral branches, with hydrodynamic dimensions varying from 1 to 30nm, and relative molar masses of 10^4–10^5 Da (Brothers et al. 1998; Campagna et al. 2015; Eichman et al. 2000; Labieniec and Watala 2009; Najlah and D'Emanuele 2006).

Tomalia and his group developed the first ''true dendrimers'' in 1980s by (Cevc and Vierl 2010; Medina and El-Sayed 2009; Tomalia et al. 1985; Tomalia and Frechet 2002). Over the past three decades, different methods were proposed to synthesize multiple dendrimer families and since then, their use in research and treatment of disease are increasing progressively.

The various types of dendrimers could be summarized as:

– Poly(amidoamine-organosilicon) dendrimers (PAMAMOS)

– Poly(amidoamine) dendrimers (PAMAM)

– Poly(propylene imine) dendrimers (PPI)

– Chiral dendrimers

– Liquid crystalline dendrimers

– Hybrid dendrimers

– Tecto dendrimers

– Multilingual dendrimers

– Micellar dendrimers (Taghavi Pourianazar et al. 2014).

1.5.1 Poly(amidoamine) Dendrimers

Poly(amidoamine) (PAMAM) dendrimers are the most common class of spherical, well-designed highly-branched dendrimers with interior cavities and abundant terminal groups on the surface (Figure 1.7). These dendrimers, also called "Starburst dendrimers", possess primary peripheral amine groups and tertiary amine branches inside the molecule (Braun et al. 2005; Buczkowski and Palecz 2014; Maiti et al. 2005). The primary amine groups have a crucial role in binding to oligonucleotides and DNA molecules and increasing the cellular uptake of these molecules. On the other hand, the buried tertiary amino groups perform as proton sponge in endosomes that result in DNA release into the cytoplasm (Inoue 2000). Accordingly, empty spaces, with hydrophobic characteristics, present in the inner part of the PAMAM dendrimers of generations higher than four (G_4) together with the abundant terminal groups, can be utilized in drug delivery applications by encapsulating various therapeutic agents.

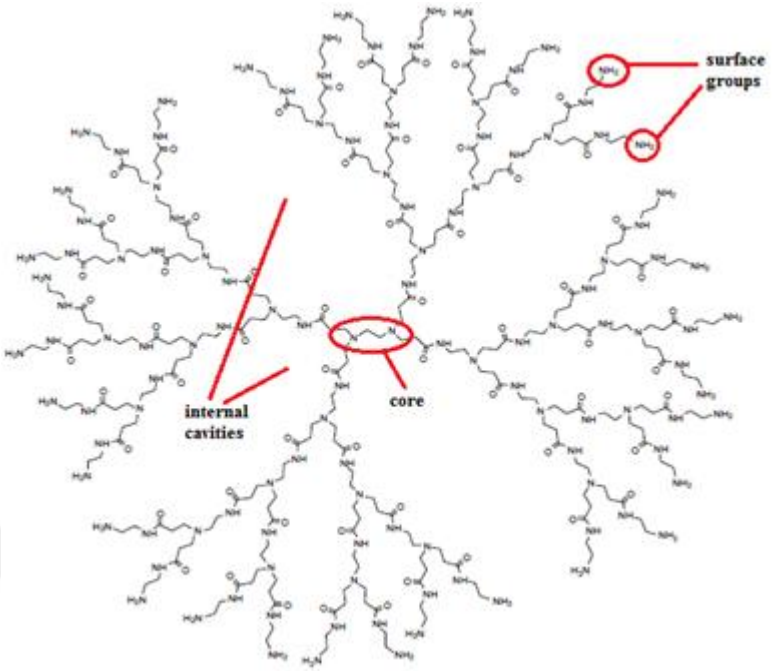

Figure 1.7 Dendrimer structure.

The main characteristics of PAMAM dendrimers could be mentioned as high solubility in water, particular architecture, abundant chemically versatile surface groups of PAMAM dendrimers which make them ideal carriers for the delivery of therapeutic agents including anticancer drugs (Sayed-Sweet et al. 1997; Taghavi Pourianazar et al. 2014).

PAMAM dendrimers comprise various specifications including high numbers of branches attached to the central core, their nanometer size, manageable molecular weight, and being non-immunogenic (Chen et al. 2000; Janaszewska et al. 2012; Mukherjee and Byrne 2013; Waite and Roth 2009). These advantageous specifications together with their spherical shape, biocompatibility, and safety are the main characteristics which make PAMAM dendrimers appropriate options as drug and gene carriers (Trivedi 2012).

Furthermore, their proper biodegradability, essential non-specific blood–protein binding characteristics, and limited drug release support PAMAM dendrimers to be efficient gene and drug delivery vehicles (Esfand and Tomalia 2001; Taghavi Pourianazar et al. 2014) .

1.5.2 Strategies for Synthesizing PAMAM Dendrimers

In order to synthesize PAMAM dendrimers, various methods have been proposed over the past decades (Maiti et al. 2004). Presently, for PAMAM dendrimers synthesis, four different methods are present (Tomalia 1994; Taghavi Pourianazar et al. 2014), including divergent synthesis, convergent synthesis, combined convergent-divergent synthesis, and click synthesis.

1.5.2.1 Divergent Synthesis

Tomalia proposed divergent method for synthesizing the first type of PAMAM dendrimers. In this method, a multifunctional core is used as initiator for the growth of the PAMAM dendrimer and the reaction occurs between the core and monomer molecules containing one reactive and two dormant groups. After this reaction, the first generation of PAMAM dendrimer is prepared. Thereafter, the surface of the molecule activates for reactions with more monomers. Different layers of the dendrimer are synthesized after these reactions are repeated (Bosman et al. 1999; Medina and El-Sayed 2009; Tomalia 2005). The initiator core for PAMAM dendrimers is an ammonia or ethylenediamine (EDA) molecule (Figure 1.8) (Eichman et al. 2000; Inoue 2000).

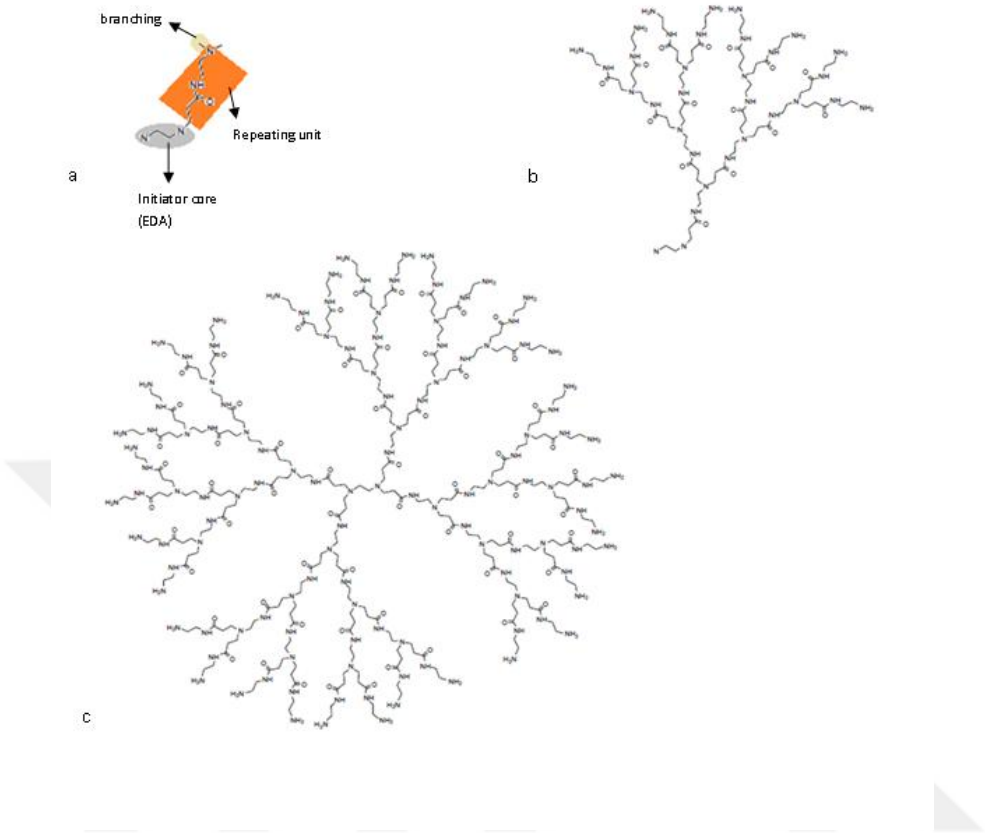

Figure 1.8 Structure of dendritic macromolecules: A) structural elements, B) dendron, and C) dendrimer.

1.5.2.2 Convergent Synthesis

The convergent method was proposed by Hawker and Frechet in 1990. In this top-down method, synthesizing of a dendrimer is started from the surface towards the core, mostly by “one to one” coupling of monomers, thereby by progressing the synthesis, the size of dendritic segments, dendrons, is enhanced. The convergent synthesis ends at the core region by joining two or more dendrons together, forming the dendrimer (Figure 1.9) (Hawker and Frechet 1990; Taghavi Pourianazar et al. 2014).

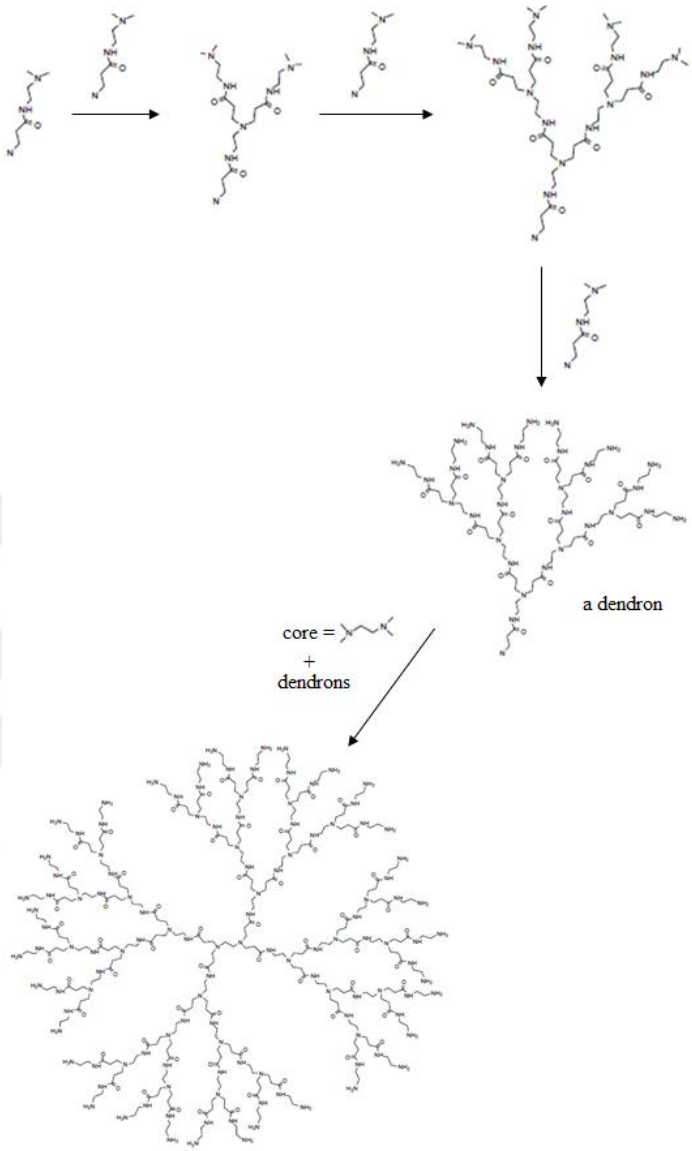

Figure 1.9 Convergent method for synthesis of dendrimers.

1.5.2.3 Combined Convergent-Divergent Synthesis

Kawaguchi and his coworkers proposed the hybrid convergent-divergent synthesis method called “double exponential growth” in which, for accelerating dendrimer preparation, orthogonally protected branched monomers are utilized with protecting groups that are stable during cleavage of the opposing functionality (Figure 1.10).

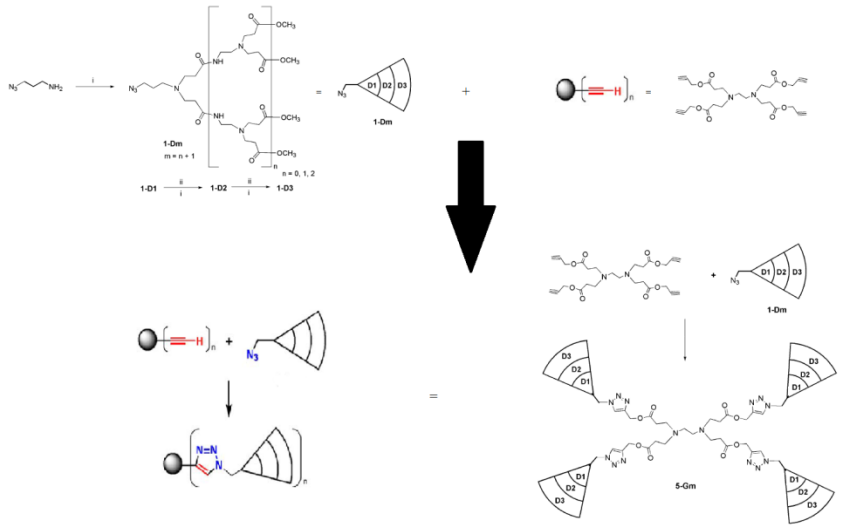

Figure 1.10 Convergent-divergent method for dendrimer synthesis.

1.5.2.4 Click Synthesis

Another facile and practical method for PAMAM dendrimer preparing is called click synthesis proposed in 2004. There are different reactions for click method, from which the copper-catalyzed azide-alkyne cycloaddition (CuAAC) is selected as the most useful one (Figure 1.11) (Astruc et al. 2012). The click chemistry refers to Cu-catalyzed cycloaddition reaction of an alkyne and an azide to form a 1,2,3-triazole ring. The main advantages of this method are the coupling specificity, mild and simple reaction conditions, oxygen and water tolerance, easy isolation of product and quantitative synthetic yields of click reactions. This reaction is considered as a breakthrough in the synthesis of dendrimers and dendritic and polymer materials. The click dendrimers present a bridge between dendritic architectures and nanomaterials (Han et al. 2012).

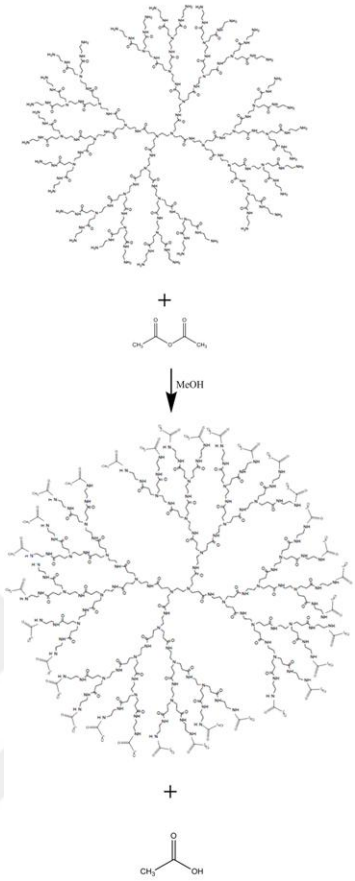

Figure 1.11 Copper-catalyzed azide-alkyne cycloaddition (CuAAC). Retrieved from (Astruc et al. 2012)

Nanoparticles are attractive delivery vehicles for CpG-ODN because, in general, nanoparticles are rapidly taken up into the endolysosomes of phagocytic immune cells. This is exactly where CpG molecules should to be delivered.

1.6 Toll-Like Receptors

Toll-like receptors (TLRs), the best characterized pattern recognition receptors (PRRs), are a family of proteins essential to the innate immune system that have been evolutionarily conserved from plants to mammals. They derive their name from the *Drosophila* Toll protein, with which they share a sequence and functional similarity (Vollmer and Krieg 2009).

In 1985, TLRs were discovered in fruit fly (*Drosophila melanogaster*) embryo as the product of the gene that controls the establishment of the dorso-ventral pattern. These were named as “Toll” meaning “weird” or “great” in German. Later, the role of “Toll” was associated with the synthesis of anti-microbial peptides, and was found to play an essential role in fly's immunity against fungal infection (Rauta et al. 2014; Zhang et al. 2014).

In human, TLRs are considered as essential receptors which recognize the pathogens and defend against their invasion. These transmembrane receptors possess the potential that could detect conserved molecular signatures of a wide range of microbial pathogens and then commence innate immune responses via specific signaling pathways (Lester and Li 2014).

Thirteen mammalian TLR members (TLR1-13) have been recognized with the expression on the cell surface (TLR 1, 2, 4, 5, and 6) or within the endosomal compartment (TLR 3, 7, 8, and 9). The cell surface-expressed TLRs mainly recognize structural components of pathogens, while the endosomal TLRs are assigned to recognizing nucleic acids (Tuomela et al. 2012).

1.6.1 Toll-Like Receptor 9

Toll-like receptor 9 (TLR9) belongs to the innate immune system and recognizes microbial and vertebrate DNA. TLR9 is a protein that in humans is encoded by the *TLR9* gene and has also been designated as CD289 (cluster of differentiation 289) (Ilvesaro et al. 2008b).

The TLR9 molecules are type I integral membrane glycoproteins that comprise a pathogen binding ectodomain (ECD) and a cytoplasmic signaling domain, attached with a single transmembrane helix (Figure 1.12). Pathogen-binding ectodomains of mammalian TLRs comprise 19–25 extracellular leucine-rich repeats (LRRs) and a cytoplasmic toll/interleukin (IL)-1R (TIR) domain. 24–29 amino acids of LRRs have the responsibility of ligand recognition and binding, and the TIR domain is responsible for downstream signaling (McKelvey et al. 2011; Zhou et al. 2013).

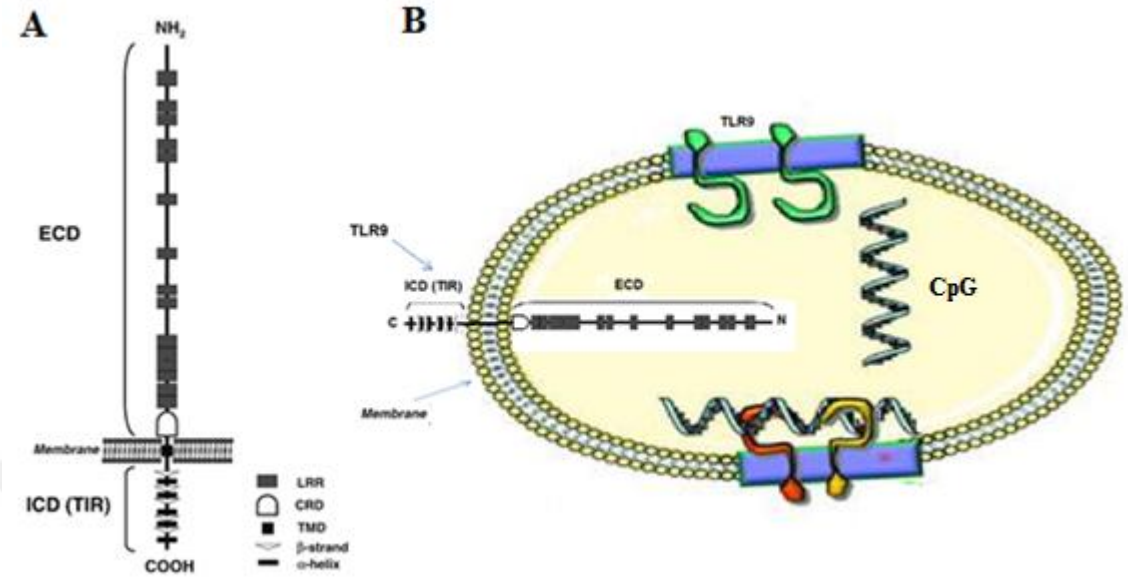

Figure 1.12 Schematic representation of A) the molecular structure of TLR9 and B) its position in lysosomes after CpG-ODN entry. Retrieved from (Takeshita et al. 2004).

1.6.2 The Expression of TLR9

Expression profiling affirmed TLR9 mRNA or protein in B cells, plasmacytoid dendritic cells (DCs), and cells of the monocyte/macrophage lineage (Eaton-Bassiri et al. 2004; Zarember and Godowski 2002). However, several studies have shown that TLR9 is not only expressed on immune cells, but is also expressed on tumor cells, including lung carcinoma, cervical cancer cells, prostate carcinoma, renal cell carcinoma, breast cancer cells, and ovarian cancer cells (Chen et al. 2008; Tanaka et al. 2010; Vollmer and Krieg 2009). Expression of TLRs on tumor cells implicates that TLRs play a role in tumor biology. Rising numbers of evidences indicated that TLRs operate as a double-edged sword in tumor cells because uncontrolled TLR signaling presents a microenvironment essential for the proliferation and evasion of cancer cells from the immune response (Basith et al. 2012).

1.6.3 CpG-ODN as TLR9 Agonist

TLR9 is normally activated by unmethylated CpG-oligodeoxynucleotides (CpG-ODN). These “CpG motifs” are commonly present in bacterial and viral DNA, but are suppressed and methylated in vertebrate DNA. For therapeutic utilizations, TLR9 is commonly activated by synthetic oligodeoxynucleotides (ODN) comprising one or more CpG motifs. To decrease nuclease degradation, therapeutic CpG-ODNs usually possess at least partially phosphorothioate-modified backbones. In 1999, the first human clinical trial of a CpG-ODN started, and indicated encouraging evidence of activity as a vaccine adjuvant (Vollmer and Krieg 2009).

1.6.3.1 Classes of Synthetic CpG-Oligodeoxynucleotides

There are various four groups of synthetic CpG-ODN described to date, each one has specific structural and biological characteristics (Table 1.1) (Bode et al. 2011).

K-type ODNs (also called B type) encoding multiple CpG motifs on a phosphorothioate backbone are more resistance to the digestion with the nucleases compared to the ODNs which have native phosphodiester nucleotides. Therefore, K-type ODNs have longer *in vivo* half-life (30–60 min while it is reduced to 5–10 min in the case of phosphodiester). K-type ODNs induce the proliferation and differentiation of plasmacytoid dendritic cells (pDCs) and trigger the release of TNF-α, and also could lead to the proliferation of B cells and induce them to secrete IgM.

D-type ODNs (also called A type) possess a mixed phosphodiester/phosphorothioate backbone, comprise a single CpG motif flanked by palindromic sequences with poly G tails at the $3'$ and $5'$ ends (the development of concatamers are facilitated by the structural motif). D-type ODNs induce pDCs to mature and secrete IFN-α, but have no influence on B cells. The specific activities of K- versus D-type ODNs have been traced to differences in the retention times of CpG/ TLR9 complexes in the endosomes of pDCs. Whereas K-type ODNs are rapidly transported through early endosomes into late endosomes, D-type ODNs are retained for longer periods in the early endosome. D-type

ODNs interact with MyD88/IRF-7 complexes, initiating a signaling cascade that leads to IFN- α production.

C-type ODNs are constructed of phosphorothioate backbone similar to K-type ODNs. However, they comprise palindromic CpG motifs resembling D-type ODNs. C-type ODNs trigger the secretions of IL-6 by B cells and IFN-α by pDCs. C-type ODNs are present in both early and late endosomes, and therefore, indicate characteristics in common with both K- and D-type ODNs.

P-type ODNs, as recently described type of immunomodulatory ODNs, comprise two palindromic sequences, so they have the potential to form higher ordered structures. P-type ODNs trigger of B cells and pDCs activation, and stimulate greater IFN-α production in comparison with C-type ODNs (Bode et al. 2011; Vollmer and Krieg 2009).

Table 1.1 Comparison of D, K, C and P-type oligodeoxynucleotide. Retrieved from (Bode et al. 2011).

ODN type	Representative sequence	Structural characteristics	Immune effects
D- also called A-class	GGTGCATCGATGCAGGGGGG	Mixed phosphodiester/phosphorothioate backbone Single CpG motif CpG flanking region forms a palindrome Poly G tail at 3′ end	Triggers strong secretion of IFN-α from pDC and maturation of APC
K- also called B-class	TCC**ATGGA**CG**TTCCT**GAGCGTT	Phosphorothioate backbone Multiple CpG motifs 5′ motif most stimulatory	Stimulates strong activation of B-cell and maturation of pDC. Induces production of TNF-α and IL-6
C Phosphorothioate backbone	T**CGTCGTT**CG**AACGACG**TTGAT	Multiple CpG motifs TCG dimer at 5′ end CpG motif imbedded in a central palindrome Stimulates proliferation and differentiation of B-cell and pDC	Induces production of IL-6 and IFN-α
P	**TCGT**CG**ACGATCGGCG**CG**CGCCG**	Phosphorothioate backbone Two palindromes Multiple CpG motifs	Stimulation of pDC and B cells. Strong secretion of IFN-α

1.6.4 CpG-ODN/TLR9 Signaling

TLR9 is localized in the endoplasmic reticulum (ER) and must traffic to endolysosomes before responding to ligands. Chaperone protein, UNC93B1, is necessary for TLR9 residence in ER and for its intracellular trafficking. When CpG-ODN is taken into the cell, TLR9 exit the ER through Golgi complex by conventional secretory pathways and reach the endolysosome where it interacts with the ligands. TLR9 is cleaved by lysosomal cysteine proteases within its ectodomain in the endolysosome (Figure 1.13) (Vollmer and Krieg 2009). After co-localization of CpG-ODN and TLR9 in these acidic compartments to stimulate cellular activation, the initial step in signal transduction involves the dimerization of two receptor chains (Basith et al. 2012; Lee et al. 2013).

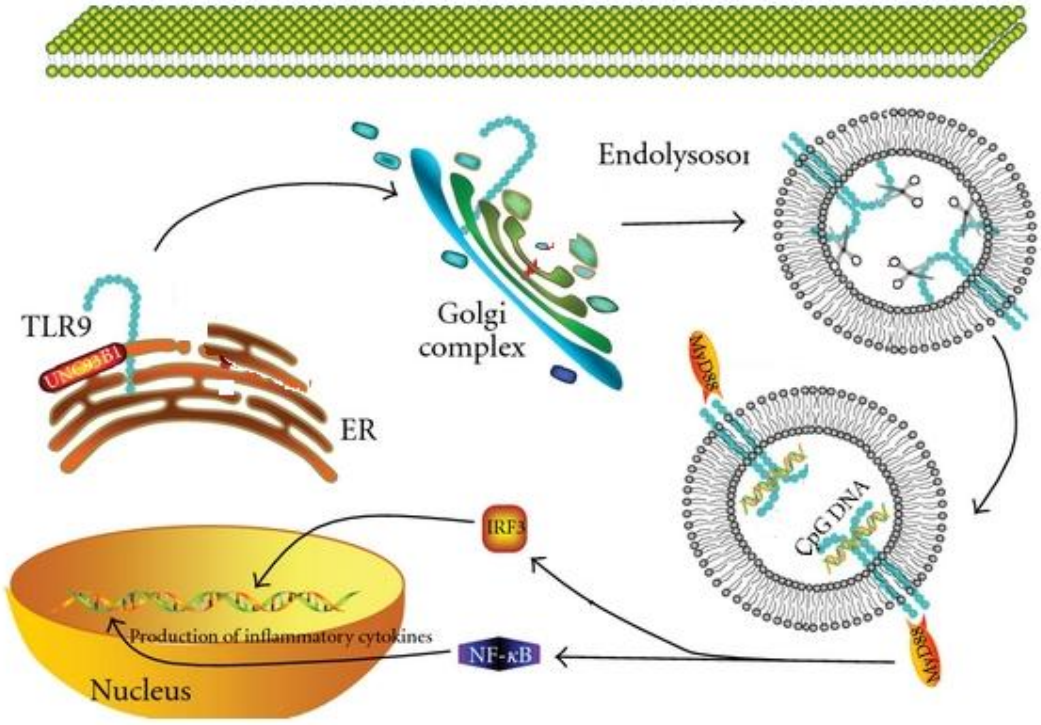

Figure 1.13 Intracellular TLR9 traffic.

Binding of CpG-ODN to TLR9 dimers causes allosteric conformational changes in the TLR9 cytoplasmic signaling domains, which leads to the recruitment of signaling adaptor molecules. TLR9 utilizes the MyD88-dependent signaling pathway (Takeda and Akira, 2004), which, in turn, recruits interleukin-1-receptor associated kinases (IRAKs)

and tumor necrosis factor (TNF) receptor-associated factor 6 (TRAF6). TRAF6, in turn, activates transforming growth factor (TGF)-activated kinase 1 (TAK1) that phosphorylates and activates the inhibitor of kappa light polypeptide gene enhancer in B-cells kinase (IKK) complex, culminating in the release and translocation of NF-κB to the nucleus, thereby inducing the synthesis of proinflammatory cytokines, such as TNF-α, IL-6 and IL-1, which are key mediators of inflammatory responses (Kawai and Akira, 2005; Akira et al., 2006; O'Neill, 2006). Additionally, TLR9 stimulation leads to the activation of other signaling pathways, such as JNKs, MAPKs, p38, ERKs and IRFs (IRF3, 5, and 7) (Basith et al., 2011; Lee and Kim, 2007; O'Neill et al., 2003). These signals are crucial for the orchestration of innate and adaptive immune responses, inflammation and tissue repair in the host (Figure 1.14) (Basith et al. 2012).

The p38, JNK and NF-kB pathways are three important pathways activated by CpG through TLR9 receptor. The p38 pathway causes premature senescence of tumor cells by inducing the expression of pro-apoptotic genes such as p53, p21, p16 and p14. The JNK related pathway like other central proteins play both proliferative and pro-apoptotic role; however, the pro-apoptotic side of this protein overweights its proliferative role (Dhanasekaran and Reddy 2008).

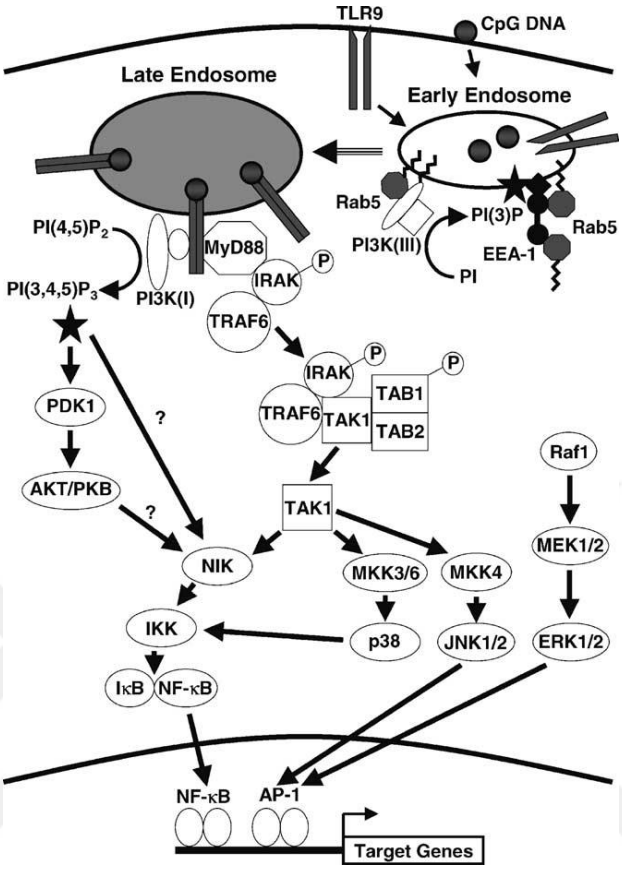

Figure 1.14 The signaling pathway for TLR9. Retrieved from (Takeshita et al. 2004).

1.6.5 Therapeutic Applications of CpG-ODN

TLR9 agonists, CpG-ODNs, have been developed in various therapeutic applications including protecting the host from infectious pathogens (Vollmer and Krieg 2009), adjuvants for use with vaccines, and in cancer therapy (Klinman 2004).

Synthetic CpG-oligodeoxynucleotides are agonists for a member of the TLR9. CpG-ODNs were shown to influence several signaling pathways in a variety of immune cells, leading to cytokine production in many mammalian species. The antigen presenting activity of dendritic cells (DCs), monocytes, and macrophages is increased by CpG administration, then the proliferation of B lymphocytes is induced and the immunoprotective function of natural killer (NK) cells is stimulated, and T cells are recruited where the CpG-ODN is administrated. The reaction of immune system after

administration of CpG-ODN is shown as activation of Th1-like immune responses which can be controlled for immune therapy of cancer, allergy, infectious diseases (Krieg 2002), autoimmune diseases, and sterile inflammation (Kanzler et al. 2007). As a consequence, CpGs could be utilized as potent vaccine adjuvant which was a principal delivery function of the synthesized nanoparticles (Bourquin et al. 2008) also by directly activating plasmoidal dendritic cells (pDCs) and then B-cells without activating the T-cells (Poeck et al. 2004).

1.6.5.1 Immunomodulation by CpG-ODN

Synthetic CpG-ODNs have been shown to exhibit immunostimulatory activity with the capacity to directly activate B cells, macrophages, and dendritic cells by cell surface binding of oligonucleotides to these cell subsets. However, T cells are not directly activated by CpG-ODNs, which correlates with the failure to bind to the T-cell surface (Oxenius et al. 1999).

CpG-ODNs have also been used in vaccination studies as adjuvants, and have induced a good Thl-type immune response. The efficiency of CpG ODNs in inducing a Thl biased response is thought to be due to synergy between TLR9 and the B-cell receptor, which results in antigen-specific B-cell stimulation, inhibition of B-cell apoptosis, enhanced IgG class switching and DC maturation and differentiation (Murad and Clay 2009).

Nearly all of the vaccine studies carried out to date have utilized B-Class CpG-ODN. However, C-Class ODN also has been used as vaccine adjuvant, and therefore, the same fundamentals could apply as well to these drug candidates. There are various mechanisms which contribute to the strong adjuvant function of these CpG-ODN for activating humoral immunity, which are the synergy between TLR9 and the B cell receptor (BCR) which stimulates antigen-specific B cells, hindrance of B cell apoptosis which leads to B cell survival, and increased IgG class switch DNA recombination, which may improve the maturation of the immune response. In contrast to B cells, TLR9 does not appear to be expressed in resting T cells. Therefore, the ability of CpG-ODN to increase the development of antigen-specific CD4 and CD8 T cell responses is probably an indirect result of the CpG-induced i) Th1-like cytokine and chemokine milieu and ii)

DC maturation and differentiation, which may explain the resulting strong CTL generation, even in the absence of CD4 T cell help. The close relation between the antigen and the CpG-ODN is critical for inducing optimal antigen-specific immunity. Antigen uptake enhancement and antigen requirements reduction could be considered as the result of conjugating a CpG-ODN directly to specific antigens. An improvement in the function of CpG-ODN as an adjuvant is considerably indicated when formulated or co-administered with other adjuvants or in formulations such as microparticles, nanoparticles, lipid emulsions, or similar formulations, which are especially required for triggering a strong response when the antigen is relatively weak (Vollmer and Krieg 2009).

1.6.5.2 Anti-tumor Therapy Using CpG-ODN

The induction of antitumor immunity through therapeutic vaccinations or the administration of immune stimulating agents is a promising approach in the treatment of cancer. Due to the importance of TLR signaling in tumorigenesis, TLR agonists have been identified as possible agents in tumor immunotherapy. Harnessing the powerful immunostimulatory properties of TLR agonists has great potential in the development of active immunotherapy against cancer. TLR-agonist linked tumor immunotherapy is still in a nascent state but growing rapidly in the area of common human malignancies. To date, the most promising and most frequently studied interaction in tumor immunotherapy trials seems to be that of TLR9 and its synthetic agonists. CpG-ODNs targeting TLR9 have shown substantial potential as vaccine adjuvants and mono- or combination therapies for the treatment of cancer (Basith et al. 2012).

In B cell lymphomas, CpG-ODN stimulates TLR9, which in turn, could trigger a Th1-like cytokine response, suggesting an essential role for this approach as one part of a combination treatment regimen. Although CpG-ODNs are strong mitogens for normal B cells, there was no apparent intensification of the lymphoma in these patients. There are various therapeutic mechanisms that have been suggested for the utilization of CpG-ODN in the treatment of such TLR9-expressing malignancies which include inducing enhanced immunogenicity of the tumor cells and the preferential stimulating of

apoptosis in cancer cells induced through TLR9. Since the immune system could be suppressed by tumors, therefore, there is an increasing interest in the utilization of combination therapies which incorporate the ways disrupting or weakening the tumor and making it more sensitive to immune-mediated attack. In mouse models, it is found a synergy between CpG-ODN with the other types of anti-tumor therapies, such as monoclonal anti-tumor antibodies, surgery, radiotherapy, and chemotherapy. Combining chemotherapy with TLR9 stimulation is unreasonable, because chemotherapy suppresses the immune system (Vollmer and Krieg 2009).

1.6.5.3 Cytokine Production

The excellent immunostimulatory properties of CpG-ODN are composed of stimulation of maturation and production of proinflammatory interleukins such as IL-6, IL-12, and tumor necrosis factor (TNF), chemokines, and IFNs (IFN-α and IFN-β) by macrophages, DCs, and B lymphocytes (Switaj et al. 2004).

Possible immunostimulating effects by CpG-ODN are achieved via a TLR9-mediated pathway and comprise the induction of cytokine production by immune cells, direct B-cell activation, activation of dendritic cells to promote a Th-1-reaction, T-helper cell-independent induction of cytotoxic T-cell activity, anti-neoplastic effects *in vivo* when applied locally into/near the tumor, and adjuvant potency in monoclonal antibody-therapy in several malignancies (Olbert et al. 2009).

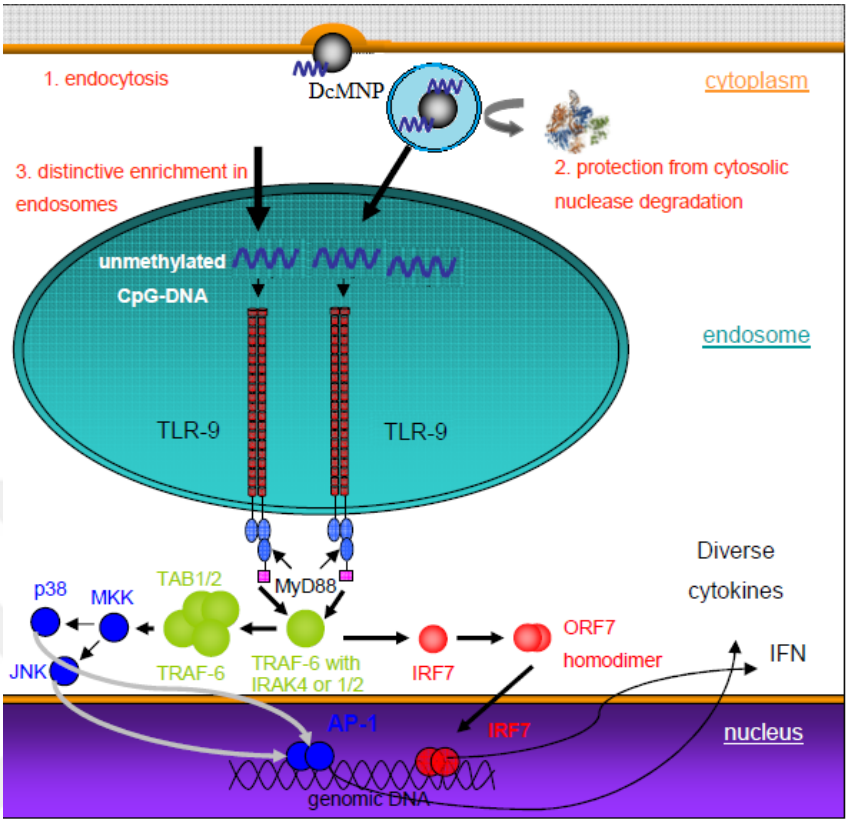

Figure 1.15 Survey on intracellular TLR-9-mediated signaling MyD88-dependent pathways and the role of nanoparticles as a potent TLR-agonist delivery device for cytokine release.

1.6.5.3.1 Interleukin 6 (IL-6)

IL-6 is a cytokine with various functions such as regulating the immune and inflammatory responses; It is indicated a relation between high expression of IL-6 and various epithelial tumors. IL-6, a glycoprotein composed of 184 amino acids and of 26 kDa in molecular weight binds to a heterodimeric receptor containing the ligand-binding IL-6α chain and the common cytokine receptor signal–transducing subunit gp130 (Guo et al. 2012; Knupfer and Preiß 2006). IL-6 receptor engagement causes the activation of the JAK family of tyrosine kinases, which in turn, triggers different pathways such as MAPKs, PI3Ks, STATs, and other signaling proteins. As it has shown that IL-6 and its downstream targets is related to the regulation of cell proliferation, survival, and metabolism, it is not surprising that IL-6 signaling has also been involved in tumorigenesis. In the case of cancer, IL-6 acts as a double-dealer, since it has

dichotomous roles in both tumor-promoting and –suppressive functions. For instance, in breast cancer cells, both pro- and anti-apoptotic functions of IL-6 have been reported (Schafer and Brugge 2007). IL-6 has also been indicated to affect the proliferation of normal and tumor-derived cells. The proliferation of hematopoietic progenitors, keratinocytes, myeloma/plastocytoma, and Kaposi's sarcoma cells is also indicated to be induced by IL-6, whereas it prevents the proliferation of M1 myeloid leukemia cells, early-stage melanoma cells, and lung and breast tumor cells. Therefore, the activity of IL-6 is dependent on the target cell which could result in contrasting biological responses (Asgeirsson et al. 1998; Badache and Hynes 2001).

1.6.5.3.2 Interleukin 10 (IL-10)

IL-10 is an immunomodulatory cytokine that is frequently upregulated in various types of cancer including ovarian, breast, renal cell, lung, and skin squamous and basal cell carcinomas as well as metastatic melanoma (Sato et al. 2011). The biological role of IL-10 in cancer is quite complex; however, the presence of IL-10 in advanced metastases and the positive correlation between serum IL-10 levels and progression of disease indicates a critical role of IL-10 in the tumor microenvironment. In other words, besides its effects on angiogenesis and cell proliferation/apoptosis, IL-10 can affect different aspects of anticancer immunity (Mocellin et al. 2005). IL-10 has been shown to directly affect the function of antigen-presenting cells by inhibiting the expression of MHC and costimulatory molecules, which in turn induces immune suppression or tolerance. Additionally, IL-10 downregulates the expression of Th1 cytokines and induces T-regulatory responses (Oft 2014).

1.6.5.3.3 Tumor necrosis factor-α (TNF-α)

Tumor necrosis factor (TNF, also referred to as TNF-α) is a multifunctional cytokine that plays important roles in apoptosis, cell survival, inflammation, and immunity acting via two receptors. It is a type II transmembrane protein consisting 157 amino acids with an intracellular N terminus. It is synthesized as a membrane-bound protein (pro-TNF) and is secreted followed by a cleavage with a TNF-converting enzyme (TACE). In inflammation-related carcinogenesis, TNF is released by inflammatory cells and considered as a pro-inflammatory cytokine (Balkwill 2006). Its secretion could lead to

the activation of specific signaling pathways such as nuclear factor-κB (NF-κB) and c-Jun N-terminal kinase (JNK). The nature of TNF's involvement in cancer has been quite controversial, since TNF could be an endogenous tumor promoter, and triggers the growth, proliferation, invasion and metastasis, and tumor angiogenesis of tumor cells. On the other hand, TNF could be a cancer killer (Horssen et al. 2006; Wang and Lin 2008).

1.7 Aim of the Study

The main goals of this thesis are listed as

- To design a CpG-bound iron oxide nanoparticles which selectively target and activate the TLR9 signaling pathway. The immobilization of CpG-ODN on magnetic nanoparticles was performed via a multifunctional polymer, PAMAM
- To visualize the targeting ability and internalization of dendrimer-coated magnetic nanoparticles by breast cancer cells
- To screen the expression of TLR9 gene in breast cancer cell lines, MDA-MB231, SKBR3, MCF7, and doxorubicin-resistant MCF7 (MCF7/Dox) cells
- To evaluate the ability of CpG-loaded magnetic nanoparticles in inducing cell death of breast cancer cell lines by XTT cell proliferation assay and flow cytometry analysis
- To check the expression profiles of apoptosis-related genes (*Bax, Noxa, Bcl-2, Survivin, PUMA,* and *c-Flip*) before and after treatment with CpG-loaded dendrimer-coated magnetic nanoparticles
- To examine the release of IL-6, IL-10, and TNF-α cytokines from breast cancer cells after treatment with various concentrations of CpG-loaded magnetic nanoparticles

CHAPTER 2

MATERIALS AND METHODS

2.1 Synthesis of Magnetic Nanoparticles

Preparation of Fe_3O_4 magnetic nanoparticles (MNPs) was carried out via the co-precipitation method. This procedure starts with dissolving of ferrous chloride tetrahydrate ($FeCl2.4H_2O$) (Sigma Aldrich, USA) and Ferric chloride hexahydrate ($FeCl_3.6H_2O$) (Sigma Aldrich, USA) (molar ratio of Fe^{+2}:Fe^{+3}=1:2) in distilled water in five-necked glass balloon followed by passing nitrogen gas and vigorous stirring (2000 rpm) at 90˚C (Figure 2.1). The nitrogen gas assembles a non-oxidizing oxygen-free environment. After about one hour constant stirring at 90˚C, ammonium hydroxide (NH_4OH) solution was added to the prepared mixture dropwise by a peristaltic pump (Liu et al. 2006). The overall chemical reaction related to this method is given in Equation 2.1 (Gupta and Gupta 2005; Tartaj et al. 2003). The precipitated magnetite is black in color. This sediment was isolated by magnetic decantation, thoroughly washed with distilled water and ethanol several times, and then dried in the air. Finally, the collected dried black particles were dispersed in ethanol (5 g L^{-1}) (Gupta and Gupta 2005; Lan et al. 2007; Liu et al. 2006; Osaka et al. 2006).

$$Fe^{2+} + Fe^{3+} + 8OH^- \rightarrow Fe_3O_4 + 4H_2O$$ **Equation 2.1**

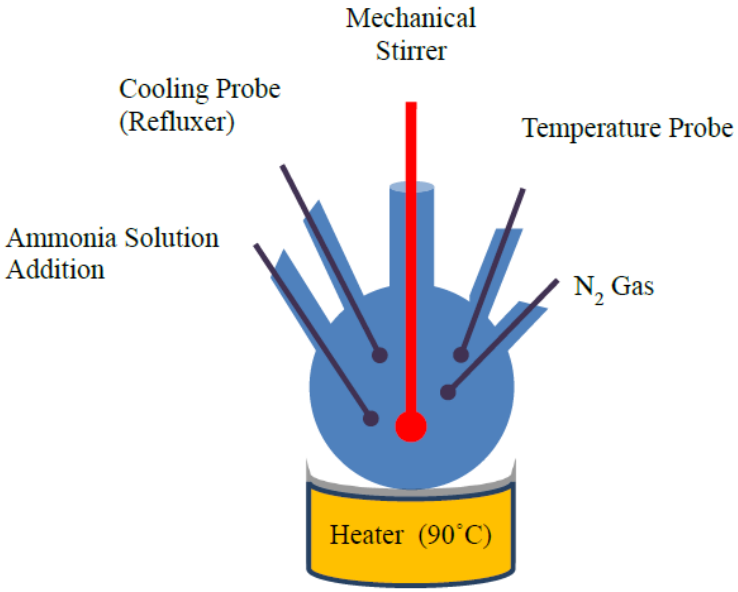

Figure 2.1 Arrangement for experimental setup for MNP synthesis. Retrieved from (Keskin and Gunduz 2012).

2.2 Surface Modification of Magnetic Core with Aminosilane

25 ml of MNP-ethanol solution (5 g L^{-1}) was mixed with 125 ml ethanol and sonicated with ultrasonicator for 30min. At the 20th min of sonication, 10 ml aminopropyltriethoxysilane (aminosilane or APTS) (NH_2 $(CH_2)_3$-Si-$(OCH_3)_3$) (Sigma Aldrich, USA) was added. After stirring mechanically for 15 h, the product was washed with methanol several times, and then dried into powder at room temperature. APTS-coated MNPs, terminated with amine groups, were called "Generation 0" (G_0) (Pan et al. 2007; Uzun et al. 2010).

2.3 Growth of PAMAM Dendrimer on the Surface of APTS-Modified MNPs

In order to obtain first generation dendrimer, 200 ml of 20% (v/v) methylacrylate methanol solution (Sigma Aldrich, USA) was added to the APTS-coated MNPs (G_0). The suspension was immersed in an ultrasonication water bath at room temperature for 7h. The particles were then rinsed with methanol five times by magnetic decantation. After rinsing, 40 ml of 50% (v/v) ethylenediamine methanol solution (Sigma Aldrich, USA) was

added and the suspension was immersed in an ultrasonication water bath at room temperature for 3 h. The particles were rinsed with methanol five times by magnetic separation. For synthesizing the desired number of generations of dendrimers, stepwise growth using methylacrylate and ethylenediamine was repeated. The synthesized dendrimer-coated MNPs (DcMNPs) were dried, weighed and dispersed in 0.01 M phosphate buffered saline (PBS) (Appendix A) (5 g L^{-1}) (Majoros et al. 2006; Pan et al. 2007; Uzun et al. 2010).

2.4 Characterization of Synthesized Bare and PAMAM-Coated Magnetic Nanoparticles

In order to characterize the bare MNP, APTS-coated MNP, and DcMNPs, Fourier transform infrared spectroscopy (FTIR) (FTIR Nicolet 6700 FTIR Spectrometer), transmission electron microscopy (TEM) (FEI Tecnai G^2 Spirit BioTwin Transmission Electron Microscope), scanning electron microscopy (SEM) (QUANTA 400F Field Emission Scanning Electron Microscope), zeta-potential (MALVERN Nano ZS90), x-ray photoelectron spectroscopy (XPS) (PHI 5000 VersaProbe), and vibrating sample magnetometer (VSM) (EV/9, ADE Magnetics) analyses were carried out.

2.5 Preparation of CpG-ODN Stock Solution

The study was carried out with the commercially available unmethylated ssDNA, CpG-ODN 2006 (K-ODN; also known as CpG-B) (InvivoGen, USA). The sequence of CpG-ODN 2006 is 5'-TCGTCGTTTTGTCGTTTTGTCGTT-3'. The CpG-ODN was dissolved in sterile endotoxin-free water to obtain a 50μM stock solution, which was a clear and colorless solution after vortexing for complete solubilization. The stock solution was aliquoted and stored at -20˚C.

2.6 CpG Binding

CpG-ODN/DcMNPs complexes were prepared by mixing different amounts of DcMNP solution (G_3-G_8) and equal amounts of the CpG-ODN solution (w/w ratio for CpG-

ODN/DcMNPs was as 1:70) in 50 µl PBS, followed by gentle rotating at 37˚C for 30 min to ensure the complex formation.

In this investigation, generation 7 (G_7) were selected as the optimum generation for loading CpG-ODN. So, after this step only G_7DcMNP was used for carrying out the experiments.

In order to investigate the best w/w ratio for CpG-ODN/DcMNP complexes, at which the highest amount of CpG-ODN loaded on the G_7DcMNP, different amounts of G_7DcMNP solution (w/w ratios were as 1:1, 1:2.5, 1:5, 1:10, 1:20, 1:30, 1:40, 1:50, 1:60, 1:70 and 1:75) and equal amounts of the CpG-ODN solution was mixed in 50 µl PBS, and rotated at 37˚C for 30 min to ensure the complex formation.

2.7 Characterization of CpG-Bound DcMNPs

In order to ensure and validate the CpG binding to the DcMNPs and determine various characteristics of the conjugate, they were characterized with the following methods.

2.7.1 NanoDrop Spectrophotometer Analysis

The loading efficiency was characterized by NanoDrop spectrophotometer. The complex solution was left on the magnet at room temperature for 10min for magnetic decantation. Then, 5 µl of the supernatant was carefully transferred into a new microcentrifuge tube without disturbing the bottom portion, and was used for measuring the ssDNA concentration by the NanoDrop spectrophotometer UV/Vis (NanoDrop 2000) (Thermo Fischer Scientific, USA) at 340nm wavelength.

The result indicates the amount of unbound or free CpG-ODN in the supernatant. If CpG-ODNs are not attached to the DcMNP efficiently, higher absorbance will be measured by NanoDrop spectrophotometer.

2.7.2 Gel Electrophoresis

The ability of DcMNP to bind CpG-ODN was evaluated by electrophoretic shift assay (Shukoor et al. 2009a). To this end, complex solutions were prepared at w/w ratios were

as 1:1, 1:2.5, 1:5, 1:10, 1:20, 1:30, 1:40, 1:50, 1:60, 1:70 and 1:75. After rotating for 30 min at room temperature, CpG-ODN binding was examined by assaying for agarose gel retardation.

For preparing 3% agarose gel, 2.4 g agarose (Applichem, Germany) was dissolved in 80 ml 1X TAE buffer (Appendix A) and boiled in a microwave oven until complete melting of agarose. Then, the gel solution was cooled and 4 µl of EtBr solution (Appendix A) was added into the gel solution. The gel solution was poured into electrophoresis tray for solidification. After the gel solidified, 10 µL of the sample was mixed with 2 µL of 6X loading dye and loaded into a well of the agarose gel which was then exposed to an electric field (50 V for 1 h). Finally, the gel was visualized by Vilber Lourmat UV imager (VILBER Lourmat UV Transilluminator).

Binding of CpG-ODN to DcMNP was validated by a lack of migration of the ssDNA in the electrophoretic field. Bare DcMNP and free CpG-ODN were used as negative and positive controls, respectively.

2.7.3 X-Ray Photoelectron Spectroscopy

X-ray photoelectron spectroscopy (XPS) is a surface-sensitive quantitative spectroscopic technique that was used for measuring and comparing the elemental compositions of bare DcMNP and CpG-ODN/DcMNP complexes. Samples of unloaded-DcMNP and CpG-loaded DcMNP in the powder form were analyzed by XPS spectrophotometer (PHI 5000 VersaProbe).

2.7.4 Scanning Electron Microscopy

Scanning electron microscopes (SEM) scan the surface of sample line by line with a fine probe of electrons and give information about sample's surface topography. SEM images of PAMAM-coated nanoparticles were taken in order to visualize the surface properties and size dispersion of nanoparticles by SEM microscope (QUANTA 400F Field Emission Scanning Electron Microscope).

2.7.5 Transmission Electron Microscopy

To visualize shape of bare MNP and DcMNPs and to learn their size, they were visualized with transmission electron microscope (TEM) (FEI Tecnai G^2 Spirit BioTwin Transmission Electron Microscope).

2.7.6 Fourier Transform Infrared Spectroscopy

To figure out the chemical composition of the naked MNP, aminosilane-modified MNP, and PAMAM-coated MNP, each of the samples was pelleted with potassium bromide (KBr) and analyzed with FTIR instrument (Nicolet 6700 FTIR Spectrometer).

2.7.7 Zeta-Potential

Zeta potential measurement is considered as an essential criterion which determines the stability of a colloid system. Therefore, bare, APTS-modified MNP, PAMAM-coated, and CpG-bound DcMNP complexes were characterized in terms of surface charge and stability by zeta-potential measurement (Nano-ZS, MALVERN Nano ZS90) at 25˚C.

2.8 *In Vitro* Stability of CpG-ODN/DcMNP Conjugate

The stability of the CpG-ODN/DcMNP complex was determined by release assay. CpG-ODN/DcMNP complex (with the best loading efficiency) was prepared and treated with 50 µl of 0.01 M PBS, pH 7.2. At predetermined time intervals, up to 8 weeks, the supernatant was taken out from the tube and analyzed with NanoDrop Spectrophotometer.

2.9 Cell Culture and Culture Conditions

MDA-MB-231 cell line was a kind gift from Prof. Dr. Ferit Avcu, Gülhane Military Medical Academy, Ankara. SK-BR-3 cell line was from Rengül Çetin-Atalay, Bilkent University, Ankara. MCF7 cell line was purchased from ŞAP Institüte, Ankara. 1000 nM doxorubicin-resistant MCF7 cells (MCF7/1000nMDox) was previously developed by the members of our laboratory (Kars et al. 2006).

Breast cancer cell lines including, MDA-MB231, SKBR3, MCF7 (MCF7/S) and MCF7/Dox cells were maintained in 12mL of RPMI 1640 medium (Appendix F) supplemented with 10% (v/v) heat inactivated fetal bovine serum (FBS) and 1% (v/v) gentamycin in T75 filter cap tissue culture flasks (Greiner Bio-one, Germany). Cells were incubated at 37˚C in a humidified atmosphere with 5% (v/v) CO_2 in a Heraeus incubator (Hanau, Germany).

2.10 Subculturing of Cells

Since all of the cell lines used in this study are adherent cells which propagate as a monolayer attached to the 75 cm^2 attached types, filter cap culture flasks (Greiner Bio-One Germany), they cease proliferating once they become confluent (i.e., when they completely cover the surface of cell culture flask), and some will die if they are left in this confluent state for too long. Therefore, need to be routinely passaged, that is, once the cells are confluent, a fraction of the cells need to be transferred to a new cell culture flask.

All cell types are subcultured at various ratios when they reached to 80% confluency. Briefly, after aspirating spent culture media from the culture flask, the cells were washed twice with 5 ml of PBS (pH 7.2). Then, 1-2 ml of trypsin-EDTA solution (Biological Industries, Israel) was added and the culture flask was rocked to coat the monolayer, and the sealed flask was returned to the incubator for 5-10 min. After incubation, the cells were examined under a microscope. Fully trypsinized cells will appear rounded up and no longer attached to the surface of the culture flask. Once the cells have detached, an appropriate volume of the resuspended cells was transferred to a fresh cell culture flask and then, clumps of cells were dissolved by pipetting. Finally, the volume of growth medium containing serum was reached to 12 ml. The serum in the medium will inhibit the trypsin.

One μM doxorubicin was added to the MCF7/Dox cells for the maintenance of resistance.

2.11 Freezing the Cells

The cells were harvested by trypsinization, resuspended in medium containing serum, centrifuged at 1000 rpm for 5 min. Supernatant was discarded and pellet was homogenized in 5mL of PBS. Then, cell suspension was centrifuged again at 1000 rpm for 5 min. After discarding supernatant, cells were resuspended in 1 mL of freezing medium consisting of 10% (v/v) DMSO and 90% heat inactivated FBS (Appendix A, A.1). The final cell suspension (approximately $3–5\times10^6$ adherent cells) was transferred into cryovials (Greiner Bio-One, Germany) and immediately immersed into ice. Then the cells were kept at -20°C for 1-2 h and transferred to -80°C for overnight incubation. Finally, the cryovials were transferred to liquid nitrogen for long term storage.

2.12 Thawing the Frozen Cells

Cryovials were removed from -80ºC freezer or liquid nitrogen container and immediately transferred to 37ºC. The thawed cell suspension was pipetted into a sterile 15 ml falcon tubes containing 4 ml growth medium, centrifuged at 1000 rpm for 5 min. After aspirating the supernatant, the cells were resuspended in fresh growth medium followed by transferring them to an appropriate culture flask. Cells were maintained in defined growth conditions.

2.13 Cell Counting

Trypan Blue is one of several stains recommended for use in dye exclusion procedures for viable cell counting. The basis of this method is that the chromophore has a negative charge and thus cannot interact with the cell with the intact membrane. Accordingly, viable cells exclude the dye and the blue stained cells are the dead ones.

The cells were trypsinized, homogenized in medium containing serum followed by mixing appropriate volume of the cell suspension with 0.5% trypan blue solution (Biological Industries, Israel) with a ratio of 9:1. The hemacytometer was moistened with exhaled breath and the cover-slip was affixed to it. A small amount of trypan blue/cell mix (approximately 10µl) was pipetted at the edge of the cover-slip and it was

allowed to run under the cover slip. Finally, the hemacytometer (Thoma, ISOLAB) was visualized under phase contrast microscope (Olympus, USA) at 40x magnification.

During cell counting, live cells (unstained with trypan blue) are always counted and blue stained cells are ignored. Cell counting was performed in triplicates. Cell concentration was calculated according to the formula below (Equation 2.2):

$$\text{Cell number}/\text{mL} = \frac{\text{Number of cells counted on 16 squares}}{256} \times 4 \times 10^6 \times \frac{10}{9} \qquad \textbf{Equation 2.2}$$

2.14 Cellular Internalization

Internalization of nanoparticles and CpG-bound DcMNPs by MDA-MB231, SKBR3, MCF7/S, and MCF7/Dox cells were investigated by using fluorescent property of fluorescein isothiocyanate (FITC) (Sigma Aldrich, Germany) bound to DcMNPs and Prussian blue staining (Sigma-Aldrich), respectively.

2.14.1 Detection of Internalized Nanoparticles by Fluorescence Microscopy

First, DcMNPs were conjugated with fluorescein isothiocyanate (FITC) (Sigma Aldrich, Germany) in EDC/NHS solution. Briefly, 20 mg 1-ethyl-3-(3-dimethylaminopropyl) carbodiimide hydrochloride (EDC) (Sigma-Aldrich) and 4.6 mg N-hydroxysuccinimide (NHS) (Sigma-Aldrich) were dissolved in 2 ml of PBS followed by the addition of 100 µl of FITC in the suspension. After 2 h, 400 µl of DcMNPs (5 mg/ml) was added to the above solution and stirred overnight at 4°C. Then, the FITC-bound DcMNPs was washed three times with PBS by magnetic decantation.

2×10^5 cells/well were seeded to each well of 6-well plate. Old medium was removed after 24 h and cells were washed with PBS solution. Then, 2 mL fresh media containing 100 µg of FITC-bound DcMNPs were added to each well. Cells were incubated at 37°C and 5% CO_2 for 5 h. Then, in order to fix the cells, they were covered with ice-cold methanol. Once covered, the cells were incubated in -20°C for 10 min. After incubation, cells were washed 5 times with PBS to get rid of the magnetic nanoparticles that have not been internalized by cells. For nuclear staining, 300 µl of 300 nM DAPI stain solution (4', 6-diamidino-2-phenylindole) (Sigma Aldrich, Germany) (Appendix A) was

added to each well, incubated for 5 min, protected from light. Then, the stain solution was removed and cells were washed 2 times with PBS. Finally, the cells are observed under fluorescence microscope (Leica DMI 4000 microscope equipped with ANDOR DSD2 spinning disk confocal) and photographed.

2.14.2 Detection of Internalized Nanoparticles by Prussian Blue Staining

The CpG-loaded nanoparticles internalized by MDA-MB231, SKBR3, sensitive MCF7, and MCF7/Dox cells were detected by Prussian blue staining method. This method provides two solutions, iron stain solution and pararosaniline solution. To prepare iron stain solution, potassium ferrocyanide solution (Sigma-Aldrich) and hydrochloride acid (1:1 v/v) were mixed in a falcon tube. Pararosaniline solution was supplied by diluting the pararosaniline solution with dH_2O to be 2% (v/v). A blue color will appear with reacting of ferrocyanide acid present in iron stain solution with iron (MNPs), while pararosaniline solution stains cells, producing red color in nucleus and pink color in cytoplasm.

Briefly, MDA-MB231, SKBR3, sensitive MCF7, and MCF7/Dox cells were seeded in 6-well plate at 2×10^5 cells/well for at least 24 h until they reached 80% confluency. After 24 h, the old medium was removed and the cells were washed with PBS solution followed by incubation with CpG-loaded DcMNP (100 μg MNP/mL) fresh medium at 37°C and 5% CO_2 for 5 h. Then, cells were washed 5 times with PBS to get rid of non-internalized DcMNPs. Iron stain solution was added (1 ml/well) in the wells and cells were incubated for 10 min. After washing the cells with distilled water, pararosaniline solution was added to the wells (1 ml/well) and incubated for 5 min. The cells were washed once with distilled water and air-dried. Finally, the cells were observed under light microscopy and photographed.

2.15 Targeting Properties of MNP Core

In order to evaluate the targeting characteristic of the magnetic core in nanoparticles, 5×10^5 cells were cultured in each well of a 6-well plate and allowed to adhere for 24h. Then, the cells were treated with 0.5 μg/ml CpG-ODN/DcMNP conjugates, with and

without the presence of the magnet. In other words, a magnet was placed under the plate so that the half of the cells in the well were exposed to the magnetic field, and the other half in the same well does not exposed to the magnet. After 48 h, the cells were fixed with 2 ml/well methanol incubating at -20°C for 10 min, washed with PBS and observed using light microscopy.

2.16 RNA Isolation

In order to prevent RNA degradation and inactivate RNases, all of the plastic and glass ware were treated with freshly prepared 0.1% (v/v) Diethyl pryrocarbonate (DEPC) in water, followed by draining and autoclaving prior to RNA isolation and cDNA synthesis.

For RNA isolation from culture flask, cells were washed with ice-cold PBS, treated with 1 mL of TRIzol® reagent for 5 min, and scraped with cell scraper. Then, cell lysate were passed several times through a pipette until viscous lysate disappeared. The lysate was transferred into a 2-mL micro-centrifuge tube (Greiner Bio-One, Germany), homogenized by pipetting several times, and incubated for 5 min at room temperature.

Then, 200 µL of chloroform (Sigma Aldrich, Germany) was added and mixed by inversions for 15 s. After incubation on ice for 15 min, the cell lysates were centrifuged at 12000 g, 4˚C for 15 min. Three layers were formed; colorless upper aqueous layer containing RNA, white interphase containing precipitated DNA and pinkish lower layer containing organic molecules. RNA remains exclusively in the aqueous phase, so the upper colorless phase was transferred carefully into a fresh 1.5 mL micro-centrifuge tube. In order to precipitate the RNA from the aqueous layer, 0.5 mL of ice-cold 2-propanol (Sigma-Aldrich, Germany) was added followed by incubation at room temperature for 10 min and centrifugation at 12000 g, 4˚C for 10 min. The supernatant was removed completely and RNA pellet was washed with 1 mL of 75% ethanol. After centrifugation at 12000 g for 10 min, supernatant was discarded and RNA pellet was air-dried. The RNA pellet was redissolved in appropriate volume of nuclease free dH_2O (HyClone, USA). In order to completely dissolve the pellet and open up any secondary

structures of RNA, the solution was incubated at 55˚C for 10 min. RNA was stored at -80˚C in several aliquots.

2.17 Quality Control of the Isolated RNA

2.17.1 Checking RNA Quantity and Purity

In order to determine the concentration and purity of isolated RNA samples, in addition to the measurements at OD260, optical densities were taken at 280 nm and 230 nm by NanoDrop spectrophotometer UV/Vis (NanoDrop 2000). RNA has a maximum absorption at 260 nm. An A260 of 1.0 is equivalent to 40 ng/µL of RNA. The A260/A280 ratio is an indication of the level of protein contamination in the sample. Pure RNA has an A260/A280 ratio of 2.1, however values between 1.8 and 2.0 are considered acceptable. A high peak at A230 indicates contamination with organic solvent contamination such as phenol.

2.17.2 Checking RNA Integrity

In order to assess the integrity of isolated RNA, an aliquot of the RNA sample was mixed with 2X RNA loading dye (Fermantas, Lithuania) and run on a 1% agarose gel stained with ethidium bromide (EtBr) (Sigma Aldrich, Germany). Finally, the gel was visualized by Vilber Lourmat UV imager (VILBER Lourmat UV Transilluminator).

Intact total RNA run on a denaturing gel will have sharp, clear 28S and 18S rRNA bands (eukaryotic samples). The upper ribosomal band (28S rRNA) band should be approximately twice as intense as the lower band (18S rRNA band) to indicate that the RNA is completely intact. A smeared appearance lacking sharp rRNA bands refers to partially degraded RNA.

2.18 DNase I Treatment

To degrade any DNA contamination in the isolated RNA and prevent their amplification in subsequent polymerase chain reactions, isolated RNA samples were treated with

DNase I prior to cDNA synthesis. To this end, 1 µg total RNA, 1 µL 10x DNAse I buffer (200 mM Tris-HCl (pH 8.4), 500 mM KCl, 20 mM MgCl2), 1 µL DNAse I (1 unit/µL) (Thermo Scientific, USA), and RNAase-free water were combine to 10 µL and incubated at 37ºC for 30 min. In order to inactivate DNAse I enzyme, 1 µL of EDTA, an exonuclease inhibitor, was added and incubated for 10min at 65ºC.

2.19 cDNA Synthesis

To convert RNA into cDNA, a polymerase called Reverse Transcriptase, primers (random hexamers), nucleotides for DNA synthesis (dNTPs); $MgCl_2$ and buffers required by the enzyme are used.

The DNase-treated RNA samples (11 µl) used as template for cDNA synthesis were mixed with 1µl Random hexamer primers (10 µM) and 0.5 µl nuclease-free water and incubated at 65ºC for 5 min. After first incubation, 7.5 µl of the prepared master mix was added and incubated at 25ºC for 10 min, 42ºC for 60 min, and 70ºC for 10 min, respectively.

The master mix includes; 4 µl 5x reverse transcriptase buffer, 1 µl RevertAid Reverse Transcriptase (200 U/µl), 0.5 µl Ribolock RNase Inhibitor (40 U/µl), 2 µl dNTPs (10 mM). After the reaction was completed, the synthesized cDNA were diluted nuclease-free water and stored at -20ºC.

2.20 Quantitative Real-Time Polymerase Chain Reaction (qRT-PCR)

TLR9 gene expression analysis was performed via TaqMan Gene Expression Assay (Roche, Germany). In this assay, a TaqMan probe was used which is a short oligonucleotide (DNA) containing a fluorescent reporter dye on the 5' end and a quencher dye on the 3' end. In the intact form of the probe, the proximity of the quencher dye greatly reduces the fluorescence emitted by the reporter dye. To generate a light signal, the probe must bind to a complementary strand of DNA at 60°C. Then, at this temperature, *Taq* DNA polymerase, the same enzyme required for the PCR, must cleave the 5' end of the TaqMan probe (5' nuclease activity), separating the fluorescent dye

from the quenching dye and increasing the reporter dye signal. Finally, the probe will be removed from the target strand, allowing primer extension to continue to the end of the template strand.

For detecting *TLR9* gene expression, *β-actin* was used as internal control. Reaction mixture and conditions for *β-actin* and *TLR9* genes are the same and listed in Table 2.1and Table 2.2.

Table 2.1 PCR mix for expression analysis of *TLR9* gene

Component	**Concentration**	**Volume**	**Final Concentration**
LightCycler 480 Probes Master	2x	10 µL	1x
Real Time Ready Assay	20x	1 µL	Primers 8 pmol each, 4pmol UPL probe
PCR grade water	---	4 µL	---
Total		15 µL	---

Table 2.2 Reaction conditions for *TLR9* gene expression

Program name	**Target** (°C)	**Hold (sec)**	**Cycles**
Pre-incubation	95	600	1
Amplification	95	10	45
	60	30	
	72	1	
Cooling	40	30	1

2.21 Analyzing qRT- PCR Data by the Comparative C_T Method

Relative quantification, also known as the $2^{-\Delta\Delta C_T}$ method, was used for analyzing data from qRT-PCR experiments (Livak and Schmittgen 2001). This method represents the changes in expression of the target gene across multiple samples and expresses it relative to some reference group such as an untreated control or an internal control gene. When comparing multiple samples using relative quantification, one sample was chosen as the calibrator (also known as control sample), and the expression of the target gene in all other samples was expressed as an increase or decrease relative to the calibrator.

First, the cycle threshold (C_T) of the target gene was normalized to that of the reference (ref) gene, for both the test sample and the calibrator sample:

$$\Delta C_{T(Test)} = C_{T(\ Target,test)} - C_{T(\ ref,test)}$$

$$\Delta C_{T(calibrator)} = C_{T(\ Target,\ calibrator)} - C_{T(\ ref,\ calibrator)}$$

Second, the ΔC_T of the test sample was normalized to the ΔC_T of the calibrator:

$$\Delta\Delta C_T = \Delta C_{T(Test)} - \Delta C_{T(calibrator)}$$

Finally, the expression ratio was calculated:

$2^{-\Delta\Delta CT}$= Normalized expression ratio

The threshold cycle (C_T) values for each gene were represented in Appendix B.

2.22 XTT Cell Proliferation Assay

The antitumor effects of free CpG-ODN, control-CpG/DcMNP, and CpG-ODN/DcMNP conjugates were measured on MDA-MB231, SKBR3, sensitive MCF7, and MCF7/Dox cells by XTT assay, which is a colorimetric test based on the reduction of tetrazolium salt, XTT, to colored formazan products by mitochondria of live cells. Intensity of color developed is proportional to relative viability.

A sample of 8×10^3 cells in 50 μL of fresh cell culture medium was seeded into each test well on a 96-well plate (Greiner). The plates were incubated for 24 h to allow the cells to

adhere, and the cells were then exposed to serial dilutions of free CpG-ODN, control-CpG/DcMNP, CpG-ODN/DcMNP complexes (each in a different plate), or medium alone (control). After incubation of plates at 37°C for 24, 48 and 72 h in an atmosphere of 5% CO_2, XTT reagent and activator (Biological Industries, Israel) were added to each well, and 4 h later, the intensity of formazan dye was measured at 500 nm with a 96-well plate reader (Spectromax 340, Molecular Devices, USA). Cell proliferation curves were constructed by conversion of dye intensity into viability percentages.

2.23 Apoptotic Gene Expression Analysis

Expression of some important apoptotic gene such as *Bax, Noxa, Bcl-2, Survivin, Puma,* and *C-Flip* were examined by qRT-PCR analysis. Cells were seeded on 6-well plate (2×10^5 cells/well) and incubated at 37°C for 24 h in an atmosphere of 5% CO_2. After 24 h, the old medium was removed; the cells were washed with PBS and treated with 0.5 µg/ml CpG-loaded DcMNPs for 48 h. Then, total RNA was extracted from treated cells followed with cDNA synthesis according to the procedure stated before (2.16-2.19) and used for quantitative real-time PCR. Untreated cells were used as control group.

QRT-PCR experiments were conducted in Rotor-Gene 6000 (Corbett Research, Australia). FastStart Universal SYBR Green Master (Rox) kit (Roche Diagnostics, Switzerland) was used to perform qRT-PCR according to the manufacturer's instructions. SYBR Green is a frequently used fluorescent dye which intercalates the double strands of DNA. The accumulation of PCR products in each cycle intensifies the signal generated by the intercalation of SYBR Green, enabling to monitor the change in the quantity of products.

The reaction mixture contained 10 µL 2x master mix, 2.8 µL template cDNA, 0.4 µL of sense and antisense primers and 6.4µL nuclease free water. The reaction was carried out in 0.2 mL PCR tubes (Greiner Bio-one, Germany). Each sample was prepared in triplicates. No template control containing nuclease free water instead of template cDNA was used to detect background signal.

Bax, Noxa, Bcl-2, Survivin, Puma, C-Flip, and *β-actin* primers were obtained from Alpha DNA, Canada. Primer sequences and amplicon sizes are shown in Table 2.3.

Table 2.3 Primers used in gene expression analyses

Primer	Sequence (5′-3′)	Amplicon Size (bp)
Bax Sense *Bax* Antisense	TCTGACGGCAACTTCAACTG TTGAGGAGTCTCACCCAACC	188
Noxa Sense *Noxa* Antisense	TGATATCCAAACTCTTCTGC ACCTTCACATTCCTCTCAA	142
Bcl-2 Sense *Bcl-2* Antisense	TGTGGCCTTCTTTGAGTTC CGGTTCAGGTACTCAGTCATC	166
Survivin Sense *Survivin* Antisense	AGCCAGATGACGACCCCATAGAGG AAAGGAAAGCGCAACCGGACGA	60
Puma Sense *Puma* Antisense	GACGACCTCAACGCACAGTA GTAAGGGCAGGAGTCCCAT	109
C-Flip Sense *C-Flip* Antisense	GAACATCCACAGAATAGACC GTATCTCTCTTCAGGTATGC	262
β-actin Sense *β-actin* Antisense	CCAACCGCGAGAAGATGA CCAGAGGCGTACAGGGATAG	97

qRT-PCR conditions for *Bax, Noxa, Bcl-2, Survivin, Puma, C-Flip,* and *β-actin* genes are represented in Table 2.4.

Table 2.4 qRT-PCR conditions of *Bax, Noxa, Bcl-2, Survivin, Puma, C-Flip,* and *β-actin* genes

	Bax	***Noxa***	***Bcl-2***	***Survivin***	***Puma***	***C-Flip***	***β-actin***
Activation	95°C, 10 min	95°C, 10 min	95°C, 10 min	95°C, 10 min	95°C, 10 min	95°C, 10 min	95°C, 10 min
Denaturation	95°C, 15 s	95°C, 15 s	95°C, 15 s	95°C, 15 s	95°C, 15 s	95°C, 15 s	95°C, 15 s
Annealing	60°C, 60 s	60°C, 60 s	60°C, 45 s	60°C, 60 s	60°C, 60 s	60°C, 60 s	60°C, 45 s
Extension	-	-	72°C, 45 s	-	-	-	72°C, 45 s
Melting (°C)	50 - 99	50 - 99	50 - 99	50 - 99	50 - 99	50 - 99	50 - 99
Cycle number	40	40	45	40	45	40	40

Fold changes of *Bax, Noxa, Bcl-2, Survivin, Puma,* and *C-Flip* genes were normalized to the internal control gene β-actin and calculated for each sample relative to no-treatment control. The threshold cycle (C_T) values for each gene were represented in Appendix B.

2.24 Evaluation of Apoptosis by Flow Cytometry

The cell death was measured using the Annexin V-fluorescein isothiocyanate apoptosis detection kit (Roche Diagnostics, Indianapolis, IN, USA) containing Annexin-V-FLUOS solution, Propidium iodide solution, and incubation buffer (HEPES Buffer).

Annexin V, a 35–36kDa protein, belonging to a family of calcium-dependent phospholipid-binding proteins, binds to phosphatidylserine (PS) with high affinity for to identify apoptotic cells. In healthy cells, PS is predominantly located along the cytosolic side of the plasma membrane. Upon initiation of apoptosis, PS loses its asymmetric

distribution in the phospholipid bilayer and translocates to the extracellular membrane, which is detectable with fluorescently labeled Annexin V.

In early stages of apoptosis, the plasma membrane remains intact and excludes viability dyes such as propidium iodide (PI), therefore cells which display only Annexin V staining (PI negative) are in early stages of apoptosis. During late-stage apoptosis and necrosis, loss of cell membrane integrity allows Annexin V binding to cytosolic PS, as well as cell uptake of PI. Annexin V staining, paired with PI is widely used to identify apoptotic stages by flow cytometry (Vermes et al. 1995).

MDA-MB231, SKBR3, MCF7/S, and MCF7/Dox cells were cultured in a 6-well plate and allowed to grow for 24h. Then, cells were treated with free CpG-ODN, free control-CpG-ODN (InvivoGen, USA) (5'- tgctgcttttgtgcttttgtgctt -3', 24 mer), unloaded DcMNP, control-CpG-ODN/DcMNP, and CpG-ODN/DcMNP complexes for 48 h (Table 2.5). As a positive control, cells were treated with etoposide (Sigma Aldrich, Germany) and the cells which have not exposed to any treatment (untreated cells) were considered as negative control.

Table 2.5 Various treatments for MDA-MB231, SKBR3, MCF7/S, and MCF7/Dox cell lines.

Cell line / **Treatment**		MDA-MB231	SKBR3	MCF7/S	MCF7/Dox
Etoposide (µM)		25	15	42	117
Free CpG (µg/ml)		0.5	0.5	0.5	0.5
Free Control-CpG (µg/ml)		0.5	0.5	0.5	0.5
Control-CpG-loaded DcMNP	CpG (µg/ml)	0.5	0.5	0.5	0.5
	DcMNP (µg/ml)	35	35	35	35
CpG-loaded DcMNP	CpG (µg/ml)	0.5	0.5	0.5	0.5
	DcMNP (µg/ml)	35	35	35	35

After 48 h incubation, the supernatant (floating apoptotic cells) was collected and the adherent cells trypsinized (combine respective floating and trypsinized cells). The

collected cells were washed twice with PBS and centrifuged (250 g, 5 min, RT). Each pellet was re-suspended in 400 µl PBS. Then, 100 µl of incubation buffer was added.

For control cells (negative and positive control),

Control 1: (Stained with both Annexin V and Propidium iodide) = (400 µl of cells + 100 µl of incubation buffer + 2 µl of Annexin-V-FLUOS solution + 2 µl of Annexin-V-FLUOS solution)

Control 2: (Annexin V only) - (400 µl of cells + 100 µl of incubation buffer + 2 µl of Annexin-V-FLUOS solution)

Control 3: (Propidium iodide only) = (400 µl of cells + 100 µl of incubation buffer + 2 µl of Propidium iodide solution)

For experimental cells: (400 µl of cells + 100 µl of incubation buffer + 2 µl of Annexin-V-FLUOS solution + 2 µl of Annexin-V-FLUOS solution).

Finally, the cells were analyzed using a flow cytometer (Accuri C6 Flow Cytometer, BD, NJ). Annexin V is excited at 488 nm and has a peak emission at 518 nm and PI can be excited at 488-540 nm and its emission wavelength is at 617 nm.

2.25 Determination of IL-6, IL-10, and TNF-α release by ELISA Assay

Human IL-6, IL-10, and TNF-α ELISA kit (Mabtech) include monoclonal antibody (1, 1, and 0.5 mg/mL for IL-6, IL-10, and TNF-α kits, respectively), biotinylated monoclonal antibody (1, 1, and 0.5 mg/mL for IL-6, IL-10, and TNF-α kits, respectively), streptavidin-alkaline phosphatase (250, 80, and 80 µL for IL-6, IL-10, and TNF-α kits, respectively) and recombinant human IL-6 standard (1 µg).

In order to coat with monoclonal human IL-6 antibody, 50 µL antibody solution was added to each well of 96-well Immulon 2B plates (Costar, USA). To equally distribute the solution, plates were tapped and incubated overnight at 4°C. Then, the plates were blocked with 200 µL of blocking buffer (Appendix A) followed by 2 h incubation at

room temperature. ELISA wash buffer (Appendix A) and then ddH_2O were used for washing the plates.

After drying the plates, 50 µL of supernatants from cultured cells and recombinant IL-6 standard was added to the wells. Recombinant IL-6 standards were serially diluted as 1:2 with 50 µL 1x PBS with 11 repeats. Plates were incubated for 2 h at room temperature or overnight at 4°C and washed again. Biotinylated-secondary antibody solution was diluted as 1:1000 in incubation buffer and 50 µL of it was added to the wells. After overnight incubation at 4°C and washed as before. Then, 50 µL of freshly prepared, 1:5000 diluted streptavidin-alkaline phosphatase solution (SA-AP) was added to the wells, then, incubated for 2 h at room temperature and washed as explained before.

A para-Nitrophenylphosphate (pNPP) tablet was dissolved in 4 ml ddH2O. 50 µL of this solution was added to the wells for the plates. Color development was determined at 405 nm at different time points with Multiskan FC Microplate Photometer (Thermo Scientific, USA). Measurements are carried out with the instrument until recombinant IL-6 standards reach a four parameter saturation forming an S-shaped curve. IL-6 concentration in supernatants was calculated using this standard curve.

2.26 Statistical Analysis

All data represent three independent experiments, each of which runs in triplicates. The data were expressed as mean ± standard error of the means (SEM). The results were analyzed using GraphPad Prism 6 with one-way ANOVA test or t-test (GraphPad Software Inc. USA). In order to compare different groups, Tukey's Multiple Comparison Analysis was utilized. The mean differences were significant at the 0.05 level.

CHAPTER 3

RESULTS AND DISCUSSION

3.1 Synthesis of DcMNPs

While a number of suitable methods have been developed for the synthesis of magnetic nanoparticles, due to some advantages such as particle size control and thus achieving a narrow particle size distribution, successful application is considered as co-precipitation method which is a facile and convenient way to synthesize iron oxides.

The size of the magnetic nanoparticles prepared with co-precipitation method in this study is below a critical value, which is typically around 10–20 nm. Moreover, the nanoparticles become a single magnetic domain and indicate superparamagnetic behavior, which makes them very attractive for a broad range of biomedical applications such as targeted drug delivery, magnetic resonance imaging (MRI), and magnetic hyperthermia.

Considering small size and thus superparamagnetism as crucial factors, we synthesized the magnetic nanoparticles by co-precipitation method.

The next step in this study was to modify the surfaces of the magnetic nanoparticles with PAMAM dendrimer to improve the biocompatibility of the nanoparticles and increasing their intracellular uptake. The polymer coating not only affords a protective organic biocompatible shell, but also provides an efficient and convenient means for loading immunostimulatory oligonucleotides, CpG-ODN. In order to prepare the magnetic nanoparticles for dendrimer coating, first the surface modification with APTS was carried out. APTS-coated MNPs, terminated with amine groups, were called “Generation 0” (G_0) (Figure 3.1).

Finally, coating with PAMAM dendrimer were carried out by divergent synthesis method (Figure 3.1). An advantage of the divergent method is the attainable high-molecular (nano) scaffold architecture as well as the facile repetitive steps. Dendrimers, which are prepared by repetition of a given set of reactions using divergent strategy, are highly branched and regular macromolecules with well-defined structures. In this method, polymer growth arises in an outward direction from the core by a series of stepwise polymerization reactions that attach layers (i.e. generations) to form the final tree-like structure (Eichman et al. 2000; Tomalia et al. 1985).

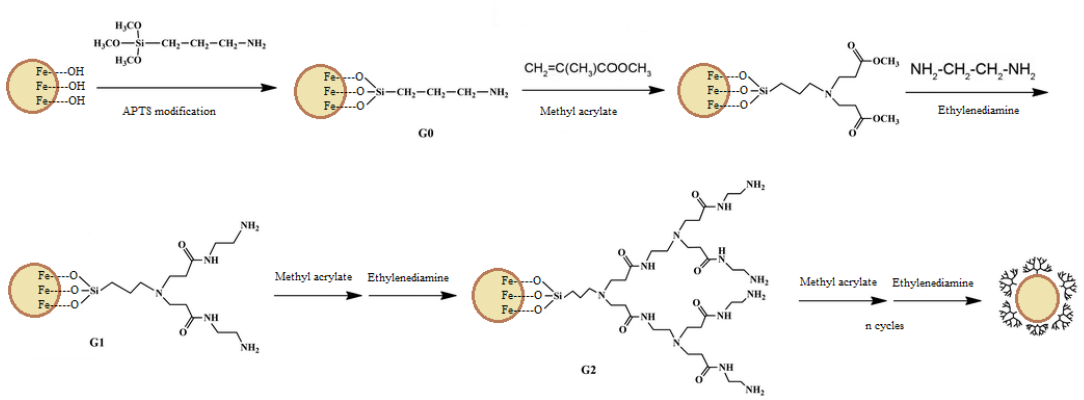

Figure 3.1 Stepwise modification of magnetic nanoparticle modified with APTS and PAMAM dendrimer.

3.2 Characterization of Bare and PAMAM-Coated Magnetic Nanoparticles

The biological behavior of magnetic nanoparticles strongly depends upon their size and shape as well as their charge and nature of the coating. Several physicochemical techniques are used to determine these parameters (Taghavi Pourianazar and Gunduz 2016).

3.2.1 Fourier Transform-Infrared Spectroscopy (FTIR)

FTIR spectroscopy was utilized to confirm that APTS and PAMAM-dendrimer was successfully coated the magnetic nanoparticles. The frequencies of the most important bands related to bare MNP, MNP-APTS, G_5DcMNP, and G_7DcMNPs which are

recorded from 4000 to 500 cm^{-1} using a FTIR spectrometer are depicted in Figure 3.2. The FTIR spectra of all the samples possess a band at 673 cm^{-1}, assigned to the magnetite (Fe_3O_4) core. The bands around 1,100 cm^{-1} are attributed to the Si–O bond which were observed after aminosilane modification. The vibration of NH_2 group is at around 3410 cm^{-1}. C–H bonds present in methylacrylate and methanol can be seen at 2840 and 3010 cm^{-1}, respectively. Vibration of –CO–NH– bonds were observed at 1450, 1490, 1530, and 1620 cm^{-1}. O–H bonds related to alcohols were at 3200–3600 cm^{-1}. FTIR spectra are compatible with the stepwise dendrimer modification process.

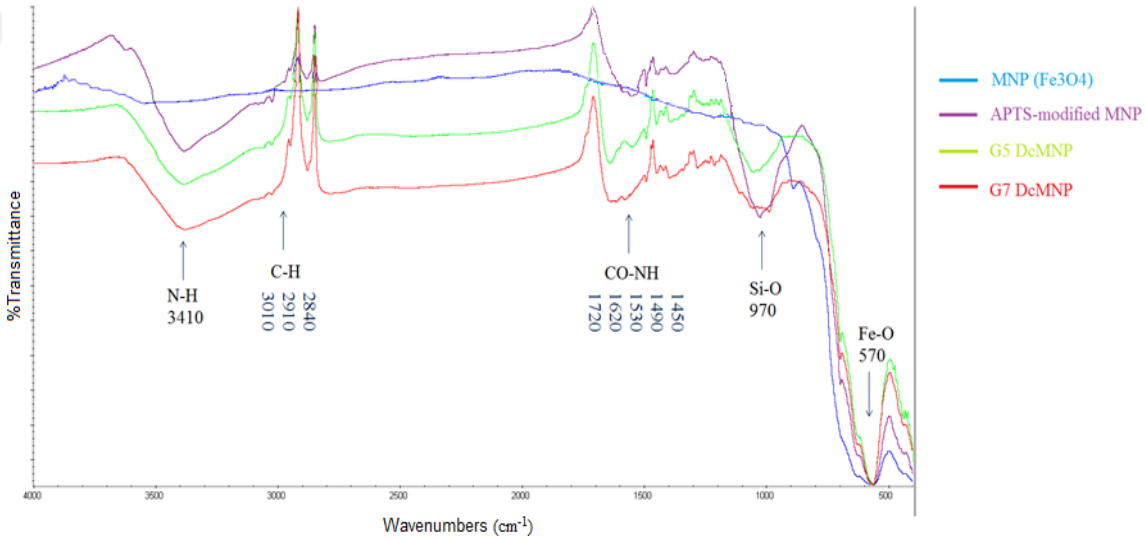

Figure 3.2 FTIR spectra of bare MNP, MNP-APTS, G5, and G7DcMNPs.

3.2.2 Transmission Electron Microscopy Analysis (TEM)

Figure 3.3 shows TEM result of synthesized bare MNP and G_7DcMNP, clearly demonstrating that the magnetic core is entirely composed of crystals with a relatively uniform and spherical morphology with average sizes of 8±5 nm. This indicates that the synthesized MNPs are potentially superparamagnetic. However, in order to confirm this, vibrating sample magnetometer analysis was done.

After coating of the magnetic core with PAMAM dendrimer, the diameter of G_7DcMNP was determined to be in the range of 40±10 nm.

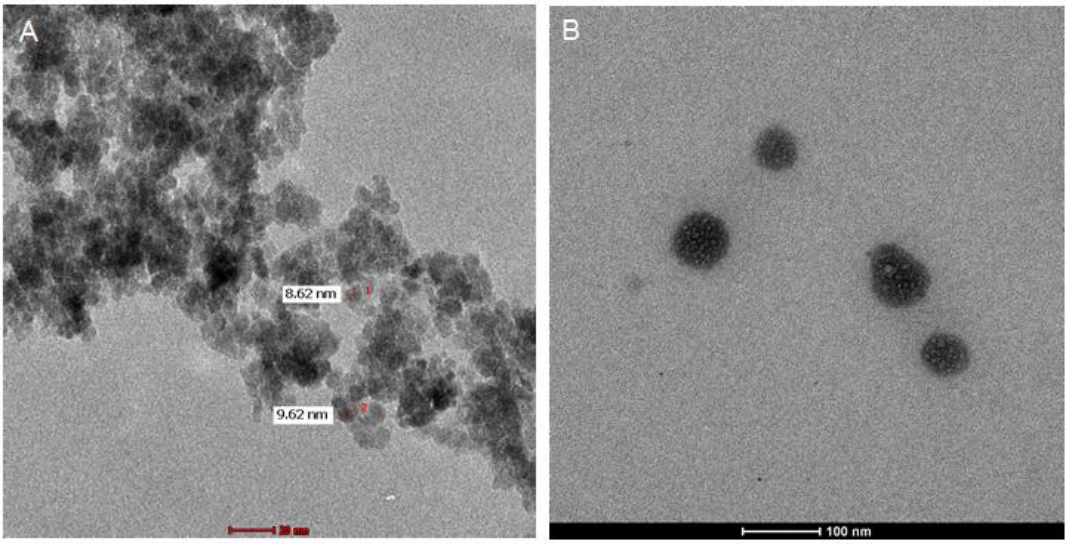

Figure 3.3 TEM results showing A) bare MNP (magnetite core) and B) G_7DcMNP. Determining the size and morphology of the nanoparticles by TEM, were performed in triplicates.

Since nanoparticles smaller than 10 nm are rapidly cleared by the kidneys or through extravasation and larger entities (~100–200 nm) are cleared by the reticuloendothelial system (Petros and DeSimone 2010), PAMAM-coated magnetic nanoparticles synthesized in this study are in the optimum size range.

3.2.3 Scanning Electron Microscopy (SEM)

SEM result of synthesized G_7DcMNP, clearly demonstrating that the average size of product is around 40±10 nm (Figure 3.4). This size is adequate to avoid entrapment by the reticuloendothelial system, leading to passive targeting to diseased parts through blood vessels; however, with the presence of magnetic core in these nanoparticles, they could be targeted to the tumor site by using a magnetic field.

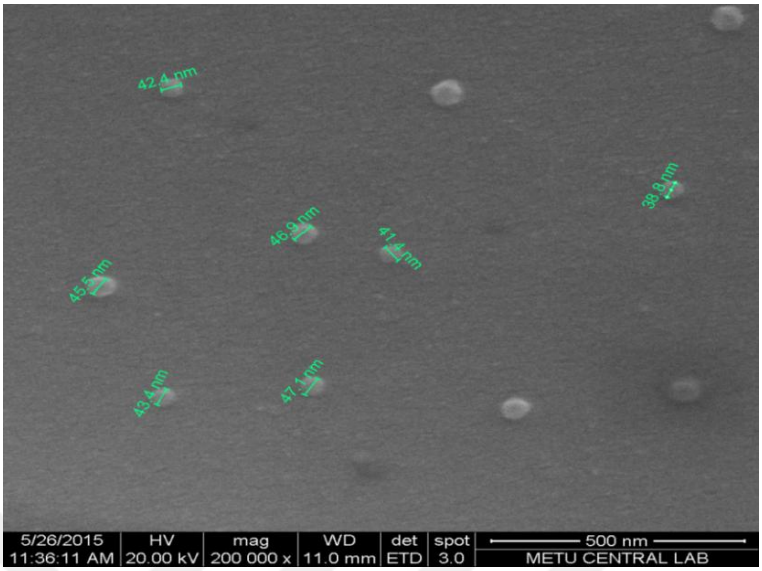

Figure 3.4 SEM results showing G_7DcMNP with an average grain size of 40±10 nm. Determining the size and morphology of the nanoparticles by SEM, were performed in triplicates.

3.2.4 Vibrating Sample Magnetometer Analysis (VSM)

Magnetization curves of the MNPs, APTS-modified MNPs, and DcMNPs at 37°C are given in Figure 3.5. Magnetic materials showing a superparamagnetic behavior have zero value of remanence (the magnetization left behind in a ferromagnetic material (such as iron) after an external magnetic field is removed.) and coercivity (a measure of the ability of a ferromagnetic material to withstand an external magnetic field without becoming demagnetized). The remanence and coercivity observed in the hysteresis loops of MNPs, APTS-coated MNPs, G_5DcMNP, and G_7DcMNP at 37°C were negligible. VSM results of bare MNPs analyzed at 37°C were obtained as 48.8 emu g^{-1}.

These results together with the results obtained related to the size of magnetic nanoparticles validate their superparamagnetic behavior.

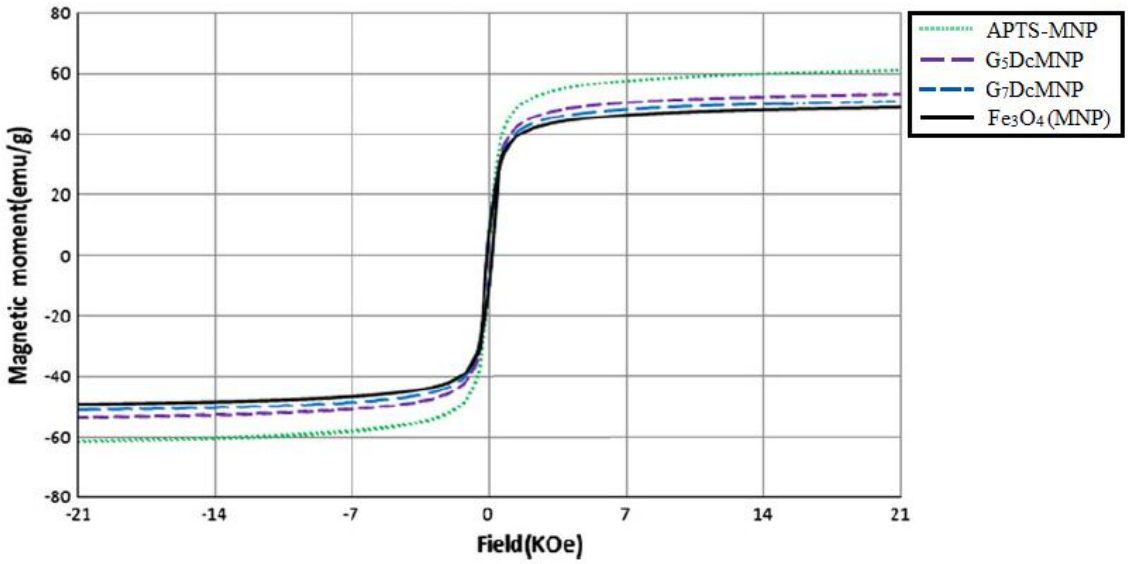

Figure 3.5 Variation of magnetization of the MNPs, APTS-modified MNPs, G_5DcMNP, and G_7DcMNP with applied field at 37°C showing superparamagnetic nature of MNPs with zero coercivity.

3.2.5 Zeta (ζ) Potential Analysis

ζ Potential is a physical property displayed by particles in suspension and is a significant indicator of stability of the particles in colloidal systems which indicates the amount of repulsion between similarly charged molecules. Therefore, if the ζ potential is very low, attractive forces surpass repulsive forces and particles will come together to form aggregates. Particles with large negative or positive ζ potentials that are small in size resist attraction and are hence electrically stabilized. In general, particles with ζ potentials larger than +30 mV or smaller than −30 mV are considered as stable (Gungor et al. 2014; Taira et al. 2012).

The surface charge and hence, stability of bare MNP, APTS-modified MNP, and G_7DcMNP were evaluated by ζ Potential measurements (Figure 3.6 and Figure 3.7) which indicated that the G_7DcMNPs had sufficiently high values (>+30 mV) that could be considered as stable nanoparticles (Figure 3.7B).

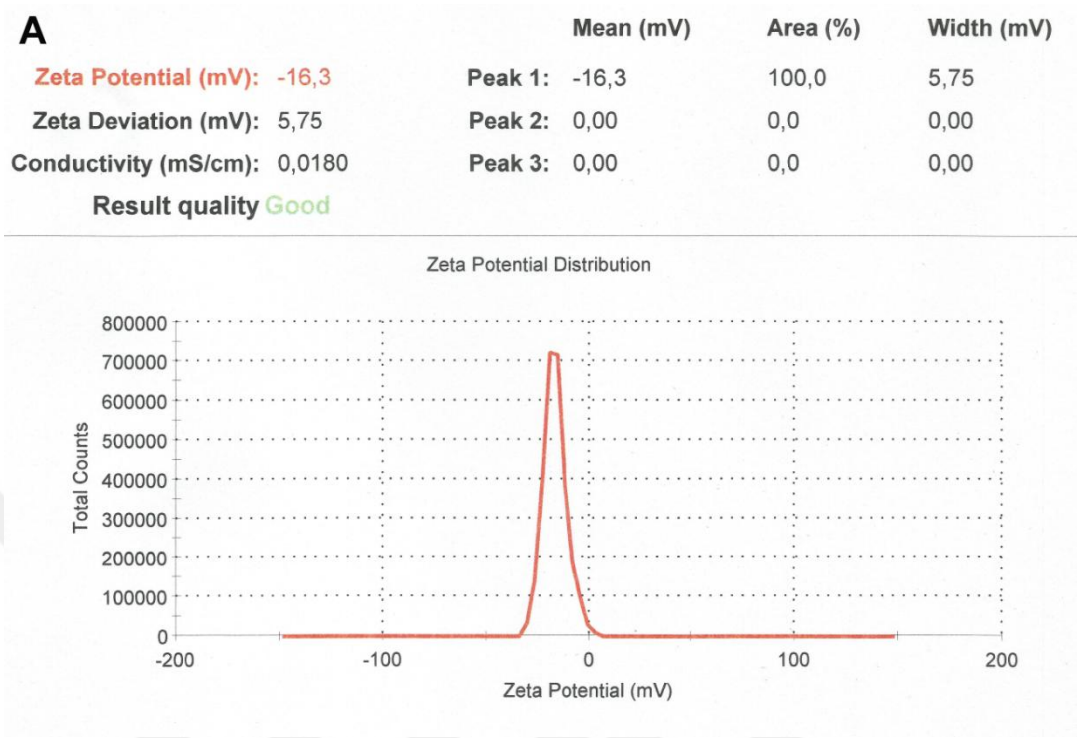

Figure 3.6 ζ Potential measurements of free MNP.

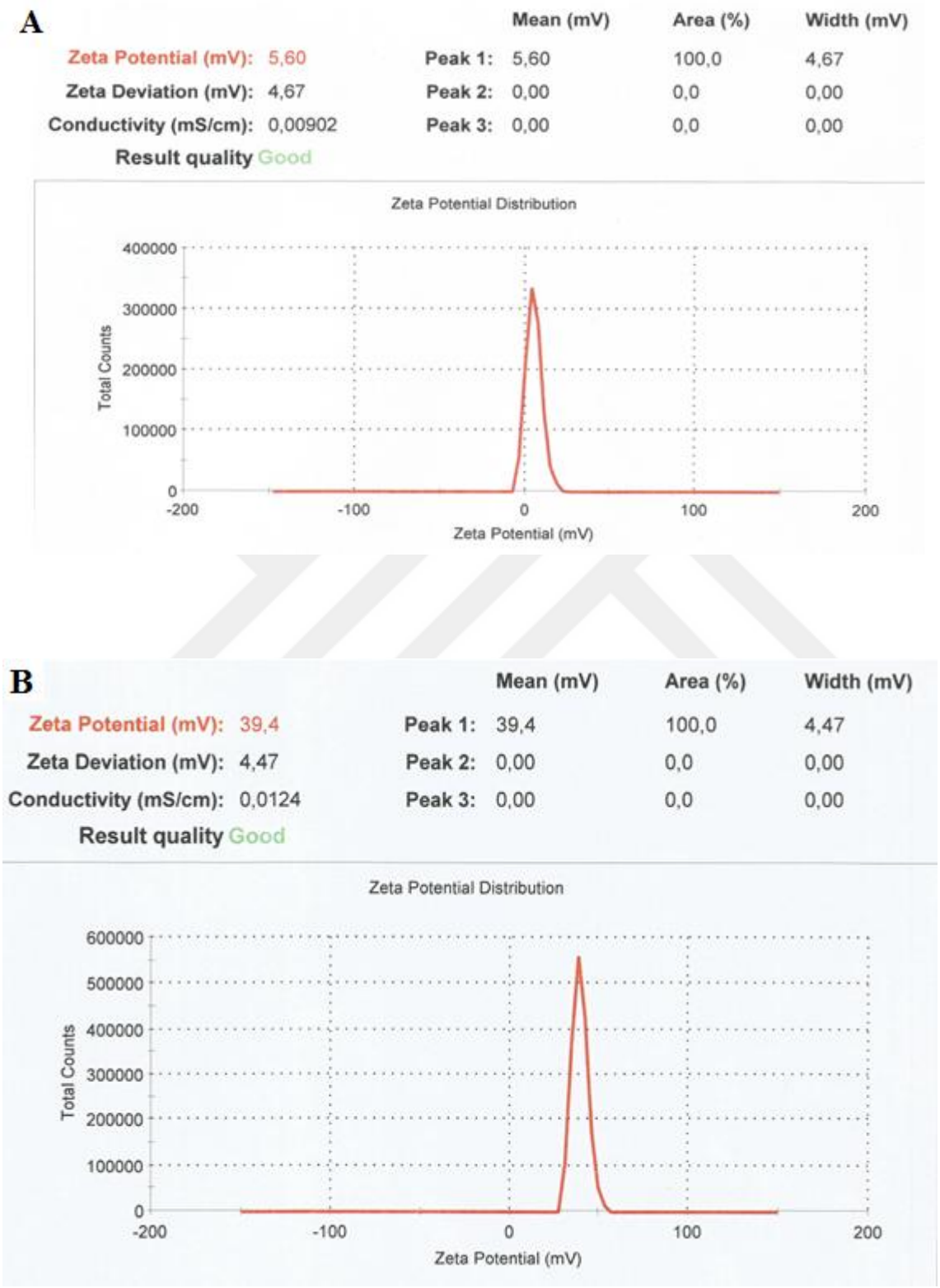

Figure 3.7 ζ Potential measurements of A) APTS-modified MNP and B) G7DcMNP.

3.3 Cellular Internalization of Dendrimer-Coated Magnetic Nanoparticles

Internalization of nanoparticles by MDA-MB231, SKBR3, MCF7, and MCF7/Dox cells was investigated by using fluorescent microscopy.

3.3.1 Fluorescence Microscopy

One of the desirable characteristics for drug carriers is to be taken up by cancer cells. In this study, cellular uptake of the DcMNPs could facilitate the intracellular delivery of CpG-ODN, and thereby enhancing its anticancer activity. To verify the cell uptake of the DcMNPs, the nanoparticles hybridized with FITC, and the DcMNP–FITC complexes were incubated with MDA-MB231, SKBR3, MCF7/S, and MCF7/Dox cells for 5 h. As shown in Figure 3.8, green fluorescence from the DcMNP-FITC complexes were distributed in the cells and primarily located in cytoplasm (stained in blue color with DAPI), which suggest that the complexes were taken up into the cells after endocytosis. Therefore, loading of anticancer drugs in the DcMNPs to deliver in cancer cells could significantly enhance the efficiency of drug delivery and thereby promote cancer therapy.

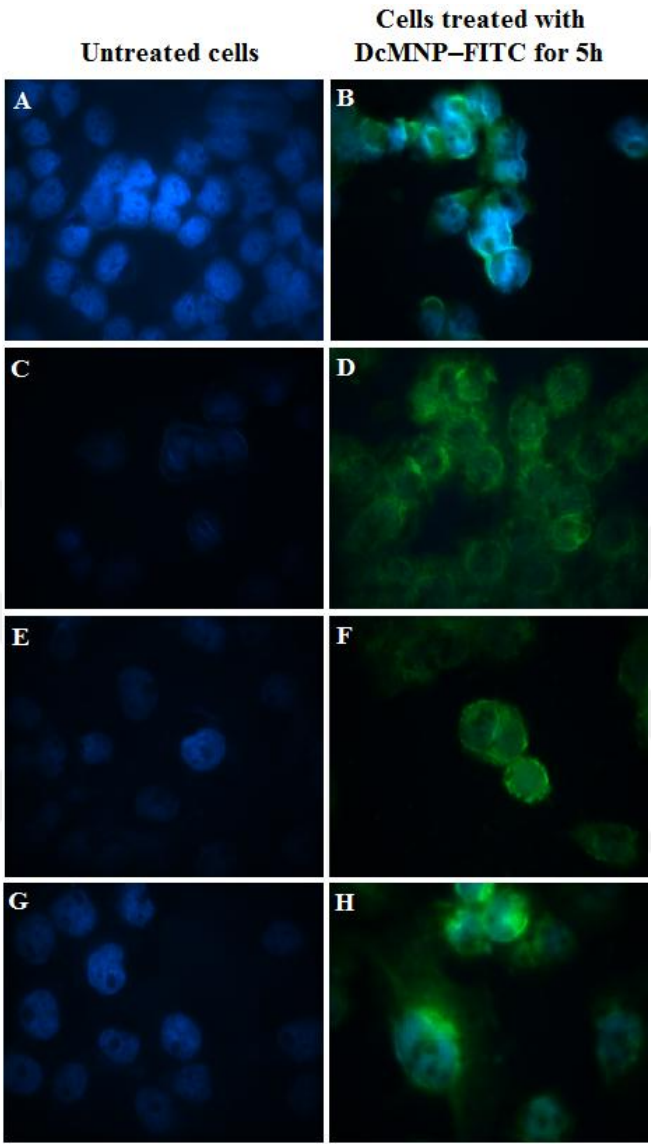

Figure 3.8 Fluorescence microscope images of (A) and (B) MDA-MB231, (C) and (D) SKBR3, (E) and (F) MCF7/S, and (G) and (H) MCF7/Dox cells. The first column from left indicates untreated cells used as control and the second column shows the cells treated with 100 μg of DcMNP-FITC complexes (after 5 h of incubation) with merged DAPI and FITC channels.

3.4 Validation of CpG Loading on DcMNPs

CpG-ODN was loaded on the surface of different generations and concentrations of DcMNPs in PBS buffer (pH 7). The complexes were characterized in terms of

movement in an electrical field, NanoDrop spectroscopy, their particle surface charge and elemental composition, by agarose gel electrophoresis, zeta-potential measurements, and XPS analyses, respectively.

3.4.1 NanoDrop Spectroscopy Analysis

In order to validate the appropriate generation on which the highest amount of CpG-ODN is loaded, a fixed amount of CpG-ODN was loaded on the different generations of DcMNPs (G_3–G_8) (CpG:DcMNP ratio (w/w) was selected as 1:70). The amount of CpG-ODN loading on the cationic nanoparticles was calculated by subtracting the ssDNA content in the supernatant from the initial concentration of CpG-ODN added.

Lower generation dendrimers (G_0–G_4) have a planar, elliptical shape, while at the higher generations (G_5–G_{10}), the densely packed branches induce the polymer to form a spherical conformation. The number of generation also affects the molecular weight, size, and the number of surface groups. “De Gennes dense packing effect” in which the steric crowding of the branches limits developing of the higher generations (G_8–G_{10}), can lead to the defective branching structures (Dufès et al. 2005; Taghavi Pourianazar et al. 2014).

The results indicated that possessing higher number of surface groups which can lead to more binding to CpG molecules and to avoid steric hindrance, G_7DcMNP has higher potential to bind CpG-ODN, compared to other synthesized generations of DcMNP (G_3-G_8) (Appendix F). This effect was dependent on cationic dendrimer surface groups and correlated with charge density (G_3-G_6) and also steric hindrance (G_8), that is, the G_7DcMNP was found to be significantly most efficient generation in terms of binding to CpG (Figure 3.9).

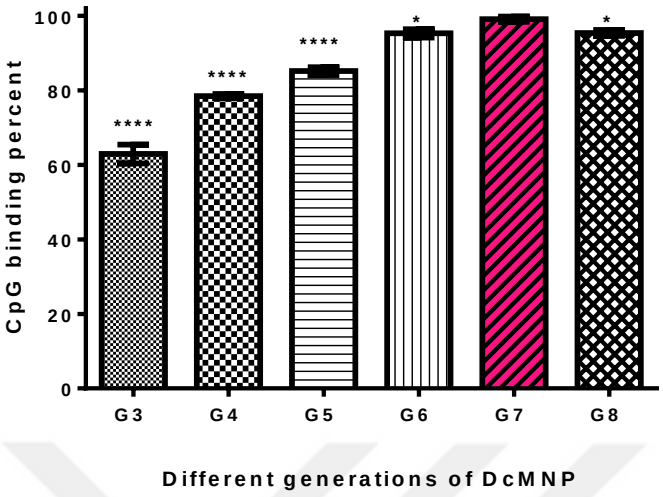

Figure 3.9 CpG binding percent on different generations of DcMNP (G_3-G_8) (CpG-ODN:DcMNP ratio (w/w) was 1:70). Experiments were run in triplicates (n = 3), *P < 0.05.

To assess whether complexation of CpG-ODN with cationic G_7DcMNPs and charge densities would generate well-defined, stable complexes suitable for clinical applications, a fixed amount of CpG-ODN was mixed with increasing amounts of nanoparticles. Figure 3.10 shows the loading optimization on G_7DcMNPs at pH 7, indicating the optimum w/w ratio of CPG-ODN:G_7DcMNPs as 1:70, at which the highest amount of CpG-ODN binds to the DcMNPs. The values measured by NanoDrop spectroscopy were listed in Appendix F.

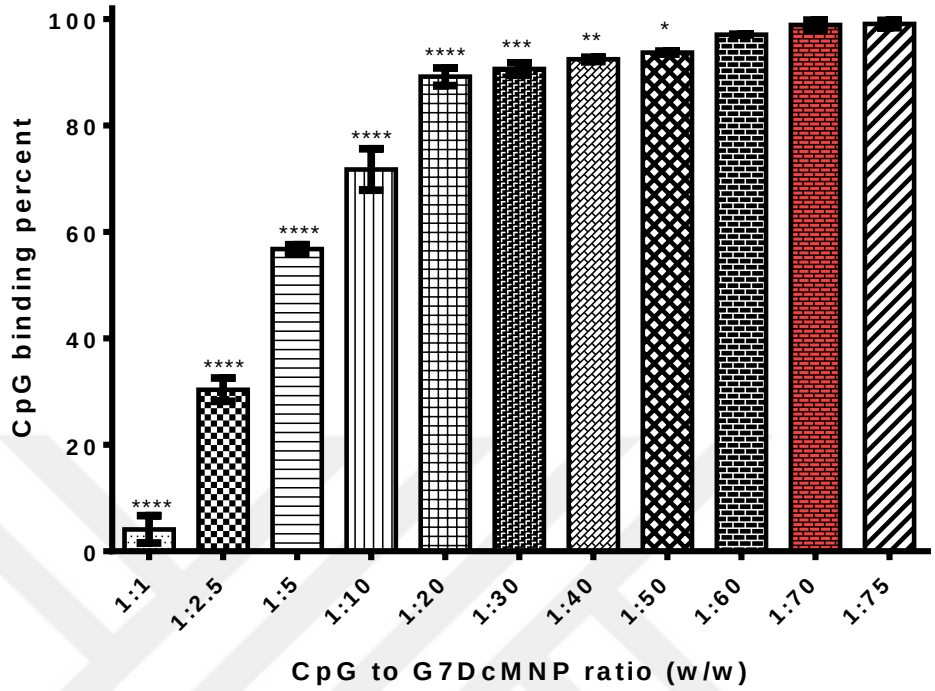

Figure 3.10 CpG binding percent on different ratios of CPG-ODN:G_7DcMNP (w/w). Experiments were run in triplicates (n = 3), *P < 0.05.

3.4.2 Agarose Gel Electrophoresis Shift Assay

The formation of CpG-ODN:G_7DcMNP complexes and the binding of dendrimers to CpG were analyzed by examining the migration of the CpG-ODN during agarose gel electrophoresis. Figure 3.11 shows the electrophoretic shift assay result of CpG-ODN loading on different generations of DcMNP (G_3-G_8) and on different concentrations of G_7DcMNP and also different concentrations of free CpG-ODN.

The positive control (1, 1:2, 1:4, 1:8, 1:16, 1:32, 1:64, and 1:128 dilutions of free CpG) and negative control (Unloaded DcMNP) were loaded in lanes 1-8 and lane 9, respectively. The CpG-loaded to different generations of DcMNP (G_3-G_8) were in lanes 10-15, CpG-bound to different concentrations of G_7DcMNP were in lanes 17-26 (Figure 3.11).

The loading efficiencies on different generations of DcMNPs (G_3–G_8) were also studied at pH 7. It was observed in NanoDrop spectroscopy and agarose gel electrophoresis analyses that the loading efficiency of CpG-ODN on G_2, G_3, G_4, G_5, G_6, and G_8DcMNPs was lower than G_7DcMNP. Moreover, Figure 3.11 indicates that increasing the amounts of nanoparticles in CpG-ODN/G_7DcMNP complex resulted in a more electrophoretic retardation of DNA which indicates the higher amount of binding of CpG to DcMNPs and these results validate the findings from NanoDrop spectroscopy.

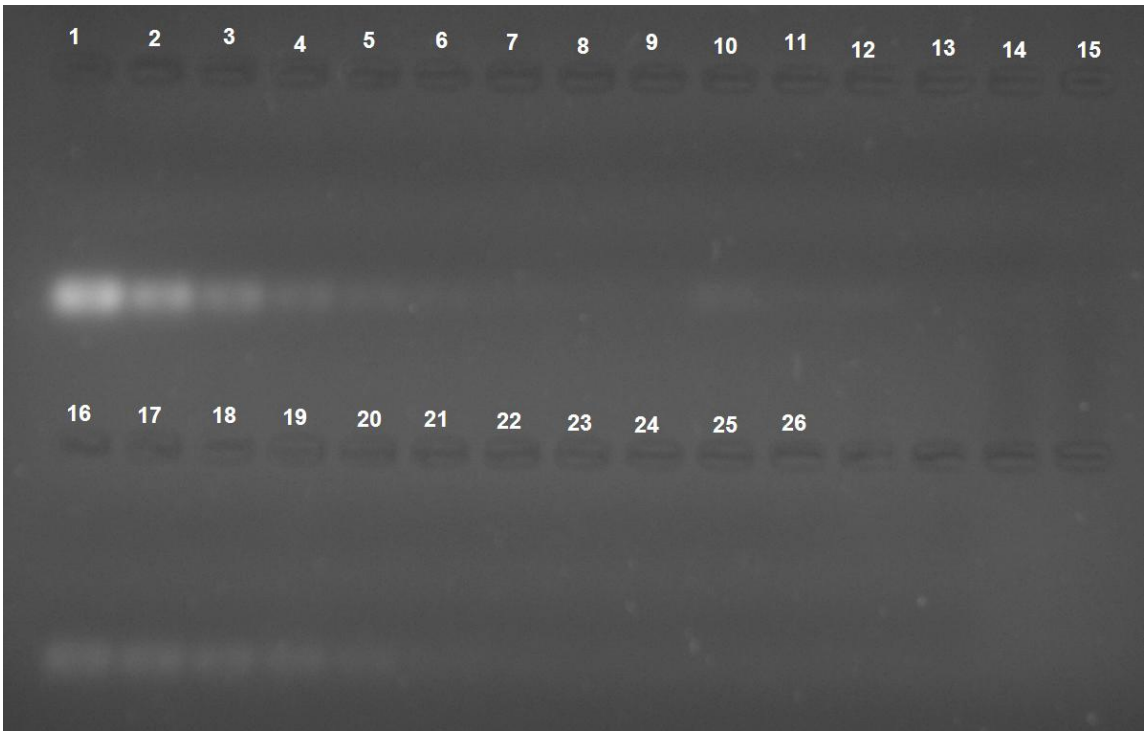

Figure 3.11 Agarose gel electrophoresis of loading optimization of CpG-ODN on DcMNPs at pH 7. Lanes 1-8: Free CpG, Lane 9: Free DcMNP, Lanes 10-15: CpG bound to different generations of DcMNPs (G_3-G_8), Lane 16: Free CpG, and Lanes 17-26: CpG bound to different concentrations of G_7DcMNP.

3.4.3 CpG-ODN Loading Validation by Zeta-Potential Analysis

Figure 3.12 shows the zeta potential of the CpG-loaded G_7DcMNPs. The zeta potential of approximately -16 mV at pH 7.0 was observed in MNPs due to the abundant OH^- ions (Figure 3.6). When MNPs were modified with PAMAM dendrimer, zeta potential

increased and reached +39.4 mV at pH 7.0 for G_7DcMNP due to the increasing positive charges of $-NH^{3+}$ on the magnetic surface (Figure 3.7). After CpG-ODN was electrostatically bound to the PAMAM-conjugated nanoparticle surface, the zeta potential was reduced to approximately +34 mV (Figure 3.12). The difference between surface charge of DcMNPs and CpG-ODN/G7DcMNP complex showed that upon conjugation of CpG-ODN to DcMNPs, the positive charges of DcMNPs is neutralized partly, and the surface charge of the complex becomes less positive compared to free DcMNPs. The zeta-potential results for bare MNP, APTS-modified MNP, unloaded DcMNP, CpG-loaded DcMNP were summarized in Figure 3.13.

In a research performed by Pan et al., the G5DcMNP was used for loading antisense *Survivin* oligodeoxynucleotide (asODN). The zeta potential results indicated a statistical difference between surface charge of DcMNPs and DcMNP-asODN ($P < 0.05$) (Pan et al. 2007c; Zhang et al. 2007). The literature indicates that a positive surface charge of composites is required for binding to anionic cell surfaces, which consequently facilitates uptake by the cell (Jiang et al. 2007; Zhang et al. 2007).

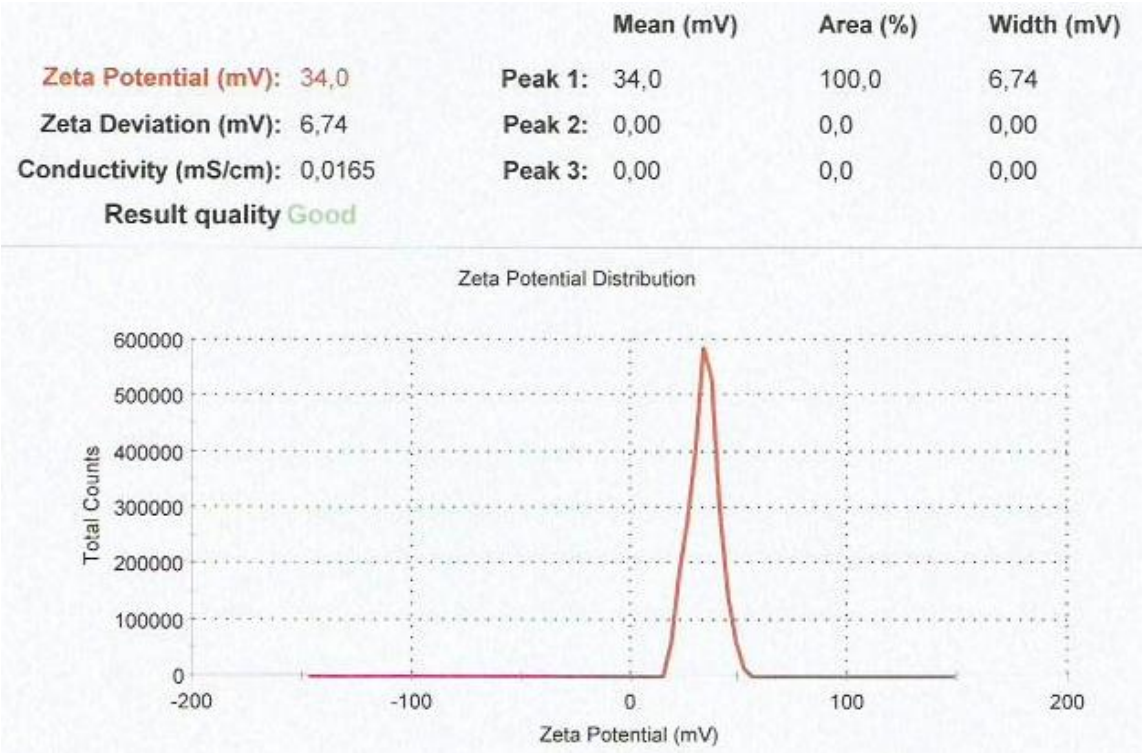

Figure 3.12 Zeta Potential Analysis of CpG-ODN/G7DcMNP Complex

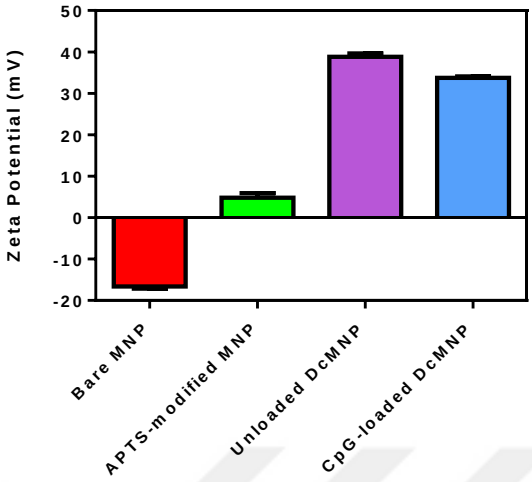

Figure 3.13 Zeta potentials of bare MNP, APTS-modified MNP, unloaded DcMNP, CpG-loaded DcMNP in H_2O.

3.4.4 Validation of CpG-ODN Loading by X-ray photoelectron spectroscopy (XPS)

To intuitively evaluate qualitative and quantitative surface characterizations and determine the composition of the synthesized DcMNPs and CpG-ODN-loaded G_7DcMNP, X-ray photoelectron spectroscopy (XPS) was utilized. As shown in Figure 3.14A, the XPS full-spectrum indicates only iron, oxygen, nitrogen and carbon, the absence of phosphorus indicating that no CpG molecules are on the surface of the unloaded DcMNPs. Figure 3.14B further shows double peaks with binding energies at 140 eV and 190 eV, corresponding to $P2_P$ and $P2_S$, respectively, assigned to phosphate groups of CpG-ODN, which can be considered as further evidence confirming that the CpG molecules were adsorbed on the surface of the nanoparticles.

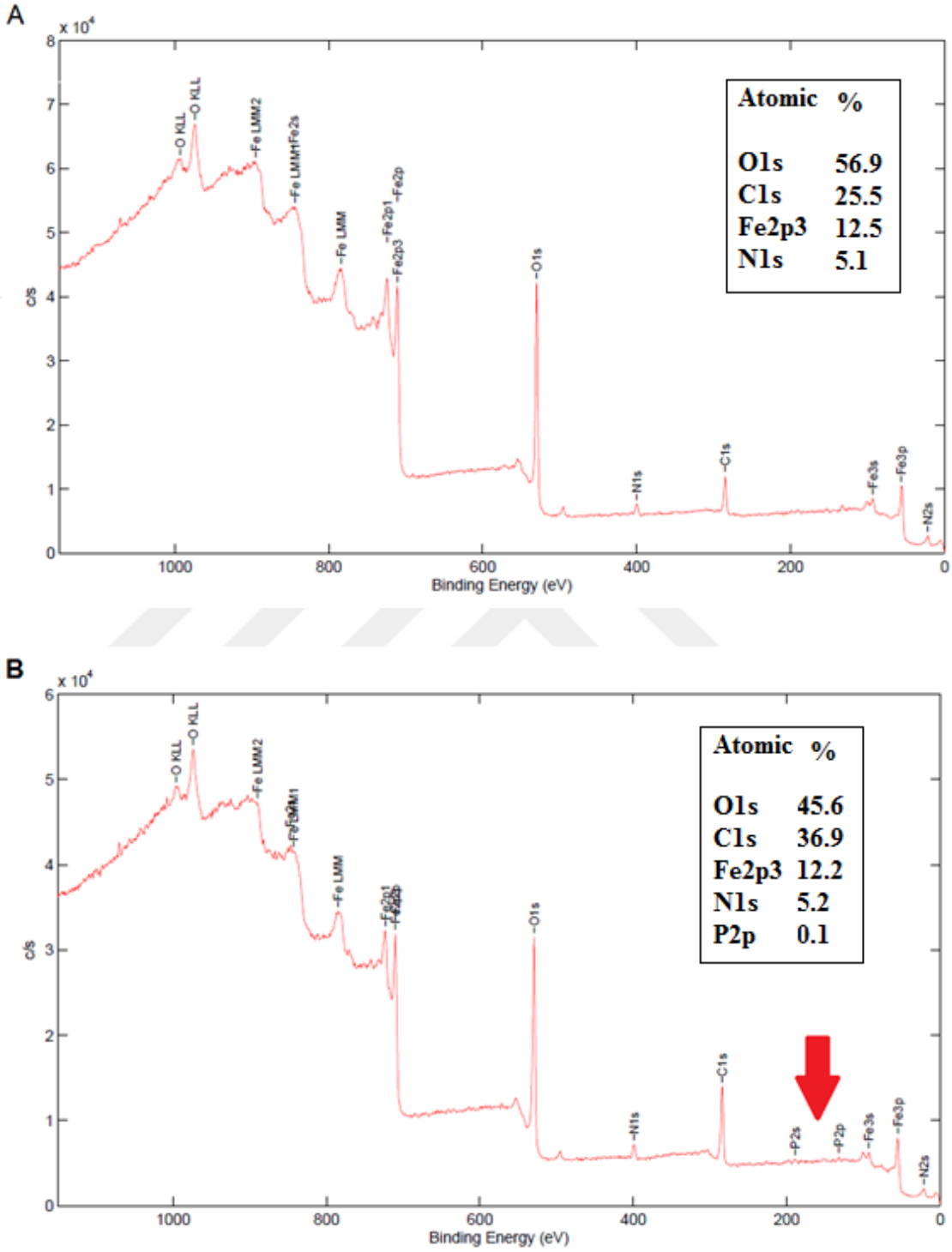

Figure 3.14 X-ray photoelectron spectroscopy (XPS) spectra of A) unloaded G_7DcMNP and B) CpG/G7DcMNP conjugates (The arrow indicates the P bands).

3.4.5 The Hydrodynamic Size Measurement of G_7DcMNP by Dynamic Light Scattering (DLS)

The hydrodynamic size of G_7DcMNP was measured by dynamic light scattering (DLS; Zetasizer Nano ZS, Malvern Instruments) as shown in Figure 3.15. The diameter was determined to be in the range of 50±10nm. The size of nanoparticles did not change after binding to CpG-ODN molecules, indicating that the dendrimers efficiently bind to CpG-ODN molecules and condense them into spherical nano-sized particles. In other words, these dendrimers self-assemble with ssDNAs into nano-sized particles, similar to what has been observed with RNA–dendrimer (Zhou et al. 2006) and ribozyme–dendrimer complexes (Zhou et al. 2006).

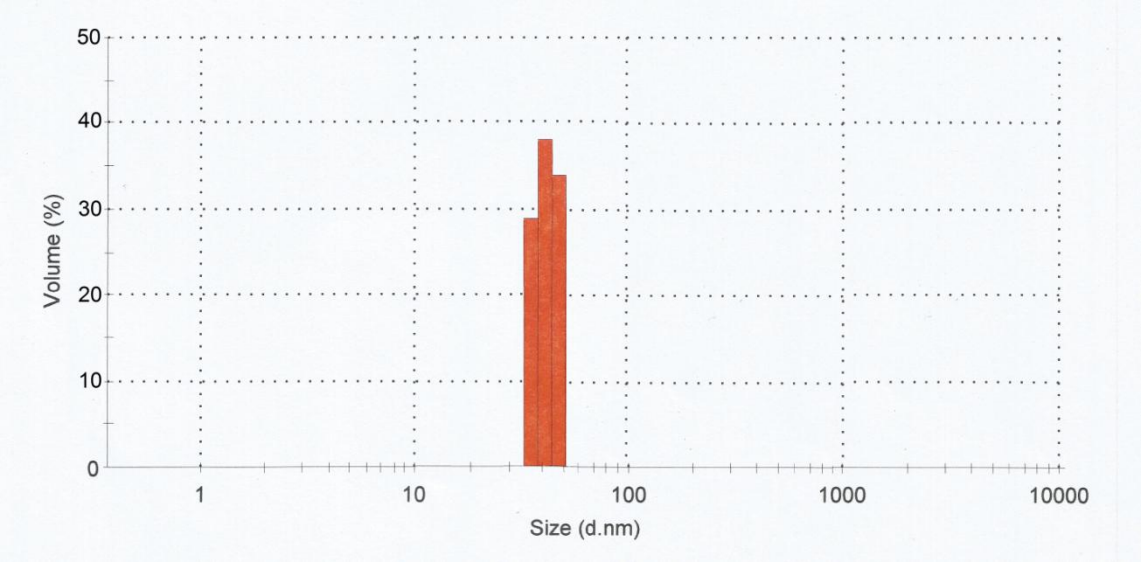

Figure 3.15 The hydrodynamic size distribution of G_7DcMNPs measured by DLS analysis.

3.4.6 Evaluation of CpG-DcMNP Internalization by Cells Using Prussian Blue Staining Assay

Prussian blue staining was utilized to determine the internalization and presence of CpG-DcMNP complexes in the cells. Untreated cells stained with Prussian blue are indicated in Figure 3.16. It was demonstrated in Figure 3.17 that most of the CpG-loaded

DcMNPs were taken up by MDA-MB231, SKBR3, MCF7, and MCF7/Dox cells (at 37°C, 5h) which are visualized by light microscopy after Prussian blue staining.

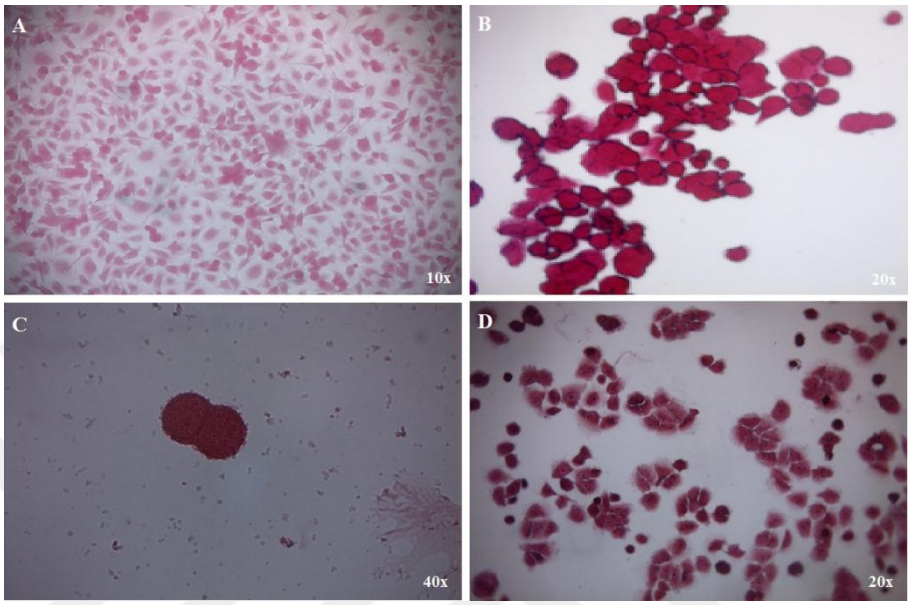

Figure 3.16 Prussian blue stained images of untreated (A) MDA-MB231, (B) SKBR3, (C) MCF7/S, and (D) MCF7/Dox cells.

Prussian blue staining was carried out to detect the presence of CpG-DcMNP complexes in MDA-MB231, SKBR3, MCF7, and MCF7/Dox cells after incubation of the cells with the 100 μg of CpG-DcMNP complexes for 5 h. As shown in Figure 3.17, CpG-DcMNP complexes show cellular uptake by all of the cells after five hours of incubation.

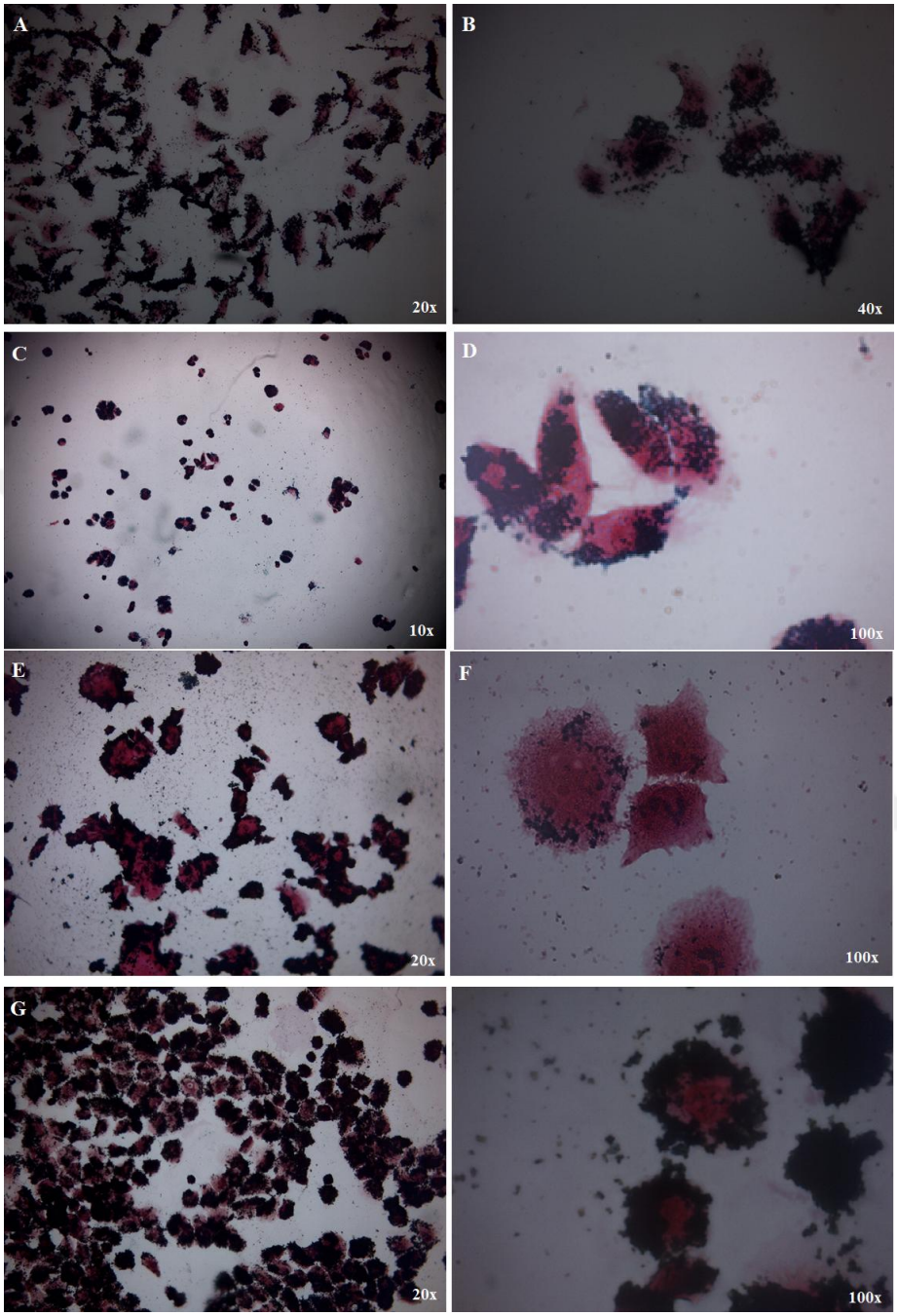

Figure 3.17 Prussian blue stained images of (A) and (B) MDA-MB231, (C) and (D) SKBR3, (E) and (F) MCF7/S, and (G) and (H) MCF7/Dox cells. Cells were incubated with CpG-DcMNP complexes with a concentration of 100 µg/ml DcMNP for 5 h.

3.5 Targeting Properties of Free and CpG-Loaded DcMNP

To show the potency of targeting, the cells were cultured in a 6-well plate and incubated for 24h. Then, the cells were treated with CpG-loaded DcMNPs and incubated for 48h, while a magnet was placed under the half of the well. On application of an external magnetic field to the treated cells, the nanoparticles were attracted towards the magnet and the cellular internalization and therefore, cell death was enhanced in these cells. Such active targeting strategies in *in vivo*, can not only effectively deliver CpG-ODN into cancer cells, but may reduce the amounts of the anticancer agent used by improving the delivered amount to the cancer cells.

As negative group, untreated MDA-MB231cells were used (Figure 3.18A).

A **B**

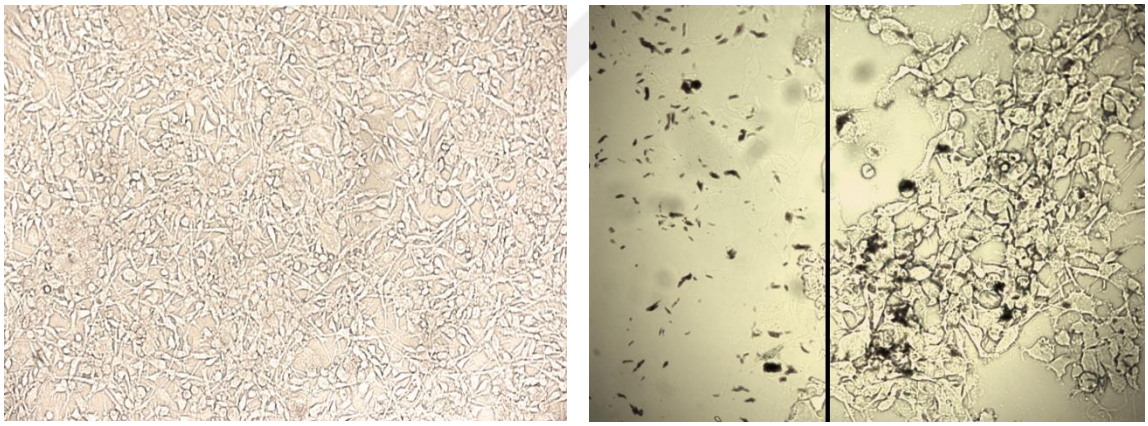

Figure 3.18 Evaluation of the role of MNP core as targeting agent in MDA-MB231 cells. A) Control MDA-MB231 cells. B) MDA-MB231 cells treated with CpG-loaded DcMNPs. A magnet was placed under the left half of the well, so as it can be seen, the CpG-loaded DcMNPs were shifted to the left side of the well and caused high accumulation of these nanoparticles. The result was cellular death in this side of the well, while the cells in the right side of the well are alive because of the lower presence of the CpG-loaded nanoparticles.

3.6 CpG-Loaded DcMNPs Stability Studies

The stability of CpG-ODN-loaded nanoparticles was determined by release assay followed up to 8 weeks in PBS (pH 7.2) at 37˚C, which mimics the pH of the physiological conditions. The results of analyzing the supernatant with NanoDrop spectrophotometer indicated that CpG-loaded G_7DcMNP were quite stable at pH 7.2, and there were only 1.15% release up to 8 weeks (Figure 3.19). The values measured by NanoDrop spectroscopy were listed in Appendix F.

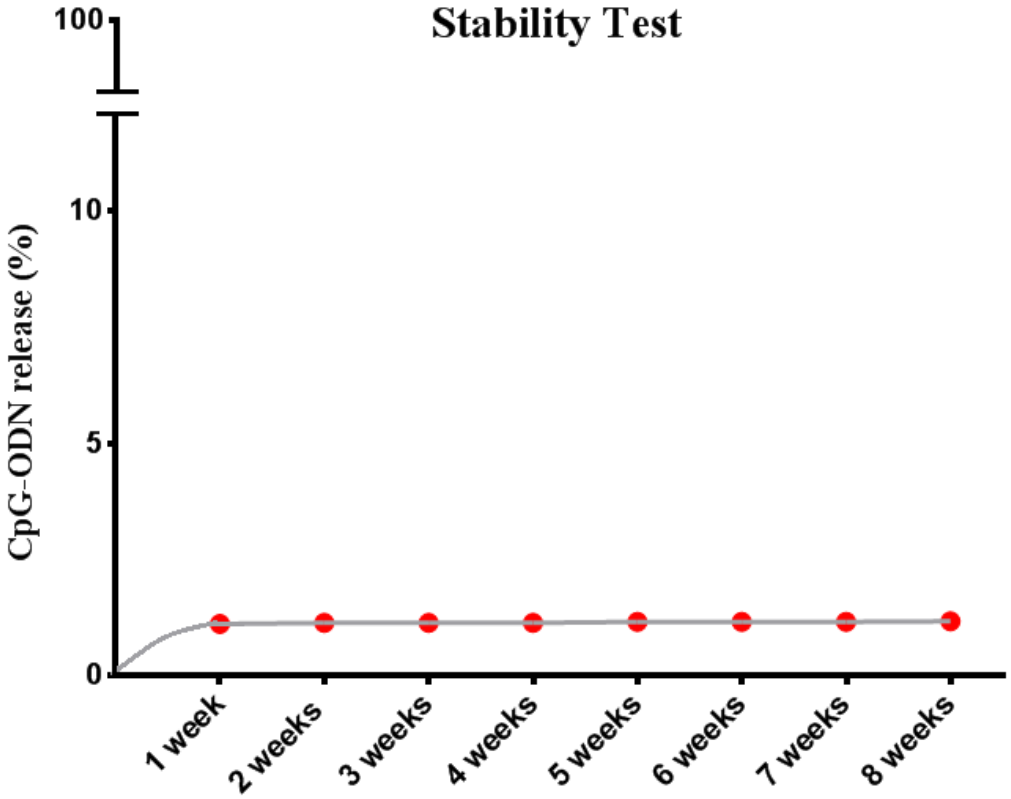

Figure 3.19 CpG-ODN release percent determined by release assay followed up to 8 weeks in PBS (pH 7.2) at 37˚C.

3.7 *TLR9* Expression Analysis

3.7.1 Isolation of Total RNA

RNAs isolated from different cell lines, MDA-MB231, SKBR3, MCF7/S, and MCF7/Dox cells were analyzed on 1% agarose gel prior to cDNA synthesis (Figure 3.20). Ribosomal RNAs (rRNAs) comprise approximately 80-85% of total RNA sample. Therefore, they could be visualized on agarose gel. The presence of distinct and sharp bands which corresponded to 28S and 18S rRNA, respectively, without any smear appearance indicated that the isolated RNA samples were intact and suitable for further analysis. The RNA samples were further examined by NanoDrop 2000 spectrophotometer (Thermo Fischer Scientific, USA) to check the purity of sample (Table 3.1). The RNA samples with the nucleic acid/protein (A260/A280) ratio of 1.8-2.0 were used in gene expression analyses.

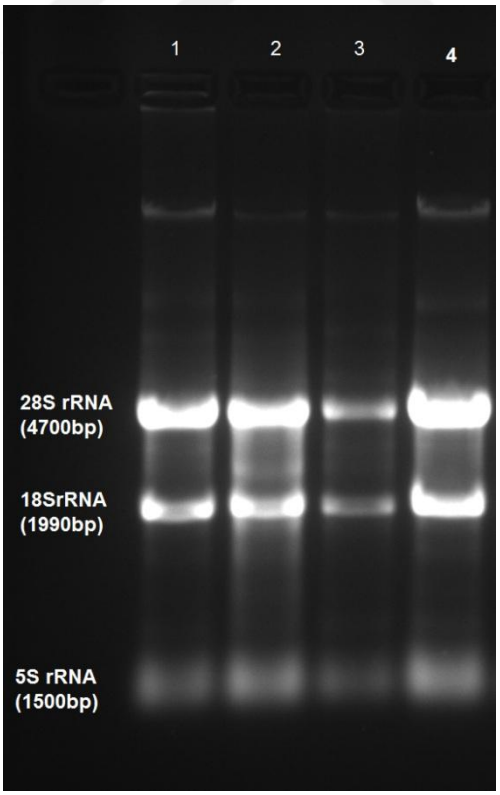

Figure 3.20 Total RNAs isolated from MDA-MB231 (Lane 1), SKBR3 (Lane 2) and MCF7/S (Lane 3), MCF7/Dox cells (Lane 4) on 1% agarose gel.

Table 3.1 Determination of RNA concentration (ng/µl) and the purity of sample using NanoDrop spectrophotometer.

	RNA concentration (ng/µl)	260/280	260/230
MDA-MB231	1942.8	1.98	1.88
SKBR3	1380	1.98	2
MCF7	1299.3	1.99	2
MCF7/Dox	928.8	2	1.94

3.7.2 Quantitative Real-Time Polymerase Chain Reaction (qRT-PCR)

The expression of *TLR9* and *β-actin* genes in parental MDA-MB231, SKBR3, MCF7/S, and MCF7/Dox cells were quantified by qRT-PCR. Amplification curves were displayed as fluorescence vs. threshold cycle number (Figure 3.21).

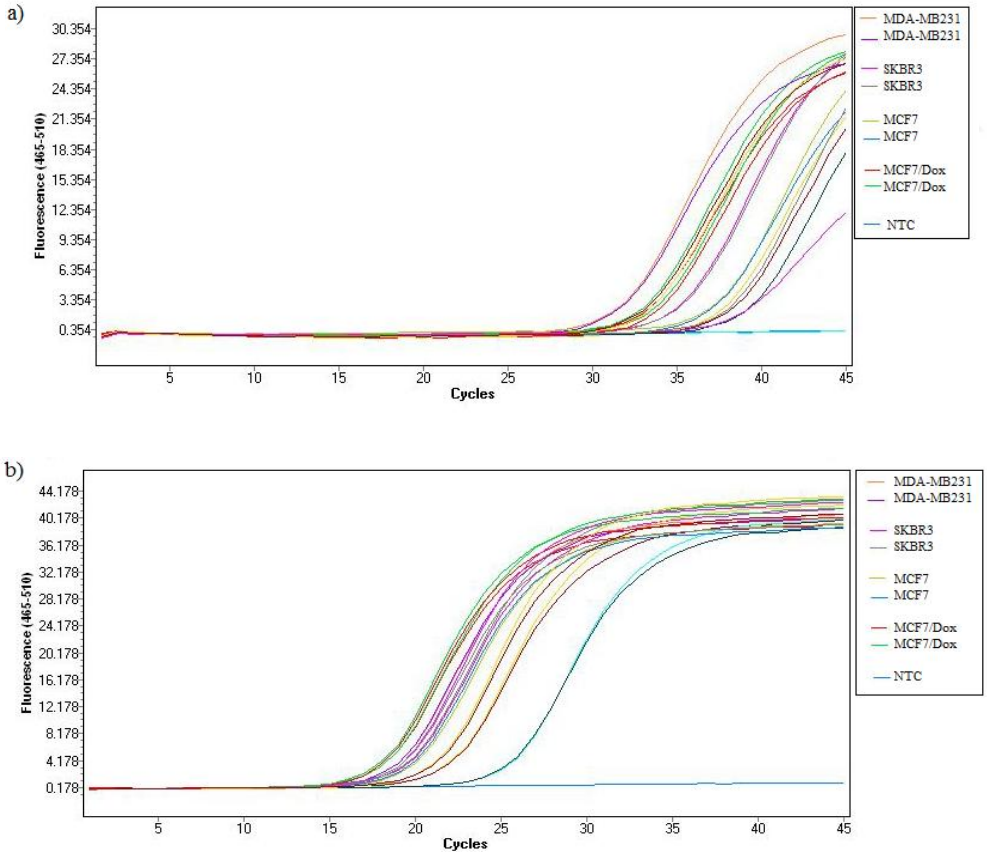

Figure 3.21 Amplification curves for a) *TLR9* and b) *β-actin* genes in MDA-MB231, SKBR3, MCF7/S, and MCF7/Dox cell lines.

Although TLR expression was first observed in immune cells, several reports have described the expression of TLRs in malignant epithelial cells. The level of *TLR9* mRNA in MDA-MB231, SKBR3, MCF7/S, and MCF7/Dox cell lines were determined by qRT-PCR and normalized with respect to the house keeping control gene *β-actin*. The fold changes in the expression of *TLR9* were determined relative to MCF7/S parental cell line by $2^{-\Delta\Delta C_T}$ method (Livak and Schmittgen 2001). The relative fold changes were indicated as bar graphs in Figure 3.22.

As it can be seen in the Figure 3.21, sensitive MCF7 cells had very low *TLR9* expression, whilst MDA-MB231 and SKBR3 cell lines expressed high level of *TLR9* mRNA among tested groups. *TLR9* mRNA is also expressed in MCF7/Dox cells.

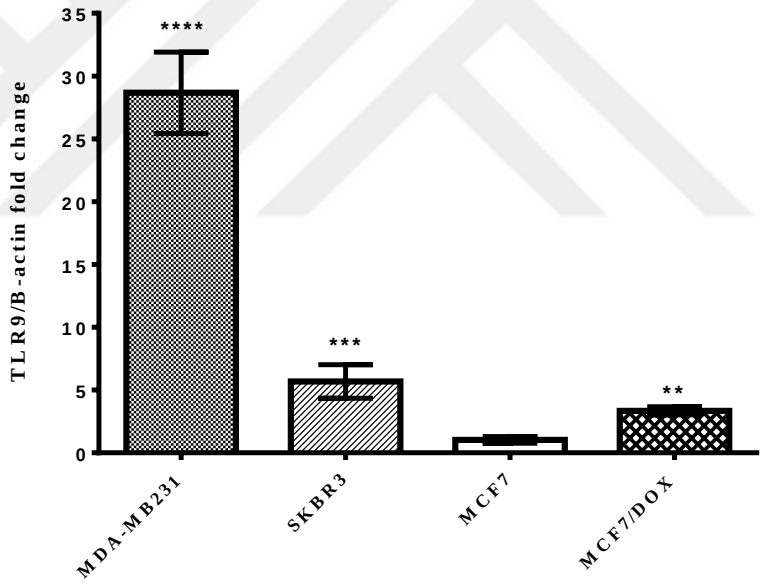

Figure 3.22 *TLR9* mRNA-expression in MDA-MB231, SKBR3, MCF7/S, and MCF7/Dox cell lines (*p<0.05, n=2).

According to Berger et al., high *TLR9* expression is related with estrogen receptor-negative (ER^-) status in the breast cancer cells (Berger et al. 2010). Since both of MDA-MB231 and SKBR3 cell lines are considered as ER-negative cell lines and MCF7 cells are shown to be ER-positive (Holliday and Speirs 2011; Subik et al. 2010), our findings are in parallel with the results of Berger et al.

Merrell et al. performed a study indicating that MDA-MB-231 cells express relatively high levels of mRNA for *TLR9*. They also found that MCF7 cells did not express *TLR9* mRNA and they selected MCF7 cells as a negative control (Merrell et al. 2006). These findings also confirm our results.

In a research performed by Ilvesaro et al., the cellular localization of TLR9 in MDA-MB231 breast cancer cells was verified by immunofluorescent stainings. They also indicated that *TLR9* is widely expressed in MDA-MB231human breast cancer samples (Ilvesaro et al. 2008).

3.8 Cytotoxicity of CpG-Loaded DcMNPs

Figure 3.23, Figure 3.24, and Figure 3.25 show the viability of MDA-MB-231, SKBR3, MCF7, and MCF7/Dox cell lines after incubation with unloaded DcMNP, free CpG, and DcMNPs bearing CpG-ODN, respectively. To quantify the cytotoxicity effects of these treatments on the cells, XTT cell viability assays were performed and inhibitory concentration 50 (IC_{50}) values, which show the toxic doses of the treatments. IC_{50} values were evaluated after 24, 48, and 72 h treatment, as shown in Table 3.2.

Survival rates indicated that at this range, there is no significant cytotoxic effect of free CpG-ODN and unloaded G_7DcMNPs on these cell lines (Figure 3.23 and Figure 3.24).

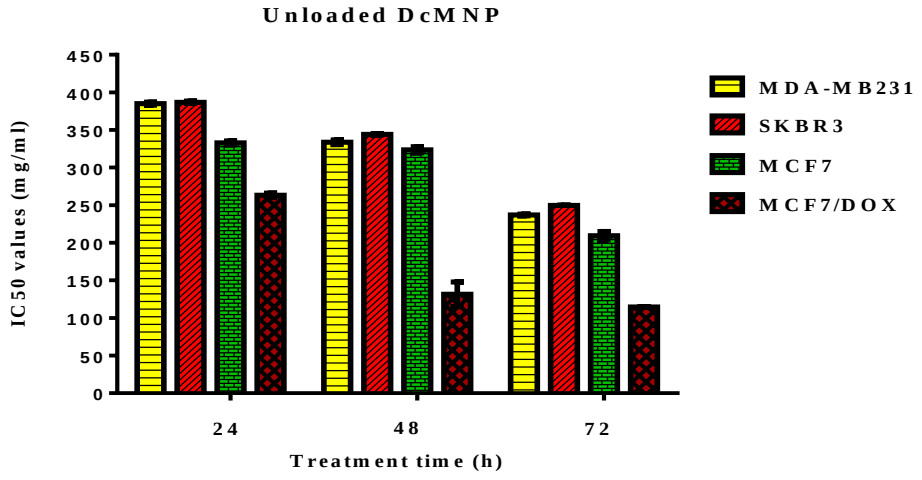

Figure 3.23 Cytotoxicity of unloaded G_7DcMNPs on MDA-MB-231, SKBR3, MCF7, and MCF7/Dox cell lines.

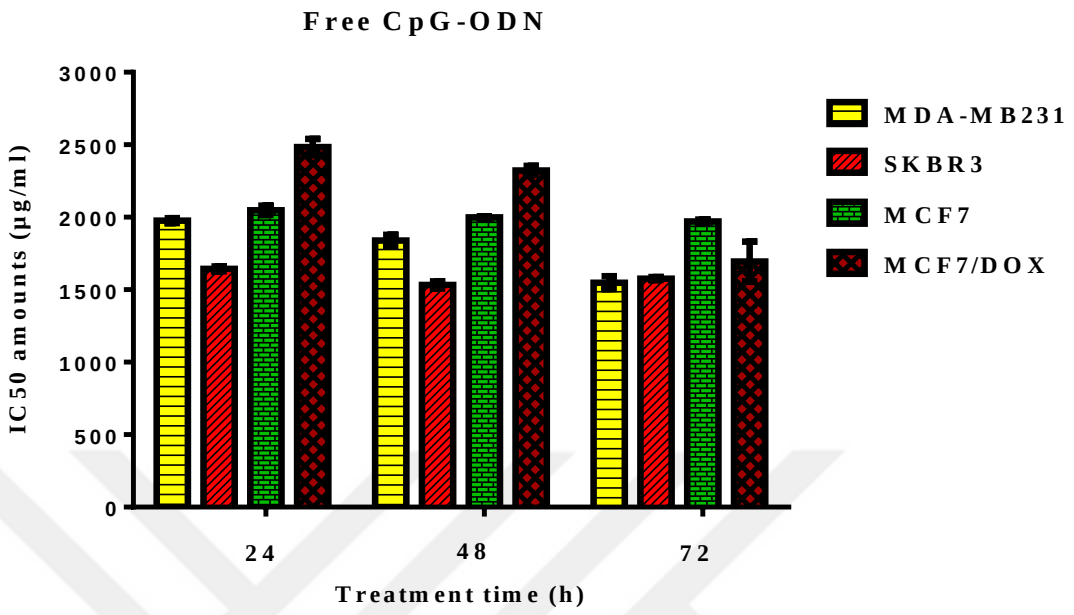

Figure 3.24 IC50 amounts (µg ml^{-1}) of free CpG-ODN for MDA-MB-231, SKBR3, MCF7, and MCF7/Dox cell lines.

The IC_{50} values of CpG-bound DcMNPs for MDA-MB231, SKBR3, MCF7, and MCF7/Dox cells were found as 0.609, 1.325, 2.296, and 0.313 µg/ml, respectively after 24 h treatment (Figure 3.25 and Table 3.2). These amounts were decreased to 0.518, 0.732, 0925, and 0.297 µg/ml, respectively after 48h treating with CpG-bound DcMNPs. Finally, the IC_{50} values of 72 h treatment with CpG-bound DcMNPs were 0.416, 0.680, 0.908, and 0.246 µg/ml, respectively. These results indicated that by increasing the duration of treatment from 24 h to 48 and 72 h in the case of MDA-MB231, SKBR3, and MCF7 cell lines, the cell viability and therefore, IC_{50} values significantly decreased. Moreover, loading of the CpG-ODN onto nanoparticles not only changes its effectiveness, but also facilitates its delivery to the cancer cells.

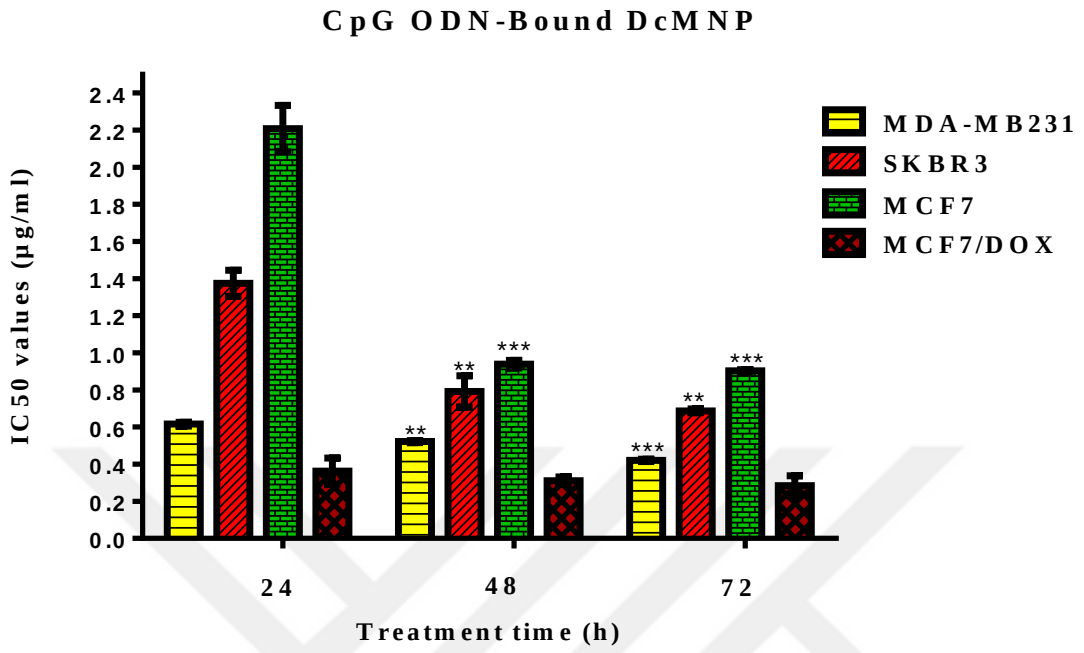

Figure 3.25 Cytotoxicity of CpG ODN-loaded G_7DcMNPs on MDA-MB-231, SKBR3, MCF7, and MCF7/Dox cell lines. The IC_{50} values are in terms of CpG-ODN used in the CpG ODN/G_7DcMNPs conjugate. The 48 and 72 h IC_{50} values of each cell line are compared with the 24 h IC_{50} value of the same cell line.

Table 3.2 IC_{50} amounts of unloaded DcMNP, free CpG, and DcMNPs bearing CpG-ODN treatments after on MDA-MB-231, SKBR3, MCF7, and MCF7/Dox cell lines.

Treatment	Unloaded DcMNP (mg/ml)			Free CpG-ODN (µg/ml)			CpG-bound DcMNP (µg/ml)		
Time (h) / Cell lines	24h	48h	72h	24h	48h	72h	24h	48h	72h
MDA-MB231	387.0	335.1	238.2	1.98×10^3	1.84×10^3	1.55×10^3	0.609	0.518	0.416
SKBR3	387.3	344.6	249.8	1.64×10^3	1.53×10^3	1.57×10^3	1.325	0.732	0.680
MCF7	333.4	322.7	203.9	2.05×10^3	1.99×103	1.97×10^3	2.296	0.925	0.908
MCF7/Dox	264.5	119.4	114.9	2.48×10^3	2.32×10^3	1.67×10^3	0.313	0.297	0.246

The cytotoxicity of CpG-bound DcMNPs on cells increased several folds compared to free CpG (Figure 3.25). For MDA-MB231 cell line, the IC_{50} of free CpG was 1980,

1840, and 1550 μg/ml after 24, 48, and 72 h, respectively. These values was dropped to 0.609, 0.518, and 0.416 μg/ml, which had a 3251, 3552, and 3726-fold decrease for 24, 48, and 72 h treatment, respectively.

In the case of SKBR3 cells, the IC_{50} of free CpG was 1640, 1530, and 1570 μg/ml after 24, 48, and 72 h, respectively. IC_{50} of CpG after loading on DcMNP was decreased to 1.325, 0.732, and 0.680 μg/ml, respectively. The results indicated a 1238, 2090, and 2309-fold decrease for 24, 48, and 72 h treatment, respectively.

After treating the MCF7 cells with free CpG for 24, 48, and 72h, the IC_{50} values were recorded as 2050, 1990, and 1970 μg/ml, respectively. These values declined significantly after treating with CpG-loaded DcMNPs to 2.296, 0.925, and 0.908 μg/ml. There was an 893, 2151, and 2170-fold decrease for 24, 48, and 72 h treatment, respectively.

Finally, in the case of MCF7/Dox cells, the IC_{50} of free CpG was 2480, 2320, and 1670 μg/ml after 24, 48, and 72 h treatment, respectively. These values was declined to 0.313, 0.297, and 0.246 μg/ml, which there was a 7923, 7811, and 6789-fold decrease for 24, 48, and 72 h treatment, respectively.

These results demonstrated that binding of CpG on DcMNPs increased the cytotoxicity of CpG by facilitating its cellular internalization. There might be several explanations for this observation. First of all, loading of CpG-ODN on the nanoparticles improve the delivery system by increasing the toxicity when inside tumor cells. The reduction in cytotoxicity of DcMNP can be explained by shielding of the positively charged amine groups to interact with negatively charged CpG molecules (Sadekar and Ghandehari 2012). CpG-loaded DcMNPs will make the system safer when in blood stream and more toxic when they are inside the tumor cells.

The cell proliferation assay demonstrated that CpG-bound DcMNPs were most effective on MCF7/Dox cells (Figure 3.25) since the highest decrease amount was seen in these cells.

It is worth noting that the IC_{50} values for unloaded DcMNPs are dedicated in mg, while the IC_{50} values for free CpG and CpG-loaded DcMNPs are given in µg (Table 3.2). Although unloaded DcMNPs could have cytotoxic effects at very high doses, the amounts of them utilized in this study for triggering cell death in cancer cells are non-toxic.

The results of a research carried out by Wu et al. showed that CpG-ODN 2216 of different concentrations (0.1, 0.5, 5 and 10 mg/mL) had inhibitory effects on pancreatic carcinoma cell line (PANC-1) and the IC_{50} at 24, 48, and 72 h was 65.1, 16.43 and 4.47 mg/mL, respectively (Wu et al. 2011).

3.9 Annexin V/PI Staining (Flow Cytometry)

To quantify cell apoptosis, the MDA-MB231, SKBR3, MCF7/S, and MCF7/Dox cells exposed to CpG-loaded DcMNP at concentrations of 0.5 µg/ml were stained using Annexin V-FITC/propidium iodide double-staining and analyzed by flow cytometry.

Three main populations of cells were distributed in dot-plots for viable cells Q3 (Annexin V-negative/propidium iodide-negative), early apoptotic cells Q4 (Annexin V-positive/propidium iodide-negative), and late apoptotic and necrotic cells Q2 (Annexin V-positive/propidium iodide-positive). In other words, to describe the selection of a subpopulation of cells for analysis, “Gating” is used. After gating, the lower left quadrant of the cytograms shows the viable cells, which exclude PI and are negative for FITC-Annexin V binding. The upper right quadrant represents the non-viable, late apoptotic and necrotic cells, positive for FITC-Annexin V binding and showing PI uptake. The lower right quadrant represents the early apoptotic cells, FITC-Annexin V positive and PI negative, demonstrating Annexin V binding and cytoplasmic membrane integrity.

Etoposide, an effective anti-cancer drug, is a topoisomerase II inhibitor which is used to treat the cells that were considered as positive control.

Figure 3.26, Figure 3.27, Figure 3.28, and Figure 3.29 indicate the flow cytometer results of Annexin V/PI staining for MDA-MB231, SKBR3, MCF7/S, and MCF7/Dox

cell lines, respectively. The plot A in each group indicate the untreated cells (negative control). According to the results, more than 93% of untreated cells were alive. The plot B show the etoposide-treated cells (positive control), which more than 25% of them were apoptotic after treatment. The result of treatment with free control CpG-ODN, free CpG-ODN, control CpG-loaded DcMNP, and CpG-loaded DcMNP were indicated in the plot C, D, E, F, and G, respectively.

The flow cytometer results of Annexin V/PI staining for MDA-MB231, SKBR3, MCF7/S, and MCF7/Dox cell lines were summarized as bar graphs in Appendix G.

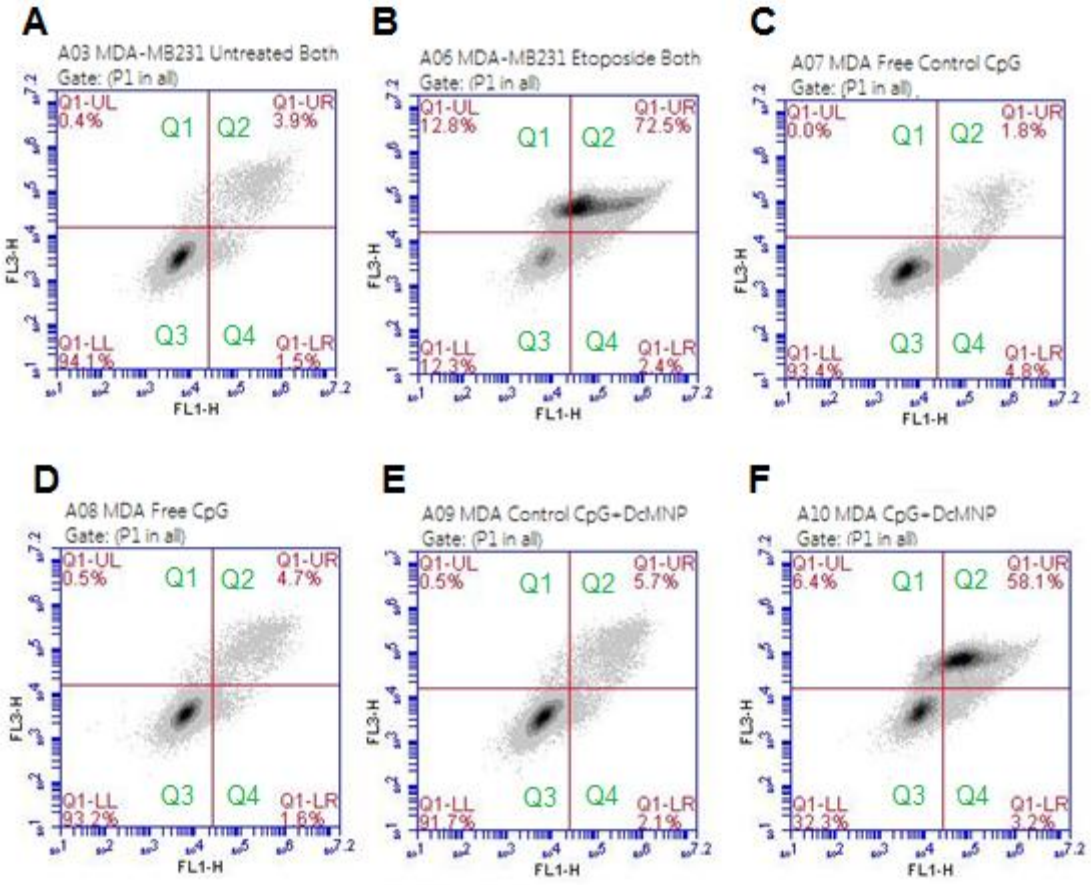

Figure 3.26 Flow cytometric analysis of MDA-MB231 cells by double labeling with Annexin V-FITC and PI. Quadrants are viable cells Q3 (Annexin V-negative/propidium iodide-negative), early apoptotic cells Q4 (Annexin V-positive/propidium iodide-negative), and late apoptotic and necrotic cells Q2 (Annexin V-positive/propidium iodide-positive). A) Negative control cells, B) Etoposide-treated positive control cells, 25 µM C) Free control CpG-treated cells, 0.5 µg/ml, 48 hours, D) Free CpG-treated cells, 0.5 µg/ml, 48 hours, E) Control CpG-DcMNP-treated cells, 0.5 µg/ml, 48 hours, F) CpG-DcMNP-treated cells, 0.5 µg/ml, 48 hours.

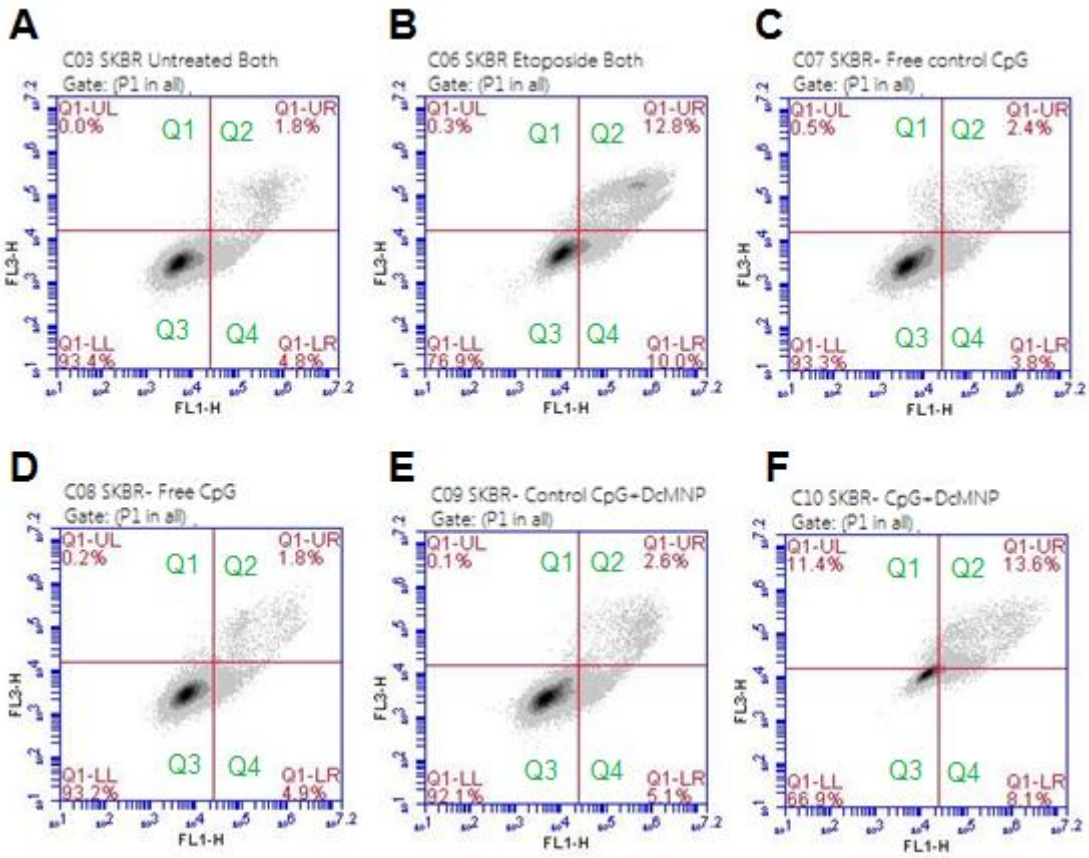

Figure 3.27 Flow cytometric analysis of SKBR3 cells by double labeling with Annexin V-FITC and PI. Quadrants are viable cells Q3 (Annexin V-negative/propidium iodide-negative), early apoptotic cells Q4 (Annexin V-positive/propidium iodide-negative), and late apoptotic and necrotic cells Q2 (Annexin V-positive/propidium iodide-positive). A) Negative control cells, B) Etoposide-treated positive control cells, 15 µM C) Free control CpG-treated cells, 0.5 µg/ml, 48 hours, D) Free CpG-treated cells, 0.5 µg/ml, 48 hours, E) Control CpG-DcMNP-treated cells, 0.5 µg/ml, 48 hours, F) CpG-DcMNP-treated cells, 0.5 µg/ml, 48 hours.

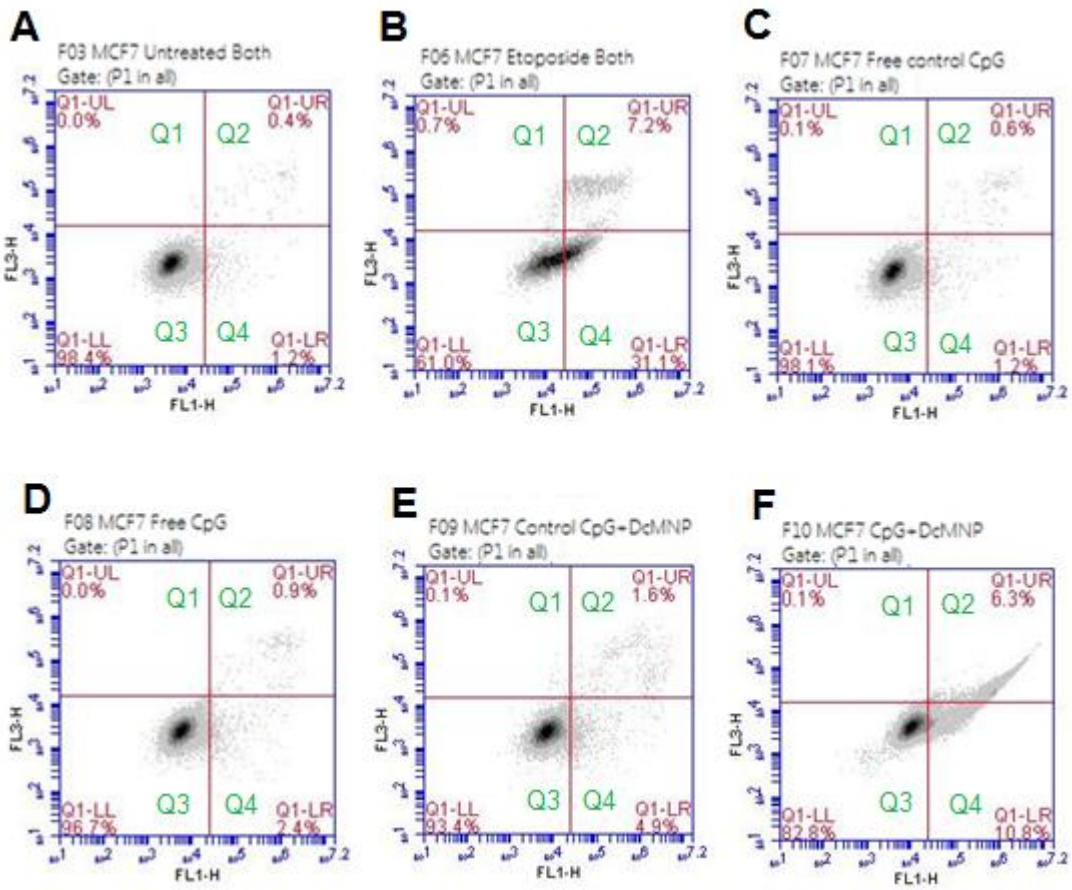

Figure 3.28 Flow cytometric analysis of MCF7 cells by double labeling with Annexin V-FITC and PI. Quadrants are viable cells Q3 (Annexin V-negative/propidium iodide-negative), early apoptotic cells Q4 (Annexin V-positive/propidium iodide-negative), and late apoptotic and necrotic cells Q2 (Annexin V-positive/propidium iodide-positive). A) Negative control cells, B) Etoposide-treated positive control cells, 42 µM C) Free control CpG-treated cells, 0.5 µg/ml, 48 hours, D) Free CpG-treated cells, 0.5 µg/ml, 48 hours, E) Control CpG-DcMNP-treated cells, 0.5 µg/ml, 48 hours, F) CpG-DcMNP-treated cells, 0.5 µg/ml, 48 hours.

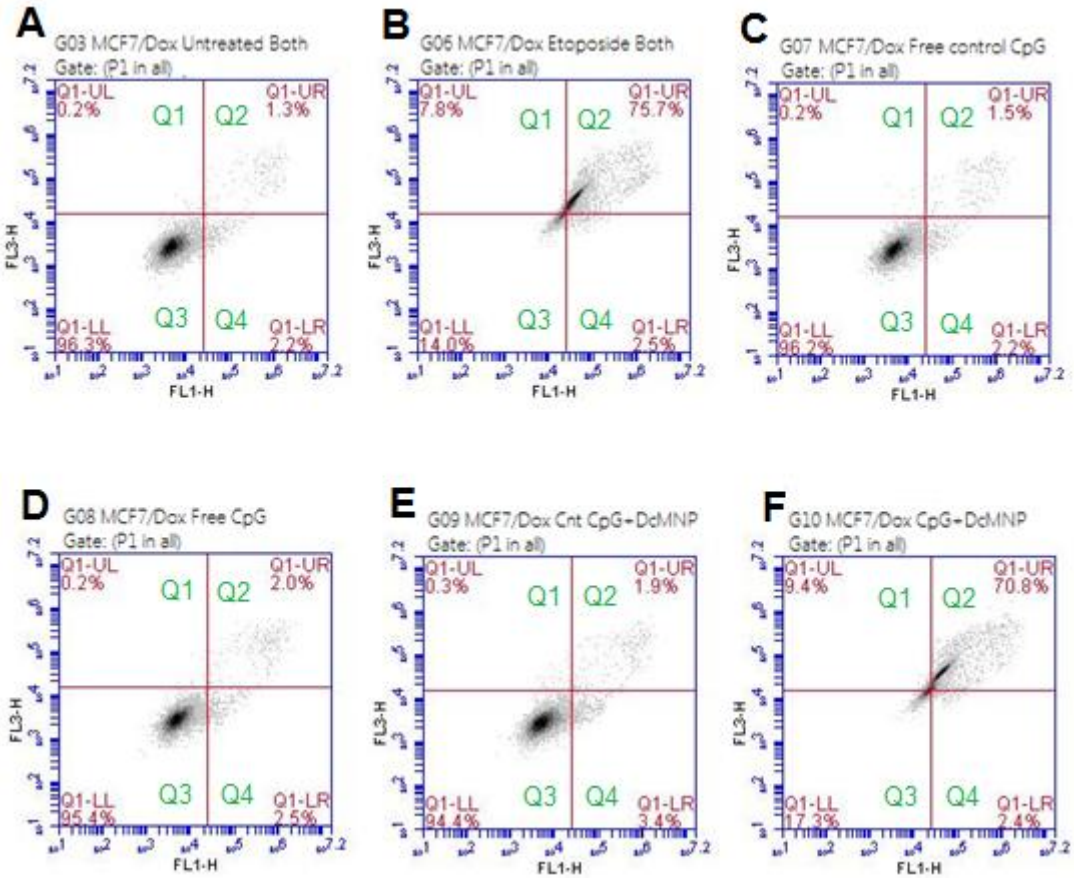

Figure 3.29 Flow cytometric analysis of MCF7/Dox cells by double labeling with Annexin V-FITC and PI. Quadrants are viable cells Q3 (Annexin V-negative/propidium iodide-negative), early apoptotic cells Q4 (Annexin V-positive/propidium iodide-negative), and late apoptotic and necrotic cells Q2 (Annexin V-positive/propidium iodide-positive). A) Negative control cells, B) Etoposide-treated positive control cells, 117 µM C) Free control CpG-treated cells, 0.5 µg/ml, 48 hours, D) Free CpG-treated cells, 0.5 µg/ml, 48 hours, E) Control CpG-DcMNP-treated cells, 0.5 µg/ml, 48 hours, F) CpG-DcMNP-treated cells, 0.5 µg/ml, 48 hours.

As it can be seen, significant difference in the percentages of the early, late apoptosis and necrotic cells was observed between CpG-loaded G_7DcMNP treated and other groups.

These results illustrated that the cellular death and apoptosis rate enhanced after treatment with the CpG-loaded G_7DcMNP. The amount of CpG-loaded G_7DcMNP which was used for treatment was set as IC_{50} value for MDA-MB231 cells (0.5 µg/ml CpG-ODN for 48h). At this condition, the cell death percent for MDA-MB231 cells was consistent with the results obtained from XTT assay. However, at this value, the cell death was lower in the case of SKBR3 and MCF7 cells, since the IC_{50} value for these cell lines was higher (0.732 and 0.925 µg/ml CpG-ODN, respectively) than IC_{50} value for MDA-MB231 cells. Since the IC_{50} value for MCF7/Dox cells (0.297 µg/ml CpG-ODN) was lower that for MDA-MB231 cells, more than 50% of the cells were undergone to cell death.

At this condition, the results of cell death percent for the cells were consistent with XTT assay data.

3.10 Apoptotic Gene Expression Analysis after Treatment with CpG-Loaded DcMNPs

3.10.1 Isolation of Total RNA

RNAs isolated from untreated and CpG-DcMNP treated (0.5 µg/ml) MDA-MB231, SKBR3, MCF7/S and MCF7/Dox cells were analyzed on 1% agarose gel prior to cDNA synthesis (Figure 3.30). The RNA samples were then tested by NanoDrop 2000 spectrophotometer (Thermo Fischer Scientific, USA) to examine the purity of sample (Table 3.3).

From isolated RNAs, cDNAs were synthesized which were used for qRT-PCR analysis.

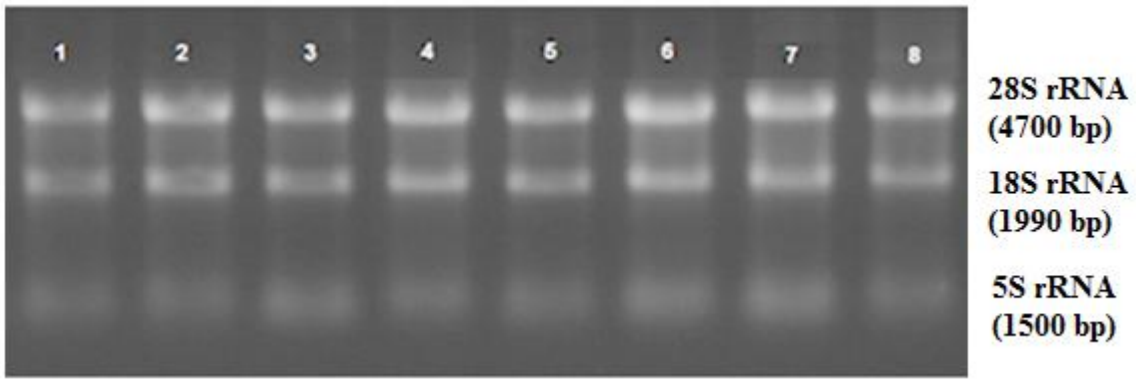

Figure 3.30 Total RNAs isolated from untreated MDA-MB231 cells (Lane 1), MDA-MB231 cells treated with 0.5 µg/ml CpG-DcMNP complex (Lane 2), untreated SKBR3 cells (Lane 3), SKBR3 cells treated with 0.5 µg/ml CpG-DcMNP complex (Lane 4), untreated MCF7 cells (Lane 5), MCF7 cells treated with 0.5 µg/ml CpG-DcMNP complex (Lane 6), untreated MCF7/Dox cells (Lane 7), and MCF7/Dox cells treated with 0.5 µg/ml CpG-DcMNP complex (Lane 8) on 1% agarose gel.

Table 3.3 Determination of RNA concentration (µg/ml) and the purity of sample using NanoDrop spectrophotometer.

	RNA concentration (µg/ml)	260/280	260/230
Untreated MDA-MB231 cells	693.2	2.197	1.898
MDA-MB231 cells treated with 0.5 µg/ml CpG-DcMNP	600.2	2.054	1.898
Untreated SKBR3 cells	586.5	1.889	1.908
SKBR3 cells treated with 0.5 µg/ml CpG-DcMNP	456.8	1.969	1.891
Untreated MCF7 cells	516.0	1.937	1.903
MCF7 cells treated with 0.5 µg/ml CpG-DcMNP	699.8	1.820	1.919
Untreated MCF7/Dox cells	832.6	1.897	1.925
MCF7/Dox cells treated with 0.5 µg/ml CpG-DcMNP	865.3	1.972	1.929

3.10.2 Quantitative Real-Time Polymerase Chain Reactin (qPCR): Expression analysis of *Bax, Noxa, Bcl-2, Survivin, Puma, C-Flip,* and *β-actin* genes

To elucidate the difference in apoptotic status between untreated and treated breast cancer cells, the expression pattern of apoptosis-related genes, *Bax, Noxa, Bcl-2, Survivin, Puma, C-Flip,* and *β-actin* genes in MDA-MB231, SKBR3, parental MCF7/S, and MCF7/Dox cell lines was examined by qRT-PCR before and after treatment of the cells with 0.5 µg/ml CpG-loaded DcMNPs for 48 h. Amplification curves were displayed as fluorescence vs. threshold cycle number (Appendix C).

Melting curve analysis was carried out after each run by measuring the signal which is generated from dissociation of DNA along with the rise of temperature. The presence of nonspecific amplification was tested by monitoring the dissociation kinetics of the qRT-PCR products (Appendix C).

Amplification products produced by a particular gene-specific primer had melting peaks at the same temperature, showing that only the expected products were amplified (Appendix C). The absence of melting peaks corresponding to other temperatures indicated that there was no generation of nonspecific products. The qRT-PCR products of *Bax, Noxa, Bcl-2, Survivin, Puma, C-Flip,* and *β-actin* genes were further examined by agarose gel electrophoresis (Appendix C).

Apoptosis is the orderly and tightly regulated cellular programmed cell death involving signal transduction pathways that induce cells to self-destruct during embryonic development, or in response to environmental hazards or anticancer therapeutics. The molecular mechanism for drug-induced apoptosis is associated with a mitochondrial dysfunction that is characterized by an increase in mitochondrial membrane permeability and a release of cytochrome c from mitochondria. The mitochondrial release of cytochrome c through anion channel is regulated by Bcl-2 and Bcl-xL, indicating that Bcl-2 plays a critical role in anticancer drug-induced apoptosis. Bcl-2 also interacts with the pro-apoptotic proteins Bax and Bak to block their pro-apoptotic activity, which is activated by apoptotic signals of anticancer drugs (Kim et al. 2004). In evaluation of expression analysis of *Bcl-2* and *Bax*, ratio of pro-apoptotic *Bax* to anti-apoptotic *Bcl-2*

expression was considered as an apoptotic parameter. According to Figure 3.31 and Figure 3.33, *Bcl-2/Bax* ratio increased with CpG-loaded DcMNPs stimulation at the mRNA level in MDA-MB231 and MCF7/Dox cells. This ratio altered 1.2 fold in MDA-MB231 cell line and 1.46 fold in MCF7/Dox cell line. Increased ratio might be correlated to enhanced apoptotic potential of MDA-MB231 and MCF7/Dox cells.

Puma and Noxa are two members of the Bcl-2 family that are also involved in pro-apoptosis. Puma plays an important role in *p53*-mediated apoptosis. It was shown that, *in vitro*, overexpression of *Puma* is accompanied by increased *Bax* expression, Bax conformational change, translocation to the mitochondria, cytochrome c release and reduction in the mitochondrial membrane potential (Liu et al. 2003). *Noxa* is also a candidate mediator of *p53*-induced apoptosis. Studies show that this protein can localize to the mitochondria and interact with anti-apoptotic Bcl-2 family members, resulting in the activation of caspase-9 (Oda et al. 2000). Since both *Puma* and *Noxa* are induced by *p53*, they might mediate the apoptosis (Meyer et al. 2006). A significant increase in the amount of *Noxa* mRNA expression has detected in treated MDA-MB231, MCF7, and MCF7/Dox cells which may contribute to apoptosis in these cell lines.

Survivin is considered as a member of the inhibitor of apoptosis protein (IAP) family which can bind to some caspases and then influence both the extrinsic and intrinsic caspase pathways. However, Survivin becomes prominently expressed in transformed cell lines and in all the most common human cancers of lung, colon, pancreas, prostate and breast, *in vivo* (Ambrosini et al. 1997), suggesting that during tumorigenesis, some changes commonly takes place in the regulation of *Survivin* gene. *Survivin* is expressed in G2-M in a cell cycle-dependent manner, and binds directly to mitotic spindle microtubules. Therefore, it could be suggested that Survivin plays an important role as an apoptotic checkpoint during cell division. In cancer therapy, Survivin is recommended as a new biomarker or therapeutic target. Survivin could essentially prevent apoptosis, especially it could directly inhibit caspases-3 and 7 (Nomi et al. 2010). The expression of *Survivin* was down-regulated in apoptotic pathway induced with CpG-loaded DcMNPs at the mRNA level in MDA-MB231. These results suggest that TLR9 might be a new therapeutic target for breast cancer patients.

No significant difference was found between the expression levels of *Bcl-2* (p=0.54), *Puma* (p=0.39), and *C-Flip* (p=0.28) in untreated and treated MDA-MB231 cells (Figure 3.31).

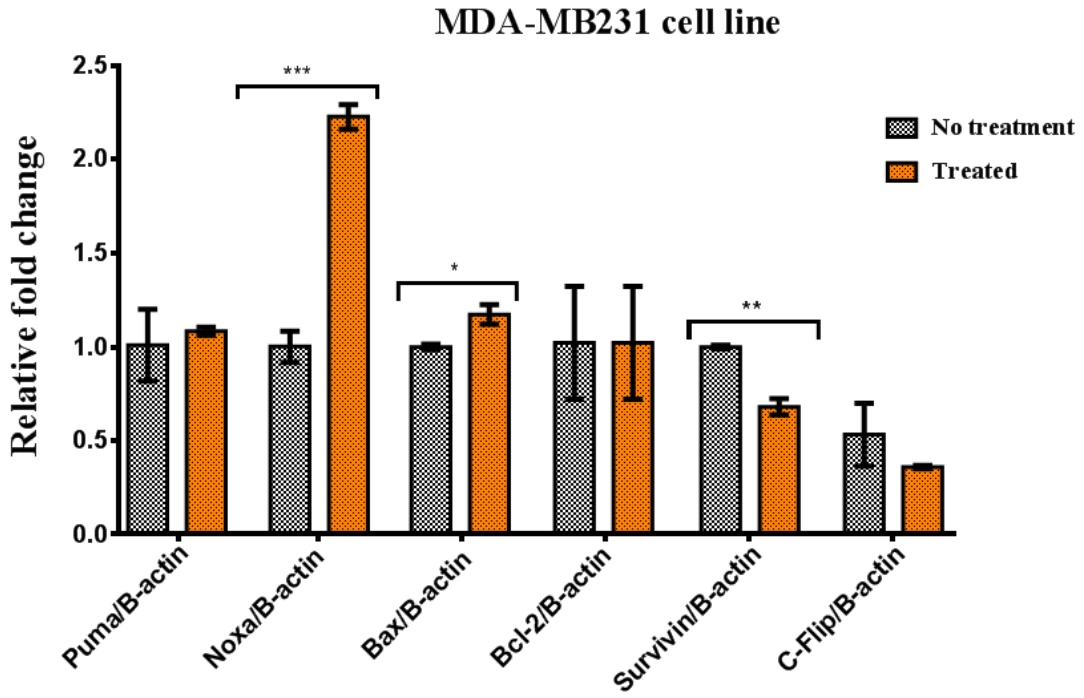

Figure 3.31 Expression levels of apoptotic-related genes in untreated and treated MDA-MB23 cell line with 0.29 mg/ml CpG-loaded DcMNPs for 48 h, when p<0.05.

The anti-apoptotic protein c-FLIP is a FLICE-inhibitory protein (C-Flip) which regulates activation of caspases-8 and -10 in the death receptor signaling pathways (Safa 2016). A significant decrease in the level of *C-Flip* mRNA was observed in SKBR3 and MCF7/Dox cells after stimulating with CpG-loaded DcMNPs (Figure 3.32 and Figure 3.33). *C-Flip* inhibits death receptor-induced apoptosis by interacting with the receptor-associated initiator caspase-8 and -10. It is a protein similar to caspase-8, but which lacks a catalytic domain, and which inhibits the activation mediated by Fas associated protein with death domain (FADD) protein by competitively interacting with caspase-8 and -10 (Lim et al. 2010). A decline in the *C-Flip* mRNA level in SKBR3 and MCF7/Dox cells could commit the cells to apoptosis.

No significant difference was found between the expression levels of *Puma* (p=0.06), *Noxa* (p=0.17), *Bax* (p=0.29), *Bcl-2* (p=0.53), and *Survivin* (p=0.90) in untreated and treated SKBR3 cells (Figure 3.32).

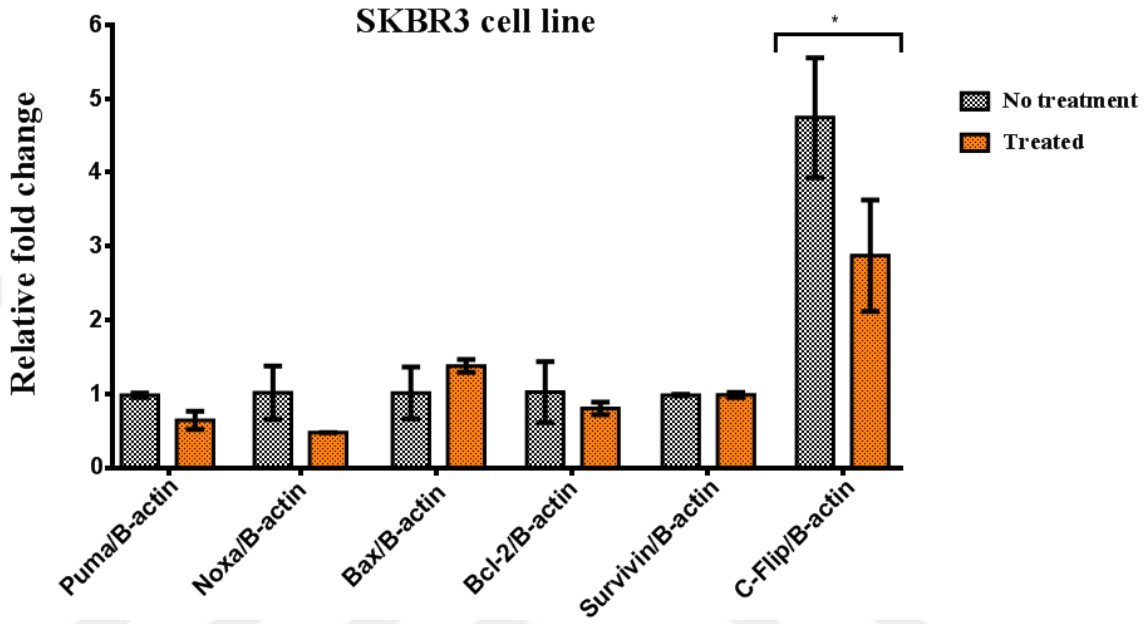

Figure 3.32 Expression levels of apoptotic-related genes in untreated and treated SKBR3 cell line with 0.29 mg/ml CpG-loaded DcMNPs for 48 h, when p<0.05.

No significant difference was found between the expression levels of *Puma* (p=0.19) in untreated and treated MCF7/Dox cells (Figure 3.32). However, the expression of *Survivin* was increased in MCF7/Dox cells, which its anti-apoptotic effect can be compensated by the effects of other proteins which lead the cell to the apoptosis.

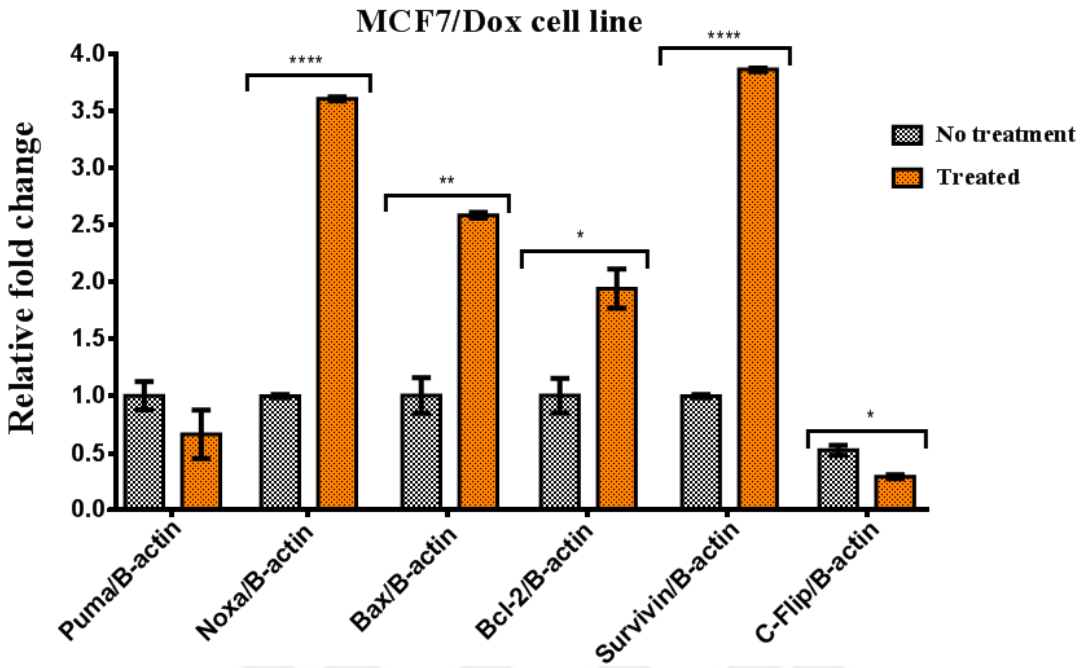

Figure 3.33 Expression levels of apoptotic-related genes in untreated and treated MCF7/Dox cell line with 0.29 mg/ml CpG-loaded DcMNPs for 48 h, when $p<0.05$.

Results indicated that *Noxa* was overexpressed in MCF7 cell line after stimulating with CpG-loaded DcMNPs (Figure 3.34).

No significant difference was found between the expression levels of *Puma* (p=0.24), *Bax* (p=0.40), *Bcl-2* (p=0.62), *Survivin* (p=0.12), and *C-Flip* (p=0.18) in untreated and treated MCF7 cells (Figure 3.34).

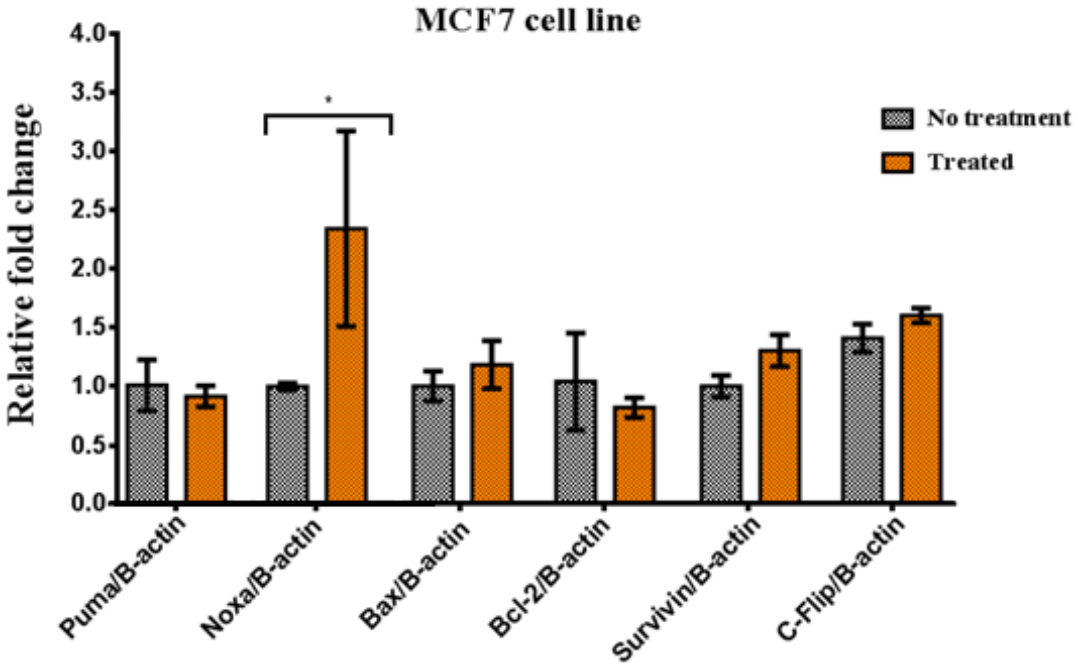

Figure 3.34 Expression levels of apoptotic-related genes in untreated and treated MCF7 cell line with 0.29 mg/ml CpG-loaded DcMNPs for 48 h, when $p<0.05$.

The results for expression levels of apoptotic-related genes in untreated and treated cell lines with 0.5 µg/ml CpG-loaded DcMNPs for 48 h were summarized in Table 3.4.

Table 3.4 Expression levels of apoptotic-related genes in untreated and treated MDA-MB231, SKBR3, MCF7, and MCF7/Dox cell lines. The amount of stars show how significant is the difference.

	MDA-MB231	SKBR3	MCF7	MCF7/Dox
Puma (Pro-apoptotic gene)	-	-	-	-
Noxa (Pro-apoptotic gene)	↑ ***	-	↑ *	↑ ****
Bax (Pro-apoptotic gene)	↑ *	-	-	↑ **
Bcl-2 (Anti-apoptotic gene)	-	-	-	↑ *
Survivin (Anti-apoptotic gene)	↓ **	-	-	↑ ****
C-Flip (Anti-apoptotic gene)	-	↓ *	-	↓ *

3.11 Enzyme-Linked Immunosorbent Assay (ELISA): Changes in secreted IL-6, TNF-α, and IL-10 levels

It was previously shown in internalization assays that CpG-DcMNPs are taken up by the MDA-MB231, SKBR3, MCF7, and MCF7/Dox cells after 5 h (13.4.6), so the release of IL-6, TNF-α, and IL-10 after stimulation with unloaded DcMNP, free CpG-ODN (1, 2, and 3 µM), and CpG-loaded DcMNP (1, 2, and 3 µM) for 14 and 24 h was assessed using ELISA on supernatants from stimulated cells. Based on the demonstrated uptake of unloaded-DcMNP and CpG-loaded DcMNP after 5 h, this time period is considered to be sufficient for stimulation of the cells. Finally, expression of the cytokines was compared to control untreated cells.

Figure 3.35 represents the amount of IL-6 secreted to medium by MDA-MB231, SKBR3, parental MCF-7, and MCF7/Dox cell lines. All of these cells secrete some amount of IL-6; however, MCF7 cell line was found to release very low amount of IL-6 to medium (0.277 ng/ml after 14h and 0.283 ng/ml after 24h).

This is supported by previous results of our group that there is very low expression of IL-6 by MCF7 cells. However, upon developing resistance to doxorubicin, those cells begin to express and secrete IL-6 (Cakmak 2013).

In a study carried out by Conze et al., it was stated that breast cancer cells that are sensitive to drug treatment do not express IL-6, whereas high levels of IL-6 are produced by multidrug-resistant breast cancer cells. The results indicated that IL-6 can be produced by some tumor cells in breast cancer patients (Conze et al. 2001).

Our results are in consistent with the data obtained from the study performed by Hartman et al. which indicates that triple-negative breast cancer (e.g. MDA-MB231 cell line) express high amounts of IL-6 cytokine (Hartman et al. 2013).

In the case of MDA-MB231 cells, after treatment of the cells with 2 and 3 µM CpG-bound DcMNPs, it could be seen a significant increase in the amount of released IL-6. However, an enhancement was indicated in the case of treating with 1 µM CpG-bound DcMNPs for 14h. Although after stimulation with 2 µM (only for 14 h) and 3 µM free CpG, there was also an increase, but it can be compared with treatment of the cells with 2 and 3 µM CpG-bound DcMNPs.

For SKBR3 cell line, there was a rise only after 24 h stimulation with 1, 2, and 3 µM CpG-bound DcMNPs.

In MCF7 cells, no significant change was indicated after treatment except for 2 µM CpG-bound DcMNPs after 24h. However, it was changed to 3 µM CpG-bound DcMNPs after 24h in the case of MCF7/Dox cell line.

In conclusion, the enhancement of IL-6 release after treating with CpG-DcMNP was higher for MDA-MB231 and SKBR3 cells. This could be related to the high expression

of TLR9 gene in these cell lines, so the cells could be highly stimulated by CpG molecules.

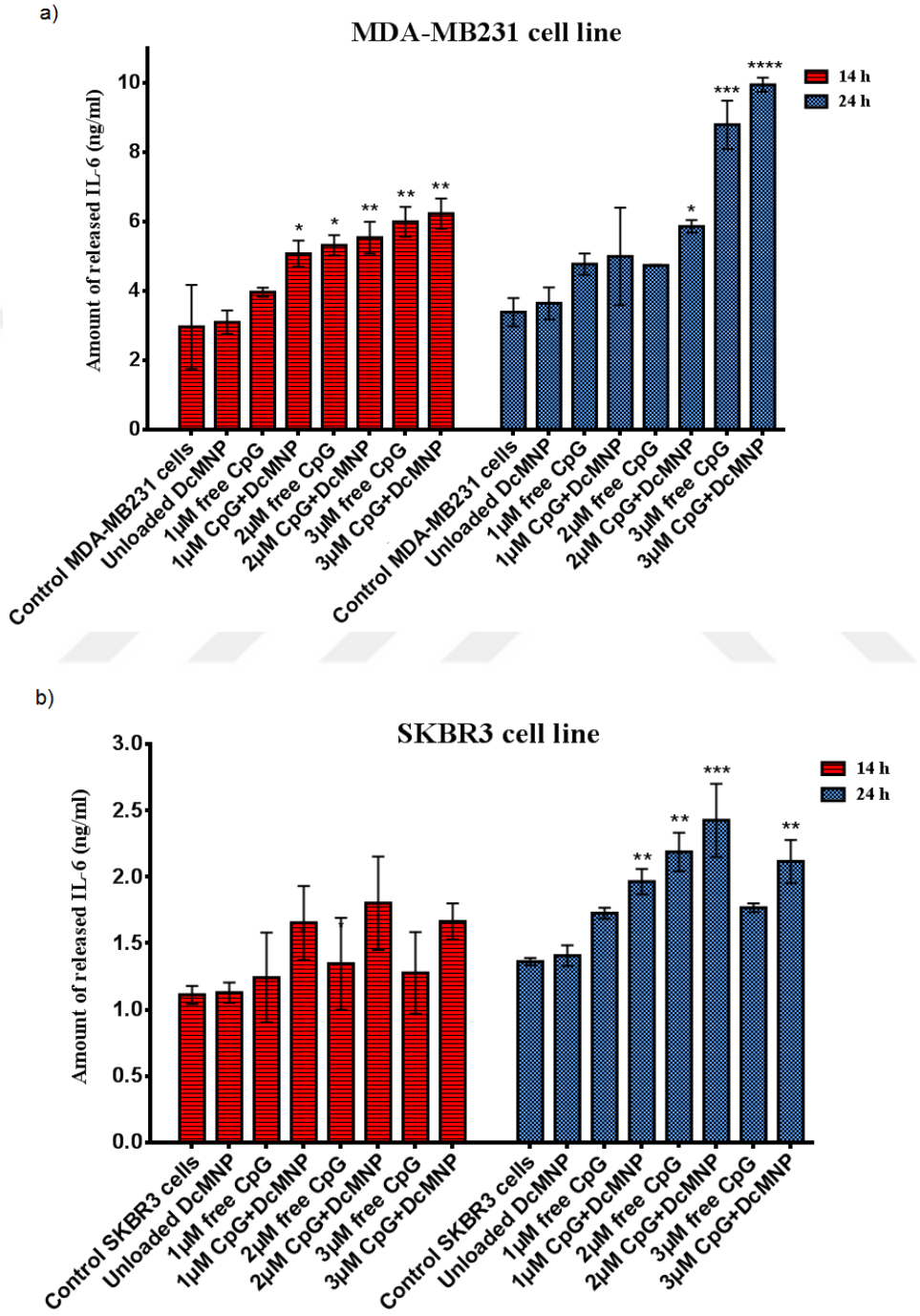

Figure 3.35 Quantification of released IL-6 in a) MDA-MB231, b) SKBR3, c) MCF7, and d) MCF7/Dox cell lines. Each bar graph in the 14 and 24 h groups is compared to the control cells. (Continued)

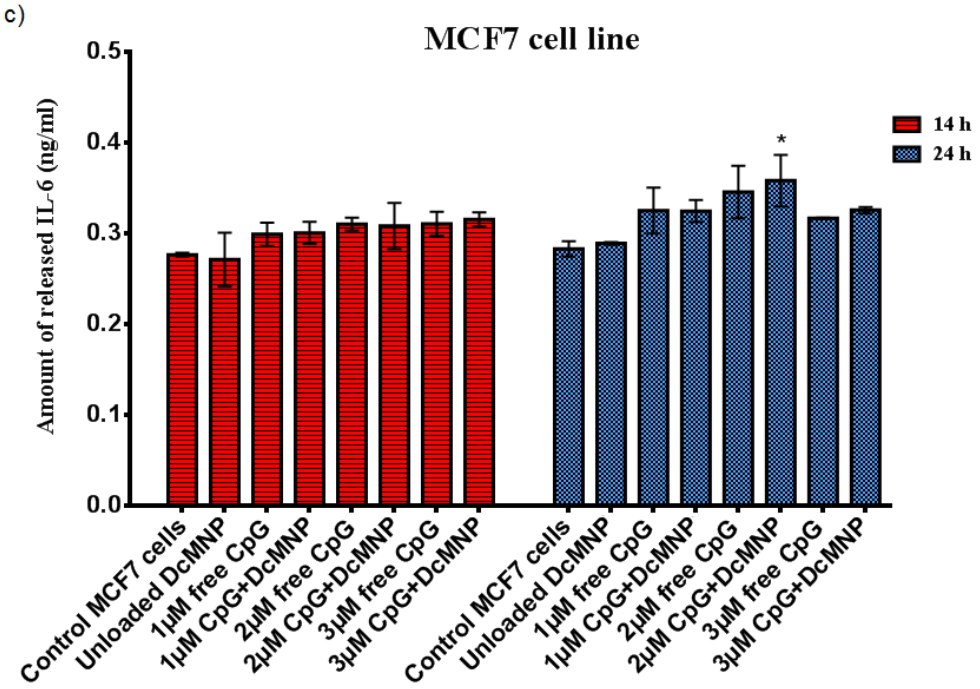

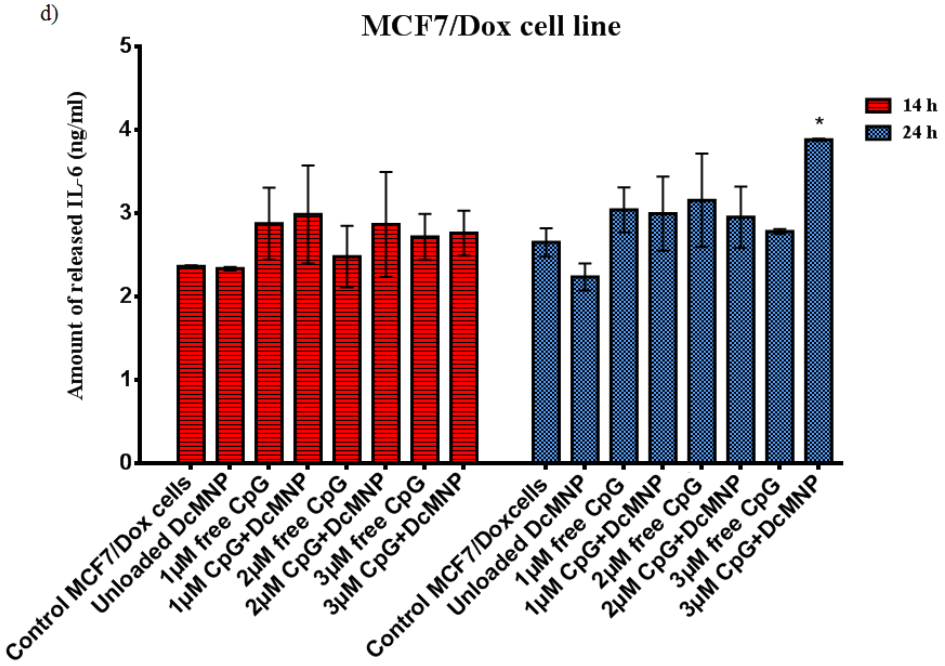

Figure 3.35 Quantification of released IL-6 in a) MDA-MB231, b) SKBR3, c) MCF7, and d) MCF7/Dox cell lines. Each bar graph in the 14 and 24 h groups is compared to the control cells. (Continued)

In a research, it was indicated that Interleukin-6 is able to inhibit growth of breast carcinoma cells in culture. Interleukin-6 exerts its activity through the membrane-bound receptor complex consisting of IL-6 binding protein (IL-6R, α-subunit and glycoprotein 130, gp130, β-subunit that functions as a signal transducer). Interleukin-6 first binds to IL-6R and then the complex attracts gp130 molecules that dimerize leading to a signal transduction. They also have found that expression of IL-6, gp130, and IL-6R in the tumor microenvironment is correlated with a favorable prognosis. Finally, they concluded that expression of IL-6, IL-6R, and gp130 in breast carcinoma tissue is associated with less advanced stages of the disease. Expressions of IL-6 and its receptor subunits, IL-6R and gp130, in cancer tissue are correlated and the presence of their specific transcripts (mRNAs) is a remarkable positive prognostic factor (Karczewska et al. 2000).

There is increasing evidence pointing to a role for IL-6 as a regulator of cancer cell proliferation. IL-6 treatment results in different biological responses, depending on the target cell type. Indeed, whereas IL-6 stimulates proliferation of myeloma/plasmocytoma, renal cell carcinoma, or Kaposi's sarcoma cells, it inhibits the growth of cells derived from melanomas and lung or breast carcinomas. In another study done by Badache and Hynes, they have found that IL-6-type cytokines inhibit T47D cell proliferation and they have delineated IL-6-induced signaling pathways in the T47D breast carcinoma cell line. It is found in this study that biological effects are mediated by independent pathways involving STAT3 activity (Figure 3.36). In the cells, the biological effect of IL-6 depends on the balance of a growth-inhibitory STAT3-dependent pathway and a growth-promoting MAPK/PI3K-dependent pathway (Badache and Hynes 2001).

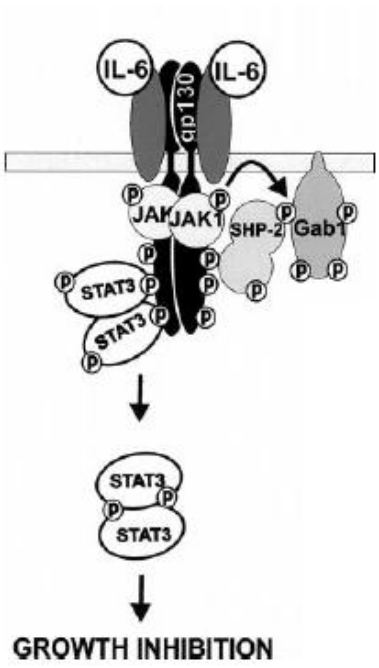

Figure 3.36 Model for the role of the EGF receptor in IL-6-induced STAT3 signaling.

K-type ODN (K-ODN), which have progressed into human clinical trials as vaccine adjuvants and immunotherapeutic agents, are strong activators of B cells and trigger plasmacytoid dendritic cells (pDCs) to differentiate and produce TNF-α through the TLR9-MyD88-IRF5 pathway (Gungor et al. 2014). TNF-α is primarily expressed by macrophages and monocytes, but is also expressed by neutrophils, NK-cells, mast-cells, endothelial cells, activated lymphocytes, and various tissue-specific cell types including certain cancers (Seruga et al. 2008).

Although, the MyD88-coupled TLRs induce the synthesis of cytokines such as TNF-α, IL-6, and IL-1, breast cancer cells, MDA-MB231, SKBR3, parental MCF-7, and MCF7/Dox cell lines, release very low amounts of TNF-α. Recent investigations strongly suggest that the chronic expression of TNF-α in breast tumors actually supports tumor growth (Ben-Baruch 2003). As it was indicated that patients with more progressed tumor phenotypes were shown to have significantly higher TNF-α serum concentration, it can be accepted as a promising result that the fore-mentioned cells express low amounts of TNF-α (Figure 3.37).

After treating with CpG-bound DcMNPs, there was not a significant change in the amount of TNF-α release in the MDA-MB231 cells except for treating with 1 µM CpG-bound DcMNPs for 24 h.

In the case of SKBR3 cell line, released TNF-α value declined after treating with 1 µM CpG-bound DcMNPs (14 h) and with unloaded DcMNP (14 and 24 h).

However, no change was detected in sensitive and MCF7/Dox cells after any treatments except for 2 µM free CpG in MCF7/Dox (14 h).

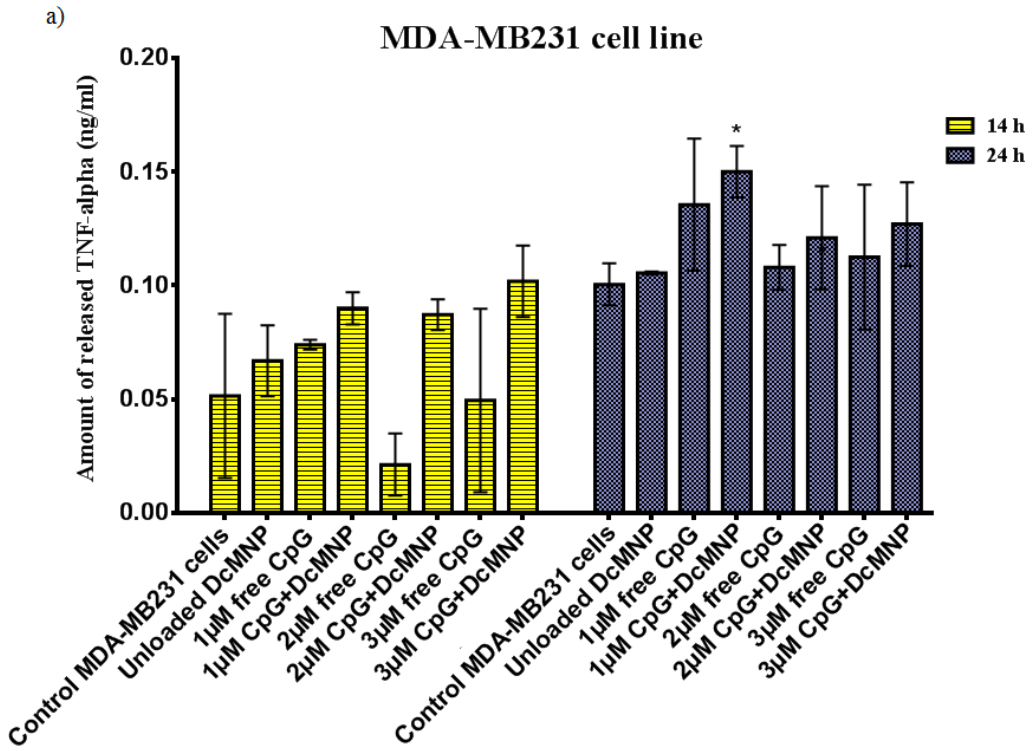

Figure 3.37 Quantification of released TNF-α in a) MDA-MB231, b) SKBR3, c) MCF7, and d) MCF7/Dox cell lines. Each bar graph in the 14 and 24 h groups is compared to the control cells. (Continued)

b)

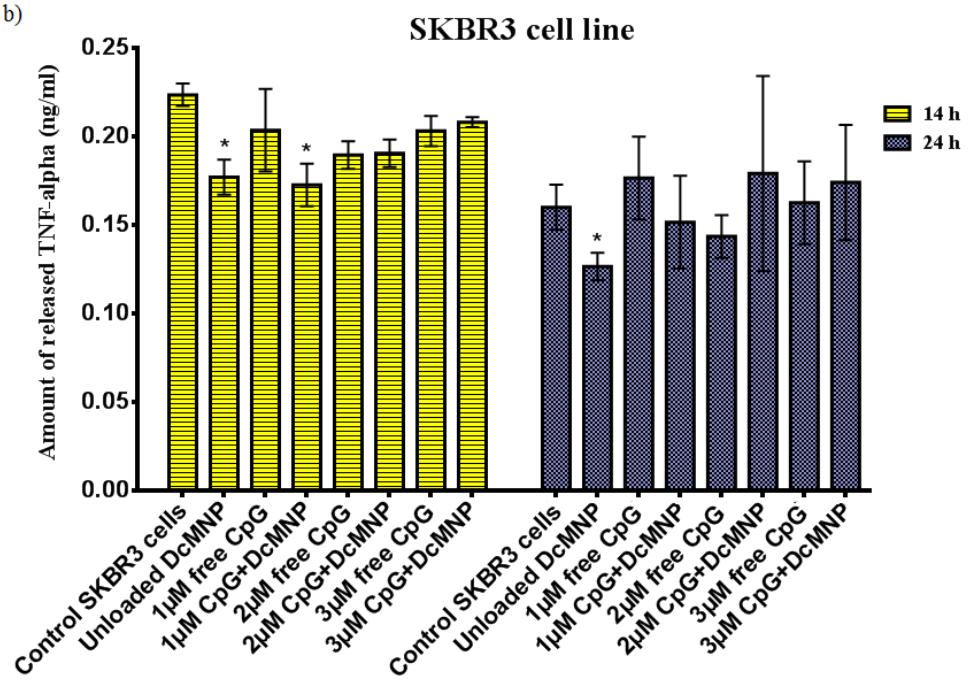

c)

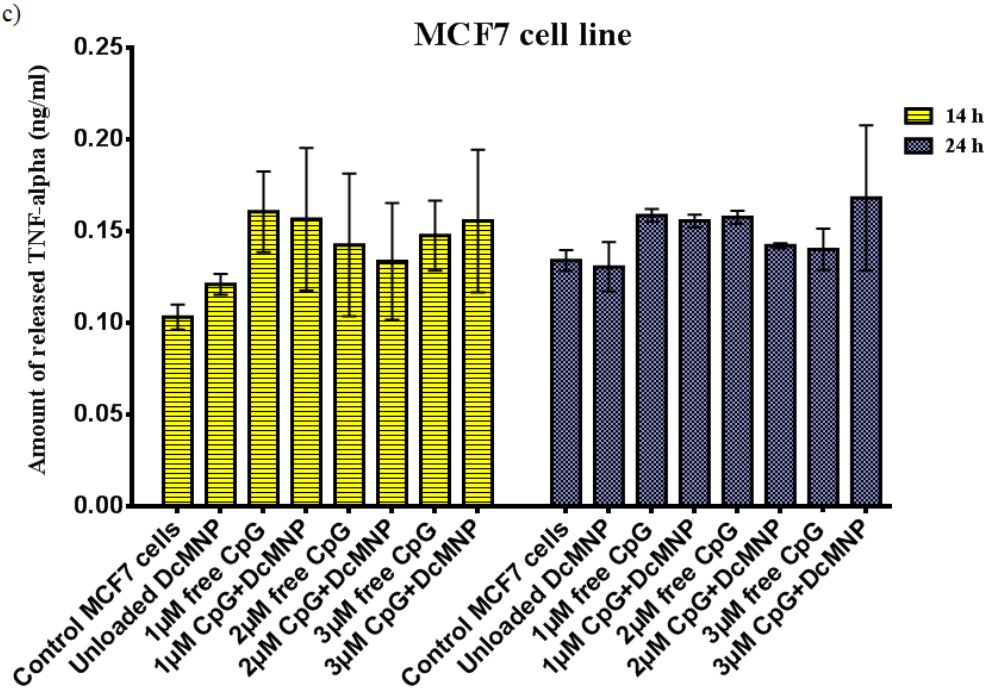

Figure 3.37 Quantification of released TNF-α in a) MDA-MB231, b) SKBR3, c) MCF7, and d) MCF7/Dox cell lines. Each bar graph in the 14 and 24 h groups is compared to the control cells. (Continued)

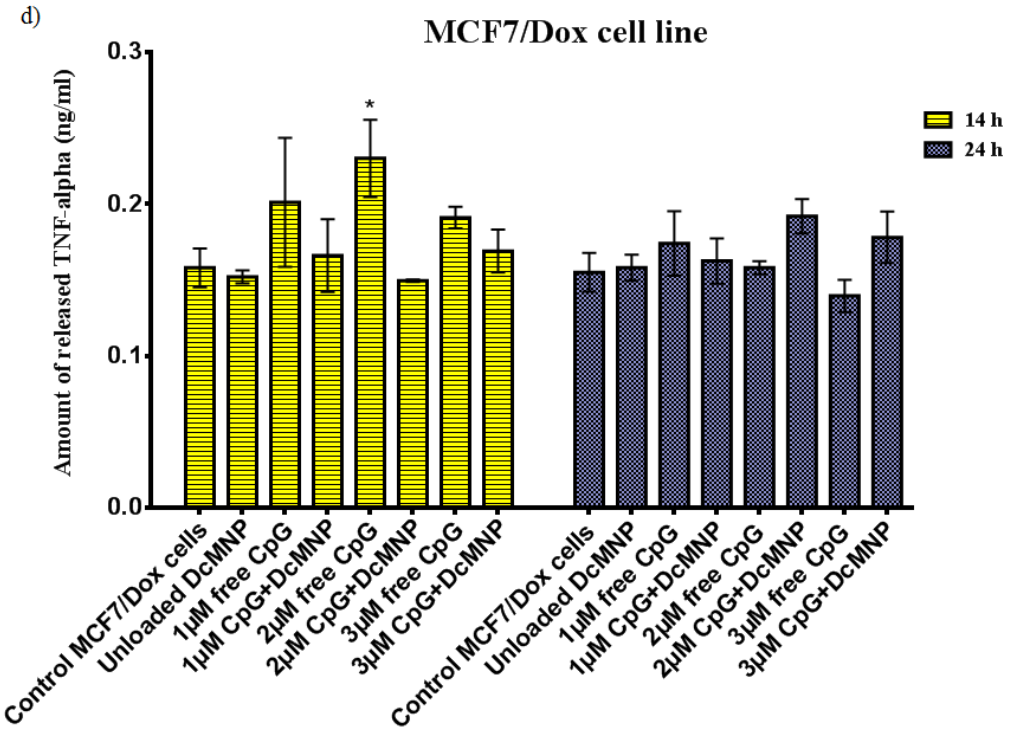

Figure 3.37 Quantification of released TNF-α in a) MDA-MB231, b) SKBR3, c) MCF7, and d) MCF7/Dox cell lines. Each bar graph in the 14 and 24 h groups is compared to the control cells. (Continued)

There was no significant increase triggered by any treatment in IL-10 concentration in any cell line (Figure 3.38). While supernatants of untreated MDA-MB231 and SKBR3 cells featured 0.006 and 0.012 ng/ml after 24 h respectively, IL-10 concentrations of treated MDA-MB231 and SKBR3 lay below in the case of 24h. IL-10 concentration was below the detection threshold in MCF7 (24 and 48 h) and MDA-MB231 (24 h), consequently could not be evaluated. In MCF7/Dox (24 and 48 h) and SKBR3 (24 h), there was not any significant change in the amount of released IL-10. It can be concluded that IL-10 release amount did not differ significantly with applying any of the fore-mentioned treatments on the cells.

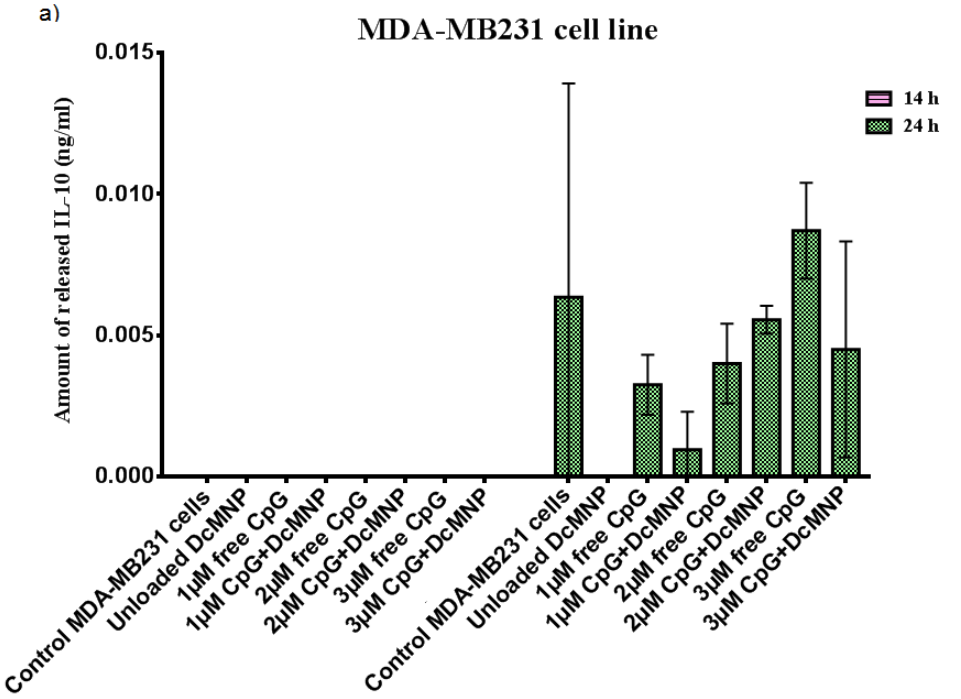

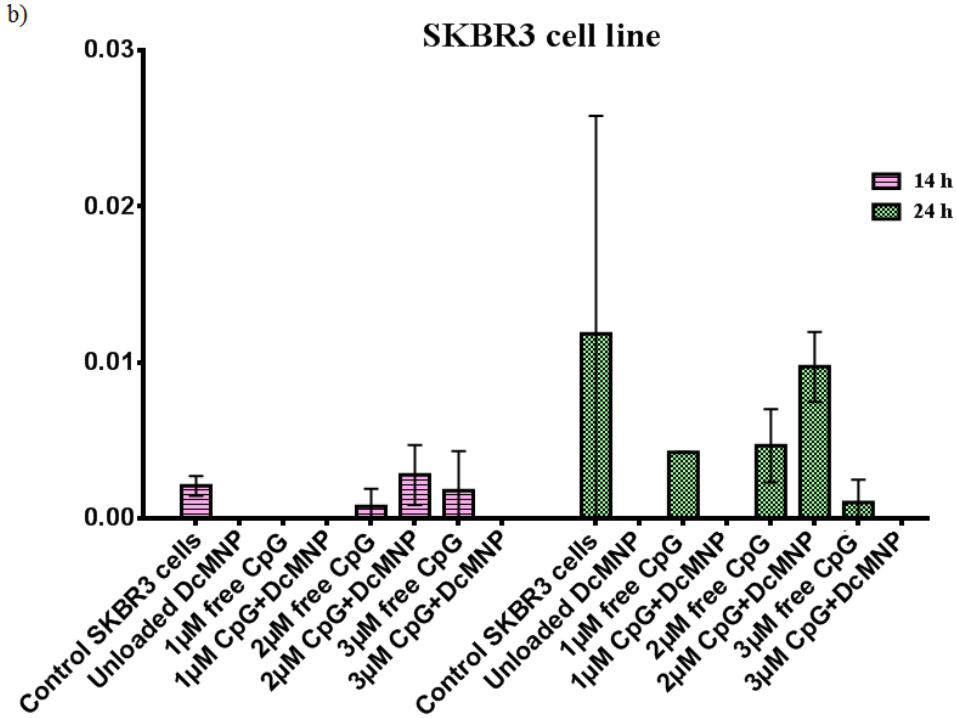

Figure 3.38 Quantification of released IL-10 in a) MDA-MB231, b) SKBR3, c) MCF7, and d) MCF7/Dox cell lines. Each bar graph in the 14 and 24 h groups is compared to the control cells. (Continued)

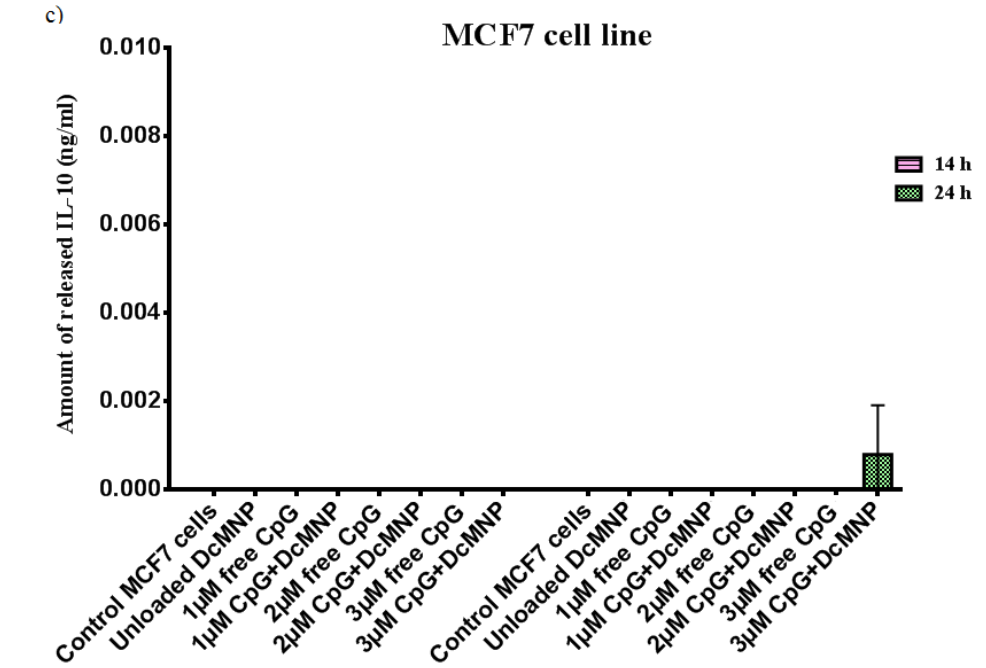

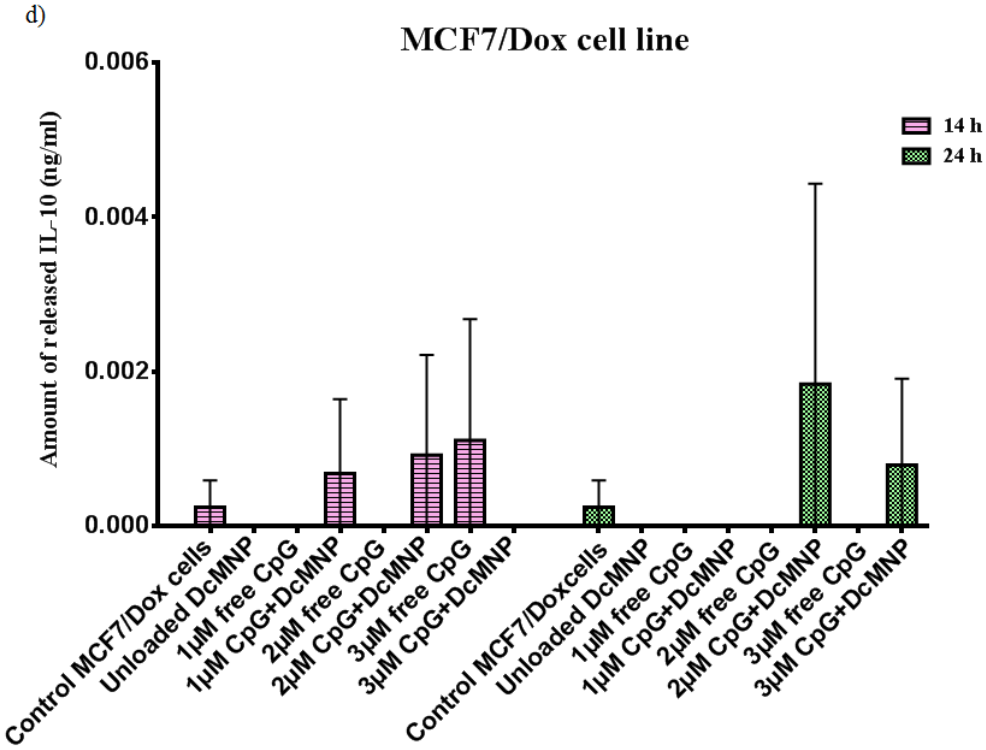

Figure 3.38 Quantification of released IL-10 in a) MDA-MB231, b) SKBR3, c) MCF7, and d) MCF7/Dox cell lines. Each bar graph in the 14 and 24 h groups is compared to the control cells. (Continued)

Since IL-10, a pleiotropic anti-inflammatory cytokine, induces immunosuppression and assists in escape from tumor immune surveillance, it can be adopted as a promising result that none of the cells released significant higher amount of IL-10 after treatment.

The mode of attachment of the CpGs to the nanoparticle can play an important role in the activity of the CpGs. In a recent report, it was found that when a class-B CpG was randomly adsorbed to a silica nanoparticle, the activation of IL-6 in peripheral blood mononuclear cells was attenuated and the activation of IFN-α was dramatically enhanced. However, when the same CpG sequence was coated onto the same nanoparticles via a linker that enforced a regular orientation of the oligonucleotides, the opposite outcome was observed, with enhanced IL-6 production and no activation of IFN-a. It is clear that as CpG delivery by nanoparticles is developed, a number of functionalization strategies will have to be evaluated for each nanoparticle (Badie and Berlin 2013).

Preclinical and early clinical experiments indicate that synthetic unmethylated CpG-ODN have potent immunostimulatory effects and can increase the anticancer activity of a variety of cancer treatments (Jahrsdorfer and Weiner 2008). CpG-ODN has to be delivered intracellularly into endosomes in order to bind to TLR9. The loading of CpG-ODN onto magnetic nanoparticles is an important tool for successful transfer of the CpG-ODN to the tumor. Endocytosis of these nanoparticles leads them directly to the endosomal sites (Pan, Gao, and Gu 2005; Pan et al. 2007c). In order to prevent their rapid clearance by nucleases, there is a need for carrier systems for CpG-ODN treatment. There are reports about the loading of the CpG-ODN on various nanoparticles which are described below; however they utilized neither iron oxide magnetic nanoparticles nor PAMAM dendrimers.

Previously, a CpG-ODN/gold nanoparticle conjugates were designed to target innate immune cells *in vitro* and *in vivo* in order to organize an anti-tumor immune response (Lin et al. 2013). They demonstrated that CpG conjugated gold nanoparticles significantly increase the macrophage stimulation *in vitro* and inhibit tumor growth *in vivo* when compared to treatments with the equivalent dose of free CpG. The antitumor effect of these conjugates is potent and there is no need for combination treatment,

suggesting that these complexes are clinically applicable and can be used for CpG monotherapy.

In another study, CpG motifs were appended to the functionalized silver nanoclusters (AgNCs) that exhibit high immunostimulatory activity while simultaneously acting as an imaging agent (Tao et al. 2013). The results indicated that the cellular internalization of these conjugates is easier than free CpG-ODNs. Additionally, the bioactivity of the CpG-ODN was enhanced, since conjugation of CpG on AgNCs effectively protects them from nuclease degradation.

Shukoor et al. performed the immobilization of CpG-ODN on manganese oxide (MnO) nanoparticles using a multifunctional polymer (Shukoor et al. 2009b; Shukoor et al. 2012). The synthesized conjugates were incubated with Caki-1 (human kidney cancer) cells and the targeting and TLR9 cascade activation potential of these CpG-ODN-loaded nanoparticles were evaluated. The findings suggest a contribution of TLR9 triggered NF-kB signaling pathway in these cell lines.

Zhi et al. synthesized boron nitride nanospheres (BNNSs) and adopted it for delivering CpG-ODN into cells for activation of TLR9 (Zhi et al. 2011). They demonstrated that BNNSs can easily be taken into cells and located in the lysosome compartments. The results of their study showed that CpG-ODN loaded BNNSs exhibited significantly higher NF-kB activity compared with free CpG-ODNs and can be used as carriers of CpG-ODN to activate TLR9. In order to increase the loading of CpG-ODN onto BNNS and cellular uptake efficiency of CpG-ODN, the boron nitride nanospheres were coated with chitosan (Zhang et al. 2013). It was indicated that chitosan-coated BNNS/CpG oligodeoxynucleotide complexes induced approximately two-fold higher amounts of cytokines than chitosan/CpG oligodeoxynucleotides because of the improved cellular uptake of CpG oligodeoxynucleotides.

CHAPTER 4

CONCLUSIONS

The main goal of this study was to synthesize PAMAM dendrimer-coated magnetic nanoparticles and evaluate their binding potential to CpG-ODN molecules. Biocompatibility and selective targeting to the desired cell or tissue under the guidance of external magnetic field are the major characteristics of these nanoparticles.

The core of prepared nanoparticles comprised magnetite (Fe_3O_4), which had superparamagnetic characteristics. The core was modified with aminosilane layer and then, coated with PAMAM dendrimer. The polymer coating not only affords a protective organic biocompatible shell but also provides an efficient and convenient means for loading immunostimulatory oligonucleotides, CpG-ODN. Synthesized DcMNPs had an average particle diameter of 40±10 nm and a spherical shape.

The interaction of prepared DcMNPs and CpG-ODN was studied for the first time in this investigation, and it was indicated that the DcMNPs had great ability to form a complex with CpG-ODN and showed suitable physicochemical properties for a CpG delivery system. The results, coupled with the high internalization and apoptotic characteristics of these conjugates for breast cancer cells, make DcMNPs attractive candidates for further *in vivo* study in the context of targeted delivery agents of CpG-oligonucleotides.

Additionally, these CpG-loaded DcMNPs may provide many advantages for *in vivo* applications, which include extending circulation life time, increasing the accessibility of CpG-ODN to the tumor cells and enhancing effective concentration at target site and therefore these could be considered as effective options for targeting and treatment of the tumor.

In vitro cytotoxicity study on MDA-MB231, SKBR3, MCF7, and MCF7/Dox breast cancer cell lines indicated that CpG-bound DcMNPs are more effective than free CpG. The most efficient cytotoxicity of CpG-bound DcMNPs was observed in MCF7/Dox cells. CpG-bound DcMNPs application seems to be a suitable replacement anticancer drug for the treatment of breast cancer cells. Flow cytometry results validated the data obtained from XTT assay, which also indicates that CpG-bound DcMNPs could be considered as an efficient therapeutic delivery system for breast cancer treatment.

In order to clarify the apoptotic pathway by which the breast cancer cells undergo apoptosis, the expression patterns of apoptosis-related genes, *Bax, Noxa, Bcl-2, Survivin, Puma, C-Flip,* and *β-actin* genes in MDA-MB231, SKBR3, parental MCF7/S, and MCF7/Dox cell lines were examined by qRT-PCR before and after treatment of the cells with CpG-loaded DcMNPs. In evaluation of expression analysis of *Bcl-2* and *Bax*, ratio of pro-apoptotic *Bax* to anti-apoptotic *Bcl-2* expression was considered as an apoptotic parameter. This ratio altered 1.2 fold in MDA-MB231 cell line and 1.46 fold in MCF7/Dox cell line. Increased ratio might be correlated to enhanced apoptotic potential of MDA-MB231 and MCF7/Dox cells. Down-regulation of *Survivin* gene and up-regulation of *Noxa* gene may contribute to apoptosis in MDA-MB231 cell line.

A significant decrease in the level of *C-Flip* mRNA was observed in SKBR3 and MCF7/Dox cells after stimulating with CpG-loaded DcMNPs which could commit the cells to apoptosis.

Noxa is also a candidate mediator of *p53*-induced apoptosis. A significant increase in the amount of *Noxa* mRNA expression has detected in treated MDA-MB231, MCF7, and MCF7/Dox cells which may contribute to apoptosis in these cell lines.

The expression of *Survivin* was down-regulated in apoptotic process with CpG-loaded DcMNPs stimulation at the mRNA level in MDA-MB231. These results suggest that TLR9 might be a new therapeutic target for breast cancer patients.

IL-6 was overexpressed in the cells. In the case of MDA-MB231 cells, after treatment of the cells with 2 and 3 µM CpG-bound DcMNPs, it could be seen a significant increase in the amount of released IL-6. For SKBR3 cell line, there was a rise only after 24 h

stimulation with CpG-bound DcMNPs. In MCF7 cells, no significance was determined except for treatment with 2 µM CpG-bound DcMNPs after 24h. However, it was changed to 3 µM CpG-bound DcMNPs after 24h in the case of MCF7/Dox cell line.

After treating with CpG-bound DcMNPs, there was an increase in the amount of TNF-α release in the MDA-MB231 cells. In the case of SKBR3 cell line, released TNF-α value declined after treating with CpG-bound DcMNPs (14 h) and with unloaded DcMNP (14 and 24 h). However, no change was detected in sensitive and MCF7/Dox cells after any treatments except for 2 µM free CpG in MCF7/Dox (14 h).

In addition, stimulation of the cells with CpG-DcMNPs did not resulted in a significant increase of IL-10 production.

In conclusion, according to these results, the synthesized CpG-loaded magnetic nanoparticles offer the potential to achieve selective and efficient delivery of CpG-ODN by using external magnetic fields. Moreover, CpG-ODN-loaded DcMNP could be utilized in various therapeutic applications such as adjuvants for use with vaccines.

REFERENCES

Ambrosini, G., Colette, A., and Dario C., A. (1997). A Novel Anti-Apoptosis Gene, Survivin, Expressed in Cancer and Lymphoma. *Nature Medicine*, 3 (8): 917–21. doi:10.1038/nm0897-917.

Asgeirsson, K., Olafsdottir, K., Jonasson, J. G., and Ogmundsdottir, H. M., (1998). The Effects of IL-6 on Cell Adhesion and E-Cadherin Expression in Breast Cancer. *Cytokine*, 10 (9): 720–28. doi:10.1006/cyto.1998.0349.

Astruc, D., Liang, L., Rapakousiou, A., and Ruiz, J. (2012). Click Dendrimers and Triazole-Related Aspects: Catalysts, Mechanism, Synthesis, and Functions. A Bridge between Dendritic Architectures and Nanomaterials. *Accounts of Chemical Research*, 45 (4): 630–40. doi:10.1021/ar200235m.

Badache, A., and Hynes, N. E. (2001). Interleukin 6 Inhibits Proliferation and, in Cooperation with an Epidermal Growth Factor Receptor Autocrine Loop, Increases Migration of T47D Breast Cancer Cells. *Cancer Research*, 61 (1): 383–91.

Badie, B., and Berlin, J. M. (2013). The Future of CpG Immunotherapy in Cancer. *Immunotherapy*, 5(1): 1-3. doi: 10.2217/imt.12.148.

Balkwill, F. (2006). TNF-A in Promotion and Progression of Cancer. *Cancer and Metastasis Reviews*, 25 (3): 409–16. doi:10.1007/s10555-006-9005-3.

Basith, S., Manavalan B., Yoo, H. T., Kim, S. G., and Choi, S. (2012). Roles of Toll-like Receptors in Cancer: A Double-Edged Sword for Defense and Offense. *Archives of Pharmacal Research*, 35 (8): 1297–1316. doi:10.1007/s12272-012-0802-7.

Ben-Baruch, A. (2003). Host microenvironment in breast cancer development: Inflammatory Cells, Cytokines and Chemokines in Breast Cancer Progression: Reciprocal Tumor–microenvironment Interactions. *Breast Cancer Res.* 5(1): 31–36. doi: 10.1186/bcr554.

Berger, R., Fiegl, H., Goebel, G., Obexer, P., Ausserlechner, M., Doppler, W., Hauser-Kronberger, C., et al. (2010). Toll-Like Receptor 9 Expression in Breast and Ovarian Cancer Is Associated with Poorly Differentiated Tumors. *Cancer Science,* 101 (4): 1059–66. doi:10.1111/j.1349-7006.2010.01491.x.

Bode, Ch., Zhao, G., Steinhagen, F., Kinjo, T., and Klinman, D. M. (2011). CpG DNA as a Vaccine Adjuvant. *Expert Review of Vaccines,* 10 (4): 499–511. doi:10.1586/erv.10.174.

Bosman, A. W., Janssen, H. M., and Meijer, E. W. (1999). About Dendrimers: Structure, Physical Properties, and Applications. *Chemical Reviews,* 99 (7): 1665–88. doi:10.1021/cr970069y.

Bourquin, C., Anz, D., Zwiorek, K., Lanz, A. L., Fuchs, S., Weigel, S., Wurzenberger, C., et al. (2008). Targeting CpG Oligonucleotides to the Lymph Node by Nanoparticles Elicits Efficient Antitumoral Immunity. *The Journal of Immunology,* 181 (5): 2990–98. doi:10.4049/jimmunol.181.5.2990.

Braun, C. S., Vetro, J. A., Tomalia, D. A., Koe, G. S., Koe, J. G., and Middaugh, C. R. (2005). Structure/function Relationships of polyamidoamine/DNA Dendrimers as Gene Delivery Vehicles. *Journal of Pharmaceutical Sciences,* 94 (2): 423–36. doi:10.1002/jps.20251.

Brothers II, H. M., Piehler, L. T., and Tomalia, D. A. (1998). Slab-Gel and Capillary Electrophoretic Characterization of Polyamidoamine Dendrimers. *Journal of Chromatography, A* 814 (1–2): 233–46. doi:10.1016/S0021-9673(98)00419-1.

Bucak, S., Yavuztürk, B., and Sezer, A. D. (2012). Magnetic Nanoparticles: Synthesis, Surface Modifications and Application in Drug Delivery. DOI: 10.5772/52115.

Buczkowski, A., and Palecz, B. (2014). Study of the Interactions of PAMAM-NH2 G4 Dendrimer with Selected Natural Amino Acids in Aqueous Solutions. *The Journal of Chemical Thermodynamics*, 70 (March): 95–100. doi:10.1016/j.jct.2013.10.022.

Cakmak, N. (2013). Reversal of Mutidrug Resistance in MCF-7 Breast Adenocarcinoma Cell Line by Silencing Interleukin 6 with RNA Interference. *Thesis*, http://etd.lib.metu.edu.tr/upload/12616111/index.pdf.

Campagna, S., Ceroni, P., and Puntoriero, F. (2015). Designing Dendrimers. ISBN: 978-0-470-43355-3.

Cevc, G., and Vierl, U. (2010). Nanotechnology and the Transdermal Route: A State of the Art Review and Critical Appraisal. *Journal of Controlled Release, Pharmaceutical Nanotechnology: Unmet Needs in Drug Delivery*, 141 (3): 277–99. doi:10.1016/j.jconrel.2009.10.016.

Cheng, Y., Xu, Z., Ma, M., and Xu, T. (2008). Dendrimers as Drug Carriers: Applications in Different Routes of Drug Administration. *Journal of Pharmaceutical Sciences*, 97 (1): 123–43. doi:10.1002/jps.21079.

Chen, T. J., Cheng, T. H., Hung, Y. C., Lin, K. T., Liu, G. Ch., and Wang, Y. M. (2008). Targeted Folic Acid-PEG Nanoparticles for Noninvasive Imaging of Folate Receptor by MRI. *Journal of Biomedical Materials Research Part A*, 87A (1): 165–75. doi:10.1002/jbm.a.31752.

Chen, W., Tomalia, D. A., and Thomas, J. L. (2000). Unusual pH-Dependent Polarity Changes in PAMAM Dendrimers: Evidence for pH-Responsive Conformational Changes. *Macromolecules*, 33 (25): 9169–72. doi:10.1021/ma000791p.

Conze, D., Weiss, L., Regen, P. S., Bhushan, A., Weaver, D., Johnson, P., and Rincon, M. (2001). Autocrine Production of Interleukin 6 Causes Multidrug Resistance in Breast Cancer Cells. *Cancer Research,* 61 (24): 8851–58.

Danhier, F., Feron, O., and Preat, V. (2010). To Exploit the Tumor Microenvironment: Passive and Active Tumor Targeting of Nanocarriers for Anti-Cancer Drug Delivery. *Journal of Controlled Release,* 148 (2): 135–46. doi:10.1016/j.jconrel.2010.08.027.

Dhanasekaran, D. N., and Reddy, E. P. (2008). JNK Signaling in Apoptosis. *Oncogene,* 27 (48): 6245–51. doi:10.1038/onc.2008.301.

Dufes, Ch., Uchegbu, I. F., and Schatzlein, A. G. (2005). Dendrimers in Gene Delivery. *Advanced Drug Delivery Reviews, Dendrimers: a Versatile Targeting Platform,* 57 (15): 2177–2202. doi:10.1016/j.addr.2005.09.017.

Eaton-Bassiri, A., Dillon, S. B., Cunningham, M., Rycyzyn, M. A., Mills, J., Sarisky, R. T., and Mbow, M. L. (2004). Toll-Like Receptor 9 Can Be Expressed at the Cell Surface of Distinct Populations of Tonsils and Human Peripheral Blood Mononuclear Cells. *Infection and Immunity,* 72 (12): 7202–11. doi:10.1128/IAI.72.12.7202-7211.2004.

Eichman, J. D., Bielinska, A. U., Kukowska-Latallo, J. F., and Baker Jr., J. R. (2000). The Use of PAMAM Dendrimers in the Efficient Transfer of Genetic Material into Cells. *Pharmaceutical Science & Technology Today,* 3 (7): 232–45. doi:10.1016/S1461-5347(00)00273-X.

Esfand, R., and Tomalia, D. A. (2001). Poly(amidoamine) (PAMAM) Dendrimers: From Biomimicry to Drug Delivery and Biomedical Applications. *Drug Discovery Today,* 6 (8): 427–36. doi:10.1016/S1359-6446(01)01757-3.

Fang, J., Nakamura, H., and Maeda, H. (2011). The EPR Effect: Unique Features of Tumor Blood Vessels for Drug Delivery, Factors Involved, and Limitations and Augmentation of the Effect. *Advanced Drug Delivery Reviews, EPR Effect Based Drug Design and Clinical Outlook for Enhanced Cancer Chemotherapy,* 63 (3): 136–51. doi:10.1016/j.addr.2010.04.009.

Gang, J., Park, S. B., Hyung, W., Choi, E. H., Wen, J., Kim, H. S., Shul, Y. G., Haam, S., and Song, S. Y. (2007). Magnetic Poly E-Caprolactone Nanoparticles Containing Fe3O4 and Gemcitabine Enhance Anti-Tumor Effect in Pancreatic Cancer Xenograft Mouse Model. *Journal of Drug Targeting,* 15 (6): 445–53. doi:10.1080/10611860701453901.

Greish, Kh. Edited by Grobmyer, S. R. and Moudgil, B. M. (2010). Enhanced Permeability and Retention (EPR) Effect for Anticancer Nanomedicine Drug Targeting. In *Cancer Nanotechnology,* 624:25–37. Totowa, NJ: Humana Press. http://link.springer.com/10.1007/978-1-60761-609-2_3.

Grobmyer, S. R., Zhou, G., Gutwein, L. G., Iwakuma, N., Sharma, P., and Hochwald, S. N. (2012). Nanoparticle Delivery for Metastatic Breast Cancer. *Maturitas, Nanotechnology: From fundamental concepts to clinical applications for healthy aging A special joint publication with Nanomedicine: Nanotechnology, Biology and Medicine,* 73 (1): 19–26. doi:10.1016/j.maturitas.2012.02.003.

Gungor, B., Yagci, F. C., Tincer, G., Bayyurt, B., Alpdundar, E., Yildiz, S., Ozcan, M., Gursel, I., and Gursel, M. (2014). CpG ODN Nanorings Induce IFNα from Plasmacytoid Dendritic Cells and Demonstrate Potent Vaccine Adjuvant Activity. *Science Translational Medicine,* 6 (235): 235ra61–235ra61. doi:10.1126/scitranslmed.3007909.

Guo, Y., Xu, F., Lu, T. J., Duan, Z., and Zhang, Z. (2012). Interleukin-6 Signaling Pathway in Targeted Therapy for Cancer. *Cancer Treatment Reviews,* 38 (7): 904–10. doi:10.1016/j.ctrv.2012.04.007.

Gupta, A. K., and Gupta, M. (2005). Synthesis and Surface Engineering of Iron Oxide Nanoparticles for Biomedical Applications. *Biomaterials*, 26 (18): 3995–4021. doi:10.1016/j.biomaterials.2004.10.012.

Hanahan, D., and Weinberg, R. A. (2000). The Hallmarks of Cancer. *Cell*, 100 (1): 57–70. doi:10.1016/S0092-8674(00)81683-9.

Han, S. C., Kim. J. H., and Lee, J. W. (2012). Convergent Synthesis of PAMAM Dendrimers Containing Tetra(ethyleneoxide) at Core Using Click Chemistry. *Bulletin of the Korean Chemical Society*, 33 (10): 3501–4. doi:10.5012/bkcs.2012.33.10.3501.

Hariani, P. L., Faizal, M., Ridwan, R., Marsi, M., and Setiabudidaya, D. (2013). Synthesis and Properties of Fe3O4 Nanoparticles by Co-Precipitation Method to Removal Procion Dye. *International Journal of Environmental Science and Development*, 336–40. doi:10.7763/IJESD.2013.V4.366.

Hartman, Z. C., Poage, G. M., Hollander, P. d., Tsimelzon, A., Hill, J., Panupinthu, N., Zhang, Y., et al. (2013). Growth of Triple-Negative Breast Cancer Cells Relies upon Coordinate Autocrine Expression of the pro-Inflammatory Cytokines IL-6 and IL-8. *Cancer Research*, 73 (11). doi:10.1158/0008-5472.CAN-12-4524-T.

Hawker, C. J., and Frechet, J. M. J. (1990). Preparation of Polymers with Controlled Molecular Architecture. A New Convergent Approach to Dendritic Macromolecules. *Journal of the American Chemical Society*, 112 (21): 7638–47. doi:10.1021/ja00177a027.

Holliday, D. L., and Speirs, V. (2011). Choosing the Right Cell Line for Breast Cancer Research. *Breast Cancer Research: BCR*, 13 (4): 215. doi:10.1186/bcr2889.

Horssen, R. V., Hagen, T. L. M., and Eggermont, A. M. M. (2006). TNF-A in Cancer Treatment: Molecular Insights, Antitumor Effects, and Clinical Utility. *The Oncologist*, 11 (4): 397–408. doi:10.1634/theoncologist.11-4-397.

Huang, B., Zhao, J., Unkeless, J. C., Feng, Z. H., and Xiong, H. (2008). TLR Signaling by Tumor and Immune Cells: A Double-Edged Sword. *Oncogene,* 27 (2): 218–24. doi:10.1038/sj.onc.1210904.

Ilvesaro, J. M., Merrell, M. A., Li, L., Wakchoure, S., Graves, D., Brooks, S., and Rahko, E., et al. (2008). Toll-like Receptor 9 Mediates CpG Oligonucleotide-Induced Cellular Invasion. *Molecular Cancer Research: MCR,* 6 (10): 1534–43. doi:10.1158/1541-7786.MCR-07-2005.

Inoue, K. (2000). Functional Dendrimers, Hyperbranched and Star Polymers. *Progress in Polymer Science,* 25 (4): 453–571. doi:10.1016/S0079-6700(00)00011-3.

Iyer, A. K., Khaled, G., Fang, J., and Maeda, H. (2006). Exploiting the Enhanced Permeability and Retention Effect for Tumor Targeting. *Drug Discovery Today,* 11 (17–18): 812–18. doi:10.1016/j.drudis.2006.07.005.

Jahrsdorfer, B., and Weiner, G. J. (2008). CpG Oligodeoxynucleotides as Immunotherapy in Cancer. *Update on Cancer Therapeutics,* 3 (1): 27–32. doi:10.1016/j.uct.2007.11.003.

Janaszewska, A., Maczynska, K., Matuszko, G., Appelhans, D., Voit, B., Klajnert, B., and Bryszewska, M. (2012). Cytotoxicity of PAMAM, PPI and Maltose Modified PPI Dendrimers in Chinese Hamster Ovary (CHO) and Human Ovarian Carcinoma (SKOV3) Cells. *New Journal of Chemistry,* 36 (2): 428–37. doi:10.1039/C1NJ20489K.

Jiang, H. L., Kim, Y. K., Arote, R., Nah, J. W., Cho, M. H., Choi, Y. J., Akaike, T., and Cho, C. S. (2007). Chitosan-Graft-Polyethylenimine as a Gene Carrier. *Journal of Controlled Release,* 117 (2): 273–80. doi:10.1016/j.jconrel.2006.10.025.

Kandpal, N. D., Sah, N., Loshali, R., Joshi, R., and Prasad, J. (2015). Co-Precipitation Method of Synthesis and Characterization of Iron Oxide Nanoparticles. *Journal of scientific and industrial research,* 73(2): 87-90.

Kanzler, H., Barrat, F. J., Hessel, E. M., and Coffman, R. L. (2007). Therapeutic Targeting of Innate Immunity with Toll-like Receptor Agonists and Antagonists. *Nature Medicine,* 13 (5): 552–59. doi:10.1038/nm1589.

Karczewska, A., Nawrocki, S., Breborowicz, D., Filas, V., and Mackiewicz, A. (2000). Expression of Interleukin-6, Interleukin-6 Receptor, and Glycoprotein 130 Correlates with Good Prognoses for Patients with Breast Carcinoma. *Cancer,* 88 (9): 2061–71.

Kars, M. D., Darcansoy İşeri, O., Gunduz, U., Ural, A. U., Arpaci, F., and Molnar, J. (2006). Development of Rational In Vitro Models for Drug Resistance in Breast Cancer and Modulation of MDR by Selected Compounds. *Anticancer Research,* 26 (6B): 4559–68.

Keskin, T., and Gunduz, U. (2012). Preparation of Polyethylene Glycol Coated Magnetic Nanoparticles for Targeting of Cancer Cells. *Thesis,* Ankara : METU; 2012.

Kim, R., Emi, M., Tanabe, K., and Toge, T. (2004). Therapeutic Potential of Antisense Bcl-2 as a Chemosensitizer for Cancer Therapy. *Cancer,* 101 (11): 2491–2502. doi:10.1002/cncr.20696.

Klinman, D. M. (2004). Immunotherapeutic Uses of CpG Oligodeoxynucleotides. *Nature Reviews Immunology,* 4 (4): 249–59. doi:10.1038/nri1329.

Knupfer, H., and Preiß, R. (2006). Significance of Interleukin-6 (IL-6) in Breast Cancer (review). *Breast Cancer Research and Treatment,* 102 (2): 129–35. doi:10.1007/s10549-006-9328-3.

Krieg, A. M., edited by Stuhler, G. and Walden, P. (2002). Applications of CpG Motifs from Bacterial DNA in Cancer Immunotherapy. *Cancer Immune Therapy,* 268–86. Wiley-VCH Verlag GmbH & Co. KGaA. doi: 10.1002/3527600795.ch13.

Labieniec, M., and Watala, C. (2009). PAMAM Dendrimers — Diverse Biomedical Applications. Facts and Unresolved Questions. *Central European Journal of Biology*, 4 (4): 434–51. doi:10.2478/s11535-009-0056-7.

Lan, Q., Liu, C., Yang, F., Liu, S., Xu, J., and Sun, D. (2007). Synthesis of Bilayer Oleic Acid-Coated Fe3O4 Nanoparticles and Their Application in pH-Responsive Pickering Emulsions. *Journal of Colloid and Interface Science*, 310 (1): 260–69. doi:10.1016/j.jcis.2007.01.081.

Lee, B. L., Moon, J. E., Shu, J. H., Yuan, L., Newman, Z. R., Schekman, R., and Barton, G. M. (2013). UNC93B1 Mediates Differential Trafficking of Endosomal TLRs. *eLife*, 2: e00291. doi:10.7554/eLife.00291.

Lee, J. H., and Nan, A. (2012). Combination Drug Delivery Approaches in Metastatic Breast Cancer. *Journal of Drug Delivery*, 2012, doi:10.1155/2012/915375.

Leng, S. X., McElhaney, J. E., Walston, J. D., Xie, D., Fedarko, N. S., and Kuchel, G. A. (2008). Elisa and Multiplex Technologies for Cytokine Measurement in Inflammation and Aging Research. *The Journals of Gerontology. Series A, Biological Sciences and Medical Sciences*, 63 (8): 879–84.

Lester, S. N., and Li, K. (2014). Toll-Like Receptors in Antiviral Innate Immunity. *Journal of Molecular Biology*, *Antiviral Innate Immunity (Part II)*, 426 (6): 1246–64. doi:10.1016/j.jmb.2013.11.024.

Li, Ch., Li, L., and Keates, A. C. (2012). Targeting Cancer Gene Therapy with Magnetic Nanoparticles. *Oncotarget*, 3 (4): 365–70.

Lim, E. J., Park, D. W., Lee, J. G., Lee, C. H., Bae, Y. S., Hwang, Y. C., Jeong, J. W., Chin, B. R., and Baek, S. H. (2010). Toll-like Receptor 9-Mediated Inhibition of Apoptosis Occurs through Suppression of FoxO3a Activity and Induction of FLIP Expression. *Experimental & Molecular Medicine*, 42 (10): 712–20. doi:10.3858/emm.2010.42.10.070.

Lin, A. Y., Almeida, J. P. M., Bear, A., Liu, N., Luo, L., Foster, A. E., and Drezek, R. A. (2013). Gold Nanoparticle Delivery of Modified CpG Stimulates Macrophages and Inhibits Tumor Growth for Enhanced Immunotherapy. *PLOS ONE*, 8 (5). doi:10.1371/journal.pone.0063550.

Liu, F. T., Newland, A. C., and Jia, L. (2003). Bax Conformational Change Is a Crucial Step for PUMA-Mediated Apoptosis in Human Leukemia. *Biochemical and Biophysical Research Communications*, 310 (3): 956–62. doi:10.1016/j.bbrc.2003.09.109.

Liu, X., Kaminski, M. D., Guan, Y., Chen, H., Liu, H., and Rosengart, A. J. (2006). Preparation and Characterization of Hydrophobic Superparamagnetic Magnetite Gel. *Journal of Magnetism and Magnetic Materials*, 306 (2): 248–53. doi:10.1016/j.jmmm.2006.03.049.

Livak, K. J., and Schmittgen, T. D. (2001). Analysis of Relative Gene Expression Data Using Real-Time Quantitative PCR and the 2−ΔΔCT Method. *Methods*, 25 (4): 402–8. doi:10.1006/meth.2001.1262.

Lotz, C., Kelleher, D., Gassner, B., Gekle, M., Vaupel, P., and Thews, O. (2007). Role of the Tumor Microenvironment in the Activity and Expression of the P-Glycoprotein in Human Colon Carcinoma Cells. *Oncology Reports*, January. doi:10.3892/or.17.1.239.

Maeda, H., Nakamura, H., and Fang, J. (2013). The EPR Effect for Macromolecular Drug Delivery to Solid Tumors: Improvement of Tumor Uptake, Lowering of Systemic Toxicity, and Distinct Tumor Imaging in Vivo. *Advanced Drug Delivery Reviews, Advanced Drug Delivery: Perspectives and Prospects*, 65 (1): 71–79. doi:10.1016/j.addr.2012.10.002.

Maiti, P. K., Cagın, T., Lin, S. T., and Goddard, W. A. (2005). Effect of Solvent and pH on the Structure of PAMAM Dendrimers. *Macromolecules*, 38 (3): 979–91. doi:10.1021/ma049168l.

Maiti, P. K., Cagın, T., Wang, G., and Goddard, W. A. (2004). Structure of PAMAM Dendrimers: Generations 1 through 11. *Macromolecules*, 37 (16): 6236–54. doi:10.1021/ma035629b.

Majoros, I. J., Myc, A., Thomas, T., Mehta, C. B., and Baker Jr., J. R. (2006). PAMAM Dendrimer-Based Multifunctional Conjugate for Cancer Therapy: Synthesis, Characterization, and Functionality. *Biomacromolecules*, 7 (2): 572–79. doi:10.1021/bm0506142.

Mbeunkui, F., and Johann, D. J. (2009). Cancer and the Tumor Microenvironment: A Review of an Essential Relationship. *Cancer Chemotherapy and Pharmacology*, 63 (4): 571–82. doi:10.1007/s00280-008-0881-9.

Medina, S. H., and El-Sayed, M. E. H. (2009). Dendrimers as Carriers for Delivery of Chemotherapeutic Agents. *Chemical Reviews*, 109 (7): 3141–57. doi:10.1021/cr900174j.

Merrell, M. A., Ilvesaro, J. M., Lehtonen, N., Sorsa, T., Gehrs, B., Rosenthal, E., Chen, D., Shackley, B., Harris, K. W., and Selander, K. S. (2006). Toll-Like Receptor 9 Agonists Promote Cellular Invasion by Increasing Matrix Metalloproteinase Activity. *Molecular Cancer Research*, 4 (7): 437–47. doi:10.1158/1541-7786.MCR-06-0007.

Meyer, N., Kim, S. S., and Penn, L. Z. (2006). The Oscar-Worthy Role of Myc in Apoptosis. *Seminars in Cancer Biology, 25 years of the c-Myc oncogene*, 16 (4): 275–87. doi:10.1016/j.semcancer.2006.07.011.

Mocellin, S., Marincola, F. M., and Young, H. A. (2005). Interleukin-10 and the Immune Response against Cancer: A Counterpoint. *Journal of Leukocyte Biology*, 78 (5): 1043–51. doi:10.1189/jlb.0705358.

Mody, V. V., Cox, A., Shah, S., Singh, A., Bevins, W., and Parihar, H. (2014). Magnetic Nanoparticle Drug Delivery Systems for Targeting Tumor. *Applied Nanoscience*, 4 (4): 385–92. doi:10.1007/s13204-013-0216-y.

Mukherjee, S. P., and Byrne, H. J. (2013). Polyamidoamine Dendrimer Nanoparticle Cytotoxicity, Oxidative Stress, Caspase Activation and Inflammatory Response: Experimental Observation and Numerical Simulation. *Nanomedicine: Nanotechnology, Biology and Medicine*, 9 (2): 202–11. doi:10.1016/j.nano.2012.05.002.

Murad, Y. M., and Clay, T. M. (2009). CpG Oligodeoxynucleotides as TLR9 Agonists: Therapeutic Applications in Cancer. *BioDrugs: Clinical Immunotherapeutics, Biopharmaceuticals and Gene Therapy*, 23 (6): 361–75. doi:10.2165/11316930-000000000-00000.

Najlah, M., and D'Emanuele, A. (2006). Crossing Cellular Barriers Using Dendrimer Nanotechnologies. *Current Opinion in Pharmacology, Anti-infectives/New Technologies*, 6 (5): 522–27. doi:10.1016/j.coph.2006.05.004.

Nomi, N., Kodama, S., and Suzuki, M. (2010). Toll-like Receptor 3 Signaling Induces Apoptosis in Human Head and Neck Cancer via Survivin Associated Pathway. *Oncology Reports*, 24 (1). doi:10.3892/or_00000850.

Oda, E., Ohki, R., Murasawa, H., Nemoto, J., Shibue, T., et al. (2000). Noxa, a BH3-Only Member of the Bcl-2 Family and Candidate Mediator of p53-Induced Apoptosis. *Science*, 288 (5468): 1053–58. doi:10.1126/science.288.5468.1053.

Oft, M. (2014). IL-10: Master Switch from Tumor-Promoting Inflammation to Antitumor Immunity. *Cancer Immunology Research*, 2 (3): 194–99. doi:10.1158/2326-6066.CIR-13-0214.

Olbert, P. J., Schrader, A. J., Simon, C., et al. (2009). In Vitro and In Vivo Effects of CpG-Oligodeoxynucleotides (CpG-ODN) on Murine Transitional Cell Carcinoma and on the Native Murine Urinary Bladder Wall. *Anticancer Research*, 29 (6): 2067–76.

Osaka, T., Matsunaga, T., Nakanishi, T., Arakaki, A., Niwa, D., and Iida, H. (2006). Synthesis of Magnetic Nanoparticles and Their Application to Bioassays." *Analytical and Bioanalytical Chemistry,* 384 (3): 593–600. doi:10.1007/s00216-005-0255-7.

Oxenius, A., Martinic, M. M. A., Hengartner, H., and Klenerman, P. (1999). CpG-Containing Oligonucleotides Are Efficient Adjuvants for Induction of Protective Antiviral Immune Responses with T-Cell Peptide Vaccines. *Journal of Virology,* 73 (5): 4120–26.

Pan, B., Cui, D., Sheng, Y., Ozkan, C., Gao, F., He, R., Li, Q., Xu, P., and Huang, T. (2007). Dendrimer-Modified Magnetic Nanoparticles Enhance Efficiency of Gene Delivery System. *Cancer Research,* 67 (17): 8156–63. doi:10.1158/0008-5472.CAN-06-4762.

Pan, B., Gao, F., and Gu, H. (2005). Dendrimer Modified Magnetite Nanoparticles for Protein Immobilization. *Journal of Colloid and Interface Science,* 284 (1): 1–6. doi:10.1016/j.jcis.2004.09.073.

Park, J. H., Saravanakumar, G., Kim, K., and Kwon, I. C. (2010). Targeted Delivery of Low Molecular Drugs Using Chitosan and Its Derivatives. *Advanced Drug Delivery Reviews, Chitosan-Based Formulations of Drugs, Imaging Agents and Biotherapeutics,* 62 (1): 28–41. doi:10.1016/j.addr.2009.10.003.

Petros, A. P., and DeSimone, J. M. (2010). Strategies in the design of nanoparticles for therapeutic applications. *Nature Reviews, Drug Delivery,* 9 (8): 615-27. doi: 10.1038/nrd2591.

Poeck, H., Wagner, M., Battiany, J., et al. (2004). Plasmacytoid Dendritic Cells, Antigen, and CpG-C License Human B Cells for Plasma Cell Differentiation and Immunoglobulin Production in the Absence of T-Cell Help. *Blood,* 103 (8): 3058–64. doi:10.1182/blood-2003-08-2972.

Rauta, P. R., Samanta, M., Dash, H. R., Nayak, B., and Das, S. (2014). Toll-like Receptors (TLRs) in Aquatic Animals: Signaling Pathways, Expressions and Immune Responses. *Immunology Letters,* 158 (1–2): 14–24. doi:10.1016/j.imlet.2013.11.013.

Sadekar, S., and Ghandehari, H. (2012). Transepithelial Transport and Toxicity of PAMAM Dendrimers: Implications for Oral Drug Delivery. *Advanced Drug Delivery Reviews, Advances in Oral Drug Delivery: Improved Biovailability of Poorly Absorbed Drugs by Tissue and Cellular Optimization,* 64 (6): 571–88. doi:10.1016/j.addr.2011.09.010.

Safa, A. R. (2012). C-Flip, a Master Anti-Apoptotic Regulator- Experimental Oncology. *Experimental Oncology,*34(3):176-84.

Sato, T., Terai, M., Tamura, Y., Alexeev, V., Mastrangelo, M. J., and Selvan, S. R. (2011). Interleukin 10 in the Tumor Microenvironment: A Target for Anticancer Immunotherapy. *Immunologic Research,* 51 (2-3): 170–82. doi:10.1007/s12026-011-8262-6.

Sayed-Sweet, Y., Hedstrand, D. M., Spinder, R., and Tomalia, D. A. (1997). Hydrophobically Modified Poly(amidoamine) (PAMAM) Dendrimers: Theirproperties at the Air–water Interface and Use as Nanoscopiccontainer Molecules. *Journal of Materials Chemistry,* 7 (7): 1199–1205. doi:10.1039/A700860K.

Schafer, Z. T., and Brugge, J. S. (2007). IL-6 Involvement in Epithelial Cancers. *The Journal of Clinical Investigation,* 117 (12): 3660–63. doi:10.1172/JCI34237.

Seruga, B., Zhang, H., Bernstein, L. J., and Tannock, I. F. (2008). Cytokines and Their Relationship to the Symptoms and Outcome of Cancer. *Nature Reviews Cancer,* 8 (11): 887–99. doi:10.1038/nrc2507.

Shcharbin, D. G., Klajnert, B., and Bryszewska, M. (2009). Dendrimers in Gene Transfection. *Biochemistry (Moscow)*, 74 (10): 1070–79. doi:10.1134/S0006297909100022.

Shen, L., Qiao, Y., Guo, Y., Meng, S., Yang, G., Wu, M., and Zhao, J. (2014). Facile Co-Precipitation Synthesis of Shape-Controlled Magnetite Nanoparticles. *Ceramics International*, 40 (1, Part B): 1519–24. doi:10.1016/j.ceramint.2013.07.037.

Shubayev, V. I., Pisanic, T. R., and Jin, S. (2009). Magnetic Nanoparticles for Theragnostics. *Advanced Drug Delivery Reviews*, 61 (6): 467–77. doi:10.1016/j.addr.2009.03.007.

Shukoor, M. I., Natalio, F., Tahir, M. N., Barz, M., Weber, S., Brochhausen, C., Zentel, R., Schreiber, L. M., Brieger, J., and Tremel, W. (2012). CpG-DNA Loaded Multifunctional MnO Nanoshuttles for TLR9-Specific Cellular Cargo Delivery, Selective Immune-Activation and MRI. *Journal of Materials Chemistry*, 22 (18): 8826–34. doi:10.1039/C2JM16903G.

Shukoor, M. I., Natalio, F., Tahir, M. N., Wiens, M., Tarantola, M., Therese, H. A., Barz, M., et al. (2009). Pathogen-Mimicking MnO Nanoparticles for Selective Activation of the TLR9 Pathway and Imaging of Cancer Cells. *Advanced Functional Materials*, 19 (23): 3717–25. doi:10.1002/adfm.200900635.

Stockhofe, K., Postema, J. M., Schieferstein, H., and Ross, T. L. (2014). Radiolabeling of Nanoparticles and Polymers for PET Imaging. *Pharmaceuticals*, 7 (4): 392–418. doi:10.3390/ph7040392.

Subik, K., Lee, J. F., Baxter, L., Strzepek, T., Costello, D., Crowley, P., Xing, L., et al. (2010). The Expression Patterns of ER, PR, HER2, CK5/6, EGFR, Ki-67 and AR by Immunohistochemical Analysis in Breast Cancer Cell Lines. *Breast Cancer : Basic and Clinical Research*, 4 (May): 35–41.

Sun, T., Zhang, Y. S., Pang, B., Hyun, D. C., Yang, M., and Xia, Y. (2014). Engineered Nanoparticles for Drug Delivery in Cancer Therapy. *Angewandte Chemie International Edition*, 53 (46): 12320–64. doi:10.1002/anie.201403036.

Switaj, T., Jalili, A., Jakubowska, A. B., Drela, N., Stoksik, M., Nowis, D., Basak, G., et al. (2004). CpG Immunostimulatory Oligodeoxynucleotide 1826 Enhances Antitumor Effect of Interleukin 12 Gene-Modified Tumor Vaccine in a Melanoma Model in Mice. *Clinical Cancer Research*, 10 (12): 4165–75. doi:10.1158/1078-0432.CCR-04-0022.

Taghavi Pourianazar, N., and Gunduz, U. (2016). CpG Oligodeoxynucleotide-Loaded PAMAM Dendrimer-Coated Magnetic Nanoparticles Promote Apoptosis in Breast Cancer Cells. *Biomedicine & Pharmacotherapy*, 78 (March): 81–91. doi:10.1016/j.biopha.2016.01.002.

Taghavi Pourianazar, N., Mutlu, P., and Gunduz, U. (2014). Bioapplications of Poly(amidoamine) (PAMAM) Dendrimers in Nanomedicine. *Journal of Nanoparticle Research*, 16 (4): 1–38. doi:10.1007/s11051-014-2342-1.

Takeshita, F., Gursel, I., Ishii, K. J., Suzuki, K., Gursel, M., and Klinman, D. M. (2004). Signal Transduction Pathways Mediated by the Interaction of CpG DNA with Toll-like Receptor 9. *Seminars in Immunology, Toll Receptor Families Structure and Function*, 16 (1): 17–22. doi:10.1016/j.smim.2003.10.009.

Tao, Y., Li, Z., Ju, E., Ren, J., and Qu, X. (2013). One-Step DNA-Programmed Growth of CpG Conjugated Silver Nanoclusters: A Potential Platform for Simultaneous Enhanced Immune Response and Cell Imaging. *Chemical Communications*, 49 (61): 6918–20. doi:10.1039/C3CC41972J.

Tartaj, P., Morales, M. P., Veintemillas-Verdaguer, S., González-Carreño, T., and Serna, C. J. (2003). The Preparation of Magnetic Nanoparticles for Applications in Biomedicine. *Journal of Physics D: Applied Physics*, 36 (13): R182. doi:10.1088/0022-3727/36/13/202.

Tomalia, D. A., Baker, H., Dewald, J., Hall, M., Kallos, G., Martin, S., Roeck, J., Ryder, J., and Smith, P. (1985). A New Class of Polymers: Starburst-Dendritic Macromolecules. *Polymer Journal,* 17 (1): 117–32. doi:10.1295/polymj.17.117.

Tomalia, D. A. (1994). Starburst/Cascade Dendrimers: Fundamental Building Blocks for a New Nanoscopic Chemistry Set. *Advanced Materials,* 6 (7-8): 529–39. doi:10.1002/adma.19940060703.

Tomalia, D. A. (2005). Birth of a New Macromolecular Architecture: Dendrimers as Quantized Building Blocks for Nanoscale Synthetic Polymer Chemistry. *Progress in Polymer Science, Dendrimers and Dendritic Polymers,* 30 (3–4): 294–324. doi:10.1016/j.progpolymsci.2005.01.007.

Tomalia, D. A., and Frechet, J. M. J. (2002). Discovery of Dendrimers and Dendritic Polymers: A Brief Historical Perspective. *Journal of Polymer Science Part A: Polymer Chemistry,* 40 (16): 2719–28. doi:10.1002/pola.10301.

Trivedi, V., Patel, U., Bhimani, B., Daslaniya, D., Patel, G., and Vyas, B. (2012). Dendrimer: Polymer of 21st Century. *International Journal of Pharmaceutical Research and Bio-Science,* 1(2): 1-21.

Tuomela, J., Sandholm, J., Karihtala, P., Ilvesaro, J., Vuopala, K. S, Kauppila, J. H, Kauppila, S., et al. (2012). Low TLR9 Expression Defines an Aggressive Subtype of Triple-Negative Breast Cancer. *Breast Cancer Research and Treatment,* 135 (2): 481–93. doi:10.1007/s10549-012-2181-7.

Uzun, K., Çevik, E., Senel. M., Sozeri, H., Baykal, A., Abasıyanık, M. F., and Toprak, M. S. (2010). Covalent Immobilization of Invertase on PAMAM-Dendrimer Modified Superparamagnetic Iron Oxide Nanoparticles. *Journal of Nanoparticle Research,* 12 (8): 3057–67. doi:10.1007/s11051-010-9902-9.

Vermes, I., Haanen, C., Steffens-Nakken, H., and Reutellingsperger, C. (1995). A Novel Assay for Apoptosis Flow Cytometric Detection of Phosphatidylserine Expression on Early Apoptotic Cells Using Fluorescein Labelled Annexin V. *Journal of Immunological Methods*, 184 (1): 39–51. doi:10.1016/0022-1759(95)00072-I.

Vollmer, J., and Krieg, A. M. (2009). Immunotherapeutic Applications of CpG Oligodeoxynucleotide TLR9 Agonists. *Advanced Drug Delivery Reviews, CpG Oligonucleotides as Immunotherapeutic Adjuvants: Innovative Applications and Delivery Strategies*, 61 (3): 195–204. doi:10.1016/j.addr.2008.12.008.

Wahajuddin, and Arora, S. (2012). Superparamagnetic Iron Oxide Nanoparticles: Magnetic Nanoplatforms as Drug Carriers. *International Journal of Nanomedicine*, 7: 3445–71. doi:10.2147/IJN.S30320.

Waite, C. L., and Roth, C. M. (2009). PAMAM-RGD Conjugates Enhance siRNA Delivery Through a Multicellular Spheroid Model of Malignant Glioma. *Bioconjugate Chemistry*, 20 (10): 1908–16. doi:10.1021/bc900228m.

Wang, X., and Lin, Y. (2008). Tumor Necrosis Factor and Cancer, Buddies or Foes? *Acta Pharmacologica Sinica*, 29 (11): 1275–88. doi:10.1111/j.1745-7254.2008.00889.x.

Weigelt, B., Peterse, J. L., and Van't Veer, L. J. (2005). Breast Cancer Metastasis: Markers and Models. *Nature Reviews Cancer*, 5 (8): 591–602. doi:10.1038/nrc1670.

Wu, H. Q., Wang, B., Zhu, S. K., Tian, Y., Zhang, J. H., and Wu, H. S. (2011). Effects of CPG ODN on Biological Behavior of PANC-1 and Expression of TLR9 in Pancreatic Cancer. *World Journal of Gastroenterology: WJG*, 17 (8): 996–1003. doi:10.3748/wjg.v17.i8.996.

Yigit, M. V., Moore, A., and Medarova, Z. (2012). Magnetic Nanoparticles for Cancer Diagnosis and Therapy. *Pharmaceutical Research*, 29 (5): 1180–88. doi:10.1007/s11095-012-0679-7.

Yoo, H., Sazani, P., and Juliano, R. L. (1999). PAMAM Dendrimers as Delivery Agents for Antisense Oligonucleotides. *Pharmaceutical Research*, 16 (12): 1799–1804. doi:10.1023/A:1018926605871.

Zhang, H., Chen, S., Zhi, C., Yamazaki, T., and Hanagata, N. (2013). Chitosan-Coated Boron Nitride Nanospheres Enhance Delivery of CpG Oligodeoxynucleotides and Induction of Cytokines. *International Journal of Nanomedicine*, 8: 1783–93. doi:10.2147/IJN.S43251.

Zhang, J., Kong, X., Zhou, C., Li, L., Nie, G., and Li, X. (2014). Toll-like Receptor Recognition of Bacteria in Fish: Ligand Specificity and Signal Pathways. *Fish & Shellfish Immunology*, 41 (2): 380–88. doi:10.1016/j.fsi.2014.09.022.

Zhang, X. Q., Intra, J., and Salem, A. K. (2007). Conjugation of Polyamidoamine Dendrimers on Biodegradable Microparticles for Nonviral Gene Delivery. *Bioconjugate Chemistry*, 18 (6): 2068–76. doi:10.1021/bc070116l.

Zhi, C., Meng, W., Yamazaki, T., Bando, Y., Golberg, D., Tang, C., and Hanagata, N. (2011). BN Nanospheres as CpG ODN Carriers for Activation of Toll-like Receptor 9. *Journal of Materials Chemistry*, 21 (14): 5219–22. doi:10.1039/C1JM10199D.

Zhou, J., Wu, J., Hafdi, N., Behr, J. P., Erbacher, P., and Peng, L. (2006). PAMAM Dendrimers for Efficient siRNA Delivery and Potent Gene Silencing. *Chemical Communications*, 22 (May): 2362–64. doi:10.1039/B601381C.

Zhou, J., Wu, J., Liu, X., Qu, F., Xiao, M., Zhang, Y., Charles, L., Zhang, C. C., and Peng, L. (2006). Cooperative Binding and Self-Assembling Behavior of Cationic Low Molecular-Weight Dendrons with RNA Molecules. *Organic & Biomolecular Chemistry*, 4 (3): 581–85. doi:10.1039/B515667J.

Zhou, W., Li, Y., Pan, X., Gao, Y., Li, B., Qiu, Z., Liang, L., Zhou, H., and Yue, J. (2013). Toll-like Receptor 9 Interaction with CpG ODN – An in Silico Analysis Approach. *Theoretical Biology and Medical Modelling*, 10 (1): 18. doi:10.1186/1742-4682-10-18.

APPENDIX A

BUFFERS AND SOLUTIONS

A.1 Freezing Medium

9 ml FBS (Biochrome, Germany)

1 ml DMSO (Applichem, Germany)

Mixed and stored at 4˚C

A.2 Phosphate Buffered Saline (0.01 M) (pH 7.2)

1 PBS tablet (Sigma, Germany) in 200 ml distilled water.

After the tablet dissolved PBS is autoclaved at 121˚C for 20 min.

A.3 Diethylpyrocarbonate (DEPC)-Treated dH_2O

1 mL DEPC

1 L dH2O

1 mL DEPC was vigorously mixed with 1 L dH2O. It was autoclaved at 121°C for 20 min after overnight incubation.

A.4 Ethidium Bromide (EtBr) Solution

10 mg EtBr

1 mL dH_2O

EtBr was dissolved in dH_2O and stored at 4°C in dark.

A.5 50x Tris-Acetate-EDTA (TAE) Buffer

242 g Tris base (molecular weight: 121.14 g/mol)

57.1 mL Acetic acid

100 mL 0.5 M EDTA disodium dehydrate (molecular weight: 372.24 g/mol)

Volume was completed to 1 L with dH_2O and pH was adjusted to 8.5. Solution was diluted to 1x with dH_2O after it was autoclaved at 121°C for 20 min. The solution was stored at 4°C.

A.6 Blocking Buffer

100 ml PBS

0.1 g Bovine serum albumin (BSA)

50 µl Tween20

BSA was added to PBS and vortexed until the BSA is dissolved. Then, Tween20 is added and mixed.

A.7 ELISA Washing Buffer

100 ml PBS

50 µl Tween20

Tween20 is added to PBS and mixed.

A.8 DAPI Stain Solution

Add 2 mL of deionized water (diH_2O) or dimethylformamide (DMF) to the entire contents of the DAPI vial to make a 14.3 mM (5 mg/mL) DAPI stock solution.

Note: DAPI has poor solubility in water, so it should be sonicated as necessary to dissolve. The 5 mg/mL DAPI stock solution may be stored at 2–6°C for up to 6 months or at -20°C for longer periods.

Add 2.1 µL of the 14.3 mM DAPI stock solution to 100 µL PBS to make a 300 µM DAPI intermediate dilution. Then, Dilute the 300 µM DAPI intermediate dilution 1:1000 in PBS as needed to make a 300 nM DAPI stain solution.

APPENDIX B

THRESHOLD CYCLE VALUES

Table B.1 Threshold cycle (C_t) values of qRT-PCR analysis

Cell line / Gene	MDA-MB231	SKBR3	MCF7/S	MCF7/Dox
TLR9	31.810	33.305	37.455	33.885
β-actin	18.635	18.125	19.805	19.150

Table B.2 Threshold cycle (C_t) values of qRT-PCR analysis

Cell line / Gene	MDA-MB231		SKBR3		MCF7/S		MCF7/Dox	
	Untreated	Treated	Untreated	Treated	Untreated	Treated	Untreated	Treated
Bax	23.9	22.9	21.3	20.9	22.4	22.8	23.5	21.8
Noxa	23.4	21.3	18.7	19.8	22.7	20.7	24.5	22.5
Bcl-2	23.8	22.8	20.6	20.9	22.4	22.9	22.9	22.0
Survivin	19.4	19.1	21.7	22.1	23.9	24.0	24.6	22.4
Puma	22.1	21.0	17.2	18.4	17.4	17.2	19.3	20.0
C-Flip	20.6	20.1	18.8	19.6	20.7	20.9	20.0	20.5
β-actin	7.9	7.1	6.5	6.9	6.8	7.2	7.2	7

APPENDIX C

AMPLIFICATION CURVES, MELT CURVES, STANDARD CURVES, AND AGAROSE GEL IMAGES

C.1 *Bax*

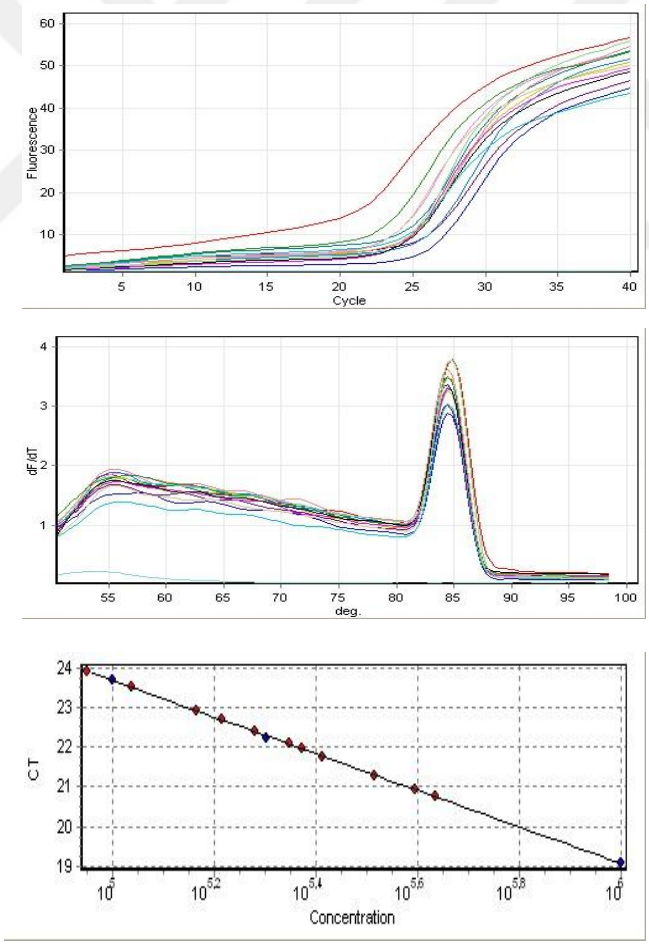

Cycling profile of *Bax*

Melt curve of *Bax* amplicon

Standard curve of *Bax* amplification

Figure C.1 Cycling profile (upper), melt curve (middle) and standard curve (lower) for *Bax* amplicon.

C.2 *Noxa*

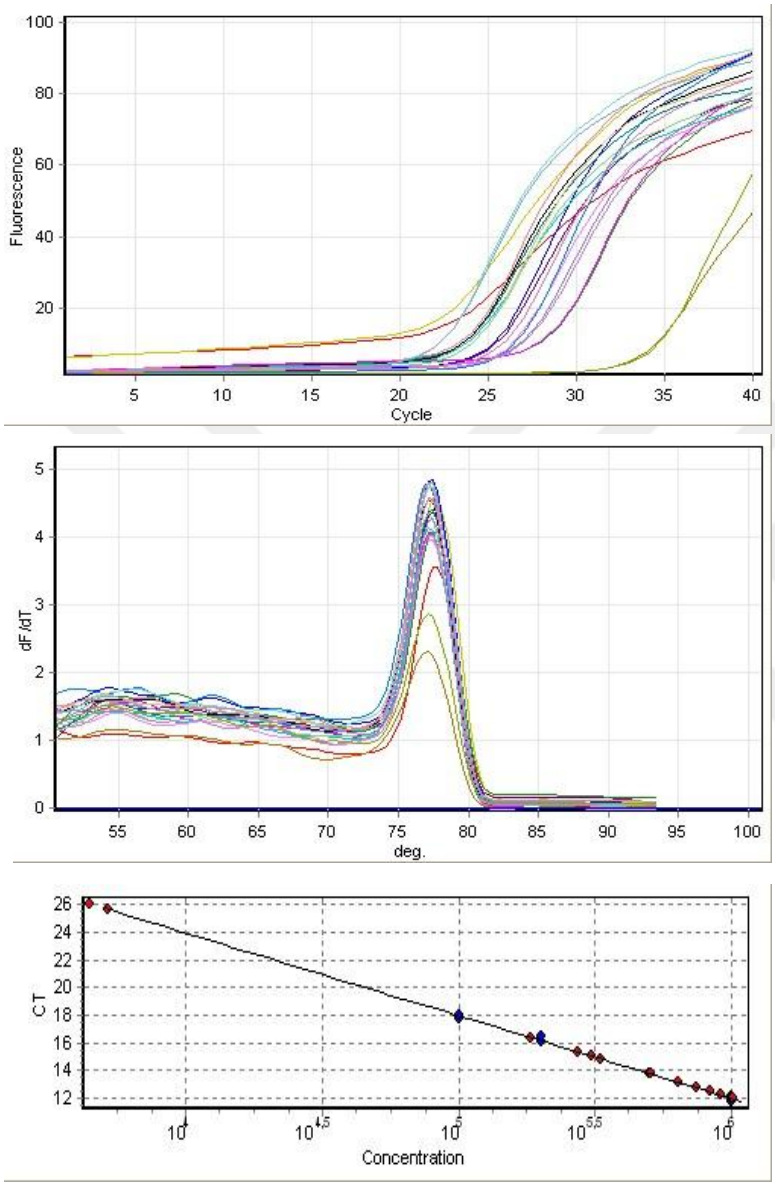

Cycling profile of *Noxa* amplification

Melt curve of *Noxa* amplicon

Standard curve of *Noxa* amplification

Figure C.2 Cycling profile (upper), melt curve (middle) and standard curve (lower) for *Noxa* amplicon.

C.3 *Bcl-2*

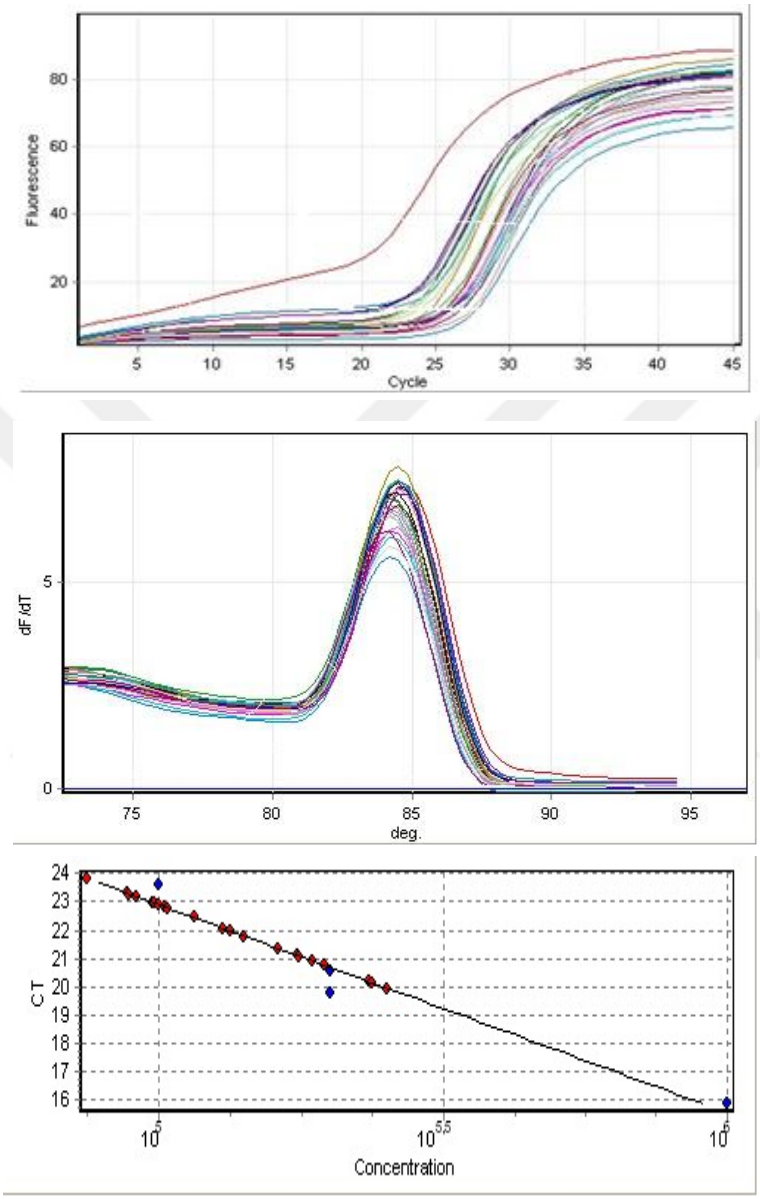

Cycling profile of *Bcl-2* amplification

Melt curve of *Bcl-2* amplicon

Standard curve of *Bcl-2* amplification

Figure C.3 Cycling profile (upper), melt curve (middle) and standard curve (lower) for *Bcl-2* amplicon.

C.4 *Survivin*

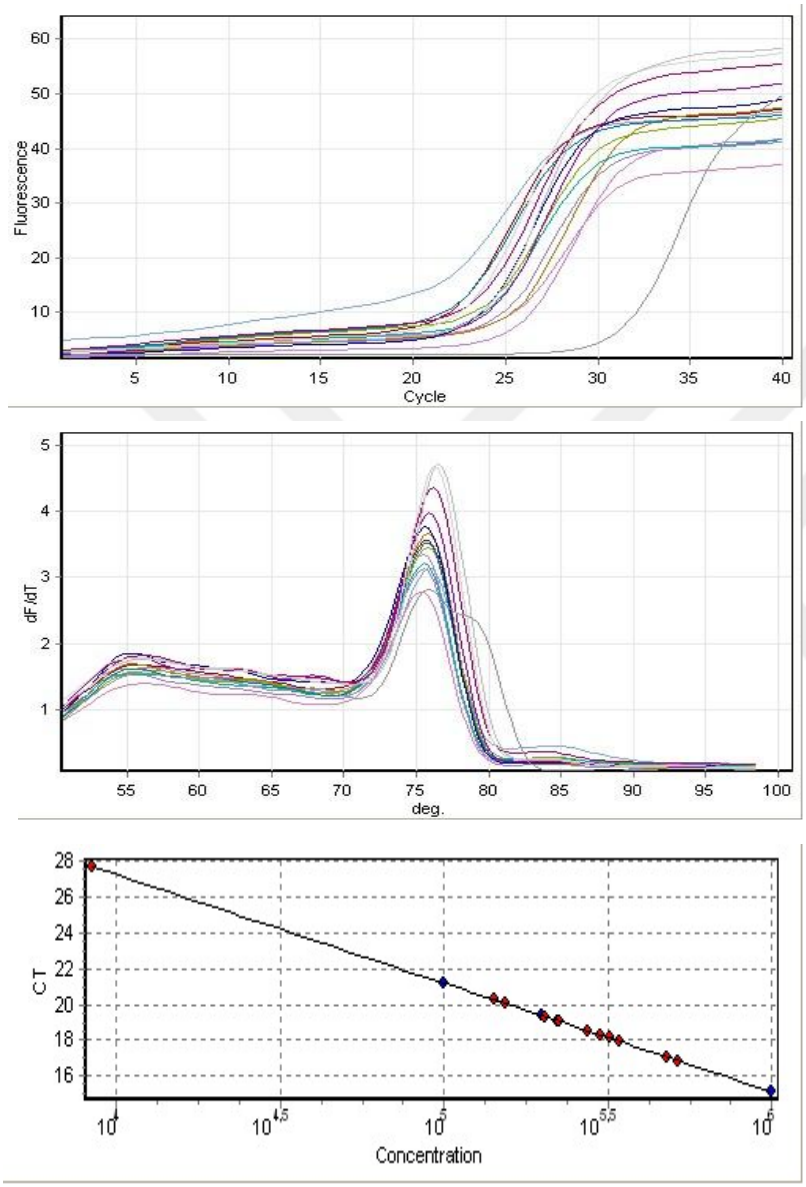

Cycling profile of *Survivin* amplification

Melt curve of *Survivin* amplicon

Standard curve of *Survivin* amplification

Figure C.4 Cycling profile (upper), melt curve (middle) and standard curve (lower) for *Survivin* amplicon.

C.5 *Puma*

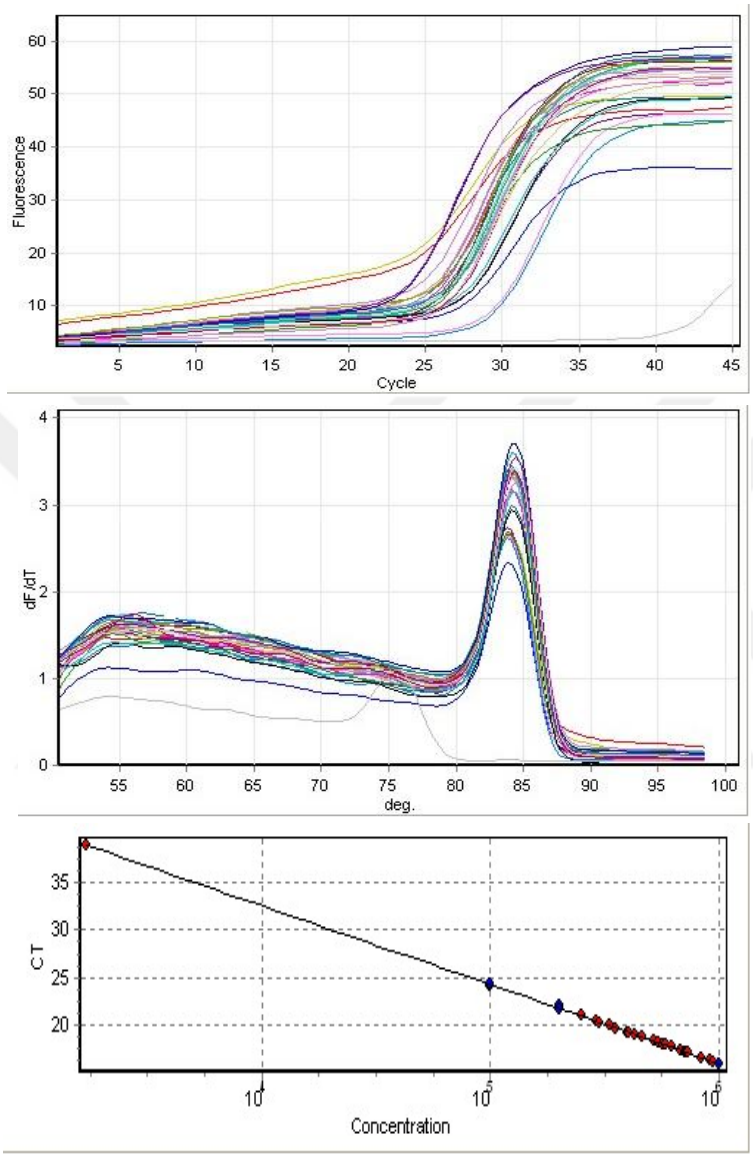

Cycling profile of *Puma* amplification

Melt curve of *Puma* amplicon

Standard curve of *Puma* amplification

Figure C.5 Cycling profile (upper), melt curve (middle) and standard curve (lower) for *Puma* amplicon.

C.6 *C-Flip*

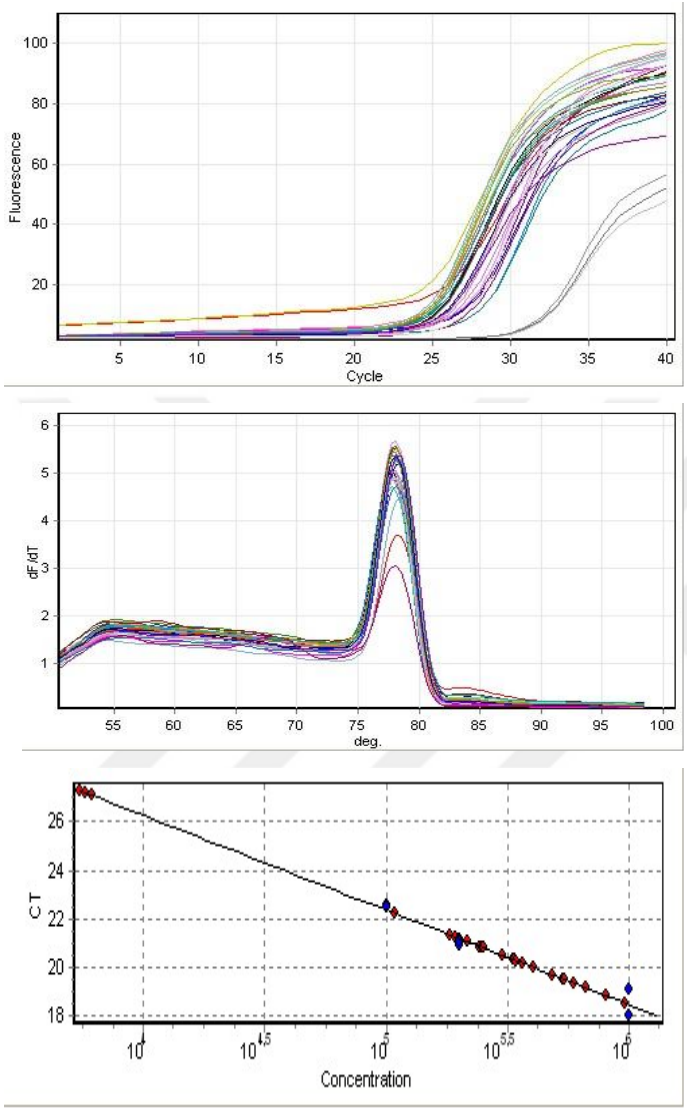

Cycling profile of *C-Flip* amplification

Melt curve of *C-Flip* amplicon

Standard curve of *C-Flip* amplification

Figure C.6 Cycling profile (upper), melt curve (middle) and standard curve (lower) for *C-Flip* amplicon.

C.7 *β-actin*

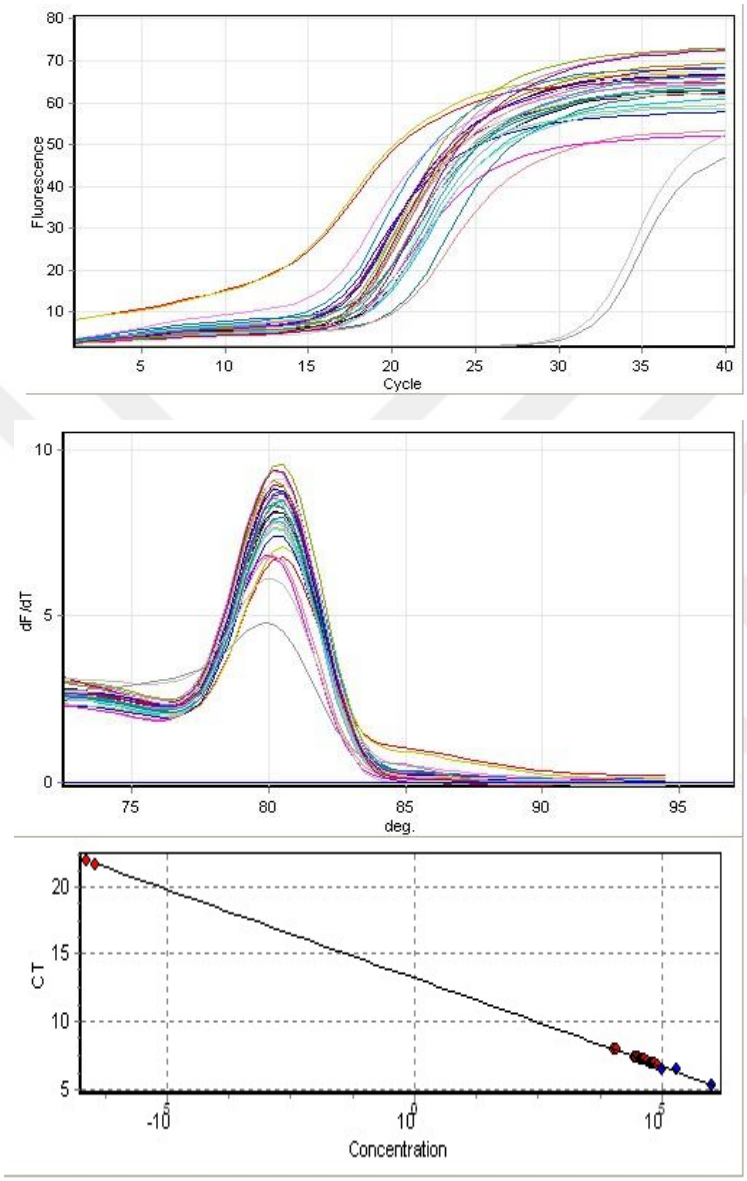

Cycling profile of *β-actin* amplification

Melt curve of *β-actin* amplicon

Standard curve of *β-actin* amplification

Figure C.7 Cycling profile (upper), melt curve (middle) and standard curve (lower) for *B-actin* amplicon.

C.8 AGAROSE GEL IMAGES

Expression levels of *Bax, Noxa, Bcl-2, Survivin, Puma, C-Flip,* and *β-actin* were determined by qRT-PCR. The products of qRT-PCR were checked by agarose gel electrophoresis. 2% agarose gel was prepared and qRT-PCR products were run at 140 V for 90 min.

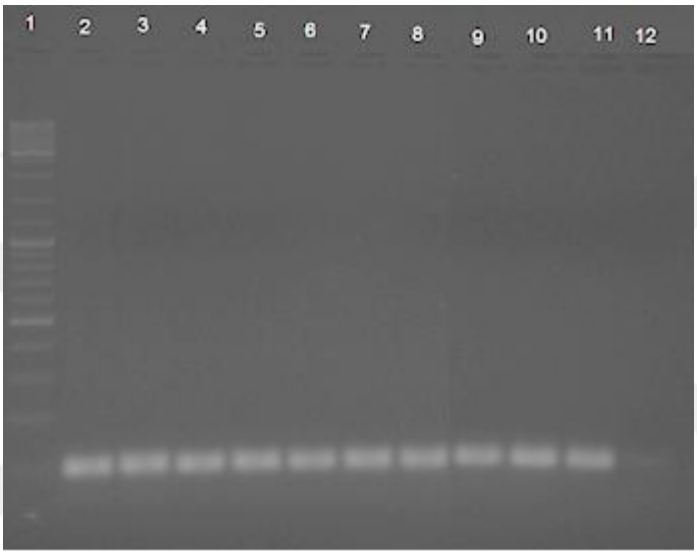

Figure C.8 Expression levels of *β-actin (ACTB)*; Lane 1: DNA ladder (Fermentas, Lithuania), Lane 2: β-actin in untreated SKBR3 cell line (Undiluted), Lane 3: β-actin in untreated SKBR3 cell line (1:5 diluted), Lane 4: β-actin in untreated SKBR3 cell line (1:10 diluted), Lane 5: β-actin in untreated MDA-MB231 cell line, Lane 6: β-actin in untreated MCF7/S cell line, Lane 7: β-actin in untreated MCF7/Dox cell line, Lane 8: β-actin in 0.5 µg/ml CpG-loaded DcMNP-treated SKBR3 cell line, Lane 9: β-actin in 0.5 µg/ml CpG-loaded DcMNP-treated MDA-MB231 cell line, Lane 10: β-actin in 0.5 µg/ml CpG-loaded DcMNP-treated MCF7/S cell line, Lane 11: β-actin in 0.5 µg/ml CpG-loaded DcMNP-treated MCF7/Dox cell line, Lane 12: Negative control

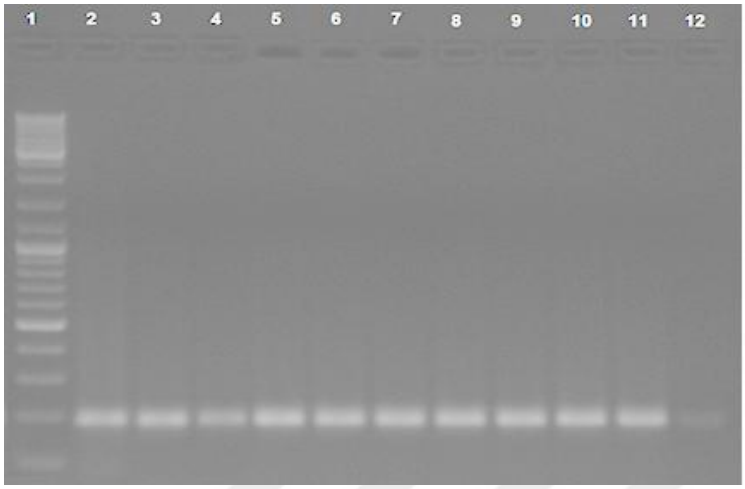

Figure C.9 Expression levels of *Bax*; Lane 1: *Bax* in untreated MCF7/S cell line (Undiluted), Lane 2: *Bax* in untreated MCF7/S cell line, Lane 3: *Bax* in untreated MCF7/S cell line (1:10 diluted), Lane 4: *Bax* in untreated MDA-MB231 cell line, Lane 5: *Bax* in untreated SKBR3 cell line, Lane 6: *Bax* in untreated MCF7/Dox cell line, Lane 7: *Bax* in 0.5 µg/ml CpG-loaded DcMNP-treated MCF7/S cell line, Lane 8: *Bax* in 0.5 µg/ml CpG-loaded DcMNP-treated MDA-MB231 cell line, Lane 9: *Bax* in 0.5 µg/ml CpG-loaded DcMNP-treated SKBR3 cell line, Lane 10: *Bax* in 0.5 µg/ml CpG-loaded DcMNP-treated MCF7/Dox cell line, Lane 12: Negative control.

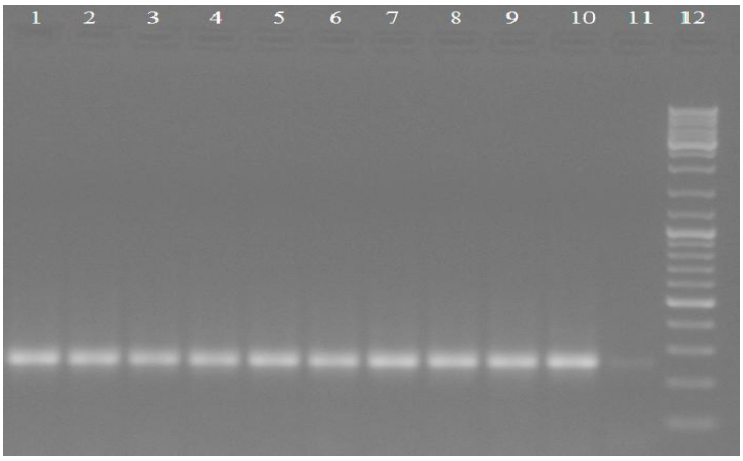

Figure C.10 Expression levels of *Noxa*; Lane 1: *Noxa* in untreated SKBR3 cell line (Undiluted), Lane 2: *Noxa* in untreated SKBR3 cell line, Lane 3: *Noxa* in untreated SKBR3 cell line (1:10 diluted), Lane 4: *Noxa* in untreated MDA-MB231 cell line, Lane 5: *Noxa* in untreated MCF7/S cell line, Lane 6: *Noxa* in untreated MCF7/Dox cell line, Lane 7: *Noxa* in 0.5 µg/ml CpG-loaded DcMNP-treated SKBR3 cell line, Lane 8: *Noxa* in 0.5 µg/ml CpG-loaded DcMNP-treated MDA-MB231 cell line, Lane 9: *Noxa* in 0.5 µg/ml CpG-loaded DcMNP-treated MCF7/S cell line, Lane 10: *Noxa* in 0.5 µg/ml CpG-loaded DcMNP-treated MCF7/Dox cell line, Lane 11: Negative control, Lane 12: DNA ladder (Fermentas, Lithuania).

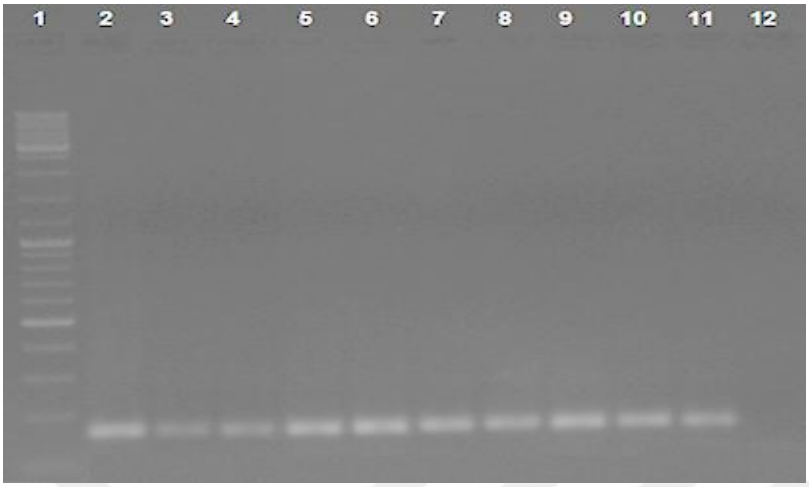

Figure C.11 Expression levels of *Bcl-2*; Lane 1: DNA ladder (Fermentas, Lithuania), Lane 2: *Bcl-2* in untreated SKBR3 cell line (Undiluted), Lane 3: *Bcl-2* in untreated SKBR3 cell line, Lane 4: *Bcl-2* in untreated SKBR3 cell line (1:10 diluted), Lane 5: *Bcl-2* in untreated MDA-MB231 cell line, Lane 6: *Bcl-2* in untreated MCF7/S cell line, Lane 7: *Bcl-2* in untreated MCF7/Dox cell line, Lane 8: *Bcl-2* in 0.5 µg/ml CpG-loaded DcMNP-treated SKBR3 cell line, Lane 9: *Bcl-2* in 0.5 µg/ml CpG-loaded DcMNP-treated MDA-MB231 cell line, Lane 10: *Bcl-2* in 0.5 µg/ml CpG-loaded DcMNP-treated MCF7/S cell line, Lane 11: *Bcl-2* in 0.5 µg/ml CpG-loaded DcMNP-treated MCF7/Dox cell line, Lane 12: Negative control.

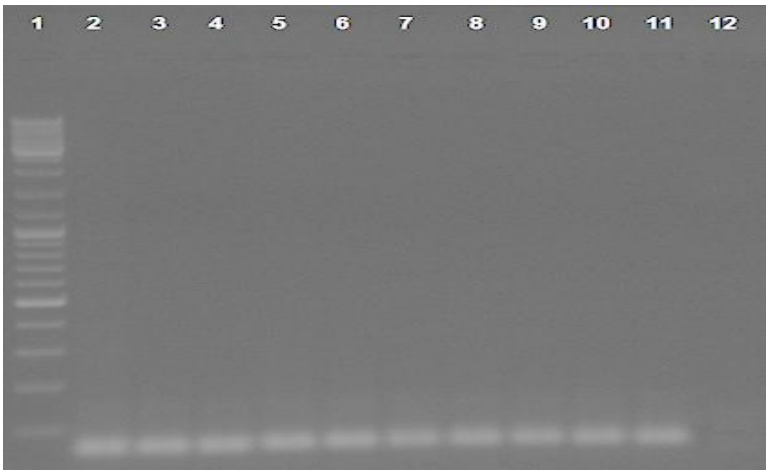

Figure C.12 Expression levels of *Survivin*; Lane 1: DNA ladder (Fermentas, Lithuania), Lane 2: *Survivin* in untreated SKBR3 cell line (Undiluted), Lane 3: *Survivin* in untreated SKBR3 cell line, Lane 4: *Survivin* in untreated SKBR3 cell line (1:10 diluted), Lane 5: *Survivin* in untreated MDA-MB231 cell line, Lane 6: *Survivin* in untreated MCF7/S cell line, Lane 7: *Survivin* in untreated MCF7/Dox cell line, Lane 8: *Survivin* in 0.5 µg/ml CpG-loaded DcMNP-treated SKBR3 cell line, Lane 9: *Survivin* in 0.5 µg/ml CpG-loaded DcMNP-treated MDA-MB231 cell line, Lane 10: *Survivin* in 0.5 µg/ml CpG-loaded DcMNP-treated MCF7/S cell line, Lane 11: *Survivin* in 0.5 µg/ml CpG-loaded DcMNP-treated MCF7/Dox cell line, Lane 12: Negative control.

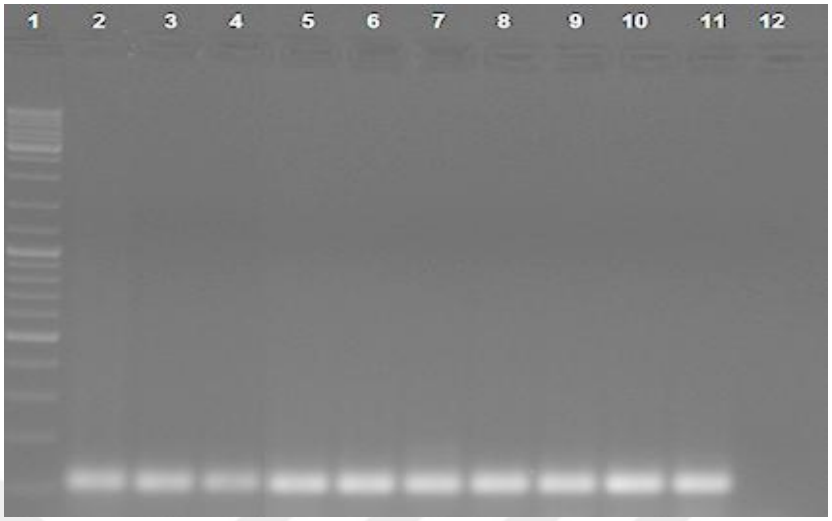

Figure C.13 Expression levels of *Puma*; Lane 1: DNA ladder (Fermentas, Lithuania), Lane 2: *Puma* in untreated SKBR3 cell line (Undiluted), Lane 3: *Puma* in untreated SKBR3 cell line, Lane 4: *Puma* in untreated SKBR3 cell line (1:10 diluted), Lane 5: *Puma* in untreated MDA-MB231 cell line, Lane 6: *Puma* in untreated MCF7/S cell line, Lane 7: *Puma* in untreated MCF7/Dox cell line, Lane 8: *Puma* in 0.5 µg/ml CpG-loaded DcMNP-treated SKBR3 cell line, Lane 9: *Puma* in 0.5 µg/ml CpG-loaded DcMNP-treated MDA-MB231 cell line, Lane 10: *Puma* in 0.5 µg/ml CpG-loaded DcMNP-treated MCF7/S cell line, Lane 11: *Puma* in 0.5 µg/ml CpG-loaded DcMNP-treated MCF7/Dox cell line, Lane 12: Negative control.

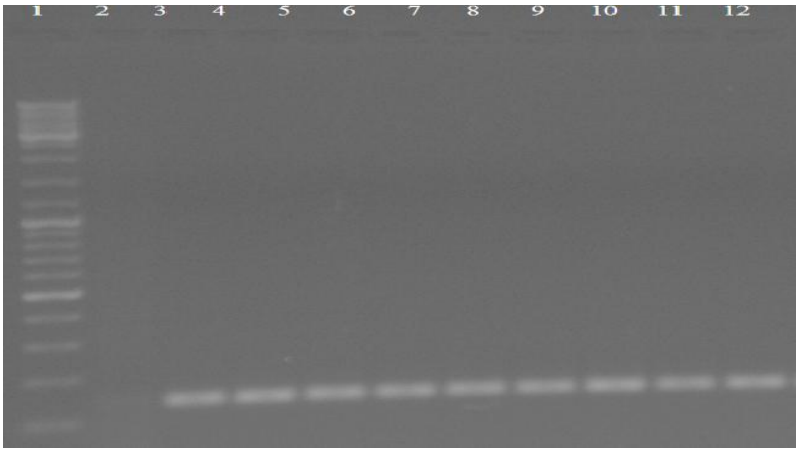

Figure C.14 Expression levels of *C-Flip* (long); Lane: DNA ladder (Fermentas, Lithuania), Lane 2: Negative control, Lane 3: *C-Flip* in untreated MCF7/S cell line (Undiluted), Lane 4: *C-Flip* in untreated MCF7/S cell line, Lane 5: *C-Flip* in untreated MCF7/S cell line (1:10 diluted), Lane 6: *C-Flip* in untreated MDA-MB231 cell line, Lane 67: *C-Flip* in untreated SKBR3 cell line, Lane 8: *C-Flip* in untreated MCF7/Dox cell line, Lane 9: *C-Flip* in 0.5 µg/ml CpG-loaded DcMNP-treated MCF7/S cell line, Lane 10: *C-Flip* in 0.5 µg/ml CpG-loaded DcMNP-treated MDA-MB231 cell line, Lane 11: *C-Flip* in 0.5 µg/ml CpG-loaded DcMNP-treated SKBR3 cell line, Lane 12: *C-Flip* in 0.5 µg/ml CpG-loaded DcMNP-treated MCF7/Dox cell line.

APPENDIX D

CELL CULTURE MEDIUM

Table D.1 Formulation of RPMI 1640 Medium (Lonza, Germany) (Continued)

Substance	Concentration (mg/L)
L-Glutamine	300.000
Sodium Bicarbonate	2.000E+03
Ca(NO3)2.4H2O	100.000
Choline Chloride	3.000
D-Biotin (Vitamin H) (00129)	0.200
D-Calcium Pantothenate (Vitamin B5)	0.250
D-Glucose anhydrous	2.000E+03
Folic Acid	1.000
Glutathione Reduced	1.000
Glycine	10.000
Potassium Chloride	400.000
L-Arginine Hydrochloride (00095)	241.860
L-Asparagine Monohydrate	56.810
L-Aspartic Acid	20.000
L-Cysteine Monohydrochloride Monohydrate	65.190
L-Glutamic Acid	20.000
L-Histidine Monohydrochloride Monohydrate	20.270
L-Hydroxyproline	20.000
L-Isoleucine	50.000
L-Leucine	50.000
L-Lysine Monohydrochloride	40.000

Table D.1 Formulation of RPMI 1640 Medium (Lonza, Germany) (Continued)

Substance	Concentration (mg/L)
L-Methionine	15.000
L-Phenylalanine	15.000
L -Proline	20.000
L-Serine	30.000
L-Threonine	20.000
L-Tryptophane	5.000
L-Tyrosine Disodium Salt, Dihydrate	28.830
L-Valine	20.000
Magnesium Sulfate Anhydrous	48.830
Myo-Inositol	35.000
Sodium Phosphate Monobasic, Anhydrous	800.490
Sodium Chloride	6.000E+03
Niacinamide (Nicotinamide)	1.000
P-Aminobenzoic Acid	1.000
Phenol Red	5.100
Pyridoxine Monohydrochloride	1.000
Riboflavin (Vitamin B2)	0.200
Thiamine Monohydrochloride (Vitamin B1)	1.000
Cyanocobalamin (Vitamin B12)	5.000E-03

Retrieved from http://bio.lonza.com/uploads/tx_mwaxmarketingmaterial/Lonza_ProductDataSheets_Formulation_-_RPMI_1640_Medium_12-702.pdf.

APPENDIX E

CELL PROLIFERATION GRAPHS

All cytotoxicity experiments were carried out in triplicate 96-well plates. Cytotoxicity of Biochanin A and zoledronic acid (before and after Biochanin A treatment at different concentrations) were assessed by plotting cell proliferation (%) versus concentration graphs for each plate in triplicates. The data were represented as mean ± standart error of the mean (SEM).

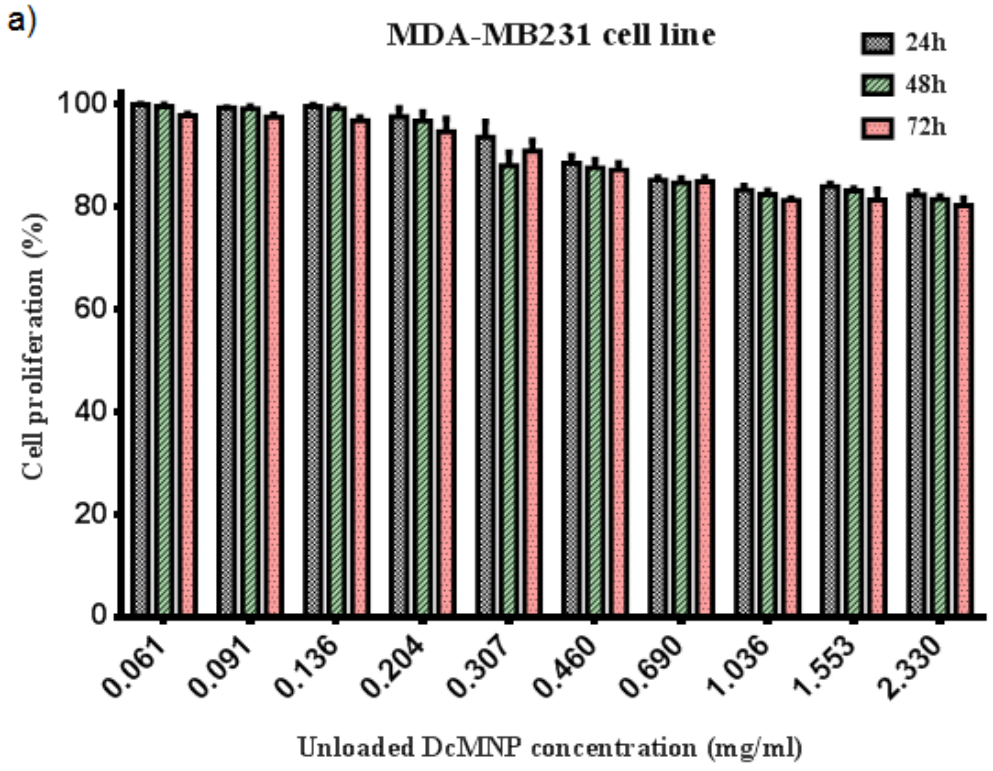

Figure E.1 Profile of cell proliferation of a) MDA-MB231, b) SKBR3, c) MCF7/S, and d) MCF7/Dox cell lines at increasing concentrations of unloaded DcMNP at three different incubation times. (Continued)

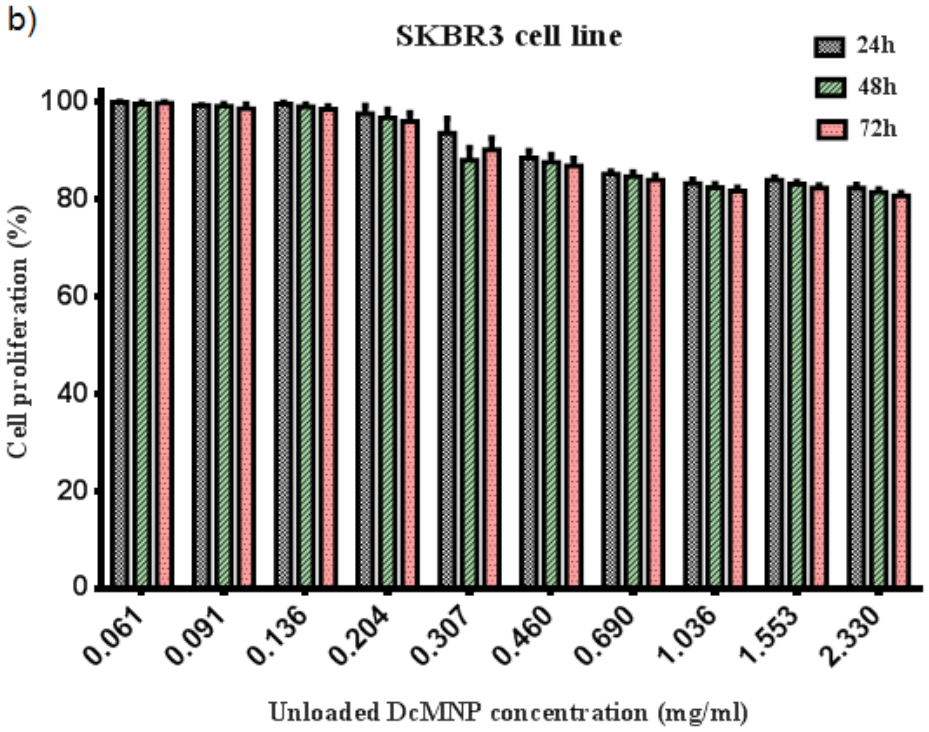

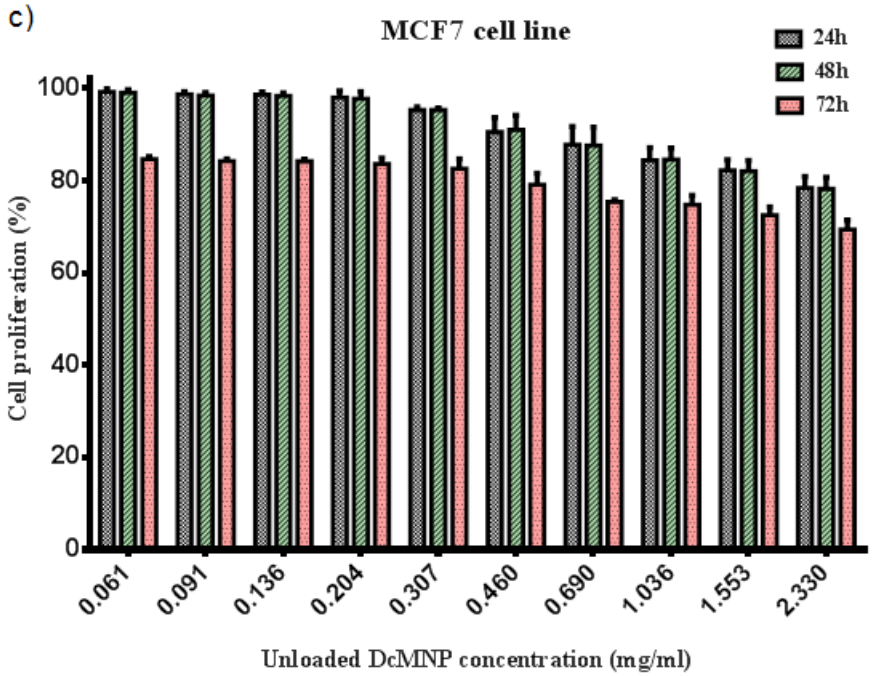

Figure E.1 Profile of cell proliferation of a) MDA-MB231, b) SKBR3, c) MCF7/S, and d) MCF7/Dox cell lines at increasing concentrations of unloaded DcMNP at three different incubation times. (Continued)

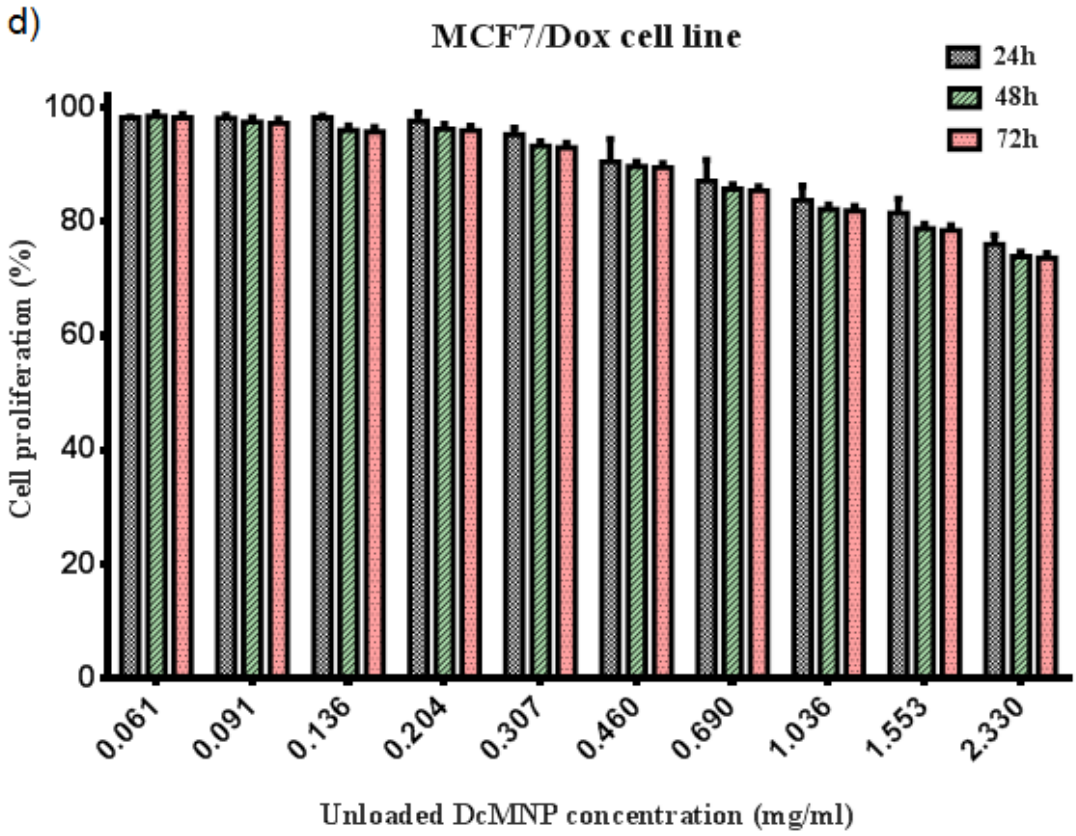

Figure E.1 Profile of cell proliferation of a) MDA-MB231, b) SKBR3, c) MCF7/S, and d) MCF7/Dox cell lines at increasing concentrations of unloaded DcMNP at three different incubation times. (Continued)

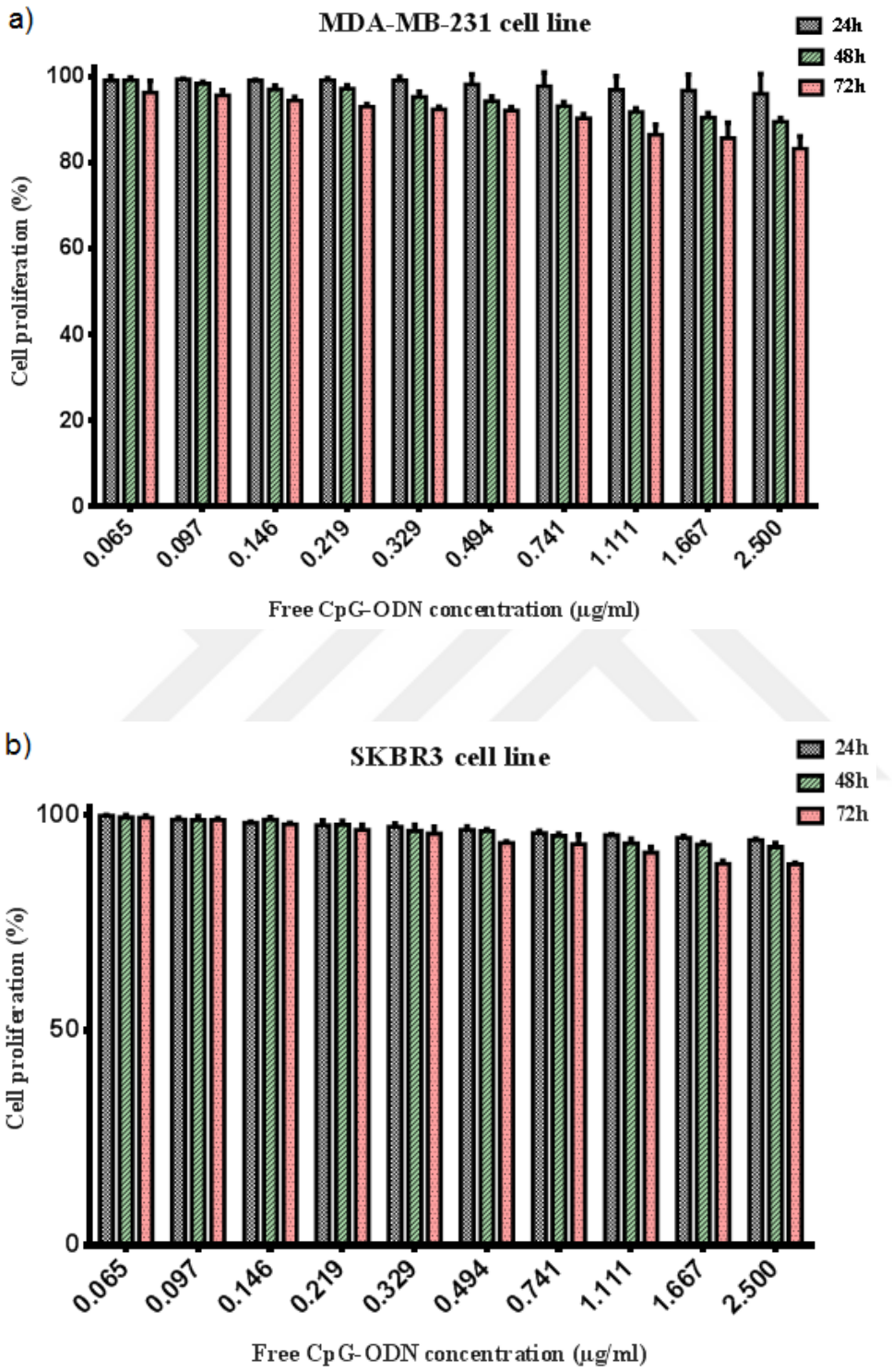

Figure E.2 Profile of cell proliferation of a) MDA-MB231, b) SKBR3, c) MCF7/S, and d) MCF7/Dox cell lines at increasing concentrations of free CpG-ODN at three different incubation times. (Continued)

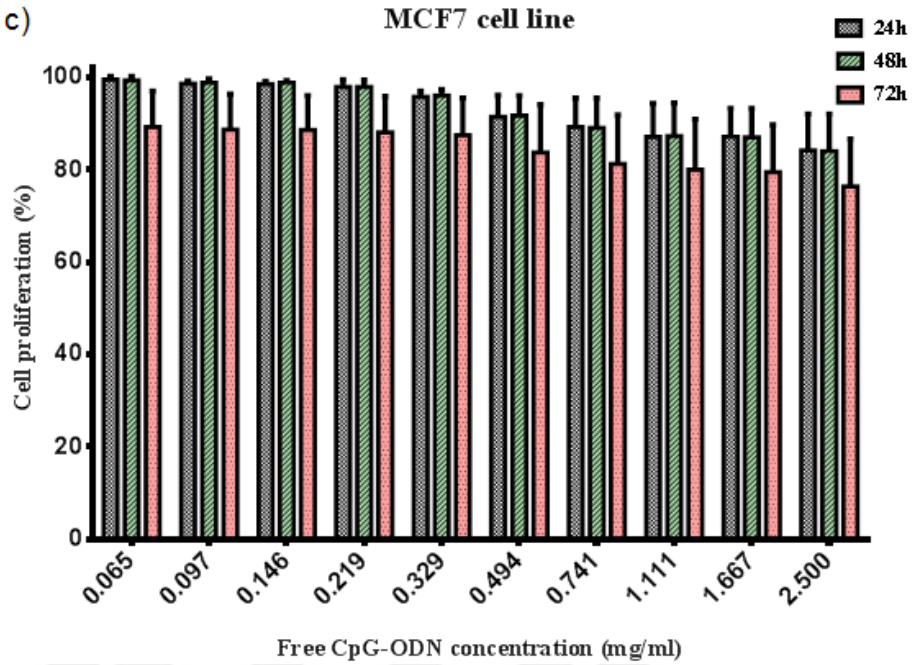

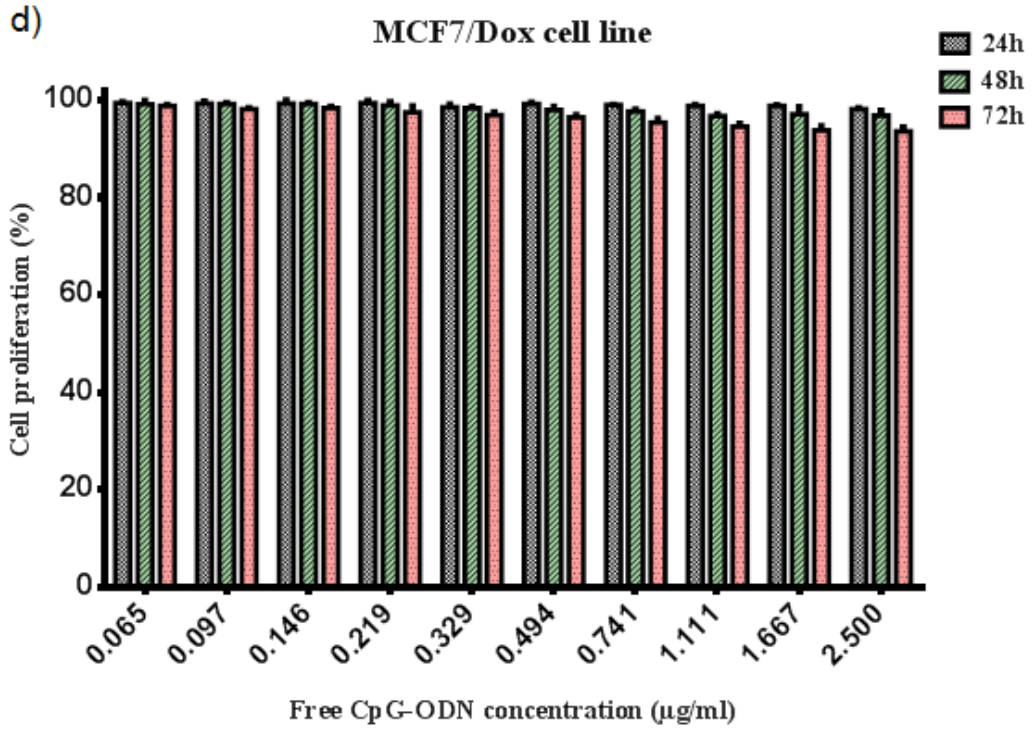

Figure E.2 Profile of cell proliferation of a) MDA-MB231, b) SKBR3, c) MCF7/S, and d) MCF7/Dox cell lines at increasing concentrations of free CpG-ODN at three different incubation times. (Continued)

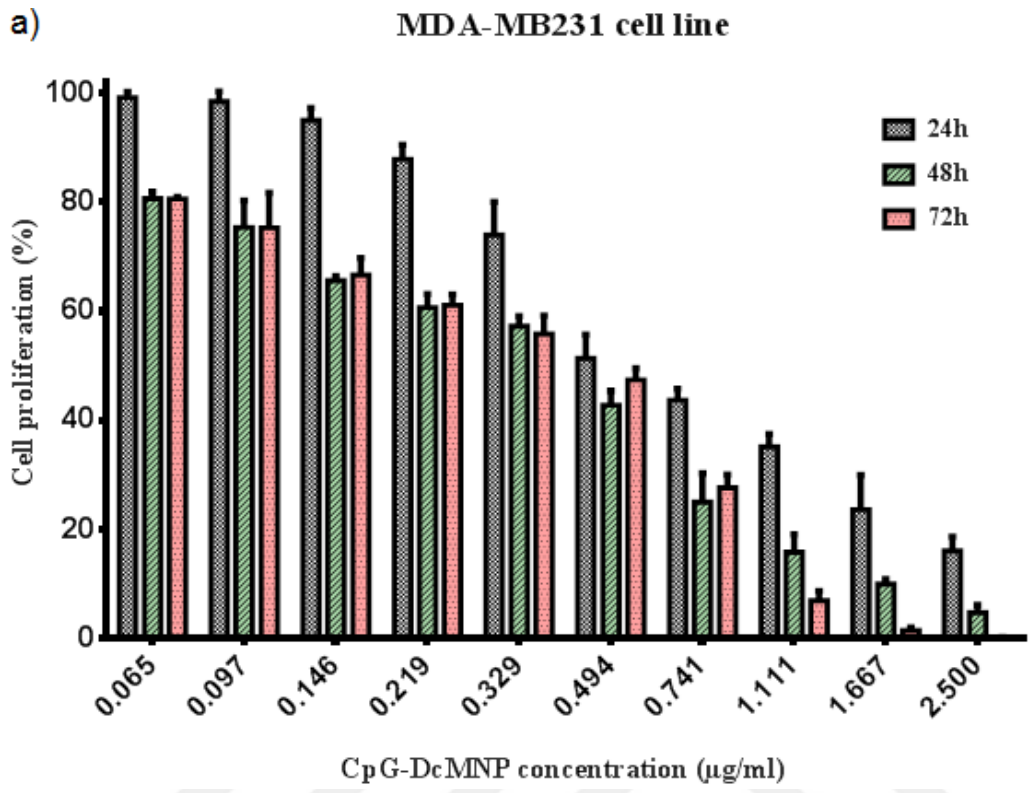

Figure E.3 Profile of cell proliferation of a) MDA-MB231, b) SKBR3, c) MCF7/S, and d) MCF7/Dox cell lines at increasing concentrations of CpG-loaded DcMNP at three different incubation times. (Continued)

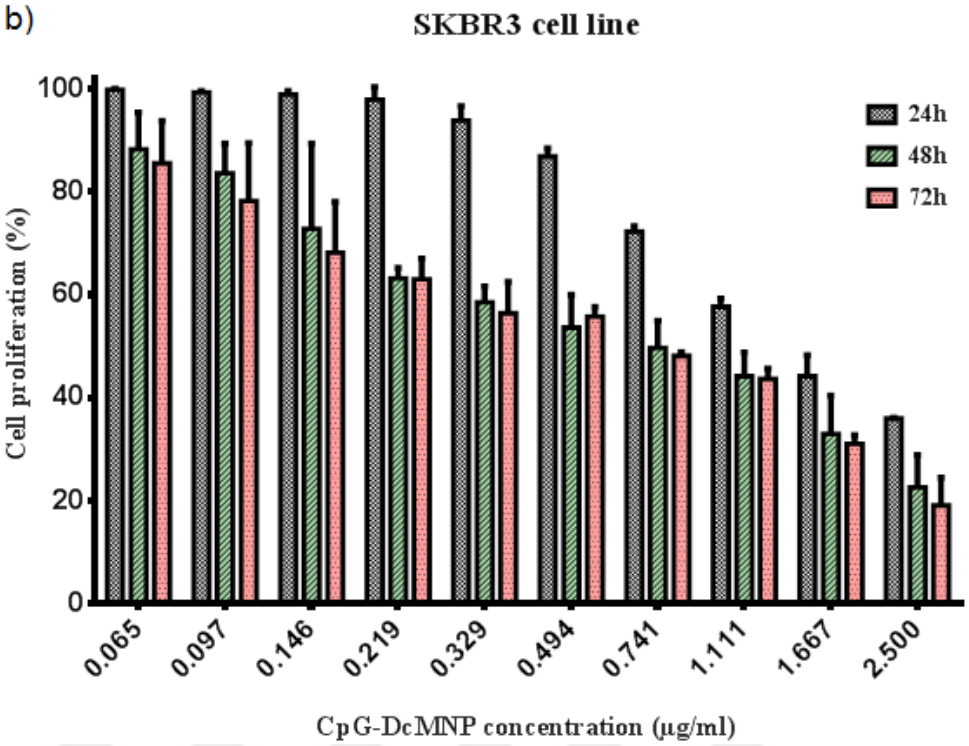

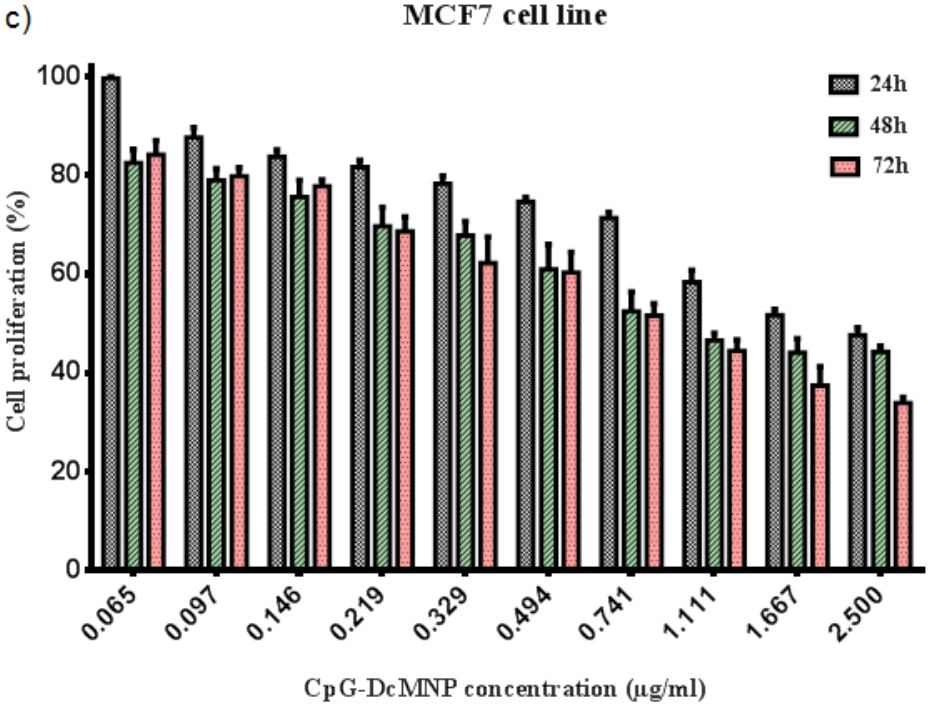

Figure E.3 Profile of cell proliferation of a) MDA-MB231, b) SKBR3, c) MCF7/S, and d) MCF7/Dox cell lines at increasing concentrations of CpG-loaded DcMNP at three different incubation times. (Continued)

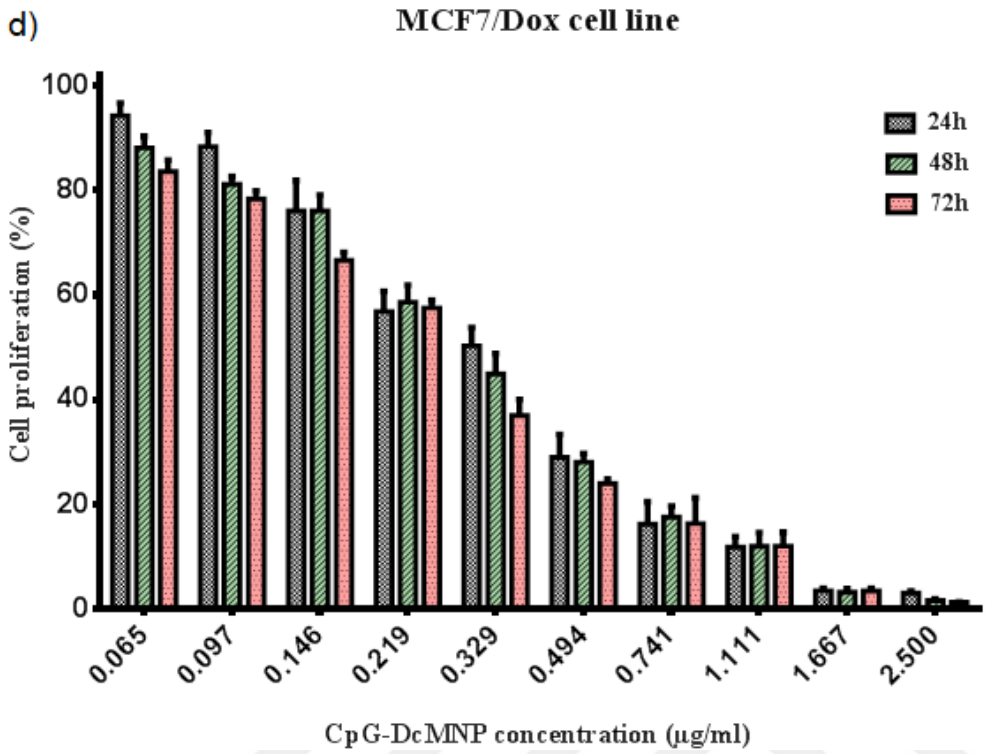

Figure E.3 Profile of cell proliferation of a) MDA-MB231, b) SKBR3, c) MCF7/S, and d) MCF7/Dox cell lines at increasing concentrations of CpG-loaded DcMNP at three different incubation times. (Continued)

APPENDIX F

NANODROP SPECTROPHOTOMETER

Table F.1 Determination of ssDNA concentration (free CpG-ODN) using NanoDrop spectrophotometer. (Continued)

#	Sample ID	Nucleic Acid Conc.	Unit	Sample Type	Factor
1	50 µM CpG	341.85	ng/µl	ssDNA	33.00
2	25 µM CpG	166.85	ng/µl	ssDNA	33.00
3	12.5 µM CpG	89.85	ng/µl	ssDNA	33.00
4	6.25 µM CpG	38.40	ng/µl	ssDNA	33.00
5	3.125 µM CpG	18.40	ng/µl	ssDNA	33.00
6	1.56 µM CpG	9.75	ng/µl	ssDNA	33.00
7	0.78 µM CpG	4.45	ng/µl	ssDNA	33.00
8	0.39 µM CpG	2.25	ng/µl	ssDNA	33.00
9	Free G7DcMNP	0	ng/µl	ssDNA	33.00
10	8.33 µM CpG + 3500 µg G3 DcMNP	16.10	ng/µl	ssDNA	33.00
11	8.33 µM CpG + 3500 µg G4 DcMNP	9.35	ng/µl	ssDNA	33.00
12	8.33 µM CpG + 3500 µg G5 DcMNP	6.45	ng/µl	ssDNA	33.00
13	8.33 µM CpG + 3500 µg G6 DcMNP	2.05	ng/µl	ssDNA	33.00
14	8.33 µM CpG + 3500 µg G7 DcMNP	0.40	ng/µl	ssDNA	33.00
15	8.33 µM CpG + 3500 µg G8 DcMNP	1.86	ng/µl	ssDNA	33.00
16	8.33 µM CpG	43.42	ng/µl	ssDNA	33.00
17	8.33 µM CpG + 50 µg G7 DcMNP	41.63	ng/µl	ssDNA	33.00
18	8.33 µM CpG + 125 µg G7 DcMNP	30.23	ng/µl	ssDNA	33.00
19	8.33 µM CpG + 250 µg G7 DcMNP	18.77	ng/µl	ssDNA	33.00
20	8.33 µM CpG + 500 µg G7 DcMNP	12.27	ng/µl	ssDNA	33.00
21	8.33 µM CpG + 1000 µg G7 DcMNP	4.70	ng/µl	ssDNA	33.00
22	8.33 µM CpG + 1500 µg G7 DcMNP	2.33	ng/µl	ssDNA	33.00

Table F.1 Determination of ssDNA concentration (free CpG-ODN) using NanoDrop spectrophotometer. (Continued)

#	Sample ID	Nucleic Acid Conc.	Unit	Sample Type	Factor
23	8.33 µM CpG + 2500 µg G7 DcMNP	1.00	ng/µl	ssDNA	33.00
24	8.33 µM CpG + 3250 µg G7 DcMNP	0.83	ng/µl	ssDNA	33.00
25	8.33 µM CpG + 3500 µg G7 DcMNP	0.41	ng/µl	ssDNA	33.00
26	8.33 µM CpG + 3750 µg G7 DcMNP	0.20	ng/µl	ssDNA	33.00

Table F.2 Determination of ssDNA concentration (free CpG-ODN) in the stability test using NanoDrop spectrophotometer.

#	Time intervals after mixing	Nucleic Acid Conc.	Unit	Sample Type	Factor
1	1 h	0.41	ng/µl	ssDNA	33.00
2	3 h	0.41	ng/µl	ssDNA	33.00
3	5 h	0.42	ng/µl	ssDNA	33.00
4	7 h	0.43	ng/µl	ssDNA	33.00
5	10 h	0.43	ng/µl	ssDNA	33.00
6	14 h	0.43	ng/µl	ssDNA	33.00
7	24 h (1 day)	0.44	ng/µl	ssDNA	33.00
8	48 h (2 days)	0.44	ng/µl	ssDNA	33.00
9	72 h (3 days)	0.45	ng/µl	ssDNA	33.00
10	96 h (4 days)	0.46	ng/µl	ssDNA	33.00
11	5 days	0.47	ng/µl	ssDNA	33.00
12	6 days	0.48	ng/µl	ssDNA	33.00
13	7 days	0.48	ng/µl	ssDNA	33.00
14	14 days (2 weeks)	0.49	ng/µl	ssDNA	33.00
15	3 weeks	0.49	ng/µl	ssDNA	33.00
16	4 weeks	0.49	ng/µl	ssDNA	33.00
17	5 weeks	0.5	ng/µl	ssDNA	33.00
18	6 weeks	0.5	ng/µl	ssDNA	33.00
19	7 weeks	0.5	ng/µl	ssDNA	33.00
20	8 weeks	0.5	ng/µl	ssDNA	33.00

APPENDIX G

FLOW CYTOMETRY GRAPHS

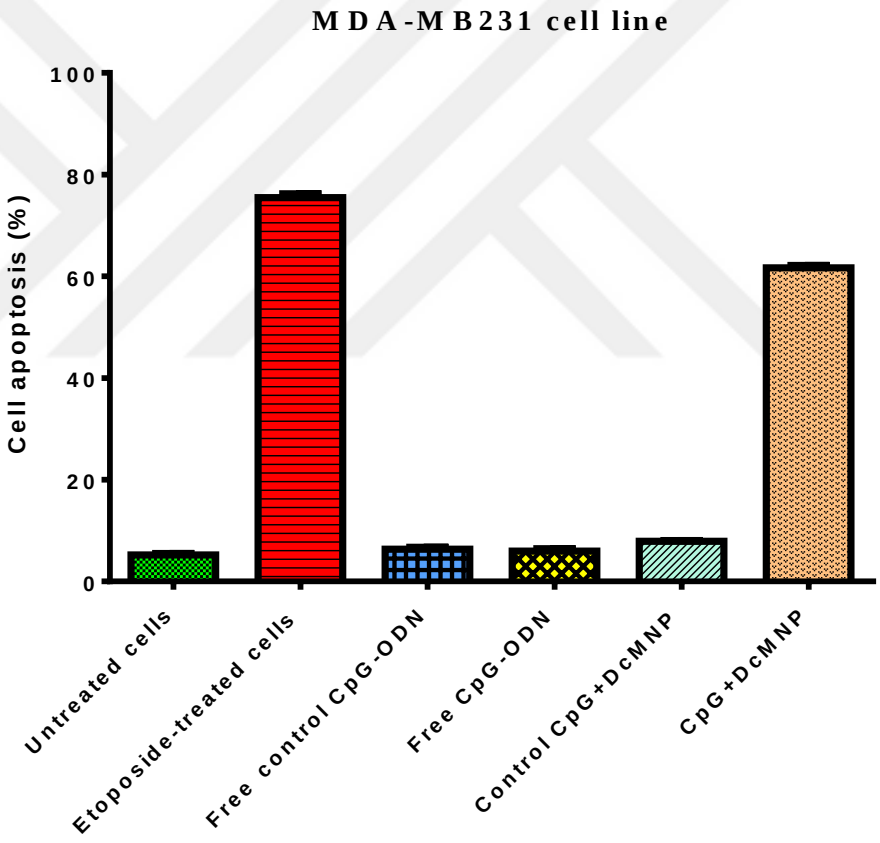

Figure G.1 Profile of programmed cell death of untreated and treated MDA-MB231 cells determined by flow cytometric analysis.

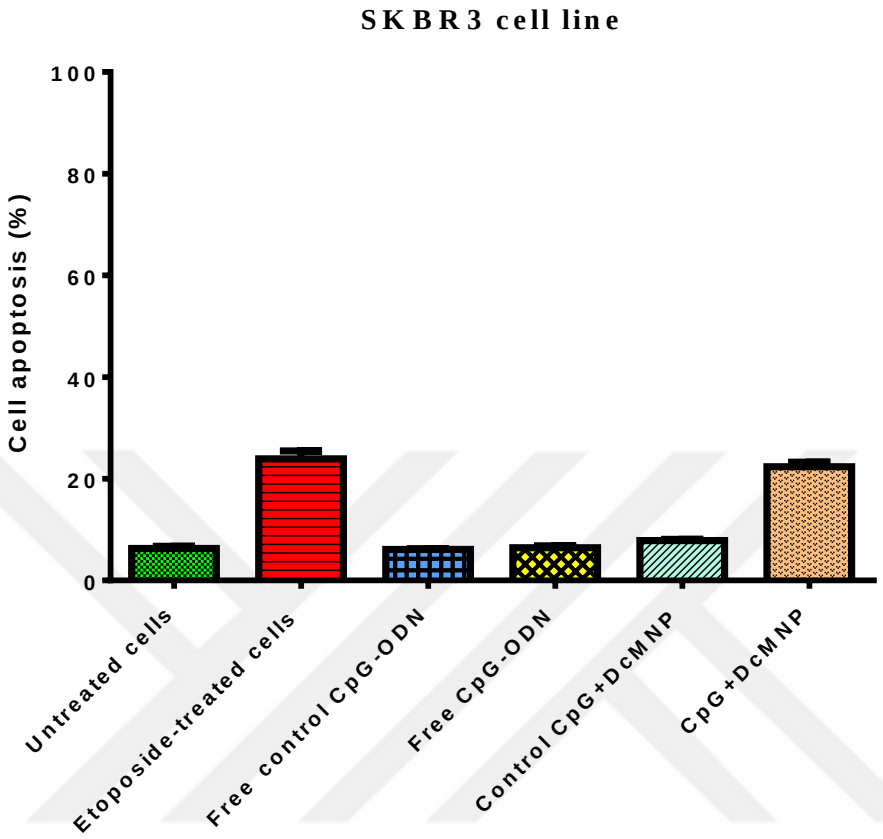

Figure G.2 Profile of programmed cell death of untreated and treated SKBR3 cells determined by flow cytometric analysis.

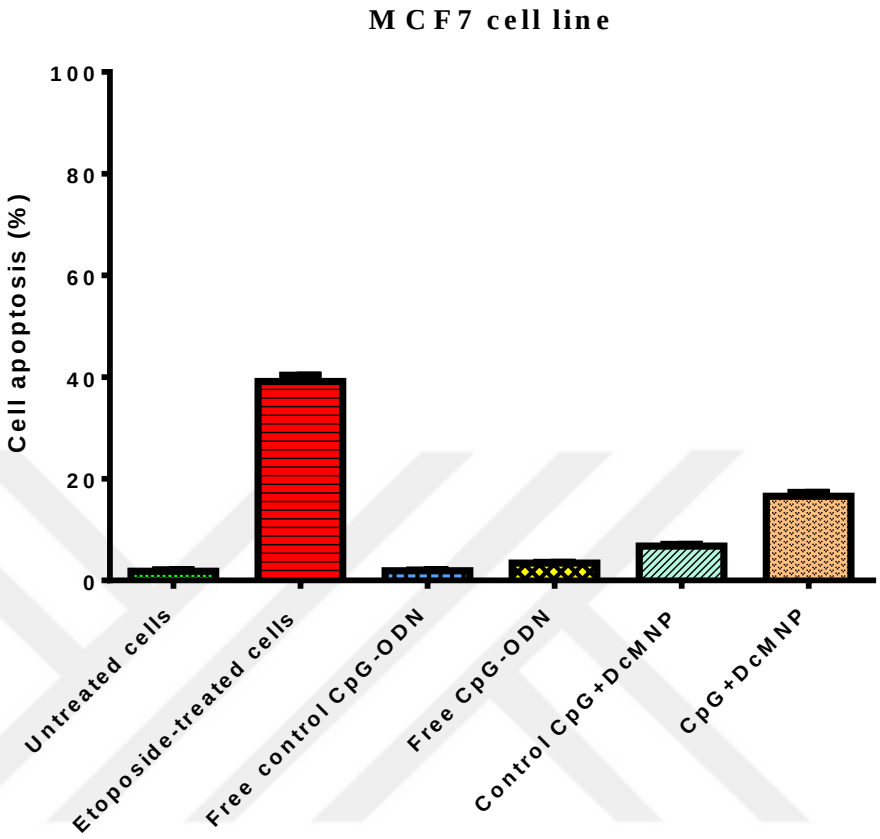

Figure G.3 Profile of programmed cell death of untreated and treated MCF7 cells determined by flow cytometric analysis.

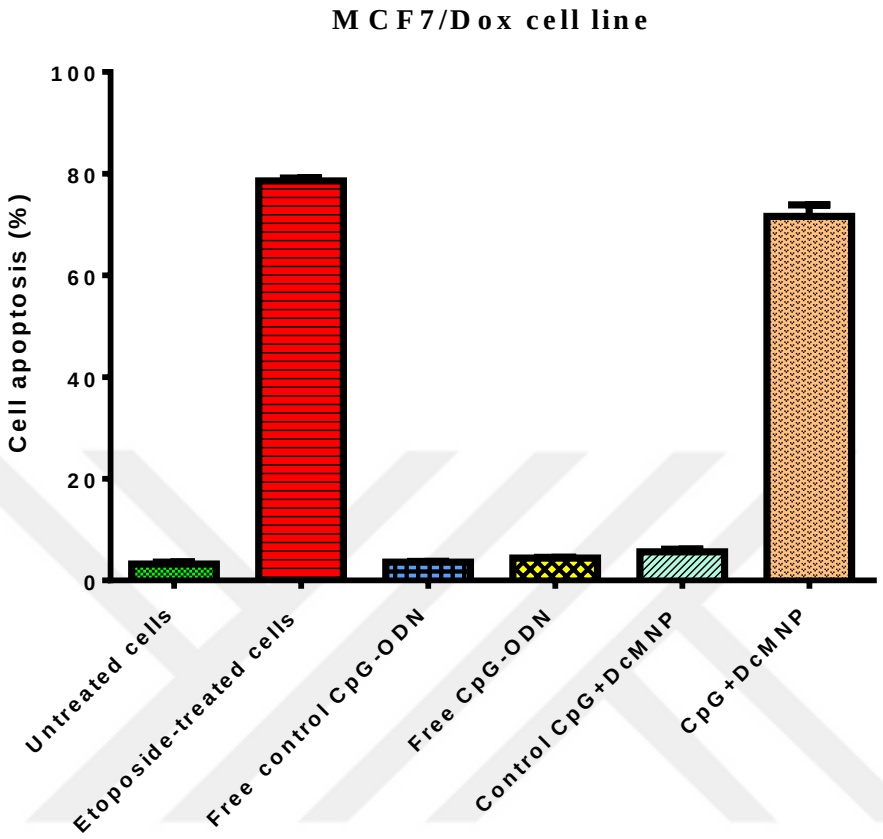

Figure G.4 Profile of programmed cell death of untreated and treated MCF7/Dox cells determined by flow cytometric analysis.

CURRICULUM VITAE

PERSONAL INFORMATION

Surname, Name: Taghavi PourianAzar, Negar

Nationality: Iranian

Date and Place of Birth: 21 March 1980, Tabriz

Marital Status: Married

Phone: +90 531 518 9932

Fax: +90 312 210 7976

Email: e176406@metu.edu.tr, negartaghavi22@gmail.com

EDUCATION

Degree	Institution	Year of Graduation
MS	University of Lahijan (Iran), Microbiology	2004
BS	University of Zanjan (Iran), Microbiology	2002
High School	Fatemiyyeh High School, Tabriz	1998

WORK EXPERIENCE

Year	Place	Enrollment
2008-2009	Nobel Food Quality Determination Laboratory	Head of Microbiological Laboratory
2000-2001	Iran Medical and Pathology Laboratory	Laboratory Assistant

FOREIGN LANGUAGES

English (Fluent)

Azeri (Mother tongue)

Farsi (Fluent)

Turkish (Fluent)

German (Intermediate)

French (Beginner)

PUBLICATIONS

A) JOURNAL PAPERS

1. Taghavi Pourianazar N., Nahaei M. R., "Using of Bacteria for Refining Wastewaters Produced in Factories on the basis of Linear Alkyl Benzene Sulfonates", Medical Journal of Tabriz University of Medical Sciences and Health services, 1(27), 21-25 (2005)

2. Taghavi Pourianazar N., Mutlu P., Khodadust R., Gunduz U., "Poly(amidoamine) (PAMAM) Nanoparticles: Synthesis and Biomedical Applications", Hacettepe J. Biol. & Chem., 41(3), 289-299 (2013)

3. Taghavi Pourianazar N., Mutlu P., Gunduz U., "Bioapplications of Poly(amidoamine) (PAMAM) Dendrimers in Nanomedicine", J Nanopart Res, 16(4), 2342 (2014)

4. Taghavi Pourianazar N., Gunduz U., "CpG Oligodeoxynucleotide-loaded PAMAM dendrimer-coated magnetic nanoparticles promote apoptosis in breast cancer cells", Biomedicine and Pharmacotherapy, 78, 81-91 (2016)

B) CONFERENCES

1. Taghavi Pourianazar N., Nahaei M. R., "Abilities of Bacteria for Degrading Linear Alkyl Benzene Sulfonates in Sewages of Detergent Producing Factories", Oral presentation, The 7th Iranian Congress of Microbiology, Semnan-Iran (2005)

2. Taghavi Pourianazar N., Nahaei M. R., "Comparison of Pseudomaonas and Aeromonas Abilities for Degrading Linear Alkyl Benzene Sulfonates in Sewages of Detergent Producing Factories", Oral presentation, The 8th National Congress of Enivronmental Health, Tehran-Iran (2005)

3. Khodadust R., Mutlu P., Yalcin S., Unsoy G., Taghavi Pourianazar N., Gunduz U., "Loading Efficiency Optimization of Doxorubicin on Dendrimer Coated Magnetic Nanoparticles using Different Buffers", Poster, 4th International Conference: NANOCON, Brno-Czech Republic (October 23rd - 25th 2012)

4. Unsoy G., Yalcin S., Khodadust R., Mutlu P., Taghavi Pourianazar N., Gunduz U., "In Situ Synthesis and Characterization of Chitosan Coated Iron Oxide Nanoparticles", Poster, 4th International Conference: NANOCON, Brno-Czech Republic (October 23rd - 25th 2012)

5. Yalcin S., Unsoy G., Khodadust R., Mutlu P., Taghavi Pourianazar N., Gunduz U., "The Cytotoxicity Analysis of PHB Coated Magnetic Nanoparticles on Sensitive and Doxorubicin Resistant MCF-7 Cell Lines", Poster, 4th International Conference: NANOCON, Brno-Czech Republic (October 23rd - 25th 2012)

6. Taghavi Pourianazar N., Khodadust R., Mutlu P., Gunduz U., "Doxorubicin loading, release and stability in dendrimer coated magnetic nanoparticles for targeted drug delivery", Oral presentation, International Porous and Powder Materials: PPM 2013, Cesme-Izmir-Turkey (September 3rd -6th 2013)

7. Taghavi Pourianazar N., Gunduz U., "Synthesis, surface modification, and characterisation of CpG-ODN loaded magnetic nanoparticles for biomedical applications", Oral presentation, EACR-sponsored 2nd Anticancer Agents Congress and 5th Multidisciplinary Cancer Research Congress, Bodrum-Turkey (April 23th-27th 2014)

8. Taghavi Pourianazar N., Parsian M., Unsoy G., Yalcin S., Gunduz U., "Comparison of two polymeric nanocarriers for targeted CpG-ODN delivery: chitosan- and poly (amidoamine) dendrimer-coated magnetic nanoparticles", Poster, The FEBS-EMBO 2014 Conference, Paris- France (30 August -4 September 2014)

9. Taghavi Pourianazar N., Gunduz U., "PAMAM coated magnetic nanoparticles as CpG-ODN carriers for activation of toll-like receptor 9", Poster, The FEBS-EMBO 2014 Conference, Paris- France (30 August -4 September 2014)

10. Unsoy G., Yalcin S., Khodadust R., Mutlu P., Taghavi Pourianazar N., Gunduz U., "Loading and release efficiencies of Bortezomib on chitosan coated magnetic nanoparticles", Poster, The FEBS-EMBO 2014 Conference, Paris- France (30 August -4 September 2014)

11. Unsoy G., Yalcin S., Khodadust R., Mutlu P., Taghavi Pourianazar N., Gunduz U., "Cellular internalization of Bortezomib loaded CS MNPs by cervical cancer cells", Poster, The FEBS-EMBO 2014 Conference, Paris- France (30 August -4 September 2014)

12. Yalcin S., Mutlu P., Unsoy G., Parsian M., Taghavi Pourianazar N., Gunduz U., "Cellular internalization of polyhydroxybutyrate coated magnetic nanoparticles in SKBR-3 cell lines", Poster, The FEBS-EMBO 2014 Conference, Paris- France (30 August -4 September 2014)

13. Parsian M., Unsoy G., Mutlu P., Yalcin S., Taghavi Pourianazar N., Gunduz U., "Chitosan-coated magnetic nanoparticles as vehicles for the delivery of the antitumor drug gemcitabine", Poster, The FEBS-EMBO 2014 Conference, Paris- France (30 August -4 September 2014)

14. Parsian M., Taghavi Pourianazar N., Yalcin S., Mutlu P., Gunduz U., "Conjugation of gemcitabine to PAMAM dendrimer-coated magnetic nanoparticles for targeted delivery", Poster, The FEBS-EMBO 2014 Conference, Paris- France (30 August -4 September 2014)

15. Unsoy G., Khodadust R., Yalcin S., Mutlu P., Taghavi Pourianazar N., Parsian M., Gunduz U., "Effect of doxorubicin loaded CS MNPs on cell proliferation in sensitive and doxorubicin resistant MCF-7 cell lines", Poster, The FEBS-EMBO 2014 Conference, Paris- France (30 August -4 September 2014)

16. Yalcin S., Unsoy G., Taghavi Pourianazar N., Gunduz U., "Preparation of fluorescent IgG monoclonal antibody conjugated PHB coated magnetic nonoparticles for imaging and cancer therapy", Poster, The FEBS-EMBO 2014 Conference, Paris- France (30 August -4 September 2014)

17. Yalcin S., Unsoy G., Mutlu P., Khodadust R., Taghavi Pourianazar N., Parsian M., Gunduz U., "The cytotoxic analysis of free doxorubicin and doxorubicin loaded PHB-MNPs on sensitive and doxorubicin resistant MCF-7 cell lines", Poster, The FEBS-EMBO 2014 Conference, Paris- France (30 August -4 September 2014)

18. Taghavi Pourianazar N., Gunduz U., "Co-delivery of doxorubicin and CPG-oligodeoxynucleotıde on PAMAM-coated magnetic nanoparticles", Poster, EACR-sponsored 3rd Anticancer Agent Development Congress, Izmir-Turkey (May 18th-19th 2015)

19. Taghavi Pourianazar N., Gunduz U., "The *in vitro* effects of CpG oligodeoxynucleotides-loaded dendrimer-coated magnetic nanoparticles on the expression of IL-6 cytokine gene in breast cancer cell lines", Poster, MolBiyoKon 2015-4th International Congress of the Molecular Biology Association of Turkey, Ankara-Turkey (November 27-29 2015)

PROJECT COLLABORATIONS

1. Research fund project (BAP1) Funding agency: BAP1. Project code: BAP-07-02-2012-101-70. Project name: Preparation of Anti-HER2 bound PHB polymer coated magnetic nanoparticles and application of them to MCF-7 Breast Cancer Cell Line. Institution: METU. Start: 01/01/2012, Finish: 31/12/2012

2. Research fund project (BAP1) Funding agency: BAP1. Project code: BAP-07-02-2012-101-71. Project name: Preparation of Anti-HER2 bound PHB polymer coated magnetic nanoparticles and application of them to MCF-7 Breast Cancer Cell Line. Institution: METU. Start: 01/01/2013, Finish: 31/12/2013

3. 1002 - Short Term R&D Funding Program (TUBITAK). Project name: Poly-amidoamine (PAMAM) Dendrimer Modified Magnetic Nanoparticle Synthesis for CpG Oligodeoxynucleotide Delivery in Breast Cancer Cell Lines

4. 3001 - R&D Funding Program (TUBITAK). Project name: Determination of the Relationship between the Expression Levels of Genes Involved in Doxorubicin Resistance and WNT Signaling Pathways

FELLOWSHIPS AND AWARDS

October 2010-2014	PhD Fellowship for Foreign Citizens (TUBITAK)
April 2014	Young Investigator scholarship of MOKAD (Molecular Cancer Research Association)
April 2014	Travel award of MOKAD (Molecular Cancer Research Association**)**
September 2014	Registration award of FEBS congress (The Federation of European Biochemical Societies)
September 2014	Travel award of FEBS congress (The Federation of European Biochemical Societies)
October 2014- 2015	Success Scholarship Program (Turkey)
May 2015	Young Investigator scholarship of MOKAD (Molecular Cancer Research Association)

TRANSLATIONS

Solomon Biology. 3rd volume. (Eldra Solomon) 2010, English to Farsi

MEMBERSHIPS

European Association for Cancer Research (EACR)

Molecular cancer research center (MOKAD)-Turkey

HOBBIES

Swimming, Volleyball, Learning Languages, Reading Books